



UNIVERSITAT DE
BARCELONA

Photo-Fenton at Circumneutral pH for Agricultural Water Reuse

Núria López Vinent

ADVERTIMENT. La consulta d'aquesta tesi queda condicionada a l'acceptació de les següents condicions d'ús: La difusió d'aquesta tesi per mitjà del servei TDX (www.tdx.cat) i a través del Dipòsit Digital de la UB (diposit.ub.edu) ha estat autoritzada pels titulars dels drets de propietat intel·lectual únicament per a usos privats emmarcats en activitats d'investigació i docència. No s'autoritza la seva reproducció amb finalitats de lucre ni la seva difusió i posada a disposició des d'un lloc aliè al servei TDX ni al Dipòsit Digital de la UB. No s'autoritza la presentació del seu contingut en una finestra o marc aliè a TDX o al Dipòsit Digital de la UB (framing). Aquesta reserva de drets afecta tant al resum de presentació de la tesi com als seus continguts. En la utilització o cita de parts de la tesi és obligat indicar el nom de la persona autora.

ADVERTENCIA. La consulta de esta tesis queda condicionada a la aceptación de las siguientes condiciones de uso: La difusión de esta tesis por medio del servicio TDR (www.tdx.cat) y a través del Repositorio Digital de la UB (diposit.ub.edu) ha sido autorizada por los titulares de los derechos de propiedad intelectual únicamente para usos privados enmarcados en actividades de investigación y docencia. No se autoriza su reproducción con finalidades de lucro ni su difusión y puesta a disposición desde un sitio ajeno al servicio TDR o al Repositorio Digital de la UB. No se autoriza la presentación de su contenido en una ventana o marco ajeno a TDR o al Repositorio Digital de la UB (framing). Esta reserva de derechos afecta tanto al resumen de presentación de la tesis como a sus contenidos. En la utilización o cita de partes de la tesis es obligado indicar el nombre de la persona autora.

WARNING. On having consulted this thesis you're accepting the following use conditions: Spreading this thesis by the TDX (www.tdx.cat) service and by the UB Digital Repository (diposit.ub.edu) has been authorized by the titular of the intellectual property rights only for private uses placed in investigation and teaching activities. Reproduction with lucrative aims is not authorized nor its spreading and availability from a site foreign to the TDX service or to the UB Digital Repository. Introducing its content in a window or frame foreign to the TDX service or to the UB Digital Repository is not authorized (framing). Those rights affect to the presentation summary of the thesis as well as to its contents. In the using or citation of parts of the thesis it's obliged to indicate the name of the author.



UNIVERSITAT_{DE}
BARCELONA

Programa de doctorat d'Enginyeria i Ciències Aplicades

Photo-Fenton at Circumneutral pH for Agricultural Water Reuse

Núria López Vinent

Directors:

Dr. Jaume Giménez Farreras

Dr. Santiago Esplugas Vidal

Tutor:

Dr. Jaume Giménez Farreras

Departament d'Enginyeria Química i Química Analítica

El Dr. JAUME GIMÉNEZ FARRERAS, Catedràtic del Departament d'Enginyeria Química i Química Analítica de la Universitat de Barcelona i el Dr. SANTIAGO ESPLUGAS VIDAL, Catedràtic del mateix departament:

CERTIFIQUEN QUE:

El treball de recerca titulat “PHOTO-FENTON AT CIRCUMNEUTRAL PH FOR AGRICULTURAL WATER REUSE” constitueix la memòria que presenta l’Ambientòloga Núria López Vinent per a aspirar al grau de Doctor per la Universitat de Barcelona. Aquesta tesi doctoral ha estat realitzada dins del programa de doctorat “Enginyeria i Ciències Aplicades”, en el Departament d’Enginyeria Química i Química Analítica de la Universitat de Barcelona.

I per a que així consti als efectes oportuns, signen el present certificat a Barcelona, 11 de maig de 2021.

Dr. Jaume Giménez Farreras

i

Dr. Santiago Esplugas Vidal

Director i tutor de la tesi doctoral

Director de la tesi doctoral

A sa meua família

Agradecimientos

Siempre que me preguntan si volvería a adentrarme en el mundo de la investigación -en concreto la misma temática de tesis- sabiendo lo que se a día de hoy, mi respuesta es claramente un sí. La investigación durante estos cuatro años no ha sido fácil. Mejor dicho: ¡ha sido una aventura! Pero no sólo me ha servido para avanzar a nivel profesional y científico, sino que también me ha hecho crecer como persona. Los momentos vividos al límite no han sido pocos. Aun así, desde mi humilde perspectiva, los he afrontado de la mejor manera posible, siempre teniendo en mente mis metas. No obstante, ha habido muchas personas que me han ayudado a conseguir estos objetivos. Agradecer en pocas palabras, es siempre una tarea difícil, ya que para cada una de las personas que han estado siempre a mi lado durante este camino no sería suficiente una página. De todas formas, lo voy a intentar.

Primero de todo, me gustaría agradecer al Dr. Santiago Esplugas, quién ha sido director del grupo de Ingeniería de Procesos de Oxidación Avanzada durante los primeros años de tesis y codirector, la confianza depositada en mí para poder formar parte de su equipo. Su amabilidad y generosidad siempre han ayudado a trabajar mucho mejor. A la Dra. Carme Sans, quien a su vez también ha sido directora del grupo en los últimos años. Agradecerle la preocupación por mi tesis, siempre queriendo ayudar en todo lo que podía y por creer en los jóvenes investigadores y cuidarlos. A la Dra. Pilar Marco agradecerle la confianza asentada en mi des de mi trabajo final de grado y por acogerme en el grupo que me ha llevado a escribir estas palabras. A la Dra. Carme González, directora del programa de doctorado en el que se engloba mi tesis, Ingeniería y Ciencias Aplicadas, por su constante simpatía y amabilidad. Siempre dispuesta a ayudar y hacer las cosas más llevaderas. Gracias por creer en los jóvenes y, sobre todo, por anteponer la faceta de persona ante la de directora. Agradecer también al Ministerio de Ciencia y Educación del Gobierno de España la oportunidad de brindarme un contrato predoctoral FPU en el año 2017 y poder dedicarme a lo que más me gusta, la investigación durante estos cuatro años. No me gustaría olvidar al Dr. Mohammed Gamal El-Din, de la Universidad de Alberta, quién me dio la oportunidad de realizar una estancia en su grupo de investigación. *Thank you! These months in Canada were very positive both professionally and personally.* De igual forma, agradecerle al Dr. Adrián Tavares Da Silva, de la Universidad de Porto, la confianza depositada en mí para realizar una estancia en su grupo de investigación y por su generosidad y amabilidad en el curso de toda la estancia. *Muito obrigada! Foram alguns meses muito produtivos.*

Finalmente, agradecerle al Dr. Stefanos Giannakis por acogerme en su maravilloso laboratorio de la Universidad Politécnica de Madrid durante tres meses difíciles debido a la pandemia originada por el SARS-CoV-2. Muchas gracias por enseñarme tantas cosas en un ámbito que me encanta y no dominaba. Por tu continua dedicación y por todas las risas que tuvimos en el laboratorio. *Ya sé que me regalarás cuando acabe la tesis: ¡la bandeja del agua que tanto me gustó! Espero que siga viva...*

Un agradecimiento especial al Dr. Jaume Giménez, quién ha sido mi director y tutor de tesis durante estos cuatro años. Gracias por guiarme durante estos años, sobre todo en las correcciones de los artículos y de esta forma poder aprender de cada una de ellas. Por su interés en cada una de mis ideas. Por la confianza dispuesta en mí para llevar a cabo la tesis doctoral. *Gràcies Jaume, ha estat un plaer poder compartir aquests quatre anys amb tú.*

Me faltarían palabras para agradecer a Alberto todo lo que ha hecho por mí. Los buenos consejos y sonrisas cuando más lo he necesitado. Por ser un pilar firme tanto en el laboratorio como en lo emocional. Gracias por estar siempre a mi lado, ¡en los buenos y en los malos momentos! Has sido como mi director de tesis, por lo que le estaré siempre agradecida. En muchos casos no es fácil tener a la persona con quien compartes tu vida personal compartiendo también la vida profesional. Pero, no es por nada, en este sentido creo que lo hemos llevado de maravilla. ¡Y es que somos un equipo! Como tú también me dijiste: *Junts ho aconseguirem tot! T'estim.*

No quiero dejar de mencionar a los antiguos doctorandos quién me enseñaron parte de lo que se ahora durante mi trabajo final de grado y de máster. Gracias, sobre todo, a Antonella De Luca, por su generosidad y amabilidad. Siempre dispuesta a ayudar. Y por explicarme muchas de las cosas en el laboratorio. Agradecer también a Mireia Marcé y Ángel Cruz por ayudarme con tanta paciencia siempre que lo he necesitado. Por supuesto, agradecer especialmente a los doctorandos con los que empecé la tesis, Carme y Keong, y los estudiantes que han ido llegando a lo largo de estos cuatro años. Ellos son Oriol, Noemí, Vini, Verónica, Judit, Miquel, Andreu, Sergi, Laura, Lucas, Sina y también los profesores jóvenes, Roger, Eliana y Nardi. Gracias por cada una de las comidas, las risas y los consejos, con los cuáles se ha hecho más llevadero este duro camino de investigación predoctoral. Entre ellos, especial mención a mi compañero de grupo Oriol, el que me ha tenido que aguantar día tras día en el laboratorio. Me gustaría dar las gracias a todas las personas que han ido pasando temporalmente por el laboratorio. Nahuel, Miguel, Jacqueline y Dimitrios.

Gracias por vuestra simpatía y por todos los momentos que hemos pasado. En especial quería agradecer a Jacque, con la que he pasado momentos estupendos, por explicarme muchas cosas y por la gran persona que es. *Foi o melhor ano da tese. Vejo vosê no Brasil!* Especial mención también a Dimitrios por sacarme siempre una sonrisa cuando más lo necesitaba. *I will never forget the theater in the window!* Muchas gracias también a los estudiantes de grado y de máster con los que también he aprendido muchas cosas: Coral, Margalida y Claudia. Me ha encantado poder conocerlos y poder compartir momentos maravillosos.

No quisiera olvidarme de mis amigas de siempre, las que están en los buenos y en los malos momentos. Aunque no hayamos podido disfrutar bien de estos cuatro veranos en Menorca, ¡ahora sí que sí! Os quiero Marta y Paloma. Y a los de Barcelona: ¡gracias por todas las risas que nos hemos echado y las que nos echaremos!

Por último, y no por eso menos importante, quería agradecer sobre todo a mi hermano y a mis padres, los que siempre han estado en los momentos más difíciles y por todo el esfuerzo que han hecho para que a día de hoy pueda estar escribiendo esta tesis. Gracias por los buenos consejos, siempre sacándome una sonrisa. Por confiar en mí y apoyarme en todas mis decisiones. Por creer en que podía llegar lejos cuando ni yo lo creía. *Estaré eternament agraïda. ¡Vus admir!* No quisiera olvidarme de mi madrina Ruth, espero poder llegar a ser la mitad de lo que eres como profesional y como persona. Juntamente a mi *tieta* y a Berni. También agradecer a mi familia de Barcelona por todo el cariño durante estos años, ¡y los que quedan! Finalmente, a los que ya no están, pero que han contribuido a que sea la persona que hoy soy. *Gràcies avis i concu Xe. Mai vos olvidaré.*

Contents

Contents	xi
Abstract.....	xv
Thesis directors' report and list of publications	xix
Nomenclature.....	xxiii
1 Introduction	1
1.1 State of the world's water resources	1
1.1.1 Water demand and availability	1
1.1.2 Wastewater treatment and reuse	3
1.2 Micropollutants in water resources	5
1.2.1 Diphenhydramine hydrochloride	7
1.2.2 Propranolol hydrochloride	8
1.2.3 Sulfamethoxazole	8
1.2.4 Acetamiprid	9
1.3 General legal framework of water	9
1.3.1 European regulations on micropollutants in water resources.....	9
1.3.2 Reclaimed wastewaters quality policies	13
1.4 Advanced Oxidation Processes	15
1.4.1 Fundamentals.....	15
1.4.2 AOPs implementation and application	17
1.4.3 Water quality impacts	18
1.4.4 Fenton and photo-Fenton processes	20
Chemistry of the Fenton reactions.....	20
Photo-Fenton process	22
Operative parameters of the processes	22
Main drawbacks of the processes	23
Photo-Fenton at circumneutral pH	25
2 Justification, objectives and thesis structure	31
2.1 Justification and objectives	31
2.2 Thesis structure	32
3 Materials and methods.....	35
3.1 Chemicals.....	35
3.1.1 Model micropollutants.....	35

3.1.2	Chelating agents	35
3.1.3	Other chemicals.....	36
3.2	Wastewater samples	37
3.3	Experimental devices.....	38
3.3.1	UV-A LEDs.....	38
	Photoreactor with LEDs on the cover	38
	Photoreactor with LEDs on the center	39
	Tubular photoreactor	40
3.3.2	Black-light Blue lamp photoreactor	41
3.3.3	Solar light simulator	42
3.4	Analyses.....	43
3.4.1	Actinometrical measures	43
3.4.2	Acute toxicity: Microtox [®] bioassay	44
3.4.3	Alkalinity.....	44
3.4.4	Assessment of Effluent Organic Matter fractions	44
3.4.5	Bacterial enumeration	45
3.4.6	Biochemical Oxygen Demand	46
3.4.7	Chemical Oxygen Demand	46
3.4.8	Dissolved iron determination	47
3.4.9	Hydrogen peroxide concentration	47
3.4.10	Model micropollutants concentrations	47
3.4.11	Oxidation intermediates	48
3.4.12	Phytotoxicity	49
3.4.13	Total Organic Carbon.....	50
3.4.14	Turbidity.....	50
3.4.15	Ultraviolet absorbance.....	50
4	Results and discussion.....	51
4.1	Synergies, radiation and kinetics in photo-Fenton process with UV-A LEDs.....	51
4.1.1	Determination of effective concentrations	53
4.1.2	Synergistic effects with two wavelengths combination	53
4.1.3	By-product's determination.....	55
Part I	57
4.2	Comparison of conventional BLB lamps and LEDs in photo-Fenton process for micropollutant abatement in real wastewater	73
4.2.1	Propranolol removal comparison using conventional lamps and LEDs	75

4.2.2	Efficiency of EDDS:Fe(II) in different water matrices with LEDs.....	77
Part II	79
4.3	Assessment of organic fertilizers as an iron source in photo-Fenton at circumneutral pH for wastewater treatment and its potential application in agriculture.	97
4.3.1	Micropollutant abatement and bacterial inactivation using DTPA-Fe.....	107
4.3.2	Potential improvement on photo-Fenton at circumneutral pH.....	110
4.3.3	Potential reactivity of organic fertilizers in the aquatic environment and the mainly involved reaction mechanisms	113
Part III	117
Part IV	137
Part V	155
Part VI	171
5	Conclusions and recommendations	207
5.1	Conclusions.....	207
5.2	Recommendations.....	209
6	Other contributions by the author	211
6.1	Journal articles from research stays	211
6.2	Other journal articles	212
6.3	Congress communications	212
References	215

Abstract

Water is an essential resource for life. However, the low water availability and its increasing demand has provoked worldwide water stress, which is one of the main problems to be faced in the next years. Additionally, the continuous rise in freshwater demand is associated with increased generation of wastewater. Thus, in a water scarcity scenario, the reused wastewater can play an important role to reduce freshwater demand, for instance, in agriculture with around 70% of the total freshwater demand. Nevertheless, the reused wastewater must guarantee the safety for public health and environment. In the last decades, there is an especial concern on removing micropollutants, since they are potentially harmful substances for public health and aquatic ecosystems. Wastewater treatment plants have been identified as a main pathway through which micropollutants can enter to the aquatic ecosystems. This fact is due to the conventional wastewater treatment plants are not designed to remove recalcitrant contaminants at low concentrations.

Advanced oxidation processes have been proven their efficiency in the degradation of several compounds of emerging concern, such micropollutants. Among these techniques, photo-Fenton process is one of the most effective. However, the requirement to work at acidic conditions to keep the iron in solution is one of the drawbacks of the process. Additionally, the need of irradiation rises the treatment operational costs and environmental impact since some conventional lamps comprises mercury. These inconveniences make the processes unattractive for its full scale-application.

The investigation derived from this thesis is focused on different solutions trying to solve these drawbacks. Firstly, LEDs and solar simulated irradiation were used, carrying out the photo-Fenton process more economically and ecofriendly. The employment of organic fertilizers, as a chelating agents of iron, is the second foundation on which the investigation is based. The final objective is the reuse of wastewater in agriculture, facing the current water scarcity scenario.

The study of the conventional photo-Fenton with UV-A LEDs revealed the suitability of the process to remove a recalcitrant compound (Diphenhydramine, DPH) with high conversion efficiencies (total DPH removal in 30 min). COD and TOC removals were 70.2 and 54.2% for 380-390 nm and 79.9 and 60.5% for 390-400 nm. Additionally, the results suggested that synergies on micropollutant, COD and TOC conversion were observed combining two

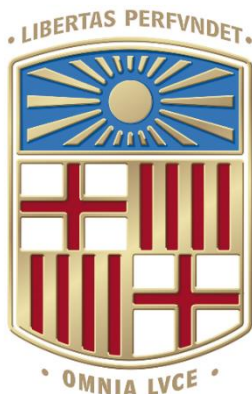
wavelength ranges, because the treatment time was reduced by half (total DPH removal in 15 min, 95.6 and 70.1% of COD and TOC removal, respectively after 1 hour. However, from the results obtained in the comparison between UV-A LEDs in wastewater effluents (52.1% of propranolol (PROP) degradation after 1 hour of treatment in MBR matrix) and BLB lamps (95.3% of PROP abatement after 1 hour of treatment, also in MBR), as a conventional ones, it was evidenced the necessity to optimize the system geometry (photoreactor + lamp) when LEDs are used as irradiation source. This fact is essential in the treatment of wastewater since the turbidity and organic matter present in these matrices influence on the radiation transfer throughout the photoreactor affecting more when LEDs are used, because they are punctual sources of irradiation.

The study in the use of organic fertilizers, as iron chelating agents, revealed that all tested agents (DTPA, HEDTA, EDDS and EDTA, except EDDHA) were effective in photo-Fenton process at circumneutral pH in MBR, CAS and CAS-NE effluents in removing micropollutants. UV-A LEDs and solar simulated light were used to perform the experiments. Propranolol, sulfamethoxazole (SMX) and acetamiprid (ACMP) were used as a model compounds. For instance, PROP degradations higher than 90% were reached in MBR effluent using organic fertilizers and both irradiation sources, UV-A LEDs and solar simulated light at the end of the treatment. The results showed that the efficiency in the degradation is linked to the stability constant of chelates with iron. Low stability corresponds to high reaction rates at initial times but also high iron release. The opposite happens with chelating agents with high stability constant with iron. EDDS and EDTA presented low stability constant, while DTPA and HEDTA have higher ones (in MBR effluent under solar simulated light, using EDTA total removal of PROP and SMX was achieved at 90 and 120 min, respectively and 67.6% of ACMP was observed at 180 min while using DTPA 89.0, 67.6 and 31.0% was reached for PROP, SMX and ACMP, respectively at 180 min). Nevertheless, the iron in solution at 180 min was 52 and 77% for EDTA and DTPA, respectively. The enhancement in removal kinetics and the decrease in iron release was achieved combining organic fertilizers with different stability constant (50%EDDS+50%EDTA, 50%EDDS+50%DTPA, 50%EDTA+50%DTPA). For instance, in MBR matrix, with the mixture 50%EDDS+50%EDTA, total PROP removal was reached 1 hour before compared to only EDTA, which presented better removal than EDDS (total PROP and SMX removal was achieved at 30 min and 90 min, respectively, and 70.0% of ACMP was observed at 180 min). In addition, the total iron in solution at the end of the

treatment was 5.5 times higher with the mixture than EDDS. The organic fertilizers mixtures were also tested in two different wastewater effluents to study the effect of the matrix on iron release. It was observed that, in wastewater with higher turbidity, alkalinity and organic matter, the iron precipitation was higher, decreasing the efficiency of the process overall in EDDS, which have the lowest stability constant with iron. Experiments performed with EDDS in CAS effluent achieved 46.8, 30.0 and 10.5% at 180 min for PROP, SMX and ACMP, respectively. While the performances of the same experiments in MBR matrix were better (94.8, 79.9 and 38.5% for PROP, SMX and ACMP, respectively). The experiments carried out in CAS matrix using DTPA the differences between two matrices were low (60.5, 38.0 and 18.3% for PROP, SMX and ACMP, respectively). Differently than MBR, in CAS effluent, the complexes of iron more stables such as DTPA, achieved better final micropollutant's degradations than iron chelates low stables like EDDS. The additional tests of BOD₅ and phytotoxicity analysis confirmed the suitability of final MBR effluent to be reused in agriculture.

Finally, the mechanisms involved in photo-Fenton process, with iron chelates in aquatic environment, cannot be generalized, since each iron complex have its stability constant with iron and its specific absorbance in solar spectrum. The irradiation experiments without H₂O₂ revealed that only EDDS and DTPA were capable to generate ROS. From the photo-Fenton experiments without O₂, it was determined that this specie is involved in the formation of final hydroxyl radicals. Finally, tests with dosing of non-chelated iron revealed that reaction with iron chelates are the main via to hydroxyl radical generation.

Thesis directors' report and list of publications



Dr. Jaume Giménez Farreras i Dr. Santiago Esplugas Vidal

Departament d'Enginyeria Química i Química Analítica

Facultat de Química

Universitat de Barcelona

Martí i Franquès 1, 6a planta

08028 Barcelona, España

Tel.: +34 934021293 (J.G.) | +34934021290 (S.E.)

e-mails.: j.gimenez.fa@ub.edu | santi.esplugas@ub.edu

Drs. JAUME GIMÉNEZ FARRERAS and SANTIAGO ESPLUGAS VIDAL, both professors at the Department of Chemical Engineering and Analytical Chemistry of the University of Barcelona and PhD thesis directors of Mrs. Núria López Vinent, issue the following report related with the participation of the PhD candidate in the publications derived from his predoctoral research and included in this dissertation:

The experimental work of the publications included in this thesis were entirely developed in the Department of Chemical Engineering of the University of Barcelona by Núria López Vinent, under the supervision of her PhD directors. These publications were not presented in other doctoral theses and are detailed below:

- I. N. López-Vinent, A. Cruz-Alcalde, L.E. Romero, M.E. Chávez, P. Marco, J. Giménez, S. Esplugas, Synergies, radiation and kinetics in photo-Fenton process with UVA-LEDs, *Journal of Hazardous Materials* 380 (2019) 120882. DOI: 10.1016/j.jhazmat.2019.120882.

-
- II. N. López-Vinent, A. Cruz-Alcalde, C. Gutiérrez, P. Marco, J. Giménez, S. Esplugas, Micropollutant removal in real WW by photo-Fenton (circumneutral and acid pH) with BLB and LED lamps, *Chemical Engineering Journal* 379 (2020) 122416. DOI: 10.1016/j.cej.2019.122416.
- III. N. López-Vinent, A. Cruz-Alcalde, J.A. Malvestiti, P. Marco, J. Giménez, S. Esplugas, Organic fertilizer as a chelating agent in photo-Fenton at neutral pH with LEDs for agricultural wastewater reuse: Micropollutant abatement and bacterial inactivation, *Chemical Engineering Journal* 388 (2020) 124246. DOI: 10.1016/j.cej.2020.124246.
- IV. N. López-Vinent, A. Cruz-Alcalde, J. Giménez, S. Esplugas, C. Sans, Improvement of the photo-Fenton process at natural condition of pH using organic fertilizers mixtures: potential application to agricultural reuse of wastewater, *Applied Catalysis B: Environmental*, 290 (2021) 120066. DOI: 10.1016/j.apcatb.2021.120066.
- V. N. López-Vinent, A. Cruz-Alcalde, J. Giménez, S. Esplugas, Mixtures of chelating agents to enhance photo-Fenton process at natural pH: influence of wastewater matrix on micropollutant removal and bacterial inactivation, *Science of the Total Environment*, 786 (2021) 147416. DOI: 10.1016/j.scitotenv.2021.147416
- VI. N. López-Vinent, A. Cruz-Alcalde, C. Lai, J. Giménez, S. Esplugas, C. Sans, Role of sunlight and oxygen on the performance of photo-Fenton process at near neutral pH using organic fertilizers as an iron chelates, submitted to *Journal of Hazardous Materials*.

Additionally, relevant information of the journals [categories, impact factor (IF) and quartile (Q)] in which the author of this thesis published or submitted the research studies is displayed further down (data from *Journal Citation Reports*[®], 2019):

- Applied Catalysis B: Environmental (IF: 16.683)

Category Name	Quartile in Category
Environmental Science	Q1

- Chemical Engineering Journal (IF: 10.652)

Category Name	Quartile in Category
Chemical Engineering	Q1
Environmental Chemistry	Q1

- Journal of Hazardous Materials (IF: 9.038)

Category Name	Quartile in Category
Environmental Engineering	Q1
Environmental Chemistry	Q1

- Science of the Total Environment (IF: 6.551)

Category Name	Quartile in Category
Environmental Science	Q1

Dr. Jaume Giménez Farreras

and

Dr. Santiago Esplugas Vidal

Barcelona, 11th May 2021

Nomenclature

The used abbreviations, acronyms and symbols are gathered below:

ACMP	Acetamiprid
ACN	Acetonitrile
AOP	Advanced Oxidation Process
AOS	Average Oxidation State
BB	Building Blocks
BLB	Black-light Blue lamp
BOD	Biochemical Oxygen Demand
BP	Biopolymers
CAS	Conventional Activated Sludge
CAS-NE	Conventional Activated Sludge with nitrogen and phosphorous elimination
CEC	Contaminant of Emerging Concern
CFU	Colony-forming-units
COD	Chemical Oxygen Demand, mg O ₂ L ⁻¹
DAD	Diode Array Detector
DBP	Disinfection-by-product
DF	Design flow
DOC	Dissolved Organic Carbon, mg C L ⁻¹
DPH	Diphenhydramine hydrochloride
DTPA	Diethylenetriaminepentaacetic acid
EC ₅₀	Sample dilution causing a 50% of the bioluminescent emission reduction after 15 min of contact.
EDDHA	Ethylenediamine- <i>N,N'</i> -bis((2-hydroxyphenyl)acetic acid)
EDDS-Na ₃	Ethylenediamine- <i>N,N'</i> -disuccinic acid trisodium salt
EDTA	Ethylenediaminetetraacetic acid
EfOM	Effluent Organic Matter
EQS	Environmental Quality Standard, µg L ⁻¹

EU WFD	European Union Water Framework Directive (Directive 2000/60/EC)
GI	Germination index
HEDTA	N-(2-Hydroxyethyl)ethylenediaminetriacetic acid
HO [•]	Hydroxyl radical
H ₂ O ₂	Hydrogen peroxide
HS	Humic Substances
HPLC	High-Performance Liquid Chromatography
IFAS	Integrated fixed-film activated sludge
<i>k</i>	Rate constant of reaction, s ⁻¹ , kJ ⁻¹ (pseudo-first order)
<i>k_i</i> ·OH	Rate constant of hydroxyl radical reaction with a compound <i>i</i> , M ⁻¹ s ⁻¹
<i>K_{ow}</i>	Octanol-water partition coefficient, dimensionless
<i>K_{stab}</i>	Stability constant of chelating agent with iron, dimensionless
LC ₅₀	Concentration of a substance required to kill 50% of the population
LED	Light emitting diode
LMCT	Ligand-metal-charge transfer
LMWA	Low Molecular Weight Acids
LMWN	Low Molecular Weight Neutrals and Amphiphilics
MBR	Membrane Bioreactor
MP	Micropollutant
MS	Mass Spectrometry
NOM	Natural Organic Matter
NTA	Nitrilotriacetic acid
OND	Organic Nitrogen Detection
PE	Population equivalent
PHS	Priority Hazardous Substances
PNEC	Predicted no-effect concentration
POP	Persistent Organic Pollutant
PROP	Propranolol hydrochloride
PS	Priority Substance
PTFE	Polytetrafluoroethylene

PVDF	Polyvinylidene fluoride
Q_{acc}	Accumulated energy per volume, kJ L^{-1}
RG	Root growth, %
RQ	Risk quotient
SEC-OCD	Size-Exclusion Chromatography with Organic Carbon Detection
SG	Seed germination, %
SMX	Sulfamethoxazole
SW	Surface water
tBuOH	<i>tert</i> -butyl alcohol
TOC	Total Organic Carbon, mg C L^{-1}
TP	Transformation product
TSS	Total Suspended Solids
US	Ultrasound
UV	Ultraviolet
UV_{254}	Ultraviolet absorbance at 254 nm, m^{-1}
WW	Wastewater
WWTP	Wastewater Treatment Plant

1 Introduction

1.1 State of the world's water resources

1.1.1 Water demand and availability

Water is an essential resource for the development of life. Water covers 70% of our planet. However, the percentage corresponding to fresh water is only 3% and two-thirds of that belongs to frozen glaciers or in another way unavailable for our use [1]. It is estimated that since 1980s water use has been rising around the world by about 1% per year [2]. The combination of population growth, socio-economic development and evolving consumption patterns are the principal causes in the surging water demand [3]. The low water availability along with increasing water demand has provoked worldwide water stress.

There are different ways to measure water stress and water scarcity. However, as the world freshwater resources are continuously renewed by water cycle, the common indicator of water scarcity is per capita renewable water per year in cubic meters (Figure 1).

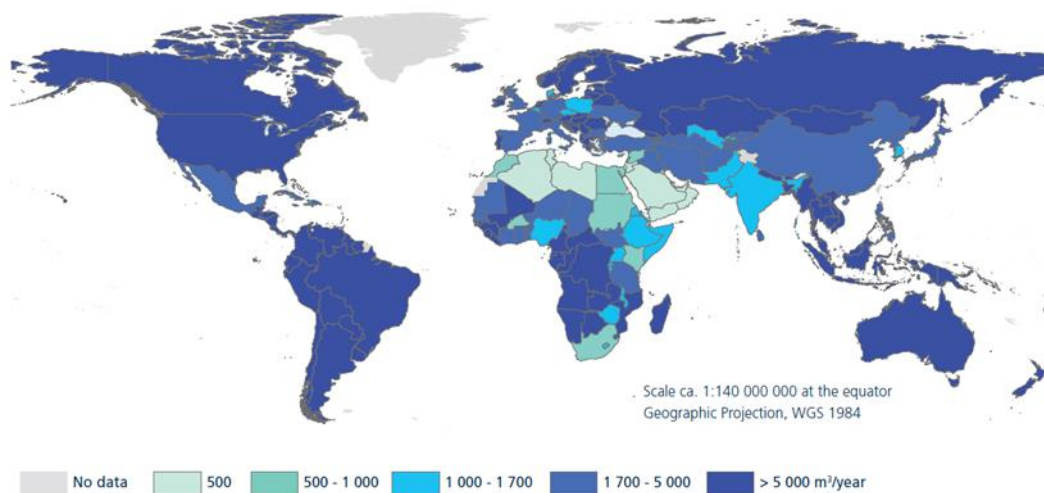


Figure 1. Total renewable water resources per capita per year (in cubic meters), 2014 [3].

An area is experiencing regular water stress when annual water supplies is between 1000 and 1700 m³ per capita. Populations face chronic water scarcity when water supplies are between 500 and 1000 m³ per capita per year. When an indicator is below 500 m³ per capita per year the populations are in absolute scarcity [3]. Currently, over 2000 million people live in countries experiencing high water stress. By 2030, with the Climate Change scenario, it

is estimated that almost half of the world's population will be living in a high water stress areas [4]. Throughout the 2010s, it has been estimated that about 4000 million people face water scarcity during at least one month of the year and 1900 million people has experienced severe water scarcity [5]. Estimations by 2050 point out that about 4800 and 5700 million people will suffer water scarcity at least one month of the year [6].

According to the projections presented by United Nations, the world population will keep increasing from 7700 million to between 9400 and 10200 million in 2050 [6]. Consequently, global water demand is expected to increase in 20 to 30% above the current water demand until 2050, mainly linked to the domestic uses, manufacturing and electricity generation. (Figure 2).

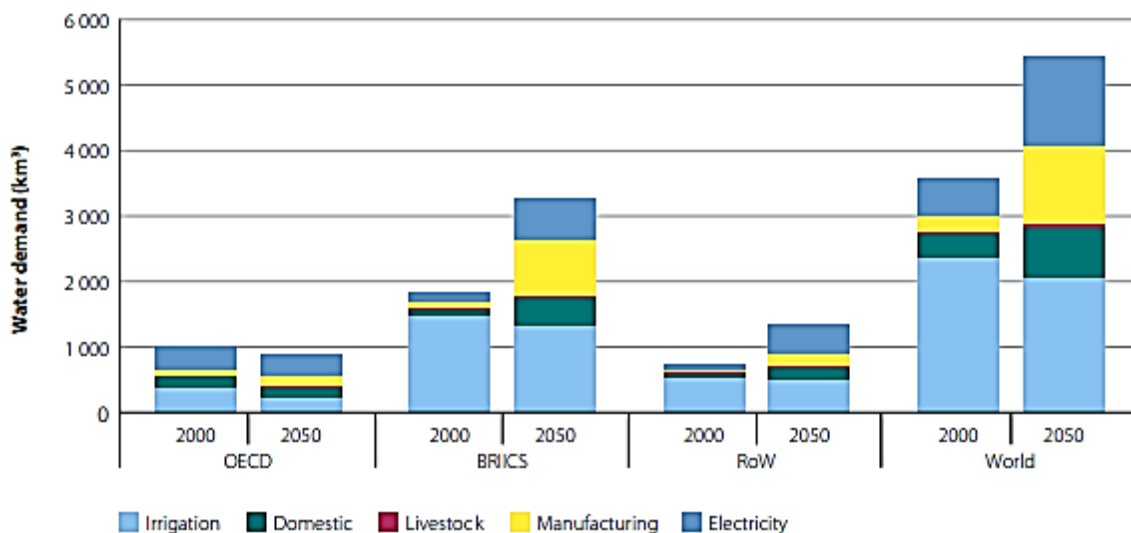


Figure 2. Predictions by 2050 of global water withdrawals based on data of 2000. The projections are divided by sector and for different groups of regions in the world, where OECD is the Organization for Economic Co-operation and Development; BRICS corresponds to Brazil, Russia, India, Indonesia, China, South Africa and RoW is the rest of world [7].

Although a decrease of water demand in agriculture is predicted by 2050, this sector is by the far the largest freshwater consumer. Water destined to agriculture is around 70% of the total freshwater demand and this percentage accounts for 90% in some developing countries. Thus, the agriculture has an important role to play on the path to sustainability.

As a consequence of the continuous growth in water demand joined to Climate Change - which directly influence on the water cycle- the water scarcity is the main problem to be faced by the World in the 21st century. Figure 3 illustrates the global distribution of physical

and economic water scarcity by 2025. Physical water scarcity is caused when there is not enough water to supply all demands. While economic water scarcity occurs when there is lack of investment in water or absence of human capacity to satisfy the water requirements.

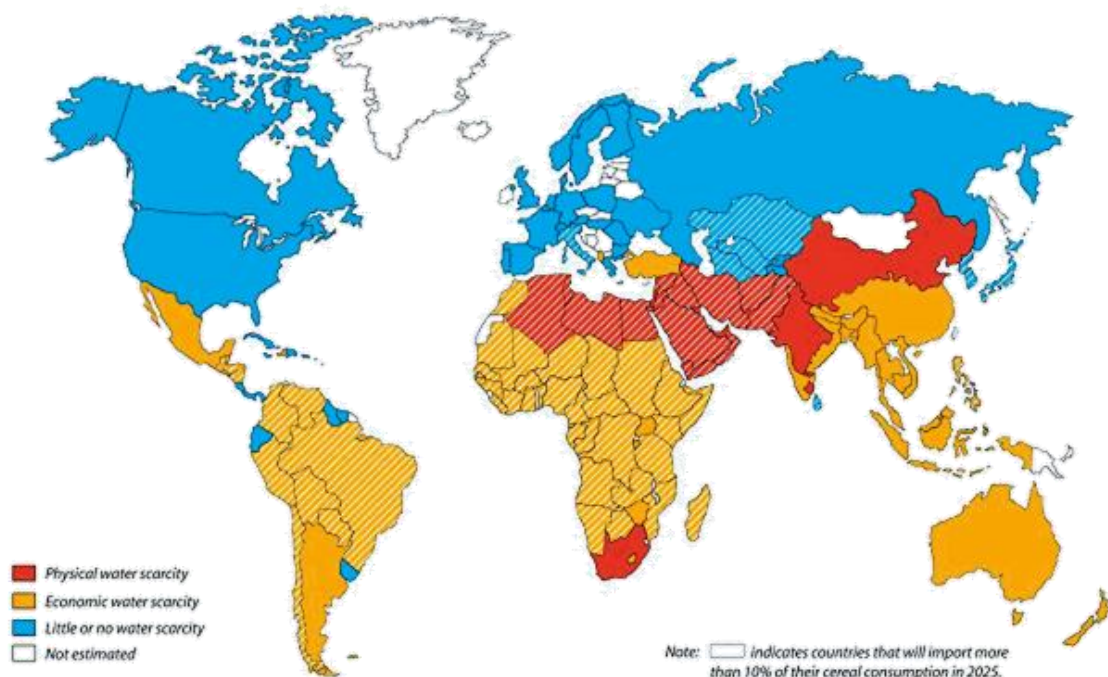


Figure 3. Projected physical and economic water scarcity by 2025 in the world. Note that grated countries indicate countries that will import more than 10% of their cereal consumption in 2025 [8].

In front of this critical scenario feasible solutions are required to face the water scarcity. The reuse of wastewater (WW) could be a partial solution to reduce the freshwater demand. However, as observed in Figure 3, investment in water infrastructures and human capacities are also required to decrease the economic water scarcity.

1.1.2 Wastewater treatment and reuse

The continuous rise in freshwater demand is associated with increased generation of wastewater. Untreated domestic wastewater contains nutrients, organics and pathogens while industrial wastewater may incorporate hazardous substances like metals, organic compounds and other pollutants. The release of these untreated wastewater to the environment poses risk to public health, food security and ecosystem services and functions. Globally, it is estimated that 80% of the untreated industrial and municipal wastewater are released to the environment causing water pollution [6, 9]. However, high differences are

observed between countries. On average, 27% of the total wastewater is not treated in high-income countries. However, the percentage increases in upper-middle-income countries and low-middle-income countries which present value of 66 and 72%, respectively [6, 9]. Additionally, the secondary effluents from conventional wastewater treatment plant (WWTP) cannot be reused directly since various organics and inorganics pollutants are not removed. This fact limits opportunities for secure and productive use and reuse of water sources to increase freshwater provisions, particularly in front of water scarcity scenario. The reuse of wastewater is an unconventional water resource for several uses, provided that it is treated and/or used safely. The potential reuse of wastewaters coming from different human activities for a secondary use, such as agriculture, decreases pressures in freshwater demand and alleviates water shortages. Figure 4 illustrates the contribution of agriculture sector to water stress, which is defined as the ratio between freshwater demand by agriculture and total renewable freshwater resources. As the freshwater demand for agriculture is about 70% of the total (Figure 2), reuse of wastewater for agricultural purposes would play an important role to face the water stress.

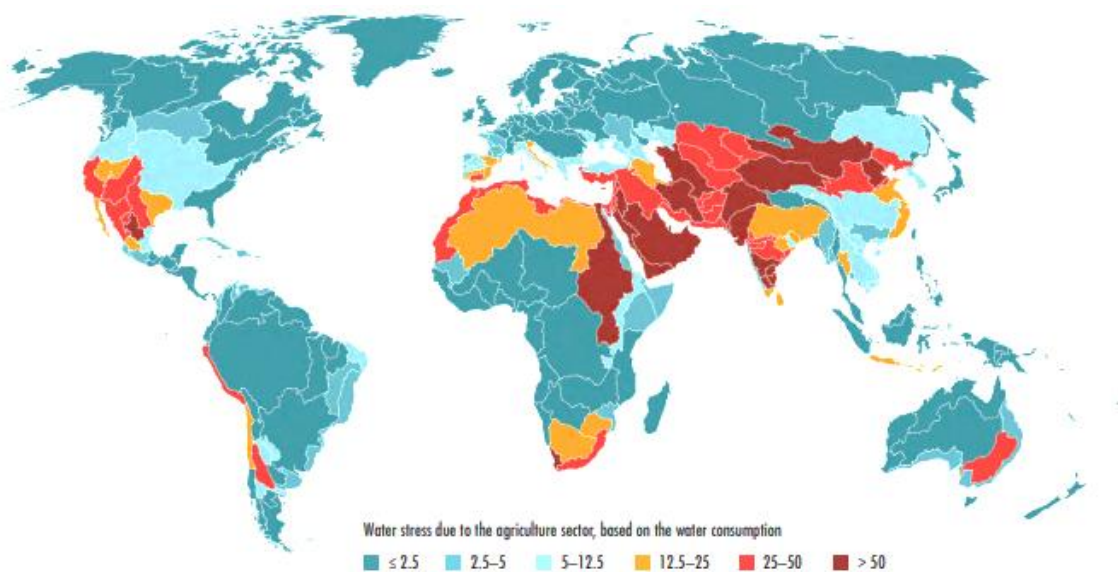


Figure 4. Contribution of the agriculture sector to the level of water stress referred to 2015, expressed in percentage. Percentages equal or below 12.5 not present water stress, medium when it ranges from 12.5 to 25 percent and high for 25 and 50 percent and very high when the percentage is higher than 50 [9].

In 2019, globally, 7.5 million m³ day⁻¹ of new water reuse capacity were forecast [9]. However, this amount only represents less than 1% of the global water use. By, 2030 it is prognosticated that this percentage will increase until to 1.66% [10].

Despite the current efforts and multiple benefits, the potential of water reuse is still highly under-explored and under-exploited [11]. Although knowledge and technologies for the development of water reuse are emerging together with an increasing number of applications, there are different impediments to exploiting their full potential. Financial, technological and policy barriers are the mainly obstacles in their development. The cost associated to development of new technologies to treat wastewater according to the end users need is a critical barrier, since withdrawing freshwater results more economically and attractive. Another obstacle is the human perception. In some countries, reusing wastewater in different sectors, overall, in agriculture, is still not culturally acceptable. Moreover, the uncertainty that this practice may cause more human and environmental risks than benefits increase the barrier. Evaluation of water quality, potential environmental and human impacts and regulatory issues are required to promote the best practices and implementation. This fact is partly due to the lack of information to society and insufficient regulations. Currently, the policies for reclaimed water are strongly fragmented and, in many countries, incomplete. The necessity of developing an appropriate legislation, regulations and planning framework for governments is essential to adopt reused wastewater as a future supply of water.

1.2 Micropollutants in water resources

The growing and widespread use of uncountable number of organic chemicals, over the last decade, generates a stream of substances, which almost immediately occur in aquatic environment, including freshwater resources [12]. Hundreds of thousands of tons of these compounds are dispensed and consumed annually worldwide [13, 14]. Many of these compounds released into the aquatic environment can cause hazardous effects on human health and ecosystems, including carcinogenicity, genotoxicity, endocrine disruption, and problems in fetal development [15, 16]. These substances can enter in the water systems from different pathways. However, the effluents from WWTPs have been identified as a major point source pollution [17, 18]. They are usually present at low concentrations in the environment (ng L⁻¹ to µg L⁻¹), reason why they are called micropollutants (MPs) [19]. The labelling contaminants of emerging concern (CECs) is also used to describe these substances, since they are a group of emerging compounds that are increasingly of concern

because of their adverse effects [12]. These include: i) substances that have been recently characterized as contaminants regarding their new toxicological data, ii) newly developed compounds that have recently entered to the environment and iii) substances that have been identified because of the development of novel or more sensitive analytical methods [20]. Pharmaceuticals, personal care products, steroid hormones, surfactants, industrial chemicals and pesticides are the principal groups [21]. Table 1 summarizes the main sources of major categories of micropollutants in aquatic environments [21].

Table 1. Principal sources of major categories of micropollutants in environment [21].

Group	Main subclasses	Main sources	
		Distinct	Nonexclusive
Pharmaceuticals	Non-steroidal Anti-inflammatory Drugs (NSAIDs), lipid regulator, anticonvulsants, antibiotics, β -blockers and stimulants	Domestic wastewater (from excretion)	
		Hospital effluents Run-off from Concentrated Animal Feeding Operations (CAFOs) and aquaculture	
Personal care products	Fragrances, disinfectants, UV filters and insect repellents	Domestic wastewater (from bathing, shaving, spraying, swimming, etc.)	Sources that are not exclusive to individual categories include: Industrial wastewater (from product manufacturing discharges) and landfill leachate (from improper disposal of used, defective or expired items)
Steroid hormones	Estrogens	Domestic wastewater (from excretion)	
		Run-off from CAFOs and aquaculture	
Surfactants	Non-ionic surfactants	Domestic wastewater (from bathing, laundry, dishwashing, etc.)	
		Industrial wastewater (from industrial cleaning discharges)	
Industrial chemicals	Plasticizers and flame retardants	Domestic wastewater (by leaching out of the material)	
Pesticides	Insecticides, herbicides and fungicides	Domestic wastewater (from improper cleaning, run-off from gardens, lawns and roadways, etc.)	
		Agricultural runoff	

The presence of micropollutants in the aquatic environment is also associated to their physico-chemical properties, which, in general, make them resistant to natural degradation processes occurring in the environment [22]. Additionally, conventional WWTPs are not

designed to eliminate these compounds. They commonly consist on a primary (physicochemical) and secondary (biological) treatments, which are not effective in removing MPs due to their trace concentrations and their biological resistance [18]. Figure 5 illustrates the occurrence of different MPs categories in wastewater influent and effluent [12].

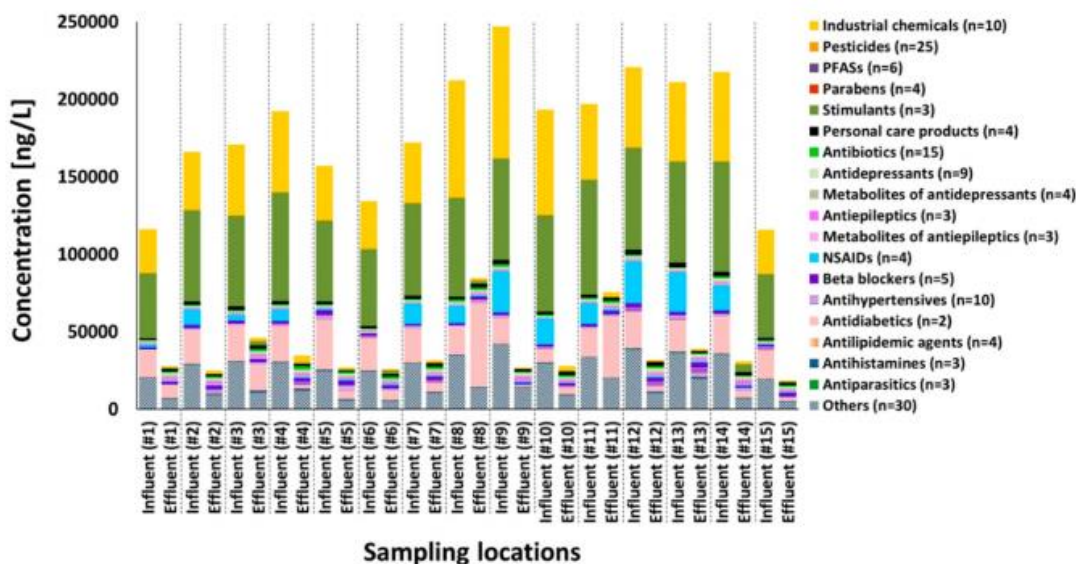


Figure 5. Concentrations (ng L^{-1}) of different micropollutants categories in influents and effluents of 15 WWTPs in Sweden [12].

The occurrence of MPs in aquatic environments even at trace concentrations poses risk human health and environment. Thus, specific treatments to remove micropollutants are required in WWTPs, especially when wastewater reuse is implemented. Advanced oxidation processes (AOPs), as a tertiary treatment, could be a feasible option in removing MPs. However, the first step is the development of legal regulations covering the limits of MPs and their metabolites in the field of water quality. Additionally, more investigations on removal technologies and toxicity are required. Currently, only a few number of compounds are regulated [23], which delays the process of implementing new treatments.

1.2.1 Diphenhydramine hydrochloride

Diphenhydramine hydrochloride (DPH) is a first generation of histamine antagonist mainly used as anti-allergic activity. It can also be used for nausea, symptoms of the common cold, tremor in Parkinson and insomnia. DPH blocks H1 receptors preventing certain effects of histamine [24]. The solubility of DPH in water is 100 mg mL^{-1} and it is moderately

hydrophobic (octanol-water partition coefficient, $\log K_{ow}=3.27$). DPH has been detected in a multiple aquatic environments and diverse studies have been reported its identification in effluents of WWTPs [25-27]. Deo's study reported the maximum detected concentrations of pharmaceuticals in surface water (SW) of the USA, and DPH was found at 1410.6 ng L^{-1} [28]. Additionally, in the same study risk quotient (RQ), related to the impact in aquatic environment, was also calculated. RQ is the ratio between maximum concentration found in SW and predicted no-effect concentration (PNEC). Pharmaceuticals were divided in three categories: high risk ($\text{RQ} \geq 1.0$), medium risk ($1.0 > \text{RQ} \geq 0.1$) and low risk ($\text{RQ} < 0.1$). For DPH, RQ was 0.39, being a medium risk quotient [28]. The acute toxicity was evaluated by Berninger and colleagues concluding that *Daphnia magna* was more sensitive ($\text{EC}_{50} = 0.374 \text{ mg L}^{-1}$) than *Pimephales promelas* (fish) ($\text{LC}_{50} = 2.09 \text{ mg L}^{-1}$) [29].

1.2.2 Propranolol hydrochloride

Propranolol hydrochloride (PROP) is a pharmaceutical belonging to beta-blockers group. It is mainly used to treat high blood pressure. It can also be used to attenuate physical manifestations of anxiety -such as tremors, rapid heartbeat, palpitations among others- and to prevent migraine headaches and chest pain. PROP acts blocking the action of beta-adrenergic receptors inhibiting the beta-adrenergic reactions which affect the heart and blood vessels [30]. PROP is soluble in water (79.4 mg mL^{-1}) and it is moderately hydrophobic ($\log K_{ow}=2.58$). PROP has been detected in effluents of WWTPs [12, 26]. In surface water was detected at 53 ng L^{-1} [31]. Its calculated RQ was very low (<0.01) [28]. However, it was reported that PROP is one of the most toxic antihypertensive drugs for invertebrates. The reported value of acute toxicity (48h- EC_{50}) for *Daphnia Magna* was 7.5 mg L^{-1} [32]. While for *Pimephales promelas* (fish), it was reported a LC_{50} value of 1.21 mg L^{-1} [33].

1.2.3 Sulfamethoxazole

Sulfamethoxazole (SMX) is a sulfonamide antibiotic widely used for humans and animals. It is mainly used to treat acute urinary tract infections. SMX is also employed against gonorrhea, meningitis and serious respiratory tract infections [34]. SMX inhibits bacterial enzyme dihydropteroate and consequently the generation of folic acid in bacteria, required for the production of nucleic acids [35, 36]. SMX is slight soluble in water (0.5 mg mL^{-1}) and hydrophilic ($\log K_{ow}=0.27$). It is the antibiotic most frequently detected in aquatic environments and its presence was reported in many effluents of WWTPs worldwide [12,

18, 20, 21, 25, 26, 37, 38]. In surface water, it was detected at 1900 ng L⁻¹ [39] and its calculated RQ was medium, obtaining a value of 0.30 [28]. The acute toxicity (24h-EC₅₀) is 25.2 mg L⁻¹ for *Daphnia Magna* [40] and the value of 48h-LC₅₀ for *Oryzias latipes* (fish) is higher than 750 mg L⁻¹ [41].

1.2.4 Acetamiprid

Acetamiprid (ACMP) is a neonicotinoid insecticide currently commercialized [42]. ACMP is slight soluble in water (4.3 mg mL⁻¹) and hydrophobic (log K_{ow} =0.8). It acts by contact and ingestion, affecting the central nervous system of insects, causing consequently paralysis and death. Because of it, ACMP is systematic for the control of insects and affects them more than other organisms [42, 43]. However, negative effects have been reported on human health due to the chronic exposure to this compound [44-46]. Some studies also reported the negative consequences of ACMP on aquatic species [47, 48] and other organisms, like honeybees [49, 50]. Although its use has not been restricted, recently ACMP has been included as one of the neonicotinoids under vigilance in Europe by the Decision 2018/840/EU [51]. ACMP has been detected in different water systems worldwide, including some in Europe, presenting concentrations up to 380 ng L⁻¹ [52-58].

1.3 General legal framework of water

1.3.1 European regulations on micropollutants in water resources

The concern about the potential risks of MPs for human health and aquatic ecosystems has led to European regulatory administration take on efforts for the development of water quality polices. Although there are no legal discharge limits for MPs some regulations have been published over the last two decades. The first mark in the European water policy was implemented in the year 2000 (Directive 2000/60/EC) –labeled European Union Water Framework Directive (EU WFD)–. The objective of this directive was to establish a list of substances or group of substances to be prioritized due to the potential risks that can cause in the aquatic environment [59]. Additionally, European Environmental Quality Standards (EQSs) were also defined in this directive, referring to the maximum concentration of substance, or group of substances, in aquatic systems.

A year later, in 2001, it was published the Decision 2455/2001/EC which approved the first list of 33 priority substances (PSs) to be supervised at EU level and amending Directive

2000/60/EC. This list was based on the volume of production and use, the potential environmental risks and occurrence of these substances on environment [60]. This same year took place the Stockholm Convention on Persistent Organic Pollutants (POPs), [61] with the objective to eliminate or restrict the production and use of some classified substances in order to protect the human health and environment from POPs. Diverse substances designated as Priority Hazardous Substances (PHSs), and listed in the Decision 2455/2001/EC, were included in this list. In 2004 the information relating to the Stockholm Convention was ratified by the Regulation 2004/850/EC [62].

The Decision 2455/2001/EC was amended by Directive 2008/105/EC. In this directive the EQSs values for 33 PSs and 8 additional contaminants were published [63]. From this information, EU countries can supervise these pollutants in aquatic systems and compare the data obtained with EQS values to determine the quality of aquatic ecosystems and adopt measures, if necessary.

Five years later, in 2013, it was published the Directive 2013/39/EU [64] amending the Directives 2000/60/EC and 2008/105/EC. In this case the PSs were extended to 45 (including 4 metals: cadmium, lead, mercury and nickel) (Table 2). In this directive EQSs more restrictive were established for PSs and it was indicated the necessity to develop new technologies for water treatment effective in removing these compounds.

Table 2. List of the priority substances in the field of water policy according to Directive 2013/39/EU [64]. Substances marked with an asterisk (*) indicates that only some substances of the groups are classified as PHS.

	Name of the PS	CAS number	Class	Identified as PHS
1	Alachlor	15972-60-8	Pesticides	
2	Anthracene	120-12-7	-	Yes
3	Atrazine	1912-24-9	Pesticides	
4	Benzene	71-43-2	Industrial compound	
5	Brominated diphenylethers	-	Industrial compound	Yes (*)
6	Cadmium and its compounds	7440-43-9	-	Yes
7	Chloroalkanes, C ₁₀₋₁₃	85535-84-8	Industrial compounds	Yes
8	Chlorfenvinphos	470-90-6	Pesticides	
9	Chlorpyrifos	2921-88-2	Pesticides	
10	1,2-dichloroethane	107-06-2	Industrial compounds	
11	Dichloromethane	75-09-2	Industrial compounds	

Table 2. (continued)

	Name of the PS	CAS number	Class	Identified as PHS
12	Di (2-ethylhexyl) phthalate (DEHP)	117-81-7	Industrial compounds	Yes
13	Diuron	330-54-1	Pesticides	
14	Endosulfan	115-29-7	Pesticides	Yes
15	Fluoanthene	206-44-0	-	
16	Hexachlorobenzene	118-74-1	Pesticides	Yes
17	Hexachlorobutadiene	87-68-3	Pesticides	Yes
18	Hexachlorocyclohexane	608-73-1	Pesticides	Yes
19	Isoproturon	34123-59-6	Pesticides	
20	Lead and its compounds	7439-92-1	-	
21	Mercury and its compounds	7439-97-6	-	Yes
22	Naphtalene	91-20-3	-	
23	Nickel and its compounds	7440-02-0	-	
24	Nonylphenols	-	Industrial compounds	Yes (*)
25	Octylphenols	-	Industrial compounds	
26	Pentachlorobenzene	608-93-5	Industrial compounds	Yes
27	Pentachlorophenol	87-86-5	Pesticides	
28	Polyaromatic hydrocarbons (PAH)	-	-	Yes
29	Simazine	122-34-9	Pesticides	
30	Tributyltin compounds	-	Pesticides	Yes (*)
31	Trichlorobenzenes	12002-48-1	Industrial compounds	
32	Trichloromethane (chloroform)	67-66-3	Industrial compounds	
33	Trifluralin	1582-09-8	Pesticides	Yes
34	Dicofol	115-32-2	Pesticides	Yes
35	Perfluorooctane sulfonic acid and its derivatives (PFOS)	1763-23-1	Industrial compounds	Yes
36	Quinoxifen	124495-18-7	Pesticides	Yes
37	Dioxins and dioxin-like compounds	-	-	Yes (*)
38	Aclonifen	74070-46-5	Pesticides	
39	Bifenox	42576-02-3	Pesticides	
40	Cybutryne	28159-98-0	Pesticides	

Table 2. (continued)

	Name of the PS	CAS number	Class	Identified as PHS
41	Cypermethrin	52315-07-8	Pesticides	
42	Dichlorvos	62-73-7	Pesticides	
43	Hexabromocyclododecanes (HBCDD)	-	Industrial compound	Yes (*)
44	Heptachlor and heptachlor epoxide	76-44-8/ 1024-57-3	Pesticides	Yes
45	Terbutryn	886-50-0	Pesticides	

Additionally, in the Directive 2013/39/EU was established a first watch list of substances for Union-wide monitoring in the field of water policy. The list was published two years later in the Decision 2015/495/EU [65]. This watch list was created with the aim to set monitoring programs on compounds of emerging concern to collect some relevant as the basis for future prioritization exercises. The watch list was repealed three years later by Decision 2018/840/EU updating the first watch list from the data accumulated by the monitoring of substances in the period between 2015 and 2017 (Table 3) [51].

Table 3. Watch list of substances for Union-wide to be supervised in the field of water policy, according to Decision 2018/840/EU [51].

	Name of the substance	CAS number	Class
1	17- α -ethinylestradiol (EE2)	57-63-6	
2	17- β -estradiol (E2)	50-28-2	Steroid hormones
3	Estrone (E1)	53-16-7	
4	Erythromycin	114-07-8	
5	Clarithromycin	81103-11-9	
6	Azithromycin	83905-01-5	Pharmaceuticals
7	Amoxicillin	26787-78-0	
8	Ciprofloxacin	85721-33-1	
9	Methiocarb	2032-65-7	
10	Imidacloprid	105827-78-9/ 138261-41-3	
11	Thiacloprid	111988-49-9	
12	Thiametoxam	153719-23-4	Pesticides
13	Clothianidin	210880-92-5	
14	Acetamiprid	135410-20-7	
15	Metaflumizone	139967-49-3	

It is important to mention that 23 substances/group of substances out of 45 from Table 2 and 7 out of 15 substances from Table 3 are pesticides, representing 50% of the total compounds of emerging concern in Europe. This fact is not coincidence given the nature of these compounds. In addition, pesticides are a key point for water reuse.

1.3.2 Reclaimed wastewaters quality policies

Although efforts have been made to address water scarcity by seeking alternatives such as wastewater reuse, the European Union did not publish any regulation or guidelines until the mid-2010s. In 2016, the European Commission launched the ‘Guidelines on Integrating Water Reuse into Water Planning and Management in the context of WFD’, complementing the European Union Water Framework Directive. This document included regulations on minimum quality requirements in the field of water reuse for agriculture and aquifer recharge [66]. A year later, in 2017, the Joint Research Center (JRC) of the European Commission published a report titled ‘Minimum quality requirements for water reuse in agricultural irrigation and aquifer recharge’ with the intention of laying the basis of the future EU reclaimed policy [67]. Two years after the first mark in the European wastewater reuse guidelines, in 2018, the European Union published a Proposal on minimum requirements for water reuse in agriculture (Proposal 2018/0169 (COD)) [68]. Finally, 25 May 2020 this proposal was amended by regulation (Regulation 2020/741/EU) [69]. This regulation establishes four reclaimed water quality classes (A-D) and the permitted uses as well as irrigation methods for each class (Table 4). Additionally, for each class it fixes the minimum requirements considering microbiological (*E.coli*, *Legionella spp.* and Intestinal nematodes) and physico-chemical parameters (Biological Oxygen Demand at 5 days (BOD₅), Total Suspended Solids (TSS) and turbidity) (Table 5). Minimum frequencies for routine monitoring of reclaimed water and their validation were also included.

Table 4. Reclaimed water quality classes, permitted agricultural use and irrigation method [69].

Reclaimed water quality class	Crop category	Irrigation method
A	Food crops, including root crops consumed raw and food crops where the edible part is in direct contact with reclaimed water	All

Table 4. (continued)

Reclaimed water quality class	Crop category	Irrigation method
B	Food crops consumed raw where the edible part is produced above ground and is not in direct contact with reclaimed water, processed food crops and non-food crops including crops to feed milk- or meat-producing animals	All
C		Drip *
D	Industrial, energy, and seeded crops	All

Table 5. Minimum requirements for different reclaimed water qualities in the field of agricultural irrigation [69]. (*) Where there is a risk of aerosolization. (†) For irrigation of pastures or forage. CFU: colony-forming-units.

Reclaimed water quality class	<i>E.coli</i> (CFU 100 mL ⁻¹)	BOD ₅ (mg L ⁻¹)	TSS (mg L ⁻¹)	Turbidity (NTU)	Other
A	≤ 10	≤ 10	≤ 10	≤ 5	<i>Legionella spp.</i> :
B	≤ 100	In accordance with		-	< 1000 CFU L ⁻¹ *
C	≤ 1000	Directive 91/271/EEC (Annex I, Table I)		-	Intestinal nematodes (helminth eggs): ≤ 1 egg L ⁻¹ †
D	≤ 10000			-	

As a consequence of the lack of European policies in the field of water reuse, some countries like Spain launched its own legislation. In 2007 the Spanish Royal Decree 1620/2007, establishing the legal regime for the reuse of treated water, was published [70]. This legislation fixed different quality criteria for the reuse of water according to their uses (urban, agrarian, industrial, recreational and environmental). Within each use different qualities were set. Maximum allowable values were regulated for intestinal nematodes, *E.coli*, TSS, turbidity and other criteria depending on the use.

Nevertheless, although the increasingly efforts carried out by European Union and some of their countries in the last decade, the legislation on wastewater reuse has some shortcomings with respect to human health and environment protection. The most important gaps are the lack of a list of chemicals and CECs and their potential toxicity. The absence of monitoring of new disinfection-by-products (DBPs) and potential transformation products (TPs) generated during the water treatments. As well as the legislation does not include microbial

regrowth, which is necessary in the field of wastewater reuse. Additionally, other aspects were also missed, such as the monitoring of the potential antibiotic resistance extent in the environment and possible transference to crops, programs to study the potential bioaccumulation of pollutants and information programs for farmers to overcome the preoccupation about the risks associated to use of reclaimed water.

1.4 Advanced Oxidation Processes

The rising concern about the occurrence of micropollutants in water resources, including freshwater, and their potential risks for human health and environment has triggered, some decades ago, the development of new technologies capable to remove MPs. This advancement was also driven due to the knowledge that conventional wastewater treatment plants are the main entry pathway of these pollutants into the environment. These substances which are hardly removed in conventional WWTPs can be degraded implementing a tertiary water treatment technology such as based on advanced oxidation processes. These technologies can alleviate the freshwater withdrawals because of the potential wastewater reuse, which is key parameter in a water scarcity scenario.

1.4.1 Fundamentals

Advanced oxidation processes are a group of oxidative water treatments for toxic effluents at industrial level, hospitals and WWTPs. AOPs were developed as an emerging degradation technology resulting in a total mineralization (conversion to CO_2) of most of the organic contaminants [71]. All these processes are based on the generation and subsequent reaction of hydroxyl radical (HO^\bullet), which is more reactive (and not selective) than other oxidizing species used in wastewater or drinking water treatment [72, 73]. However, additionally to HO^\bullet , other oxidizing species are involved in the degradation and transformation of contaminants. This fact depends on the type of oxidant used and the mechanisms of reactions [74].

The oxidation mechanisms of hydroxyl radical can be summarized throughout three pathways [75, 76].

- **Hydrogen atom abstraction** from organic compound resulting in the formation of water and organic radical (R^\bullet), which in turn can react with molecular oxygen and generate peroxy radical (ROO^\bullet) that undergoes subsequent reactions.



- **Electrophilic addition of HO[•]** to C=C double bond or to an aromatic ring obtaining an organic radical as a product. Double bond is eliminated and HO[•] incorporated into the chain.



- **Electronic transference to HO[•]**. This pathway rarely occurs in the oxidation of organic compounds.



Diverse AOPs classifications can be performed depending on different aspects such as the source of the oxidizing species or the method employed for its production. Table 6 displays one of these divisions [77]

Table 6. Classification of the most common advanced oxidation processes adapted from [77].

Classics	Dark processes	O ₃ in alkaline medium
		O ₃ /H ₂ O ₂
		H ₂ O ₂ /catalyst
		Fenton (Fe ²⁺ /H ₂ O ₂)
		Electrochemical oxidation
	Photoprocesses	UV (ultraviolet) photolysis
		Ozonation (O ₃)/UV
		Hydrogen peroxide (H ₂ O ₂)/UV
		O ₃ /H ₂ O ₂ /UV
		Photo-Fenton (Fe ²⁺ /H ₂ O ₂ /UV)
Hot	Photocatalysis	
	Non thermal plasma	
	Wet oxidation	
	Supercritical wet oxidation	
	Electron beam	
	Ultrasounds	

Table 6. (continued)

Hot	Vacuum UV Hydarulic cavitation and sonolysis
------------	---

1.4.2 AOPs implementation and application

Generally, the efficiency of different AOPs depends largely upon the physical and chemical properties of targeting pollutants and operating costs. The installation cost of AOPs is low but have high operating costs because of the continuous requirement of chemicals and/or energy [78]. To avoid high costs and make the treatment more efficient, AOPs may be used as a pre-treatment combined with a biological process. This strategy is the more suitable option when wastewater influent is not biodegradable [79]. The sequencing implementation of different AOPs as a tertiary treatment is another way to increase the removal rate of micropollutants and reducing the costs. This method is useful treating effluents characterized by the mixtures which display different reactivity towards diverse AOPs [79]. Finally, the implementation of separation process and subsequent AOP is effective, apart to reducing costs, in the elimination of non-target organic matter in the first step so that less amount of effluent with higher concentration of pollutants can be treated with AOPs [79].

Figure 6 displays the possible AOPs implementation in a wastewater and drinking water treatment plant [80].

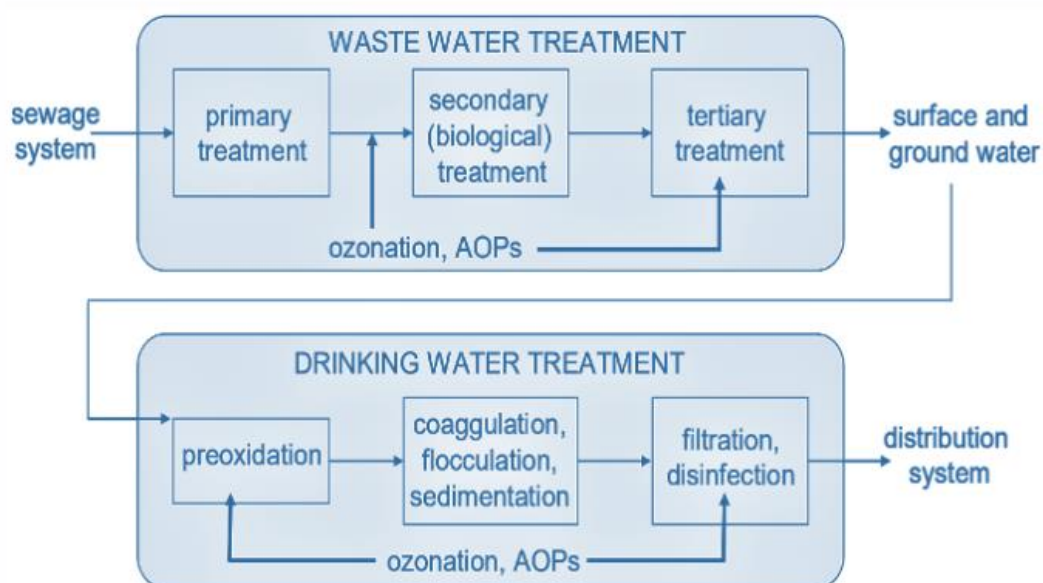


Figure 6. Possible applications of ozonation and AOPs in wastewater and drinking water treatment plants [80].

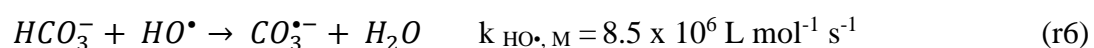
In the case of WWTP the implementation of AOPs can be performed as a pre-treatment and subsequent biological process or AOPs as a tertiary treatment. The first option is less economically viable due to influent wastewater usually contains high amount of organic matter which can compete for the oxidative species. Switzerland is the most representative country in the implementation of advanced technologies where some of its WWTPs have an ozonation process [81, 82]. However, in the case of drinking water, as the influent is from surface or groundwater, the organic matter load is low. Thus, AOPs can be implemented as a peroxidation to remove refractory trace of organic compounds or as a posttreatment. As an example, Zurich's water treatment system (Switzerland) employs natural sand and carbon filters before water being treated with ozone to get rid of microorganisms and promote oxidization [83]. Similarity, in Lucerne (Switzerland) in 2018 was installed the first water treatment plant using PWNT's CeraMac[®] system (ceramic membrane filtration process) followed by ozonation [84]. In Netherlands, Andijk III water treatment plant also uses CeraMac[®] system but, in that case, it is followed by UV/H₂O₂ treatment and activated carbon filters. The implementation of membranes as a first step reduces considerably the energy required to UV [85].

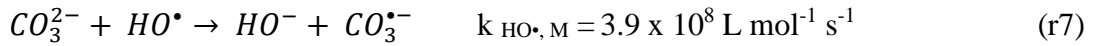
AOPs can also be used joined with other treatment systems to treat various types of industrial wastewater such as pesticides and/or herbicides, pharmaceutical industry, textile wastewaters, pulp and paper mill industry wastewaters, landfill leachate and olive or palm oil mill. The implementation of adequate AOP and best combination with other process will depends on the special characteristic of each effluent [86].

1.4.3 Water quality impacts

As mentioned in the previous section, the quality of water is a key parameter to consider defining an efficient water treatment strategy. When AOPs are involved in the process, the presence of dissolved organic or inorganic compounds can compete for hydroxyl radical, due to its non-selective character. The most important parameters influencing on the effectiveness of AOPs are detailed below:

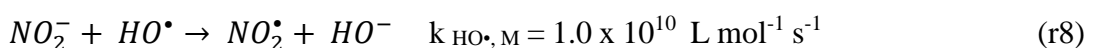
- **Alkalinity:** bicarbonate (HCO₃⁻) and carbonate (CO₃²⁻) ions react with hydroxyl radicals to form carbonate radicals according to following reactions [87, 88].





Although the reaction rate constants of two species are lower compared than most of micropollutants [88], the second order reaction rate depends on the concentration of compound. The concentration of bicarbonate and carbonate in WW influents or aquatic environment usually is much higher than recalcitrant compounds, hence hydroxyl radicals can be scavenged by these ions.

- Organic matter load:** usually quantified as a total organic carbon (TOC) or dissolved organic carbon (DOC) and called NOM (natural organic matter), if its origin is natural, or EfOM (effluent organic matter), if is coming from WWTP. Organic matter can also react with hydroxyl radicals, but there are no concrete values for these reactions, because of different types of organic matter is present in water. However, some authors have determined the second order reaction rate of dissolved organic matter (DOM) with HO^\bullet in the range of 10^8 - 10^9 $\text{L mol}^{-1} \text{ s}^{-1}$ [89-94]. Similarity to bicarbonate and carbonate ions, the concentration of DOM is always higher than micropollutants resulting in a hydroxyl radical scavenging by organic matter and decreasing the efficiency in MPs removal. Additionally, organic matter absorbs in a large UV range. The competition between DOM and oxidant, MP or catalyst, for UV light causes a decrease in the hydroxyl radicals' generation and consequently a reduction of AOP efficiency.
- Nitrates and nitrites:** these ions overall affect the AOPs which requires UV light. Nitrates absorb in the range of 230-240 nm while nitrites present the maximum peak between 300-310 nm. Equal than DOM, the competition between these ions and species involved in HO^\bullet production for UV light causes a decrease of AOP performance. Additionally, nitrite ion can react with HO^\bullet (reaction r8) [87] decreasing the efficiency of AOPs.



- Turbidity:** this parameter also affects the UV based AOPs. Higher turbidity decreases the water transmittance and consequently reduces the light penetration into

the system. This fact results in a lower generation of hydroxyl radicals and subsequent decreasing in treatment efficiency.

1.4.4 Fenton and photo-Fenton processes

Chemistry of the Fenton reactions

Fenton and related reactions comprise reactions with peroxides (usually H_2O_2) with iron ions to generate active oxygen species capable to oxidize organic or inorganic compounds when they are present. In 1894, Henry J. Fenton described the activation of H_2O_2 by Fe^{2+} salts to oxidize tartaric acid [95]. After this discovery, these reactions had turn of great interest for their importance in biological chemistry, synthesis, chemistry of natural waters and treatment of dangerous wastes [76]. In 1934, Haber and Weiss proposed that hydroxyl radical is the active oxidant formed by Fenton reaction [96]. In the last decades, the relevance of HO^\bullet reactions in the environment, biological systems and in waste treatment have been recognized and more than 1700 rate constants of HO^\bullet between organic and inorganic substances in aqueous matrix have been reported by Buxton in 1988 [87]. The Fenton and related reactions are viewed as a convenient and economical technology to treat chemical wastes. H_2O_2 and iron salts are cheap and their potential residual on the environment is considered non harmful [76].

Iron species naturally can be found as Fe(II) and Fe(III) valences. In solution, these species exist in various hydrolyzed species and/or inorganic complexes depending on the pH value of the solution. Fe(II) exists predominantly as $\text{Fe}^{2+}(\text{aq})$, at pH lower than 3, and as a $\text{Fe}(\text{OH})_2$ at pH between 3 and 7. Fe(III) can be found in different forms as displayed in Figure 7 [97].

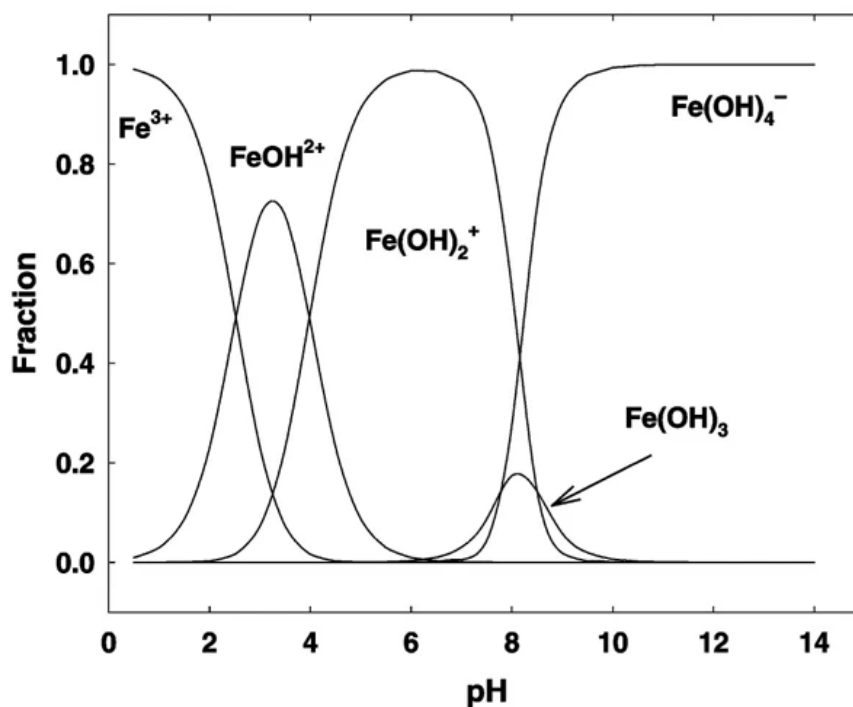


Figure 7. Speciation diagram of Fe(III) depending on the pH [97].

The Fenton mechanism is based on the decomposition of H_2O_2 catalyzed by Fe^{2+} in acidic solution (optimal pH = 2.8) near room temperature and in dark conditions. This process consists of a complex chain of radical reactions which are gathered in Table 7.

Table 7. Main reactions involved in the Fenton process.

Reaction	Rate constant of reaction	Ref.	Reaction
Initiation			
$Fe^{2+} + H_2O_2 \rightarrow Fe^{3+} + HO^- + HO^*$	$k=76 M^{-1} s^{-1}$	[98]	(r9)
$Fe^{3+} + H_2O_2 \rightarrow Fe^{2+} + HO_2^* + HO^+$	$k=0.001-0.01 M^{-1} s^{-1}$	[99]	(r10)
$2H_2O_2 \rightarrow 2H_2O + O_2$		[76]	(r11)
Propagation			
$HO^* + H_2O_2 \rightarrow HO_2^* + H_2O$	$k= 2.7 \times 10^7 M^{-1} s^{-1}$	[87]	(r12)
$HO_2^* + H_2O_2 \rightarrow HO^* + H_2O + O_2$	$k= 1.1-3.7 M^{-1} s^{-1}$	[94]	(r13)
Termination			
$Fe^{2+} + HO^* \rightarrow Fe^{3+} + HO^-$	$k= 3.2 \times 10^8 M^{-1} s^{-1}$	[87]	(r14)
$Fe^{3+} + HO_2^* \rightarrow Fe^{2+} + H^+ + O_2$	$k= 1.2 \times 10^6 M^{-1} s^{-1}$	[94]	(r15)
$Fe^{2+} + HO_2^* + H^+ \rightarrow Fe^{3+} + H_2O_2$	$k= 1.3 \times 10^6 M^{-1} s^{-1}$	[94]	(r16)
$HO^* + HO_2^* \rightarrow H_2O + O_2$	$k= 6.6 \times 10^9 M^{-1} s^{-1}$	[87]	(r17)
$HO^* + HO^* \rightarrow H_2O_2$	$k= 5.2 \times 10^9 M^{-1} s^{-1}$	[87]	(r18)
$HO_2^* + HO_2^* \rightarrow H_2O_2 + O_2$	$k= 1.3 \times 10^6 M^{-1} s^{-1}$	[87]	(r19)

In Fenton process, the hydroxyl radical is predominantly generated via reaction 9 simply by combining Fe^{2+} salt with H_2O_2 . The reduction of Fe^{3+} to Fe^{2+} is a limiting step in the generation of HO^\bullet since the rate constant of reaction 10 is very low. This fact compromises the efficiency of the process in the oxidation of organic compounds, because hydroxyl radical is the responsible of their oxidation. From reaction 12 it is observed that hydrogen peroxide can act as a hydroxyl radical scavenger, also affecting the efficiency in the degradation of compounds. Thus, an excess of this reactant is not desirable. Whereas that hydroperoxyl radical (HO_2^\bullet) ($pK_a=4.8$) [100] and its conjugate base (superoxide radical, O_2^\bullet) play an important role in the redox cycle of iron in solution (see reaction 15 and 16).

Photo-Fenton process

The modification of Fenton process including irradiation (UV or UV/Visible light), namely photo-Fenton process, increases the HO^\bullet production leading higher yields in the removal of organic contaminants. This enhance is achieved by promoting the photoreduction of Fe^{3+} to Fe^{2+} with wavelengths up to 580 nm. This photoreduction drives to a redox cycle resulting in a continuous generation of HO^\bullet (see reaction 9 and 20) [100].



From Figure 7 it was observed that at pH 3, which is the optimal condition for the process, the predominantly iron specie is FeOH^{2+} .

Operative parameters of the processes

Apart from the factors commented in section 1.4.3, related to the water quality and affecting the AOPs in general, other operational parameters can influence on the efficiency of Fenton and photo-Fenton process. The most important parameters are detailed below:

- **pH value of the solution:** this factor is a key parameter since iron ions in aqueous solution form hexacoordinate complexes with water and or hydroxyl ligands depending on the pH. For pH values lower than 2.3, the predominant ferric iron complex is $[\text{Fe}(\text{H}_2\text{O})_6]^{3+}$ which present low reactivity with H_2O_2 . While for pH higher than 3.5, the ferric iron hydroxides formed $[\text{Fe}(\text{H}_2\text{O})_4(\text{OH})_2]^+$ and $[\text{Fe}(\text{H}_2\text{O})_3(\text{OH})_3]$ and ferrous hydroxides ($\text{Fe}(\text{OH})_2$) have a low solubility in aqueous media and they precipitate reducing the efficiency of the processes. When pH is between 2.3 and 3.5, the iron aqua-complex FeOH^{2+} is the predominant specie, which has the

higher absorption coefficient in UV range and is soluble in aqueous media. Thus, optimal pH value for Fenton and photo-Fenton process is 2.8.

- **Reagents concentration:** the efficiency of the processes increases by the rise of iron and hydrogen peroxide concentrations. However, the selection of reagents concentrations fundamentally depends on the water quality of influent. For iron, a ratio between 1:10 and 1:50 (wt/wt) of iron-organic matter ensure good oxidation performances. Another important factor to consider is the intended of water reuse. In that cases the legislation fixes a maximum limit of iron emission. For instance, 5 mg L⁻¹ is the maximum concentration of iron emission in irrigation permitted by international regulations [102, 103]. Regarding H₂O₂, its selection depends on the various factors. The most important is the concentration of iron to avoid the process limitation. However, the concentration of hydrogen peroxide can not be in excess due to their scavenger effect of HO[•] (see reaction 12).
- **Fe²⁺ : H₂O₂ ratio:** is a critical parameter to promote the efficiency of the processes. Typical ratios range between 1:5 and 1:25 (wt/wt). According to these ratios, a HO[•] production is assured without limiting reactants and avoiding the scavenging of hydroxyl radicals.
- **Temperature:** for endothermic reactions the increase of temperature enhances the reaction rate. However, temperatures higher than 40 °C involves H₂O₂ decomposition reducing the oxidant available for the hydroxyl radical generation. This fact results in a decrease in Fenton and photo-Fenton efficiency. For this reason, temperatures between 20-40 °C are desirable for these processes.

Main drawbacks of the processes

Fenton and photo-Fenton processes seem useful and economically feasible to treat chemical wastes due to the cheapness of H₂O₂ and iron. However, they present some inconveniences. One of them is the requirement of the iron extraction, at the end of the process, which produces high volumes of iron wastes. The need of acidic pH (2.8), to maintain the iron in solution and achieve higher performances in micropollutants removal, is another of the great drawbacks of these processes. This condition is a critical parameter when the aqueous

solution to treat has a higher pH, such as in wastewater treatment. The continuous acidification/neutralization of water increases the cost of the treatment besides to the environmental impact due to the CO₂ generation [104, 405]. Additionally, in photo-Fenton process the requirement of irradiation increases the operational costs due to the electricity consumption and maintenance. The presence of mercury in some lamps used for that purposes increases even more the environmental impact [106, 107]. All of these inconveniences make the processes unattractive for their full scale-application [108].

To deal with the problems related to the pH and work at circumneutral pH (between 6.5 and 7.5), iron complexes as iron source have been used driving to great performances in micropollutants degradation and bacterial inactivation. Otherwise, to overcome the problems associated to the need of irradiation in photo-Fenton process, the use of solar light may be a good option, making the process more economically and environmentally sustainable. However, solar irradiation is highly dependent on location and weather. Other option studied in the last years is the use of UV light emitting diodes (LEDs) as irradiation source. Contrary to conventional lamps, UV-LEDs offer low energy consumption, long lifetime (up to 26,000 h), no mercury content, no problems associated to overheating and the possibility to select specific wavelengths and configurations of the photoreactor according to particular needs [109, 110]. Although numerous advantages presented by UV-LEDs and the good performances on micropollutant degradation by photo-Fenton with UV-LEDs, nowadays, conventional lamps are more economical than LEDs. Thus, improvements in the efficiency and power are required to apply LEDs at full-scale. Table 8 displays the efficiency of LEDs in photo-Fenton at acidic and circumneutral pH for several micropollutants.

Table 8. Efficiency of photo-Fenton process at acidic and circumneutral pH using LEDs as a radiation source in the removal of some recalcitrant organic compounds and wastewater treatment.

Target	Iron source and reagents concentrations	Water matrix	Wavelength (nm)	pH	Performance	Ref.
Losartan & Hydrochlorothiazide (20 mg L ⁻¹ each one)	[Fe ²⁺]=10 mg L ⁻¹ [H ₂ O ₂]= 100 mg L ⁻¹	Ultrapure	280-800	3.0	Removal (in % DOC) of almost 75% after 90 min. (130 kWh m ⁻³ , 60 min).	[111]
Chemical Oxygen Demand (COD) (22932 mg L ⁻¹)	Fe ³⁺ =286 mg L ⁻¹ H ₂ O ₂ = 5459 mg L ⁻¹	Crystallized-fruit effluents	365	3.0	74% of COD removal after 360 min (85 W m ⁻²)	[112]

Table 8. (continued)

Target	Iron source and reagents concentrations	Water matrix	Wavelength (nm)	pH	Performance	Ref.
Acetamiprid (200 $\mu\text{g L}^{-1}$)	[Fe ²⁺]=5.5 and 11 mg L ⁻¹ [H ₂ O ₂]= 50 mg L ⁻¹	Simulated secondary effluent (DOC= 10 mg L ⁻¹)	365 385 400	2.8	Complete removal in 10 min with 365 nm, 5 cm liquid depth and 11 mg L ⁻¹ Fe ²⁺ (10 W m ⁻²)	[113]
Acetamiprid (100 $\mu\text{g L}^{-1}$)	[Fe ²⁺]=1, 2 and 3 mg L ⁻¹ [H ₂ O ₂]= 2, 4, 6, 8 and 12 mg L ⁻¹ Ratio H ₂ O ₂ :Fe ²⁺ = 2:1 and 4:1	Synthetic secondary effluent (DOC >10 mg L ⁻¹)	256	2.8	Complete removal in 12.5 min with 3 mg L ⁻¹ Fe ²⁺ and 12 mg L ⁻¹ H ₂ O ₂ (20 W m ⁻²)	[114]
Antipyrine (50 mg L ⁻¹)	[Fe ²⁺]=5-20 mg L ⁻¹ [Oxalate]=25-100 mg L ⁻¹ [H ₂ O ₂]= 100-1000 mg L ⁻¹	Ultrapure	365	2.8	Complete removal in 2.5 min with 20 mg L ⁻¹ Fe ²⁺ , 100 mg L ⁻¹ H ₂ O ₂ and 100 mg L ⁻¹ of oxalate (3.32x10 ⁻⁶ Einstein s ⁻¹)	[115]
Salicylic acid, ketoprofen, diclofenac, paracetamol and caffeine (10 mg L ⁻¹ of each one)	[Fe ³⁺]= 15.0 mg L ⁻¹ Molar ratio (Fe ³⁺ :oxalate =1:3) [H ₂ O ₂]= 47.6 mg L ⁻¹	Ultrapure	365 400 470 515 568 624 650 White	6.5	Complete removal in 25 min of all substances with 40 LEDs of different wavelengths (68 mW) V _{sol} =200 mL	[116]

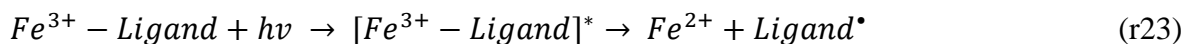
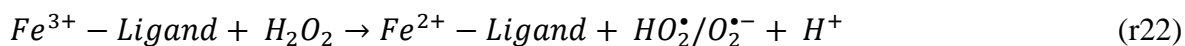
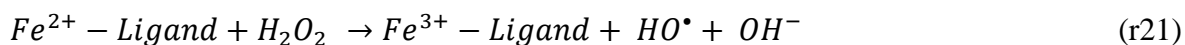
Photo-Fenton at circumneutral pH

Photo-Fenton at circumneutral pH (between 6.5-7.5) is an interesting alternative to overcome one of the biggest inconveniences of the process (work at acidic pH) for its application at full-scale. In the last decades, several studies related with the investigation of heterogeneous and homogeneous photo-Fenton at near neutral pH were reported. Heterogeneous process is performed by catalysts containing iron. Iron can be supported in a large variety of materials like neutral organic polymers, ion exchange membranes or resins, inorganic materials (clay,

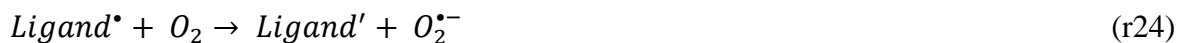
zeolites...) or even residual materials containing iron. Homogeneous treatment at circumneutral pH is carried out with compounds capable to solubilize the iron in a wide range of pH, even at high values of pH. These substances are chelating agents or ligands. As the iron is chelated and not free as in acidic pH, this process could imply a reduction of the metal ion activity for the generation of reactive oxygen species. However, the possibility to work at near neutral pH and reduce the iron sludge makes the process more attractive for its application.

Despite the mechanism of iron chelates in photo-Fenton is not clearly defined, it seems that HO^\bullet is the predominant specie in the degradation of micropollutants and bacterial inactivation [93, 117].

Like than conventional photo-Fenton, the reactions involved in the process with iron chelates are described below [118].



The UV radiation also plays an important role in enhancing the HO^\bullet generation in some chelating agents [76, 119] and the light absorption, which define the quantum yield of the photoreduction process, depends on the iron complex. The proposed mechanism lies in the photoreduction of Fe^{3+} to Fe^{2+} by ligand-metal-charge transfer (LMCT) forming a ligand radical ($Ligand^\bullet$), which requires a second electron transfer to reach its stable oxidation state. This fact can be performed by the reaction with dissolved oxygen (r24) [117].



The superoxide radical generated in r24 can take part in additional reactions as a precursor of HO^\bullet . While $Ligand^\bullet$ can also reacts with iron (III) complex increasing the Fe(III)/Fe(II) cycle.

Moreover, the stability constant (k_{stab}) of each chelating agent with iron is also a key parameter in mechanisms of photo-Fenton at near neutral pH. The stability constant depends greatly on the properties of the iron chelates such as geometry, number of coordination groups and phenolate groups. Iron complexes presenting octahedral geometry, higher

coordination groups and phenolate groups are usually more stable [119]. Higher stability of iron complexes results in a lower availability of iron to generate reactive oxygen species, but less iron release is observed. However, when the stability constant is lower, the iron is more readily, giving higher micropollutant removal performances at initial times. However, this fact results in a higher iron precipitation, causing iron sludge and decreasing the efficiency of the process. Thus, an equilibrium between stability of iron complex and iron release is essential for the efficiency of the process.

A suitable molar ratio between iron and ligand is also a key parameter in the performance of the process, assuring the complete iron chelation. However, chelating agents are organic molecules which increase the dissolved organic carbon in the solution and can scavenge hydroxyl radicals. Thus, the proper molar ratio is not always the stoichiometric one [119]. For these reasons, the selection of appropriate chelating agent and its molar ratio with iron are essential for the process efficiency. The biodegradability and toxicity of the iron complex is also an important parameter to consider for its selection.

Several chelating agents were reported in the literature for the photo-Fenton at near neutral pH. The use of simple and well-known bases of natural organic acids, like citric, gluconic, caffeic, ascorbic, oxalic, and tartaric have been widely studied since their biodegradability and natural character.

On the other hand, the employment of synthetic ligands based on aminopolycarboxylic acids, such as NTA (Nitrilotriacetic acid), EDTA (Ethylenediaminetetraacetic acid) and EDDS (Ethylenediamine-*N,N'*-disuccinic acid), has been raised in the last years. Among them, Fe^{3+} -EDDS has been the most studied due to its biodegradability and higher efficiency on MPs abatement.

In the water scarcity scenario, it also has increased the interest on the synthetic organic iron fertilizers based on aminopolycarboxylic acids to operate photo-Fenton at circumneutral pH. The use of these compounds in the process is associated to the further reuse of wastewater for agriculture, since the iron is an essential micronutrient for plants. EDDHA ((Ethylenediamine-*N,N'*-bis(2-hydroxyphenylacetic acid)), HEDTA (2-Hydroxyethyl ethylenediamine-*N,N',N'*-triacetic acid) and DTPA (Diethylene triamine pentaacetic acid) have been investigated on that purpose. All of these fertilizers are approved by the European

Commission for their agricultural use [120]. Currently, EDTA and EDDS are also included in this regulation.

Table 9 shows the efficiency of photo-Fenton at near neutral pH using different chelating agents in the abatement of micropollutants and bacterial inactivation.

Table 9. Efficiency of photo-Fenton process at circumneutral pH in the removal of some recalcitrant organic compounds and bacterial inactivation.

Target	Iron source and reagents concentrations	Water matrix	Source of light	Performance	Ref.
<i>E. coli</i> (2.4×10^4 - 8.4×10^5 CFU mL ⁻¹)	[Fe ³⁺]= 28 mg L ⁻¹ Molar ratio Fe ³⁺ : oxalate = 1:10 [H ₂ O ₂]= 68 mg L ⁻¹	Phosphate buffer solution	Black-light Blue lamp (BLB) 300-400 nm (7.9×10^{-6} Einstein L ⁻¹ s ⁻¹)	4 Log-reduction in 50 min	[121]
<i>C. parvum</i> (3.1×10^3 oocysts mL ⁻¹) <i>B. subtilis</i> (3×10^5 CFU mL ⁻¹)	[Fe ³⁺]= 28 mg L ⁻¹ Molar ratio Fe ³⁺ : oxalate = 1:10 [H ₂ O ₂]= 68 mg L ⁻¹	Phosphate buffer solution	BLB lamp 300-400 nm (7.9×10^{-6} Einstein L ⁻¹ s ⁻¹)	2 Log-reduction in 300 min	[122]
15 MPs (5 µg L ⁻¹ of each one) Total bacteria (10^4 CFU mL ⁻¹) Total coliforms (10^3 CFU mL ⁻¹)	[Fe ³⁺]= 5 mg L ⁻¹ Molar ratio Fe ³⁺ : EDDS = 1:2 [H ₂ O ₂]= 50 mg L ⁻¹	Municipal wastewater	Solar light (30 W m ⁻²)	87% of the MPs removal sum in 60 min. 2 and 3 Log-reduction of total bacteria and total coliforms, respectively in 120 min.	[123]
Bisphenol A (4.6 mg L ⁻¹)	[Fe ³⁺]= 5.6 mg L ⁻¹ Molar ratio Fe ³⁺ : EDDS = 1:1 [H ₂ O ₂]= 3.4 mg L ⁻¹	Ultrapure	Fluorescent lamp 300-500 nm (530 W m ⁻²)	85% removal in 10 min	[124]
Ciprofloxacin (1 mg L ⁻¹)	[Fe ³⁺]= 0.36 mg L ⁻¹ Molar ratio Fe ³⁺ : citrate = 1:1 Fe ³⁺ : oxalate = 1:3 [H ₂ O ₂]= 10.9 mg L ⁻¹	Ultrapure	BLB lamp (15 W) 365-410 nm V _{sol} =280 mL	50% and 30% removal in 10 min of Fe-citrate and Fe-oxalate, respectively	[125]
Sulfamethoxazole (20 mg L ⁻¹)	[Fe ³⁺]= 5 mg L ⁻¹ Molar ratio Fe ³⁺ : tartrate = 1:10 Fe ³⁺ : oxalate = 1:20 Fe ³⁺ : NTA = 1:1.5 Fe ³⁺ : EDTA = 1:1.5 [H ₂ O ₂]= 10 mg L ⁻¹	Ultrapure	BLB lamp 350-40 nm (5.05×10^{-6} Einstein s ⁻¹)	72% removal with Fe-EDTA and Fe-NTA, 50% removal with Fe-oxalate and 10% removal with Fe-Tartrate in 60 min.	[126]

Table 9. (continued)

Target	Iron source and reagents concentrations	Water matrix	Source of light	Performance	Ref.
Phenol, Bisphenol A, sulfamethoxazole, carbamazepine, pyrimethanil (100 µg L ⁻¹ of each one)	[Fe ³⁺]= 7.7 mg L ⁻¹ Molar ratio Fe ³⁺ : EDDS =1:2 [H ₂ O ₂]= 65 mg L ⁻¹	Municipal wastewater	Solar simulator Sunlight (30 W m ⁻²)	80% of the sum of five MPs in 1.8 kJ L ⁻¹	[127]
<i>E. coli</i> (10 ⁶ CFU mL ⁻¹)	[Fe ³⁺ : citrate]= 0.6 mg L ⁻¹ relative to the Fe content [H ₂ O ₂]= 10 mg L ⁻¹	Natural water	Solar simulator 300-400 nm (20.2 W m ⁻²)	Total inactivation in 30 min. (6 log-reduction)	[128]
<i>E. coli</i> (10 ⁶ CFU mL ⁻¹)	[Fe ³⁺]= 5 mg L ⁻¹ Molar ratio Fe ³⁺ : citrate =1:0.01 Fe ³⁺ : tartrate =1:0.01 Fe ³⁺ : ascorbic acid =1:0.1 Fe ³⁺ : caffeic acid =1:0.01 [H ₂ O ₂]= 25 mg L ⁻¹	Synthetic wastewater	Solar simulator 290-400 nm (600 W m ⁻²)	Total inactivation in 70 min. (6 log-reduction) for all conditions	[129]
Acetamiprid (100 µg L ⁻¹)	[Fe ³⁺]= 5.6 mg L ⁻¹ Molar ratio Fe ³⁺ : EDDS =1:1 [H ₂ O ₂]= 30 mg L ⁻¹	Synthetic wastewater	Solar simulator (40 W m ⁻²)	90% removal in 30 min.	[130]
<i>E. coli</i> and <i>E. faecalis</i> (10 ⁶ CFU mL ⁻¹ each one)	[Fe ³⁺]= 5.6 mg L ⁻¹ Molar ratio Fe ³⁺ : EDDS =1:2 [H ₂ O ₂]= 10 mg L ⁻¹	Municipal wastewater	Solar light (30 W m ⁻²)	Total inactivation in 3.5 kJ L ⁻¹ for <i>E. coli</i> and 15 kJ L ⁻¹ for <i>E. faecalis</i> (6 log-reduction)	[131]
Carbamazepine (10 mg L ⁻¹)	[Fe ³⁺]= 2.8 mg L ⁻¹ Molar ratio Fe ³⁺ : NTA= 1:2 [H ₂ O ₂]= 34 mg L ⁻¹	Ultrapure	UVA lamp 365 nm (4.05 mW cm ⁻²)	Total removal in 60 min.	[132]
45 MPs from wastewater (µg L ⁻¹)	[Fe ³⁺]= 5.6 mg L ⁻¹ Molar ratio Fe ³⁺ : EDDS= 1:1 [H ₂ O ₂]= 50 mg L ⁻¹	Municipal wastewater	Solar light (30 W m ⁻²)	> 80% degradation of the sum of MPs in 15 min	[133]
<i>E. coli</i> and <i>S. enteritidis</i> (10 ⁶ CFU mL ⁻¹)	[Fe ³⁺ : EDDHA]= 2.5 mg L ⁻¹ relative to the Fe content [H ₂ O ₂]= 5 mg L ⁻¹	Synthetic fresh-cut wastewater	Solar light (30 W m ⁻²)	Total inactivation in 30 Wh m ⁻² for <i>E. coli</i> (6 log-reduction) and 5 log-reduction for <i>S. enteritidis</i>	[134]

Table 9. (continued)

Target	Iron source and reagents concentrations	Water matrix	Source of light	Performance	Ref.
Acetaminophen, caffeine, trimethoprim, sulfamethoxazole, carbamazepine and diclofenac (100 µg L ⁻¹ each one)	[Fe ³⁺]= 3 mg L ⁻¹ Molar ratio Fe ³⁺ : EDDS= 1:2 [H ₂ O ₂]= 50 mg L ⁻¹	Natural water	Solar simulator 300-400 nm (30 W m ⁻²)	Total removal in 10 min of acetaminophen, diclofenac, trimethoprim and carbamazepine. Total removal of sulfamethoxazole at 20 min. 90% removal of caffeine at 30 min.	[135]
<i>E. coli</i> and <i>total coliforms</i> (10 ⁷ CFU mL ⁻¹ each one)	[Fe ³⁺]= 5 mg L ⁻¹ Molar ratio Fe ³⁺ : citrate= 1:1.5 Fe ³⁺ : oxalate= 1:10 Fe ³⁺ : EDTA= 1:1.5 Fe ³⁺ : NTA= 1:1.5 Fe ³⁺ : EDDS= 1:2 [H ₂ O ₂]= 90 mg L ⁻¹	Municipal wastewater	UVA lamps 365 nm (4.05x10 ⁻⁵ Einstein s ⁻¹)	With EDTA and oxalate: total inactivation of <i>E. coli</i> and <i>total coliforms</i> at 40 and 50 min. (7 log-reduction) With NTA : 7 and 6.5 log-reduction in 60 min. of <i>E. coli</i> and <i>total coliforms</i> , respectively. With citrate : 6 and 5.5 log-reduction at 60 min. of <i>E. coli</i> and <i>total coliforms</i> With EDDS: 5.5 and 4.5 log-reduction at 60 min. of <i>E. coli</i> and <i>total coliforms</i> , respectively.	[136]

2 Justification, objectives and thesis structure

2.1 Justification and objectives

The rising concern, in the last decades, on micropollutant occurrence in aquatic ecosystems, mainly from effluents of wastewater treatment plants, involves the implementation of processes capable to remove this persistent and recalcitrant compounds, such as AOPs. Although photo-Fenton process is one of the most efficient AOP, the optimal working conditions (acid pH) make the process unattractive to full-scale application. In the last years, several works in the literature have investigated the efficiency of photo-Fenton modifications linked to irradiation sources and the employment of iron complexes, to work at near neutral pH. However, further research on this area is required to improve the process efficiency for full-scale application. If the drawbacks presented by the photo-Fenton process are saved, it could be applied to the treatment of wastewater to convert it into useful water for reuse. This would be a relief given the current situation of water scarcity and the high consumption of fresh water for agriculture. In addition, organic fertilizers can be used as Fe chelating agents in photo-Fenton, obtaining water for reuse with adequate amounts of fertilizer and iron.

Summarizing, the main objective of this thesis is focused on the study of possible improvements in the photo-Fenton process for its possible implementation at full-scale, among other applications, for water reuse. It was considered that improvements could be introduced via radiation source or by working at circumneutral pH with chelating agents. Thus, the following specific objectives were proposed:

1. Exploring the efficiency of photo-Fenton using ultraviolet light emitting diodes (LEDs) as irradiation source:
 - Studying the influence of LEDs wavelength ranges on MP degradation and assessing the potential enhancement when LEDs with two wavelength ranges are combined.
 - Examining the transformation products depending on the initial concentrations of reagents and proposing degradation pathways.
2. Study and comparison of different irradiation sources (BLB lamps and LEDS) to perform photo-Fenton at acidic pH in four secondary effluents matrices, assessing the importance of radiation distribution in the photoreactor.

3. Exploring and testing new iron complexes to carry out the photo-Fenton process more efficiently in terms of iron release, MPs abatement and bacterial inactivation.

This includes:

- Assessing the potential efficiency of an organic fertilizer, as iron complex, in photo-Fenton for the abatement of MPs and bacterial inactivation, at near neutral pH using tubular photoreactor illuminated by LEDs.
- Testing the efficiency of different organic fertilizers mixtures and comparing the removal of different MPs with the single one in photo-Fenton using simulated solar light.
- Determining the BOD₅ (mgO₂ L) and *E.coli* (CFU 100mL) parameters of treated effluents and comparing the values with the maximum values allowed for European policies for the reuse of wastewater in agriculture.
- Examining the phytotoxicity of the treated effluents useful for the water reuse in irrigation.
- Study the potential reactivity of organic fertilizers in the aquatic environment and the mainly involved reaction mechanisms.

2.2 Thesis structure

This thesis consists of six chapters: introduction, justification and objectives, materials and methods, results and discussion, conclusions and recommendations and other contributions by the author. Chapter 4, referred to results, is divided in three sections, due to the specific objectives above mentioned were compiled in different publications. Each section includes their specific publications presented as a part (Part I-Part VI).

Section 4.1: Synergies, radiation and kinetics in photo-Fenton process with UV-A LEDs (Part I). This section includes the study about the use of LEDs as radiation source to carry out the photo-Fenton process. LEDs with two different wavelength ranges were used for testing the efficiency in the diphenhydramine hydrochloride removal. Additionally, the combination of LEDs with two different wavelength ranges (maintaining the same power than experiments performed with one range) enhances the efficiency of micropollutants abatement.

The following publication was derived from the results obtained in this section:

N. López-Vinent, A. Cruz-Alcalde, L.E. Romero, M.E. Chávez, P. Marco, J. Giménez, S. Esplugas, Synergies, radiation and kinetics in photo-Fenton process with UVA-LEDs, *Journal of Hazardous Materials* 380 (2019) 120882.

Section 4.2: Comparison of conventional BLB lamps and LEDs in photo-Fenton process for micropollutant abatement in real wastewater (Part II). In this section, it was compared the efficiency of BLB lamps and LEDs, emitting at 365 nm, in photo-Fenton process with different wastewater matrices. This comparison is necessary to determine the potential implementation of an alternative radiation source to reduce costs and environmental impacts. The results derived from this section also contributed to understand the importance of radiation distribution in the photoreactor.

The following publication was derived from the results obtained in this section:

N. López-Vinent, A. Cruz-Alcalde, C. Gutiérrez, P. Marco, J. Giménez, S. Esplugas, Micropollutant removal in real WW by photo-Fenton (circumneutral and acid pH) with BLB and LED lamps, *Chemical Engineering Journal* 379 (2020) 122416.

Section 4.3: Assessment of organic fertilizers as an iron source in photo-Fenton at circumneutral pH for wastewater treatment and its potential application in agriculture (Part III-VI). In this section different organic fertilizers were tested to carry out photo-Fenton process at near neutral pH, employing LEDs and solar simulated light as alternative irradiation sources. This section also includes the combination of organic fertilizers to investigate the potential enhancement in micropollutants abatement and bacterial inactivation and in the reduction of iron release in different wastewaters. Biochemical oxygen demand at 5 days and *E.coli* inactivation were followed and compared with the values proposed in the Regulation 2020/741/EU, for the potential water reuse in irrigation. Phytotoxicity was also evaluated. Summarizing, the work carried out in this section was focused on the investigation of more efficient and eco-friendlier photo-Fenton process to be applied at full-scale, including the potential reuse of wastewater in the scarcity scenario. Additionally, potential mechanisms were proposed for hydroxyl radical formation by photoexcitation of different organic fertilizers, depending on their characteristics. This fact can be important from an environmental point of view because it is related to the self-depuration of the aquatic compartments by oxidation of some persistent organic pollutants.

The following publications were derived from the results obtained in this section:

N. López-Vinent, A. Cruz-Alcalde, J.A. Malvestiti, P. Marco, J. Giménez, S. Esplugas, Organic fertilizer as a chelating agent in photo-Fenton at neutral pH with LEDs for agricultural wastewater reuse: Micropollutant abatement and bacterial inactivation, *Chemical Engineering Journal* 388 (2020) 124246.

N. López-Vinent, A. Cruz-Alcalde, J. Giménez, S. Esplugas, C. Sans, Improvement of the photo-Fenton process at natural condition of pH using organic fertilizers mixtures: potential application to agricultural reuse of wastewater, *Applied Catalysis B: Environmental*, 290 (2021) 120066.

N. López-Vinent, A. Cruz-Alcalde, J. Giménez, S. Esplugas, Mixtures of chelating agents to enhance photo-Fenton process at natural pH: influence of wastewater matrix on micropollutant removal and bacterial inactivation, *Science of the Total Environment*, 786 (2021) 147416. DOI: 10.1016/j.scitotenv.2021.147416

N. López-Vinent, A. Cruz-Alcalde, C. Lai, J. Giménez, S. Esplugas, C. Sans, Role of sunlight and oxygen on the performance of photo-Fenton process at near neutral pH using organic fertilizers as an iron chelates, submitted to *Journal of Hazardous Materials*.

3 Materials and methods

3.1 Chemicals

3.1.1 Model micropollutants

Relevant chemical information about model micropollutants and their acronyms (ACMP, DPH, PROP and SMX) are listed in Table 10. All compounds (analytical grade standards) were purchased from Sigma-Aldrich (Germany).

Table 10. Main information of model micropollutants employed in the research.

Compound	Abbreviation	Chemical formula	Molecular Weight (g mol ⁻¹)	CAS Number
Acetamiprid	(ACMP)	C ₁₀ H ₁₁ ClN ₄	222.68	135410-20-7
Diphenhydramine hydrochloride	(DPH)	C ₁₇ H ₂₁ NO · HCl	291.82	147-24-0
Propranolol hydrochloride	(PROP)	C ₁₆ H ₂₁ NO ₂ · HCl	295.80	318-98-9
Sulfamethoxazole	(SMX)	C ₁₀ H ₁₁ N ₃ O ₃ S	253.28	723-46-6

3.1.2 Chelating agents

Data on chelating agents employed in this thesis are detailed in Table 11. Organic fertilizers chelated with iron (III) (DTPA-Fe, EDDHA-Fe, EDTA-Fe and HEDTA-Fe) are also listed in the same table. All of them were purchased from Sigma-Aldrich and Phygenera (Germany), except EDDHA-Fe from Fertiberia (Spain)

Table 11. Main data of chelating agents and organic fertilizers chelated with iron (III) employed in this thesis. Sigma-Aldrich and Phygenera from Germany.

Compound	Chemical formula	Molecular Weight (g mol ⁻¹)	Iron chelated (%)	CAS Number	Company
DTPA	C ₁₄ H ₂₃ N ₃ O ₁₀	393.35	-	67-43-6	Sigma-Aldrich
DTPA-Fe	C ₁₄ H ₁₈ N ₃ O ₁₀ FeNa ₂	490.20	7.0	19529-38-5	Phygenera
EDDS-Na ₃	C ₁₀ H ₁₃ N ₂ Na ₃ O ₈	358.19	-	178949-82-1	Sigma-Aldrich
EDDHA-Fe	C ₁₈ H ₁₆ N ₂ O ₆ FeNa	435.20	6.0	16455-61-1	Fertiberia

Table 11. (continued)

Compound	Chemical formula	Molecular Weight (g mol ⁻¹)	Iron chelated (%)	CAS Number	Company
EDTA	C ₁₀ H ₁₆ N ₂ O ₈	292.24	-	60-00-4	Sigma-Aldrich
EDTA-Fe	C ₁₀ H ₁₂ N ₂ O ₈ FeNa · 3H ₂ O	421.10	13.3	18154-32-0	Phygenera
HEDTA-Fe	C ₁₀ H ₁₈ FeN ₂ O ₇ · 5H ₂ O	424.11	13.0	17084-02-5	Phygenera

3.1.3 Other chemicals

Diluent, Microtox[®] Acute Reagent, Osmotic Adjustment and Reconstitution Solution used for bioluminescent *Vibrio fischeri* assays were purchased from Modern Water (UK). Ammonium metavanadate (NH₄VO₃), catalase from bovine liver (C₉H₁₀O₃), Chromocult[®] Coliform Agar, hydrogen peroxide solution (30% w/v) and 2-chloro-6-(trichloromethyl)pyridine were acquired from Sigma-Aldrich (Germany). Acetonitrile (ACN) (CH₃CN, HPLC grade), ascorbic acid (C₆H₈O₆), iron (II) sulphate heptahydrate (FeSO₄ · 7H₂O), mercuric sulfate (HgSO₄), methanol (CH₃OH), orthophosphoric acid solution (H₃PO₄, 85% w/w), potassium dichromate solution (K₂Cr₂O₇, 4 mM with 25 g L⁻¹ of HgSO₄), silver sulfate solution (Ag₂SO₄, 10 g L⁻¹ in H₂SO₄), sodium bisulphite (NaHSO₃), sodium hydroxide (NaOH), sulfuric acid (H₂SO₄), sodium bicarbonate (NaHCO₃), 1,10-phenantroline, ethanol (C₂H₅OH), ammonium acetate (C₂H₇NO₂), acetic acid glacial (C₂H₄O₂), *tert*-butyl alcohol (tBuOH) were supplied from Panreac (Spain). Reagents to prepare solutions for BOD₅ were also purchased from Panreac (Spain): calcium chloride (CaCl₂), magnesium sulphate (MgSO₄), ferric chloride (FeCl₃), ammonium chloride (NH₄Cl), potassium hydroxide (KOH), boric acid (H₃BO₃), zinc sulphate heptahydrate (ZnSO₄ · 7H₂O), manganese sulphate hydrate (MnSO₄ · H₂O), ammonium molybdate (NH₄)₆Mo₇O₂₄ · 4H₂O, sodium phosphate hydrate (NaH₂PO₄ · H₂O). Seed lyophilized capsules were acquired from Cole-Parmer (USA). Buffered peptone water was obtained from Labkem (Spain). Pure nitrogen (≥ 99.999%) was purchased from Abelló Linde (Spain). Finally, ultrapure water (resistivity: 18.2 MΩ cm; TOC < 2 ppb) was generated by a Milli-Q[®] purification system (Millipore, USA).

3.2 Wastewater samples

The main research presented in this thesis was performed with four different secondary effluents from two WWTPs (plant of Gavà-Viladecans and plant of El Prat de Llobregat) located in the province of Barcelona (Spain).

The WWTP of Gavà-Viladecans (384000 population equivalent (PE); 64000 m³ d⁻¹ design flow (DF)) has two techniques implemented for the biological treatment, including the nitrogen and phosphorous removal in both treatments. One of the lines employs an integrated fixed-film activated sludge (IFAS) system. In this technology a hybrid attached/suspended growth mode is created due to the addition of solid media to the bioreactor. The other line uses a membrane bioreactor (MBR) technology, which is a combination of conventional activated sludge (CAS) and separation by ultrafiltration. In the same way, in the WWTP of El Prat de Llobregat (2275000 PE; 420000 m³ d⁻¹ DF) two biological treatment systems are operated. Both lines use the conventional activated sludge technology. The main difference lies in the elimination of nitrogen and phosphorous, which is only implemented in one of the lines. CAS (without nitrogen and phosphorous elimination) and CAS-NE (with nitrogen and phosphorous elimination) were the initials used in the research presented in this thesis.

For working with the same conditions in each set of experiments and avoid the degradation of the effluents, three sampling campaigns were carried out (see Parts II-IV). Each sampling was performed in January 2018, 2019 and 2020. Effluents from CAS, CAS-NE and IFAS were filtered with conventional paper to avoid any interference of largest particles in the experiments. Then, all effluents were stored at 4°C. In the experiments of Parts II and III, four effluents were used, while in the experiments of Part IV only CAS and MBR were employed. The main physicochemical parameters of the effluents for the different campaigns are shown in Table 12.

Table 12. Main physicochemical parameters of effluents employed. This includes the samples for the three sampling campaigns corresponding to the experiments of Parts II-IV. N/A: below the detection limit.

	Part II				Part III				Parts IV and V	
	IFAS	MBR	CAS	CAS-NE	IFAS	MBR	CAS	CAS-NE	MBR	CAS
pH	7.8	7.7	8.0	7.5	7.9	7.8	8.0	7.6	7.8	8.2
Turbidity (NTU)	18.5	0.5	20.1	2.6	13.9	1.0	8.9	4.0	0.3	5.3
UV₂₅₄ (m ⁻¹)	50.3	17.4	48.9	24.6	48	0.3	29	13	19.1	28.8
TOC (mg C L ⁻¹)	51.1	13.6	37.9	13.3	29.5	5.3	24.1	7.9	7.0	16.6
DOC (mg C L ⁻¹)	21.7	13.3	18.7	13.2	22.2	4.7	20.9	5.1	6.7	10.9
Alkalinity (mg CaCO ₃ L ⁻¹)	469	208	449	275	545	312	457	304	233	467
Cl⁻¹ (mg L ⁻¹)	543	565	486	464	507	470	519	482	592	406
SO₄²⁻ (mg L ⁻¹)	196	187	175	199	N/A	125	242	236	169	206
N-NO₂⁻ (mg L ⁻¹)	0.2	0.2	0.1	0.3	N/A	N/A	N/A	N/A	0.4	0.4
N-NO₃⁻ (mg L ⁻¹)	0.3	8.4	0.3	8.3	N/A	9.9	24.8	31.7	N/A	1.6

3.3 Experimental devices

3.3.1 UV-A LEDs

Photoreactor with LEDs on the cover

The research gathered in Part I was performed in 0.5 L Pyrex photoreactor (inner diameter: 8 cm; height: 12 cm) equipped with four LEDs positioned symmetrically at the top of the photoreactor (Figure 8). The nominal consumption of each LED (Intelligent LED solutions from RS Components, Spain) was 1.05 W operating at 350 mA and irradiance angle of 125°. Two wavelength ranges were used in this research: 380-390 nm and 390-400 nm. In addition,

a combination of two wavelength ranges were also employed. In that case two LEDs of 380-390 nm and two LEDs of 390-400 nm were used and situated crossed. To determine the incoming photons to the solution actinometrical analyses were performed with *o*-nitrobenzaldehyde [137, 138, 139]. The values for 380-390, 390-400 and 380-400 nm were $3.85 \cdot 10^{-7}$, $4.28 \cdot 10^{-7}$ and $5.25 \cdot 10^{-7}$ Einstein s^{-1} , respectively. The photoreactor was covered with aluminum foil to avoid loss of photons. A good mixing was assured by a magnetic stirrer and the temperature was maintained at 25°C by immersion in a Lauda Alpha thermostatic bath.

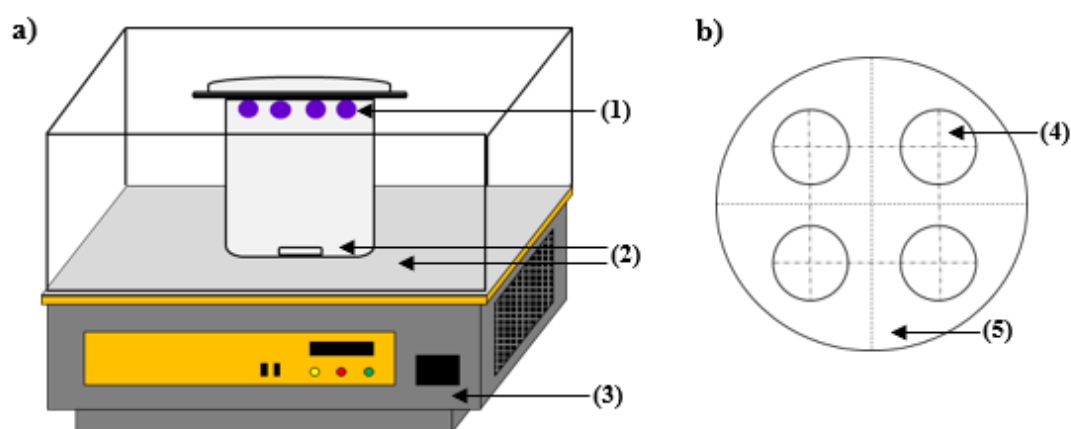


Figure 8. a) Schematic diagram of photoreactor with LEDs on the cover; b) cover of aluminum foil with four LEDs. (1) LEDs; (2) Magnetic stirrer; (3) Immersion thermostatic bath; (4) LEDs positioned symmetrically; (5) Aluminum foil cover.

Photoreactor with LEDs on the center

Part of the experiments included in Part II were carried out in a 2 L Pyrex-jacketed thermostatic photoreactor (inner diameter: 11 cm; height: 23 cm). A hand-made lamp was prepared with eight LEDs (Intelligent LED solutions), arranged on aluminum bar forming a spiral (to avoid dark zones into the photoreactor) and wrapped in a quartz glass tube (Figure 9). The lamp was located at the center of the photoreactor, which was also covered with aluminum foil. The nominal power, irradiance angle and electric current of LEDs were equal than previous photoreactor. However, in that case the emission wavelength range was 365-370 nm with an incident radiation into the photoreactor of $5.36 \cdot 10^{-7}$ Einstein s^{-1} (also calculated with *o*-nitrobenzaldehyde actinometry [137, 138, 139]). The temperature of the

solution was kept constant at 25°C with a thermostatic bath (Haake-C40). A magnetic stirrer (IKA[®] RCT basic) was used to provide a good mixing of solution.

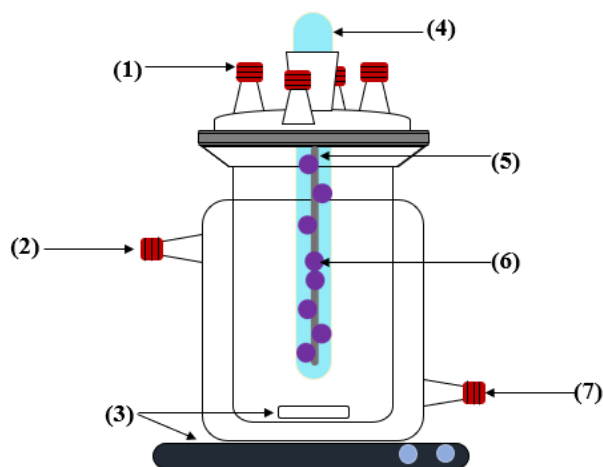


Figure 9. Schematic diagram of photoreactor with LEDs on the center. (1) Sampling point; (2) Thermostatic bath-inlet port; (3) Magnetic stirrer; (4) Quartz glass tube; (5) Aluminum bar; (6) LEDs; (7) Thermostatic bath-outlet port.

Tubular photoreactor

The research gathered in Part III was performed in a Duran glass tubular photoreactor (25 cm length; 2 cm external diameter) illuminated by eight LEDs (Intelligent LED solutions). The nominal power, electric current, irradiance angle and wavelength range were the same than previous photoreactor (photoreactor with LEDs on the center). The solution to treat was continuously recirculated with a peristaltic pump (Ismatec[®] Ecoline) from a 1 L reservoir tank to tubular photoreactor (Figure 10). The tubular photoreactor was enveloped by a cylindrical tube (30 cm length; 8 cm diameter) where the LEDs were located at the top and it was covered with aluminum foil to avoid the photon loss. The solution in the feeding tank was continuously mixed with a magnetic stirrer (IKA[®] RCT basic) and the temperature was kept constant at 25°C with a thermostatic bath (Haake-C40). Again, the o-nitrobenzaldehyde actinometry [137, 138, 139] was carried out and the value of the irradiance was $2.66 \cdot 10^{-7}$ Einstein s⁻¹.

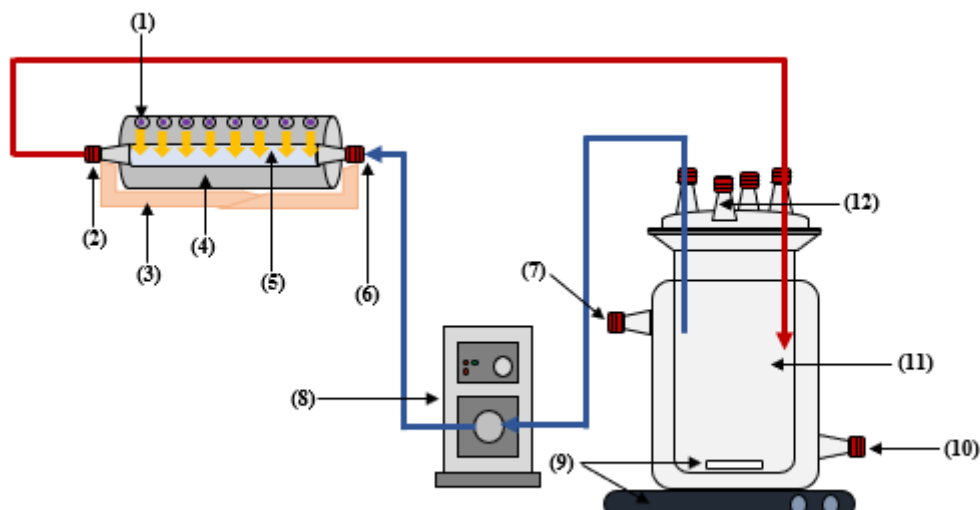


Figure 10. Schematic diagram of tubular photoreactor with LEDs. (1) LEDs; (2) Recirculation to feeding tank; (3) Support of the tubular photoreactor; (4) Cylindrical envelope covered with aluminum foil; (5) Duran glass tubular photoreactor; (6) Recirculation to photoreactor; (7) Thermostatic bath-inlet port; (8) Peristaltic pump; (9) Magnetic stirrer; (10) Thermostatic bath-outlet port; (11) Feeding tank; (12) Sampling point.

3.3.2 Black-light Blue lamp photoreactor

Other part of the experiments included in Part II were performed in the same photoreactor as in section 3.3.1 (Photoreactor with LEDs on the center). However, in that case, a BLB lamp was used (Philips TL 8W, 08 FAM). The lamp was wrapped in a quartz glass tube and located at the center of the photoreactor (Figure 11). Equal than other devices, the temperature was kept constant at 25°C with a thermostatic bath (Haake-C40) and mixing was provided with a magnetic stirrer (IKA[®] RCT basic). The photon flux into the photoreactor was $6.71 \cdot 10^{-7}$ Einstein s⁻¹ (calculated by o-nitrobenzaldehyde actinometry [137, 138, 139]).

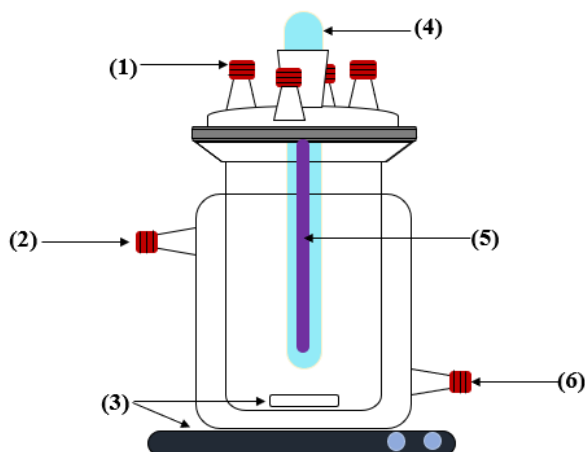


Figure 11. Black-light Blue Lamp photoreactor scheme. (1) Sampling point; (2) Thermostatic bath-inlet port; (3) Magnetic stirrer; (4) Quartz glass tube; (5) Black-light Blue Lamp; (6) Thermostatic bath-outlet port.

3.3.3 Solar light simulator

The investigation included in Parts IV-VI was performed in a solar simulator (Xenoterm-1500RF.CCI) equipped with a Xenon lamp (1.5 kW) simulating the solar spectrum. As it was equipped with a filter, the emission wavelength range was between 290-400 nm. Equal than tubular photoreactor with LEDs, the solution to treat was steadily recirculated with a peristaltic pump (Ismatec[®] Ecoline) from 1 L reservoir tank to tubular photoreactor (25 cm length; 2 cm external diameter) placed inside the simulator chamber on the axis of a parabolic mirror located at the bottom of solar simulator (Figure 12). A good mixing and temperature of 25°C were maintained in the feeding tank with a magnetic stirrer (IKA[®] RCT basic) and thermostatic bath (Haake-C40), respectively. Like the other photoreactors the photon flux was measured, and it was obtained a value of $6.60 \cdot 10^{-7}$ Einstein s^{-1} (o-nitrobenzaldehyde actinometry [137, 138, 139]).

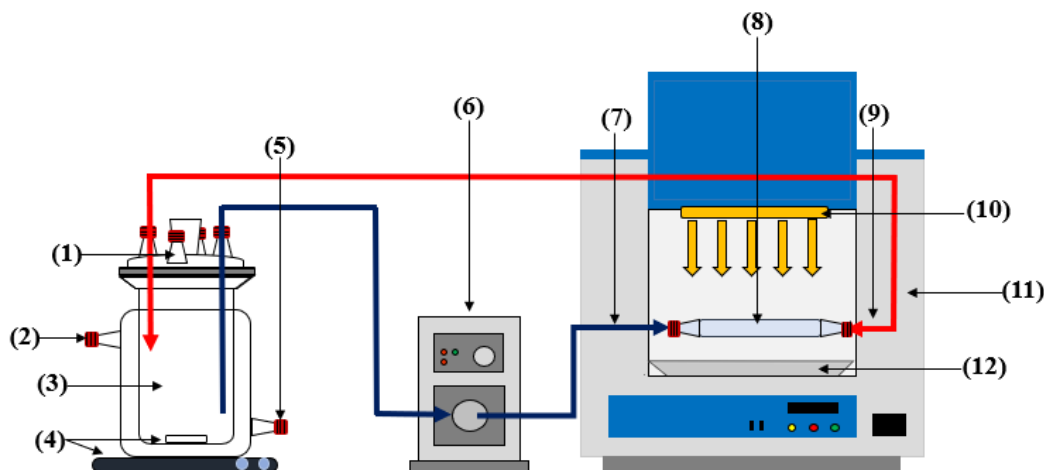


Figure 12. Solar simulator photoreactor scheme. (1) Sampling point; (2) Thermostatic bath-inlet port; (3) Feeding tank; (4) Magnetic stirrer; (5) Thermostatic bath-outlet port; (6) Peristaltic pump; (7) Recirculation inlet port; (8) Tubular photoreactor; (9) Recirculation outlet port; (10) Xenon lamp; (11) Solar simulator chamber; (12) Parabolic mirror.

3.4 Analyses

3.4.1 Actinometrical measures

The incoming photon flow to the solution was quantified through actinometric experiments according to the emission wavelength range of the lamps. In all experimental devices it was measured by actinometrical method based on *o*-Nitrobenzaldehyde reaction [137, 138, 139] adapting the method proposed by Willet and Hites [140]. This actinometer is considered suitable for these tests since absorbs radiation in the range from 290 to 400 nm. This range encloses the emission wavelength of different lamps and LEDs employed in the experimental devices.

The value of incident irradiation obtained by actinometric experiments was used to calculate the accumulated energy per volume (Q_{acc} , kJ L^{-1}). This parameter was employed in Parts IV-VI to plot the degradation of micropollutants and bacterial inactivation (where applicable) vs. Q_{acc} , which was determined according to Eq. 1 [141].

$$Q_{acc} = \sum_{i=1}^n \frac{I \cdot \Delta t_i}{V} \quad (\text{Eq. 1})$$

I is the irradiation entering the photoreactor (kJ s^{-1}), $\Delta t_i = t_i - t_{i-1}$ is the increment of the reaction time (s) and V is the reaction volume (L).

3.4.2 Acute toxicity: Microtox[®] bioassay

The ecotoxicity evolution of the treated water samples was evaluated through Microtox[®] toxicity bioassay. Microtox[®] M500 analyzer by Modern Water (UK) was used on that purpose. This technique is based on the detection of the acute effects caused by diverse substances contained in water. Microtox[®] bioassay employs the marine bioluminescent bacteria *Vibrio fischeri*, which experiences a luminescent reduction in response to the presence of toxic compounds. The bacterial bioluminescence reaction is linked to the electron transport in cellular respiration and it is indicative of the metabolism state of the cell, so that a decrease in bioluminescence indicates decreasing in cellular respiration. To perform the analysis the protocol recommended by the manufacturer was rigorously followed. The results were expressed as $1/EC_{50}$, being EC_{50} the value of the sample dilution that causes 50% of the bioluminescent emission reduction after 15 min of contact.

3.4.3 Alkalinity

The alkalinity of wastewater samples was measured employing an automatic titration method (pH Burette 24) coupled with a Basic 20 pH meter, both by CRISON (Spain). Hydrochloric acid (0.1 M) was used and pH 4.3 as endpoint was fixed in the titration. This technique allows to measure the capacity of water for neutralizing acids. In wastewater, the alkalinity is mainly associated to the bicarbonate (HCO_3^-) and carbonate (CO_3^{2-}) species. However, the presence of other buffering species (*i.e.*, ammonia, hydroxide, phosphate and sulfate) can also increase the alkalinity.

3.4.4 Assessment of Effluent Organic Matter fractions

Dissolved Effluent Organic Matter fractions were quantified by means of Size Exclusion Chromatography equipped with Organic Carbon Detection (SEC-OCD). This measurement combined with UV and Organic Nitrogen Detection (OND) was used in the identification and quantification of organic fractions listed in Table 13 [142, 143]. Samples were filtered through 0.45 μm PTFE membranes to obtain dissolved EfOM. Analyses were conducted in collaboration with the R&D Department of ACCIONA Agua. This technique provides information about chemical nature of water organic species.

Table 13. Characteristics of dissolved Effluent Organic Matter fractions [142].

Dissolved EfOM fraction	Molecular Weight	Characteristics
Biopolymers (BP)	> 50000- 2000000	<ul style="list-style-type: none"> Hydrophilic character and not UV-absorbing. Linked to amino acids and proteins.
Humic substances (HS)	100-100000	<ul style="list-style-type: none"> Combination of humic and fulvic acids, in varying concentrations.
Building Blocks (BB)	350-500	<ul style="list-style-type: none"> By-products of fluvic acids and precursors of LMWA.
Low Molecular Weight Acids (LMWA)	< 350	<ul style="list-style-type: none"> Final degradation products of organics. Also liberated by algae and bacteria.
Low Molecular Weight Neutrals and Amphiphilics (LMWN)	<350	<ul style="list-style-type: none"> Slightly hydrophobic character, like alcohols, aldehydes, ketones and amino acids.

3.4.5 Bacterial enumeration

For the quantification of colony-forming-units present in samples during the oxidation experiments the pour plate method was employed. Wild *Escherichia coli* and *Coliform* bacteria present in the secondary effluents from WWTP were selected as a microbial target. 1 mL of sample was placed in the center of Petri dish (100 mm x 10 mm). When dilutions of the sample were required, buffered peptone water was used to perform serial dilutions (1 mL of sample in 9 mL of broth). Approximately 15 mL of Chromocult® Coliform Agar was then poured into the Petri dish and mixed well with the sample aliquot. Chromocult® Coliform Agar allows the simultaneous detection of the two bacteria from the colony coloration, where *E.coli* presents blue-dark-violet colonies and *Coliform* bacteria gives cherry-red colonies. Once the agar was solidified, the plate was inverted and incubated at 37° for 24 hours. Sterile material was always used, and analyses were performed in a cabinet to avoid any contamination. Catalase from bovine liver was added to the samples (200 mg L⁻¹, 10 µL in 5 mL of sample) to remove residual H₂O₂.

Bacterial regrowth was also evaluated at the end of the treatment. This parameter is important in wastewater reuse since water is not poured out immediately after being treated. Consequently, if the damage in bacteria is repairable, they can reproduce decreasing the

quality of treated water. Regrowth-on-the-plate was used on that purpose. Quantification of new CFU was carried out after incubation of 48 and 72 hours at 37 °C.

3.4.6 Biochemical Oxygen Demand

The evaluation of Biochemical Oxygen Demand at five days was carried out according to Standard Methods 5210 D by respirometry analysis [144]. This technique provides direct quantification of oxygen consumed by microorganisms in a sealed vessel under constant stirring and fixed temperature at 20 °C for 5 days. OxiTop[®] manometric system was used as a diagnostic tool. This relates the oxygen uptake to the change in pressure due to the consumption of oxygen keeping constant volume. The value of respirometry analysis is always compared with control test performed with ultrapure water. The analysis consists on following steps:

a) Chemical Oxygen Demand evaluation to obtain the volume of BOD sample, b) seed (lyophilized capsules 5466-00, Cole-Parmer) aeration for 2 hours, c) sample preparation adding the appropriate volume of nutrients and a specific volume of the seed supernatant (detailed in the corresponding Standard Methods), d) magnetic stirrer and two pellets of NaOH addition, e) bottles closure with OxiTop[®] and its preparation to read the oxygen value, f) incubation at 20 °C and constant stirring.

3.4.7 Chemical Oxygen Demand

The Chemical Oxygen Demand was determined following the Standard Methods 5220D procedure [144]. This technique evaluates the equivalent amount of oxygen required to oxidize organic species contained in a water sample through strong oxidizing agents. It provides an indirect measurement of the organic load content in a water sample. 2.5 mL of sample were mixed with 1.5 mL of potassium dichromate solution (4 mM with 25 g L⁻¹ of HgSO₄) and 3.5 mL of silver sulfate solution (10 g L⁻¹ in H₂SO₄). The mixture was digested at 150 °C for 2 hours. Mercuric sulfate was added to avoid any interference originated by chloride anion. Organic compounds are oxidized and, consequently, Cr⁶⁺ is reduced to Cr³⁺. Once the sample is cold, this Cr⁶⁺ reduction, which is proportional to the oxidation, was evaluated by measuring absorbance at 410 nm (low COD protocol) with an Odyssey DR2500 UV-Vis spectrophotometer (Hach, USA).

3.4.8 Dissolved iron determination

Ferrous iron (Fe(II)) was evaluated by the complexation with 1,10-phenantroline according to standardized procedure (ISO 6332) (International Organization for Standardization 1988). 4 mL of sample were mixed with 1 mL of phenanthroline solution (1 g L^{-1}) and 1 mL of acetic/acetate buffer (62.5 g of ammonium acetate are dissolved in 175 mL of acetic acid and flushed until 250 mL with ultrapure water). The complex takes a red color, which was measured by a spectrophotometer (Hach Lange DR 6000) at 510 nm. The concentration of ferrous iron is proportional to the absorbance and was determined from a calibration curve (absorbance - concentration) previously prepared. Total iron (Fe_{tot}) concentration was evaluated after ferric iron reduction to ferrous form by ascorbic acid. From the difference between total and ferrous iron, it was obtained the concentration of ferric iron (Fe(III)). In the experiments performed with iron chelates at circumneutral pH, since the iron is already chelated, the differentiation between ferrous or ferric forms it is not possible. Thus, only total iron can be measured. In that cases, samples were filtered with $0.20 \mu\text{m}$ PVDF filter to ensure a good read of soluble (chelated and not) iron.

3.4.9 Hydrogen peroxide concentration

The measurement of hydrogen peroxide content was done by a metavanadate colorimetric method [145]. 1.5 mL of sample was mixed with 1.5 mL of ammonium metavanadate solution (5.14 g L^{-1}) in acidic medium ($19.2 \text{ mL H}_2\text{SO}_4 \text{ L}^{-1}$). The formation of peroxovanadium cation by reaction (reaction 25) presents an orange coloration which was measured by spectrophotometer (Hach Lange DR 6000) at 450 nm. The concentration of H_2O_2 was determined from a calibration curve since the proportionality between the absorbance and concentration.



3.4.10 Model micropollutants concentrations

The evolution of micropollutants concentration during the oxidation experiments was quantified by High Performance Liquid Chromatography with ultraviolet detection (HPLC-UV). A 1260 Infinity HPLC by Agilent Technologies (USA) provided with a Diode Array Detector (DAD) was employed. Depending on the selected micropollutant and the range of concentrations to analyze, the HPLC conditions may vary. The characteristics of different

methods used are detailed below. In all cases, a Mediterranea Sea 18 column (250 mm x 4.6 mm, 5 μm size packaging) by Teknokroma (Spain) was employed. The mobile phases were acetonitrile and ultrapure water acidified with orthophosphoric (pH 3) in different volumetric proportions depending on the method. All samples were filtered through 0.45 μm PTFE membranes before the analysis. Catalase from bovine liver was added to the samples (200 mg L^{-1} , 10 μL in 5 mL of sample) to remove residual H_2O_2 .

Experiments Part I: for the analysis of DPH, a mixture of 30% ACN and 70% acidified ultrapure water were used. Flow rate was set at 1.2 mL min^{-1} , UV absorption was fixed at 220 nm and 50 μL of injection volume was employed.

Experiments Parts II and III: for the quantification of PROP, 25% ACN and 75% acidified ultrapure water were employed. UV absorption was set at 214 nm and 0.7 mL min^{-1} was fixed as a flow rate. 10 and 100 μL of injection volume were employed in Appendix II and III, respectively, since the initial PROP concentration to determine was different.

Experiments Parts IV and V: for the simultaneous determination of PROP, SMX and ACMP, an isocratic method was used with mixture of 20% ACN and 80% acidified ultrapure water, 100 μL of injection volume and 1 mL min^{-1} of flow rate. UV absorbances were set at 214, 250 and 270 nm for PROP, ACMP and SMX, respectively.

Experiments Part VI: for the analysis of SMX, mixture of 60% ACN and 40% ultrapure water at acid pH was employed, with 1 mL min^{-1} as a flow rate, 100 μL as injection volume and 270 nm of UV absorbance.

3.4.11 Oxidation intermediates

HPLC-UV equipped with Mass Spectrometry (MS) was employed in the identification of oxidation intermediates. An Electrospray-Ionization-Time-of-Flight (ESI-TOF) MS system (Agilent G1969A) coupled in sequence to a 1100 HPLC by Agilent fitted up with a DAD, was used for that purpose. Analyses were conducted in Scientific and Technological Centers of the Universitat de Barcelona in collaboration with the Molecular Characterization Mass Spectrometry Unit.

3.4.12 Phytotoxicity

Phytotoxicity was evaluated by means of seeds of *Eruca sativa* (arugula) and *Lactuca sativa* (lettuce) according to the procedure by US EPA Protocol [146], and adapting the method proposed by Tam and Tiquia [147]. This method evaluates the suitability of the reused water or compost for agricultural purposes. It is one of the most important parameters to avoid environmental risks associated to water reuse. The evaluation of the germination index (GI), which includes measures of relative seed germination (SG, %) and root growth (RG, %), is used to determine the phytotoxicity grade. These parameters were calculated according to Eq. 2-4.

$$\% SG = \frac{n^{\circ} \text{ seeds germinated in the sample}}{n^{\circ} \text{ seeds germinated in the control}} \times 100 \quad (\text{Eq. 2})$$

$$\% RG = \frac{\text{mean root length in the sample}}{\text{mean root length in the control}} \times 100 \quad (\text{Eq. 3})$$

$$GI = \frac{\% \text{ seed germination} \times \% \text{ root growth}}{100} \quad (\text{Eq. 4})$$

To perform the analysis, 4 mL of sample were added to 100 x 10 mm culture plate, which contained 1 filter paper and 10 ecological seeds of the same plant (arugula or lettuce). The plates were incubated at 22 °C, without light, for 5 days. Control test was always carried out with distilled water. After this time, the number of seeds germinated in the sample and the control were counted to evaluate the percentage of SG. In the same way, the mean root length (cm) in both sample and control was measured to determine the percentage of RG.

To determine the phytotoxicity grade by means of GI, Zucconi and coworkers [148, 149] proposed different categories:

- Inhibition of seed germination and root elongation: <20 GI.
- Presence of phytotoxicity: 20-50 GI.
- No significant injury to the plant: >50-60 GI.
- Disappearance of phytotoxicity: >80-85 GI.
- Stimulation of the root elongation: >100 GI (better than control, which represent 100 of GI).

3.4.13 Total Organic Carbon

The quantification of Total Organic Carbon content was performed following the Standard Methods 5310 B procedure [144] and employing a 5055 TOC-VCSN analyzer equipped with an ASI-V autosampler, both by Shimadzu (Japan). Three steps are required for the analysis. In the first one, the inorganic carbon is removed by sample acidification (HCl, 2 M), followed by air bubbling. Then, at 680 °C, the catalytic combustion of the sample takes place. Finally, the quantification of CO₂ occurs. The same process was used for the determination of Dissolved Organic Carbon (DOC) with previous sample filtration by 0.45 μm syringe filters.

3.4.14 Turbidity

The turbidity was quantified according to Standard Methods 2130B procedure [144]. Portable turbidimeter Hach 2100P was used on that purpose. This parameter is understood as the degree of transparency that water loses due to presence of suspended particles and/or colloidal matter. In wastewater treatment, the turbidity is considered a good parameter to determine the water quality, the higher the turbidity the lower the quality.

3.4.15 Ultraviolet absorbance

The ultraviolet absorbance was evaluated through a spectrophotometer DR6000 UV-Vis by Hach (USA). All dissolved organic matter presents an indicative absorbance so that this parameter is typically used in the water and wastewater characterization. Especially, ultraviolet absorbance at 254 nm (UV₂₅₄) is characteristic of the level of unsaturated carbon bonds of organic compounds (aromaticity). Measurements at 254 nm were always carried out for wastewater characterization and wavelength scans in the range of 200-400 nm were also performed in experiments of Part VI for Fe-complexes.

4 Results and discussion

In this section, it is presented a summary of the most relevant results obtained in this thesis. As explained in section 2.1, results and discussion were divided in three subsections (4.1,4.2 and 4.3) and six Parts, corresponding to each one of the articles published (or submitted) with the results obtained in this thesis. Thus, subsection 1 includes only Part I, dedicated to the use of LEDs in photo-Fenton. Subsection 4.2 also includes only Part II devoted to the comparison between LEDs and BLBs. Finally, subsection 4.3 includes 6 articles (Parts III - VI) dedicated to the study of the application of fertilizers as chelating agents in photo-Fenton.

4.1 Synergies, radiation and kinetics in photo-Fenton process with UV-A LEDs

A summary of the experiments displayed in Part I is detailed in Table 14, including the operational conditions, performance, as well as the figure within the publication where each experiment is located.

Table 14. Summary of the experiments presented in Part I.

Test	Target	[Reagents]	Irradiation	Matrix	pH	Performance	Figure in publication
Influence of reagent's concentrations							
A1	[DPH] = 50 mg L ⁻¹	[Fe ²⁺] = 10 mg L ⁻¹ [H ₂ O ₂] = 150 mg L ⁻¹	No	Ultrapure water	2.8	Total DPH removal in 45 min	Figure 1A
A2	[DPH] = 50 mg L ⁻¹	[Fe ²⁺] = 10 mg L ⁻¹ [H ₂ O ₂] = 25 mg L ⁻¹	No	Ultrapure water	2.8	95% of DPH removal in 60 min	Figure 1A
A3	[DPH]= 50 mg L ⁻¹	[Fe ²⁺] = 2.5 mg L ⁻¹ [H ₂ O ₂] = 150 mg L ⁻¹	No	Ultrapure water	2.8	30% of DPH removal in 60 min	Figure 1A
A4	[DPH]= 50 mg L ⁻¹	[Fe ²⁺] = 2.5 mg L ⁻¹ [H ₂ O ₂] = 25 mg L ⁻¹	No	Ultrapure water	2.8	40% of DPH removal in 60 min	Figure 1A

Table 14. (continued)

Test	Target	[Reagents]	Irradiation	Matrix	pH	Performance	Figure in publication
Two wavelength ranges of LEDs							
A5	[DPH] = 50 mg L ⁻¹	[Fe ²⁺] = 10 mg L ⁻¹ [H ₂ O ₂] = 150 mg L ⁻¹	4 LEDs 380-390 nm on the cover	Ultrapure water	2.8	Total DPH removal in 30 min	Figure 1B
A6	[DPH] = 50 mg L ⁻¹	[Fe ²⁺] = 10 mg L ⁻¹ [H ₂ O ₂] = 25 mg L ⁻¹	4 LEDs 380-390 nm on the cover	Ultrapure water	2.8	97% of DPH removal in 60 min	Figure 1B
A7	[DPH] = 50 mg L ⁻¹	[Fe ²⁺] = 2.5 mg L ⁻¹ [H ₂ O ₂] = 150 mg L ⁻¹	4 LEDs 380-390 nm on the cover	Ultrapure water	2.8	65% of DPH removal in 60 min	Figure 1B
A8	[DPH] = 50 mg L ⁻¹	[Fe ²⁺] = 2.5 mg L ⁻¹ [H ₂ O ₂] = 25 mg L ⁻¹	4 LEDs 380-390 nm on the cover	Ultrapure water	2.8	52% of DPH removal in 60 min	Figure 1B
A9	[DPH] = 50 mg L ⁻¹	[Fe ²⁺] = 10 mg L ⁻¹ [H ₂ O ₂] = 150 mg L ⁻¹	4 LEDs 390-400 nm on the cover	Ultrapure water	2.8	Total DPH removal in 30 min	Figure 1C
A10	[DPH] = 50 mg L ⁻¹	[Fe ²⁺] = 10 mg L ⁻¹ [H ₂ O ₂] = 25 mg L ⁻¹	4 LEDs 390-400 nm on the cover	Ultrapure water	2.8	98% of DPH removal in 60 min	Figure 1C
A11	[DPH] = 50 mg L ⁻¹	[Fe ²⁺] = 2.5 mg L ⁻¹ [H ₂ O ₂] = 150 mg L ⁻¹	4 LEDs 390-400 nm on the cover	Ultrapure water	2.8	85% of DPH removal in 60 min	Figure 1C
A12	[DPH] = 50 mg L ⁻¹	[Fe ²⁺] = 2.5 mg L ⁻¹ [H ₂ O ₂] = 25 mg L ⁻¹	4 LEDs 390-400 nm on the cover	Ultrapure water	2.8	47% of DPH removal in 60 min	Figure 1C
Combination of two wavelength ranges							
A13	[DPH] = 50 mg L ⁻¹	[Fe ²⁺] = 10 mg L ⁻¹ [H ₂ O ₂] = 150 mg L ⁻¹	2 LEDs 380-390 nm and 2 LEDs 390-400 nm on the cover	Ultrapure water	2.8	Total DPH removal in 15 min	Figure 3A

4.1.1 Determination of effective concentrations

The concentration of Fenton reagents and the ratio between iron and hydrogen peroxide are the critical parameters for the Fenton and photo-Fenton processes efficiency. Thus, four sets of iron and H_2O_2 concentrations were tested. A concentration of 10 and 2.5 mg L^{-1} of Fe^{2+} were combined with 150 and 25 mg L^{-1} of H_2O_2 and the ratios $\text{Fe}^{2+}:\text{H}_2\text{O}_2$ were 1:15; 1:2.5; 1:60 and 1:10 (wt/wt). Typical ratios range between 1:5 and 1:25, hence two ratios were selected within this range and other two out of range. From the results A1-A4, it was observed that the best performances, in DPH removal by Fenton, were achieved with 1:15 and 1:2.5 $\text{Fe}^{2+}:\text{H}_2\text{O}_2$ ratios (experiments A1 and A2 respectively). A1 and A2 also corresponds to the experiments with higher iron concentration (10 mg L^{-1}) evidencing the importance of initial iron concentration. Although the ratio 1:2.5 was out of typical range, it was close to that not affecting greatly to the efficiency of the process. The experiments A3 and A4 were carried out with the lowest iron concentration (2.5 mg L^{-1}) and they achieved similar DPH abatement though the hydrogen peroxide was 6 times higher in A3 than A4. In that case, the ratios $\text{Fe}^{2+}:\text{H}_2\text{O}_2$ were 1:60 and 1:10 for A3 and A4, respectively, evidencing again that the ratio is critical for the process efficiency. Probably, in experiment A3 hydroxyl radicals scavenging by H_2O_2 was took place. Comparing the four tests, it was concluded that initial iron concentration is more critical than initial hydrogen peroxide concentration.

Photo-Fenton experiments with LEDs located at the cover of the photoreactor, using 380-390 nm (A5-A8) and 390-400 nm (A9-A12), achieved higher DPH degradations than Fenton, as expected due to the photoreduction of Fe^{3+} to Fe^{2+} leading the formation of more hydroxyl radicals. Experiments with 10 mg L^{-1} of iron achieved the best performances like in Fenton process. With 10 mg L^{-1} of Fe^{2+} and 150 mg L^{-1} of H_2O_2 , total DPH removal was obtained at 30 min, reducing 15 min treatment time compared to Fenton process. The major difference was observed using 2.5 mg L^{-1} of Fe^{2+} and 150 mg L^{-1} of H_2O_2 . In photo-Fenton process, at equal initial iron concentration, higher initial hydrogen peroxide led to a greater DPH degradation. This fact is due to the redox cycle of $\text{Fe}^{3+}/\text{Fe}^{2+}$ was accelerated by light, implying the presence of more Fe^{2+} during the reaction which can reacts with H_2O_2 and avoiding the scavenger of hydroxyl radicals.

4.1.2 Synergistic effects with two wavelengths combination

The employment of LEDs as irradiation source to perform the photo-Fenton process more efficiently needs investigation about its potential application. The efficiency of the use of

two near ranges of wavelengths was investigated in the previous section achieving better performances than Fenton process. However, the difference between two ranges were low, as expected because they were very close. To investigate possible enhancements, the combinations of two ranges were carried out maintaining the total nominal power (4.2 W), equal than one range was tested. A concentration of 10 mg L⁻¹ of Fe²⁺ and 150 mg L⁻¹ of H₂O₂ were selected because they presented the best performances. On that purpose, 2 LEDs in the range of 380-390 nm and 2 LEDs in the range of 390-400 nm were combined. The results of DPH removal indicated synergies in the combination. Thus, using 380-400 nm, DPH removal was obtained in 15 min, reducing by half the treatment time than experiments without combination and 30 min compared to Fenton process. In the case of photo-Fenton experiments, shorter treatment time also means lower cost, which makes the process more effective.

The enhancement observed combining two wavelength ranges was also evaluated for COD and TOC removal. Average Oxidation State (AOS) comparing three ranges was also evaluated. This indicator takes values between +4 (value for CO₂, state of maximum oxidation of carbon) and -4 (value for CH₄, state of maximum reduction). Table 15 displays the results of these parameters for the experiments A5, A9 and A13.

Table 15. Values of AOS, COD and TOC for the experiments A5, A9 and A13.

Test	AOS	COD	TOC
A5 (380-390 nm)	2.4	70.2	54.2
A9 (390-400 nm)	2.7	79.9	60.5
A13 (380-400 nm)	3.8	95.6	70.1

As can be observed in Table 15, the combination of two wavelengths (experiment A13), presented higher values for the three parameters, maintaining the same nominal power and only increasing the range from 10 nm to 20 nm. Although this is a basic study, it evidences the potential enhancement by the combination of selected wavelength ranges for a specific treatment. This fact is characteristic of LEDs since conventional lamps present a fixed extended range containing wavelengths useless for the treatment. Further investigations are required in this field to promote the replacement of conventional lamps for a sustainable alternative.

4.1.3 By-product's determination

HPLC-MS analyses allowed the identification of oxidation compounds of DPH for two pairs of Fe^{2+} and H_2O_2 concentrations (10 mg L^{-1} of Fe^{2+} and 150 mg L^{-1} of H_2O_2 - 2.5 mg L^{-1} of Fe^{2+} and 25 mg L^{-1} of H_2O_2). These tests were selected to bring out the importance of initial reagents concentrations not only for the degradation of a selected micropollutant, otherwise also to reach the mineralization. This fact is important due to the toxicity of some by-products may be higher than the initial compound.

Three oxidation products were found with 2.5 mg L^{-1} of Fe^{2+} and 25 mg L^{-1} of H_2O_2 (DPH-272, DPH-288 and DPH-322) while with 10 mg L^{-1} of Fe^{2+} and 150 mg L^{-1} of H_2O_2 were found four intermediates, those described before and DPH-183, which is a secondary intermediate probably from DPH-272 (see Figure 4 from publication Part I). This difference was related to the DPH initial degradation. In the last case, total removal was achieved in 30 min, while with 2.5 mg L^{-1} of Fe^{2+} only about 50% was degraded in 60 min. This fact allows the degradation of the three primary oxidation products and the formation of one secondary intermediate, in this case from the primary by-product DPH-272, when 10 mg L^{-1} of Fe^{2+} were used. However, this fact not occurred with 2.5 mg L^{-1} of Fe^{2+} , since there was still initial DPH in the solution at probably higher concentration than intermediates, hence hydroxyl radicals react greatly with initial compound. Figure S3 of additional material of Part I presents the proposed pathways and Table S1 displays information about detected oxidation intermediates.

Part I

Synergies, radiation and kinetics in photo-Fenton process with UVA-LEDs

Núria López-Vinent, Alberto Cruz-Alcalde, Luis Eduardo Romero, Marcelo Eduardo Chávez, Pilar Marco, Jaime Giménez, Santiago Esplugas

Department of Chemical Engineering and Analytical Chemistry, Faculty of Chemistry, University of Barcelona, C/Martí i Franqués 1, 08028 Barcelona, Spain.

Published in *Journal of Hazardous Materials* 380 (2019) 120882



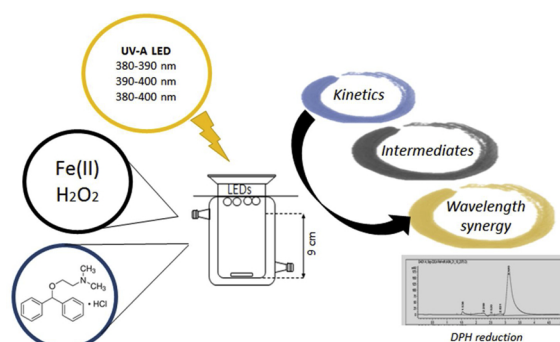
Synergies, radiation and kinetics in photo-Fenton process with UVA-LEDs

N. López-Vinent, A. Cruz-Alcalde, L.E. Romero, M.E. Chávez, P. Marco, J. Giménez*, S. Esplugas

Department of Chemical Engineering and Analytical Chemistry, Faculty of Chemistry, Universitat de Barcelona, C/Martí i Franqués 1, 08028, Barcelona, Spain



GRAPHICAL ABSTRACT



ARTICLE INFO

Editor: L. Eder

Keywords:

Synergy wavelength
UV-A LED
Photo-Fenton
Intermediates
Kinetics

ABSTRACT

The photo-Fenton process, with UV-A LED ($\lambda = 380\text{--}390, 390\text{--}400$ and $380\text{--}400$ nm) has demonstrated to be effective in the abatement of a target micropollutant, such as diphenhydramine hydrochloride (DPH). Different concentrations of iron (Fe^{2+}) and H_2O_2 were tested and monitored, and the best results in DPH removal were obtained for the highest concentrations of both iron (II) and H_2O_2 ($10 \text{ mg Fe}^{2+}/\text{L} - 150 \text{ mg H}_2\text{O}_2/\text{L}$). The evolution of iron and peroxide concentration was also monitored. Kinetic studies showed that dark Fenton process prevails at the beginning of the experiment, when Fe^{2+} concentration is higher. However, after these initial moments, the prevailing process is photo-Fenton and, in addition, wavelength radiation plays an important role. Concerning the effect of radiation, four LEDs (4.2 W total power) were used, emitting radiation in the wavelength range between $380\text{--}390$ or $390\text{--}400$ nm. Similar results were obtained in both cases in DPH removal by photo-Fenton (30 min for total elimination). However, a synergistic effect was observed when two LEDs of $380\text{--}390$ nm and two LEDs of $390\text{--}400$ nm were used. Total power was the same (4.2 W) in each experimental condition, but the increase in the wavelength range to 20 nm ($380\text{--}400$ nm) produces an increase in the rate of DPH removal, achieving its total elimination at 15 min. This fact, with the use of a simple radiation model, reveals the important role that radiation plays in the photo-Fenton process. Finally, the formed intermediates were determined and some reaction pathways were proposed.

1. Introduction

Micropollutants (MPs), especially pharmaceuticals, have been an increasing concern due to their biorecalcitrant character. Because of

that property, MPs are not completely eliminated during conventional wastewater treatments (Verlicchi et al., 2010). Moreover, they potentially affect human health as a consequence of long-term exposure (Gebhardt and Schroder, 2007). Important amounts of pharmaceuticals

* Corresponding author.

E-mail address: j.gimenez.fa@ub.edu (J. Giménez).

<https://doi.org/10.1016/j.jhazmat.2019.120882>

Received 4 March 2019; Received in revised form 6 June 2019; Accepted 8 July 2019

Available online 13 July 2019

0304-3894/ © 2019 Elsevier B.V. All rights reserved.

are used, but there is little concern about the final disposal of these drugs. In Deo's study (Deo, 2007), a risk index (RQ) was calculated for numerous micropollutants, related to the impact on the aquatic ecosystem. According to RQ, pharmaceuticals are classified in three categories: high risk ($RQ \geq 1.0$), medium risk ($1.0 > RQ \geq 0.1$) or low risk ($RQ < 0.1$). In this work, the pharmaceutical diphenhydramine hydrochloride (DPH), with RQ 0.39, has been chosen as a model compound. DPH is an antihistaminic drug that has been detected in surface waters in concentrations around 1.40 $\mu\text{g/L}$.

Advanced Oxidation Processes (AOPs) are effective options for the removal of emerging and recalcitrant contaminants from wastewaters (Comminellis et al., 2008; Kumar and Bansal, 2013; Wankhade et al., 2013; Primo et al., 2008a, b; Lee and Park, 2013). Among AOPs, the photo-Fenton process has demonstrated to be effective in the abatement of MPs. In this process, a catalytic cycle with iron (II and III), hydrogen peroxide (H_2O_2) and ultraviolet (UV) light are combined to generate hydroxyl radicals ($\text{HO}\cdot$) (Pignatello and MacKay, 2006).

Photochemical processes present several disadvantages due to the cost and electrical consumption of the UV lamps (Carra et al., 2015). Numerous studies based on AOPs use mercury lamps as a source of UV light, presenting diverse drawbacks, like high power consumption (Autin et al., 2013) and a low lifetime and overheating problems (Xiong and Hu, 2012; Verma and Sillanpää, 2015). In addition, they present problems associated with its disposal (Tayade et al., 2009; Würtele et al., 2011) due to the mercury content. In this sense, the Minamata Convention on Mercury has been approved by 128 countries in an attempt to remove mercury from several products and methods by 2020 (Matafonova and Batoev, 2018).

Due to all these disadvantages, UV light-emitting diodes (UV-LEDs), as potential substitutes, have been tested in numerous studies with AOPs (De la Obra et al., 2017; Chevremont et al., 2012). Contrary to traditional mercury lamps, UV-LEDs offer low energy consumption, long lifetime, small size, no mercury content, no problems associated with overheating and the possibility of selecting specific wavelengths and reaction configurations according to particular needs (Moreira et al., 2016; Rasoulifard et al., 2015). In spite of the numerous advantages that LEDs may provide, the use of mercury lamps is still a cheaper option nowadays as conventional lamps are really efficient in the conversion of electricity to light. Thus, improvements in the efficiency and power are required to apply LED radiation sources in AOPs. Hölz and coworkers (Hölz et al., 2017) studied the replacement of mercury lamps by LEDs in photochemistry applications. A comparison in terms of consumption and costs was conducted between both radiation sources. The investigation revealed that electricity (kWh/year) (value of 30 instead of 2600 kWh/year in LEDs and mercury lamps, respectively), initial cost (€) (12,000 € for LEDs and 1500 € for mercury lamps) and consumables (€/year) (50 €/year for LEDs instead 2400 €/year for mercury lamps) could be potentially lower in LEDs than in mercury lamps, provided that the type of LED technology required in the photochemistry area is upgraded in terms of energy conversion efficiency.

The aim of this study was to test the efficiency of UV-A LED photo-Fenton process in DPH degradation. The effect of hydrogen peroxide (H_2O_2) and initial iron (Fe^{2+}) concentrations on DPH removal was studied. LEDs with different wavelength ranges (380–390 nm and 390–400 nm) were used and the synergistic effect was also studied and explained by using a simple radiation model. Additionally, reaction pathways were proposed according to detected reaction intermediates. Although the application of photo-Fenton for MPs abatement is currently a hot research topic, further research including the use of LEDs is still needed for process intensification. In this work, the use of two wavelengths has been evaluated, and potential synergistic effects explored. The study of synergistic effect is a novel part of this paper because this is not a common topic when LEDs are used. In addition, the novelty of this work is based on the kinetic studies, which were divided in two parts. In our opinion, this double fitting contributes also to the

originality of the paper, because the interaction kinetics-radiation becomes clear and is reflected in the fittings made. This type of studies relating kinetics and radiation, and also linking it with the predominance of Fenton or photo-Fenton, is not customary and therefore represents a novelty in this work.

2. Materials and experimental set-ups

2.1. Chemicals and reagents

Diphenhydramine hydrochloride was used as a target compound. A concentration of 50 mg/L was chosen to simulate a scenario of wastewaters resulting from pharmaceutical industries (Joakim Larrson et al., 2007) and to assure the monitoring of DPH concentrations in High Performance Liquid Chromatography (HPLC) and Total Organic Carbon (TOC). Orthophosphoric acid (Panreac Quimica) and acetonitrile (Fisher Chemical) were employed in (HPLC) analyses. Hydrogen peroxide was acquired from Merck, and ferrous sulfate ($\text{FeSO}_4 \cdot 7\text{H}_2\text{O}$) from Panreac. Ascorbic acid for iron analyses was purchased from Panreac. The initial pH was adjusted with concentrated sulphuric acid (Panreac). Quenching reagents, such as NaHSO_3 and MeOH, were acquired from Panreac and used to stop the reaction after sample withdrawal.

2.2. Experimental device

The experiments were carried out in a 0.5 L Pyrex photoreactor (inner diameter 8 cm, height 12 cm, supplementary information - Fig. S1), with a magnetic stirrer. 4 LEDs (Intelligent LED solutions) were located at the top of the reactor. The nominal consumption of each LED is 1.05 W, operating at 350 mA and with a radiance angle of 125° . The wavelength ranges of the used LEDs were 380–390 and 390–400 nm. The nitrobenzaldehyde actinometry was performed to determine the incoming radiation in the UV-LED reactor (Kuhn et al., 2004; Galbavy et al., 2010) and the obtained results appear in Fig. 3B. The temperature is maintained at 25°C by immersion in a Lauda Alpha thermostatic bath.

2.3. Experimental procedure

Degradation of DPH by photo-Fenton was evaluated for one hour, based on previous experiments (López et al., 2017, 2018). The volume of DPH solution was 0.5 L, that means 9 cm of liquid depth in the photoreactor and 3 cm from the liquid level to the top of photoreactor where LEDs are located. Different concentrations of H_2O_2 (25 and 150 mg/L) and Fe^{2+} (2.5 and 10 mg/L) were tested. Four previous experiments, for each wavelength range, were done to determine the optimal concentrations of H_2O_2 and Fe^{2+} (see Fig. 1). These concentrations of peroxide and iron (10 mg/L Fe^{2+} and 150 mg/L H_2O_2) were selected to carry out the rest of the experiments. The pH was adjusted to 2.8 ± 0.2 using H_2SO_4 . Then, the $\text{FeSO}_4 \cdot 7\text{H}_2\text{O}$ was introduced in the solution and, finally, H_2O_2 was added, just before starting the experiment. During one hour samples were taken at different reaction times and analyzed. For Fe^{2+} quantification, 4 mL of each sample were mixed with 1 mL of buffer solution and 1 mL of o-phenantroline (ISO 6322). At the end of the experiment, an excess of ascorbic acid was added at each vial to determine the total iron concentration. The concentration of Fe^{3+} was calculated by the difference between the total iron and the Fe^{2+} concentration. To quantify the H_2O_2 amount, 1.5 mL of each sample were mixed with 1.5 mL of metavanadate (Pupo Nogueira et al., 2005), methanol and sodium hydrogen sulfite were employed to stop the reaction in samples containing H_2O_2 . Samples for TOC (15 mL), COD (Chemical Oxygen Demand) (2.5 mL) and UV_{254} (5 mL) were analyzed only at the initial time and at 60 min in each experiment.

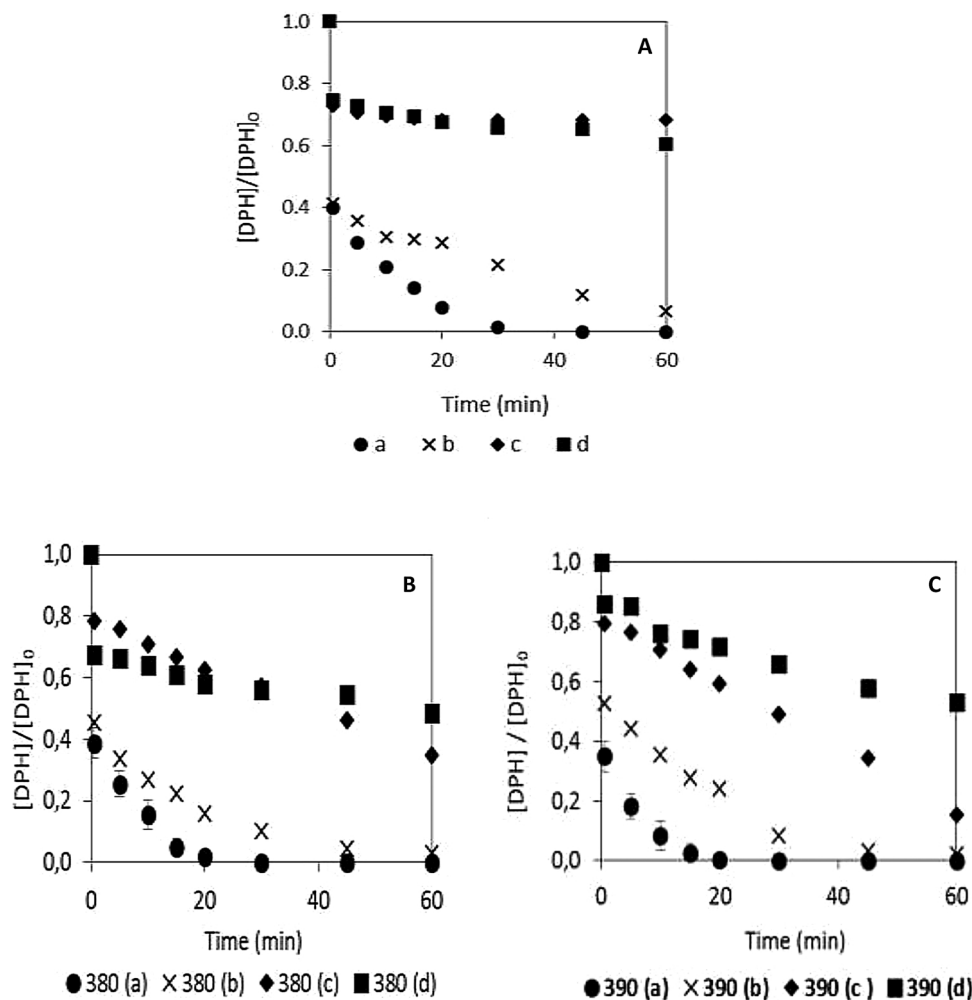


Fig. 1. DPH degradation by (A) Fenton and (B and C) photo-Fenton process. (B) 380–390 nm. (C) 390–400 nm. [DPH] = 50 mg/L. (a) 10 mg Fe^{2+} /L - 150 mg H_2O_2 /L; (b) 10 mg Fe^{2+} /L - 25 mg H_2O_2 /L; (c) 2.5 mg Fe^{2+} /L - 150 mg H_2O_2 /L; (d) 2.5 mg Fe^{2+} /L - 25 mg H_2O_2 /L.

2.4. Analytical methods

DPH was analyzed by an Infinity 1260 HPLC by Agilent with a Teknokroma Mediterranea Sea 18 column (250 × 4.6 mm i.d; 5 μ m particle size). The mobile phases were acetonitrile (30%) and ultrapure water (70%), adjusted with orthophosphoric acid at pH = 3. A flux of 1.2 mL/min was employed, and the UV detector was set at 220 nm. The TOC was measured in a Shimadzu TOC-V CNS apparatus. COD was determined following the Standard Methods (Eaton et al., 2005). UV_{254} was analyzed with a HACH DR6000 UV VIS spectrophotometer. An electrospray ESI-MS and LC/MSD-TOF from Agilent were employed for the identification of reaction intermediates.

3. Results and discussions

Preliminary tests were performed to study the interaction Fe^{2+} -light and H_2O_2 -light, separately. Experiments were carried out with 10 mg/L of Fe^{2+} and 150 mg/L of H_2O_2 . Degradation and mineralization were not observed at any tested interaction. Degradation of DPH by photolysis was also studied and no degradation was observed during 60 min.

3.1. Determination of effective concentrations

Fig. 1 shows the degradation of DPH with different concentrations of hydrogen peroxide and iron II vs. irradiation time. UV-A LEDs emitting in the range 380–400 nm, were used. In Fig. 1A the UV-A LEDs

used emit in the range 380–390 nm. However, in Fig. 1B the radiation selected was 390–400 nm.

In addition, the accumulated energy (Q_{acc} , kJ/L) was estimated for each experiment according to Eq. (1) (De la Cruz et al., 2013; Doumic et al., 2013).

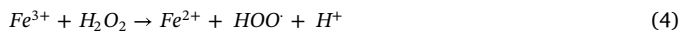
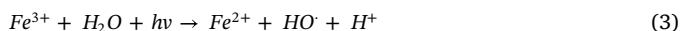
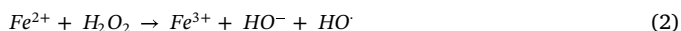
$$Q_{acc} = \sum_{i=0}^n \frac{I \cdot \Delta t_i}{V} \quad (1)$$

I is the incident radiation flow (kJ/s), Δt_i is the increment of the reaction time (s) and V stands for the reaction volume (L).

Thus, the energy accumulated in each experiment was 0.864 kJ/L (Fig. 1B) and 0.936 kJ/L (Fig. 1C), at 60 min.

The comparison of Fig. 1A and B points out that the degradation of DPH is practically the same during the first 30 s. This fact indicates that Fenton is the prevailing process, according to Eq. (2). However, after this initial period (30 s), behavior changes and photo-Fenton becomes faster than Fenton. Thus, in the best conditions (10 mg Fe^{2+} /L and 150 mg H_2O_2 /L), DPH is totally removed in 30 min with photo-Fenton and 45 min are needed to remove completely DPH by Fenton. If the results obtained for the lowest concentrations are analyzed (2.5 mg Fe^{2+} /L and 25 mg H_2O_2 /L), similar results were obtained. Thus, the DPH abatement at first 30 s with photo-Fenton was 32.4% (Fig. 1B) and in the Fenton process was 25.4% (Fig. 1A). Next 30 s of the reaction, according to Eq. (3), the Fe^{3+} is reduced to Fe^{2+} by UV-A LED, producing more hydroxyl radicals, responsible for more DPH removal than in the Fenton process. At 60 min DPH degradation was 51.6% and

39.4% for photo-Fenton and Fenton, respectively (Pulgarin et al., 1999; Carra et al., 2014).



If the wavelength range influence is considered (Fig. 1B and C), it can be observed that time for total DPH removal is the same in both cases (30 min) for the best conditions (10 mg Fe^{2+} /L and 150 mg H_2O_2 /L). The DPH removal is also similar (97.0%, for 380–390 nm, and 97.9%, for 390–400 nm, at 60 min) when 10 mg Fe^{2+} /L and 25 mg H_2O_2 /L were used. However, for the rest of Fe^{2+} and H_2O_2 concentrations tested, the shape of the graphics is close but values are a little different. Thus, the final degradation of DPH (60 min) was similar in both wavelength ranges tested for 2.5 mg Fe^{2+} /L and 25 mg H_2O_2 /L, being 51.6% and 46.9% for 380–390 nm and 390–400 nm, respectively. Differences increase for concentrations of 25 mg Fe^{2+} /L and 150 mg H_2O_2 /L, being DPH removal, at 60 min, 65.1% for 380–390 nm and 84.8% for 390–400 nm. These differences can be explained because radiation and hydrogen peroxide concentration play more important role in the second part of the process, after the initial 30 s, where photo-Fenton (reaction 3) prevails.

If the last values (2.5 mg Fe^{2+} /L and 25/150 mg H_2O_2 /L) are compared with Fenton process (Fig. 1A), as commented before, large differences were observed because in Fenton process, after the initial 30 s, the degradation rate decreases dramatically compared to the

photo-Fenton process (Fig. 1B and C). This fact points out again the important role-played by the light.

Summarizing, from these results it seems that Fe^{2+} plays an important role at the initial moments of the experiment (30 s) and the reaction 2 prevails, that means Fenton is the predominant process and a little synergistic effect of photo-Fenton can aid to DPH degradation. On the contrary, H_2O_2 concentration and light acquire the predominant role during the rest of the experiment, meaning that photo-Fenton prevails (reactions 3 and 4). Moreover, from the shape of graphics presented in Fig. 1, it seems that the influence of Fe^{2+} concentration on the degradation of DPH is higher than the influence of H_2O_2 concentration.

The consumption of hydrogen peroxide confirms all that explained in the previous paragraphs (see Fig. 2A). As expected, the H_2O_2 consumption increased with the iron and hydrogen peroxide concentrations. Thus, for the same concentration of iron (II), when the concentration of hydrogen peroxide increases, its consumption also increases, according to Eqs. (2) and (4). It has also to be said that the same trend was observed in the experiments made in the range 380–390 nm.

Iron evolution was also followed (see Fig. 2B and C). The first observation was that total iron (Fe_{tot}) remained constant during the experiment. For 10 mg Fe^{2+} /L and 150 mg H_2O_2 /L (molar ratio $\text{H}_2\text{O}_2:\text{Fe}^{2+} = 25$), at the first minute, all ferrous iron was almost oxidized to ferric iron. Thus, Fe^{2+} reacts quickly with the hydrogen peroxide to give hydroxyl radicals in large quantity, according to the Eq. (2) and as explained in Section 3.1. This behavior would explain the fast

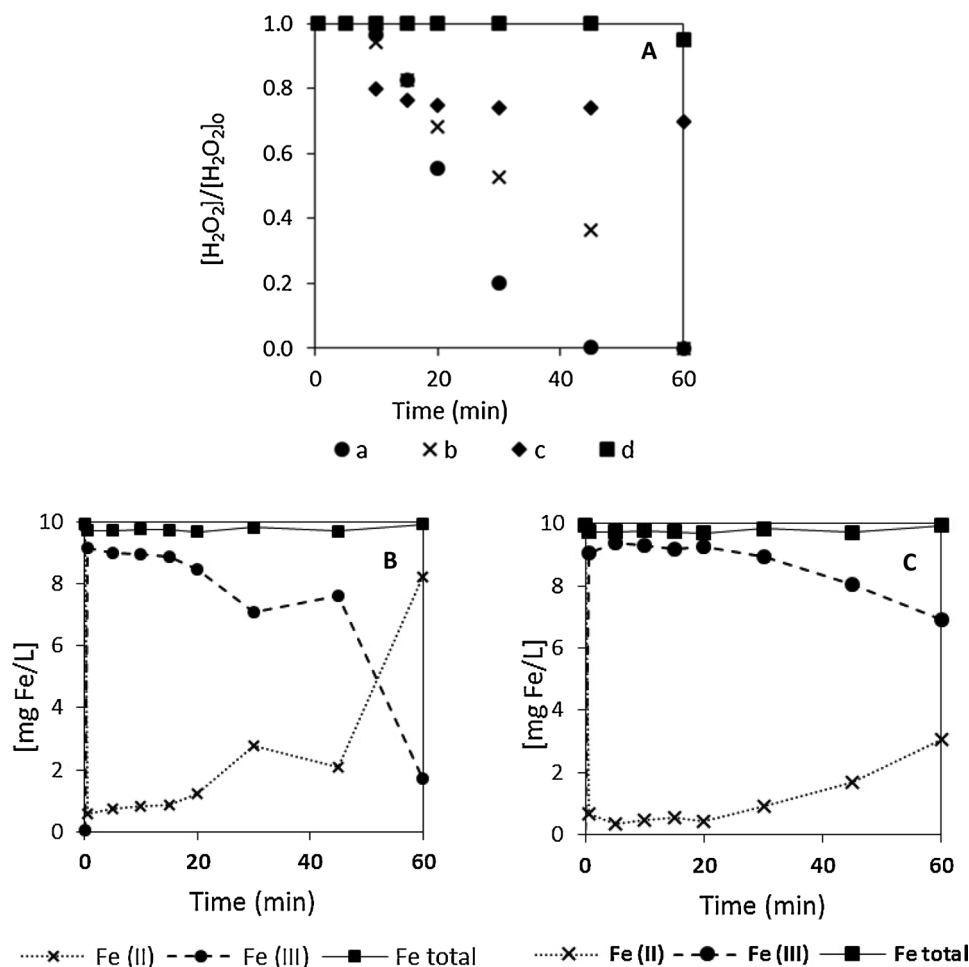


Fig. 2. (A) Hydrogen peroxide consumption in photo-Fenton process. (a) 10 mg Fe^{2+} /L - 150 mg H_2O_2 /L; (b) 10 mg Fe^{2+} /L - 25 mg H_2O_2 /L; (c) 2.5 mg Fe^{2+} /L - 150 mg H_2O_2 /L; (d) 2.5 mg Fe^{2+} /L - 25 mg H_2O_2 /L. (B and C) Species of iron vs. irradiation time. (B) 10 mg Fe^{2+} /L and 150 mg H_2O_2 /L; (C) 10 mg Fe^{2+} /L and 25 mg H_2O_2 /L. The lines show an experimental decay fit and are presented only to appreciate better the behavior of the decay.

decrease in DPH concentration observed during the first 30 s and confirms that Fenton prevails at these initial moments of the experiment (Eq. (2)), as commented before. After that, the Fe^{3+} was reduced to Fe^{2+} step by step in the course of the experiment. The Eq. (3) begins to take place and the photo-Fenton process begins to act. However, for 10 mg Fe^{2+} /L and 25 mg H_2O_2 /L (molar ratio $\text{H}_2\text{O}_2:\text{Fe}^{2+} = 4$), lower iron regeneration was seen, because the excess of hydrogen peroxide is lower and the regeneration of Fe^{2+} from Fe^{3+} (Eq. (4)) is more difficult. A proper ratio between iron (II) and hydrogen peroxide concentrations is fundamental to maximize the $\text{HO}\cdot$ production and thus the good performance of the oxidation process. The generation of hydroxyl radicals is higher when concentration of H_2O_2 and Fe (II) are higher, as commented above (Dogruel et al., 2009; Durán et al., 2011). However, to avoid scavenging effects due to excess amounts of H_2O_2 (because hydroxyl radical can also react with H_2O_2), selecting an optimal dose of this reagent is important. The needed concentrations of the reagents (H_2O_2 and Fe (II)), in turn, depend on the effluent characteristics (Cassano et al., 2011). Rodríguez-Chueca and coworkers (Rodríguez-Chueca et al., 2016), for instance, studied the effect of $\text{H}_2\text{O}_2/\text{Fe}^{2+}$ ratio on COD removal and the results revealed that a ratio of approximately 31 (5500 mg/L of H_2O_2 and 180 mg/L of Fe^{3+}) gave the best results (achieving 42.05% of COD removal in 180 min). For the same concentration of iron (III) but less concentration of H_2O_2 (1100 mg/L) (ratio $\text{H}_2\text{O}_2/\text{Fe}^{3+} = 6$ approx.), the result of COD removal at the same time was lower (23.35%). These results are in accordance with this study. When 10 mg Fe^{2+} /L and 150 mg H_2O_2 /L (which implies the highest $\text{H}_2\text{O}_2/\text{Fe}^{2+}$ ratio and high concentrations of H_2O_2 and Fe (II)) were tested, high removal of DPH was achieved. The optimal relationship between COD removal and oxidant dosage has also been studied. An increase in H_2O_2 /COD weight ratio favors an enhancement in micropollutants degradation (Bolobajev et al., 2014). Bolobajev and coworkers (Bolobajev et al., 2014), among others, studied this aspect of the process. The results revealed that a higher ratio, which means more H_2O_2 per unit of COD, leads to the best performance in terms of organic matter degradation. Like the $\text{Fe}^{2+}/\text{H}_2\text{O}_2$ ratio, the H_2O_2 /COD optimal ratio depends on a large extent on the characteristics of the effluent (Brink et al., 2017). Again, these results are in accordance with the observations in this study.

3.2. Synergistic effects of two wavelengths combination

Fig. 3A shows the influence of the wavelength range on the DPH degradation for 10 mg Fe^{2+} /L and 150 mg H_2O_2 /L. Two wavelengths were tested (380–390 nm and 390–400 nm) and the combination of both LEDs (380–400 nm). The nominal power in all experiments was 4.2 W.

As it can be observed in Fig. 3A, the use of radiation of 380–390 nm (0.432 kJ/L) or 390–400 nm (0.468 kJ/L) does not imply a significant

increase regarding total DPH removal, which is achieved at 30 min in both cases. However, there are little differences in the DPH degradation curve until 20 min and range 390–400 nm presents a faster degradation, because the accumulated radiation is always a little higher in the range 390–400 nm.

When two wavelengths were combined (15 min, $Q_{\text{acc}} = 0.288$ kJ/L, 380–400 nm), the degradation of DPH was 100% in only 15 min (the degradation time is reduced by half), due to the synergistic effect of the two wavelengths working jointly that increases the efficiency of the process. This rise of DPH degradation, for 380–390 and 390–400 nm, is logical according to the accumulated energy. As it can be observed in Fig. 3B, the accumulated energy was higher than this one corresponding to the two wavelengths acting separately at any time.

The increase in efficiency was also reflected in AOS (Eq. (5)), COD and TOC, and the highest values for these parameters were obtained for 380–400 nm (see Table 1). More explanations about this behavior can be found at the end of Section 3.3.

3.3. Kinetics, synergies and radiation

The experimental data shown in Fig. 1 were fitted to a pseudo-first order kinetics, according to Eq. (6).

$$\ln\left(\frac{C_{\text{DPH}}}{C_{\text{DPH}_0}}\right) = k \cdot t \quad (5)$$

Where C_{DPH_0} is the initial DPH concentration (mg/L), C_{DPH} is the final DPH concentration (mg/L), t is the time (min) and k is an apparent reaction rate constant (min^{-1}). From the plot of $\ln(C_{\text{DPH}}/C_{\text{DPH}_0})$ vs. time, the kinetics were obtained for each experimental conditions. However, looking at Fig. 1, two zones can be clearly seen for all experiments. In the initial moments, up to 30 s, a very fast decrease in the concentration of DPH can be seen. After 30 s, the decrease is much smoother. Therefore, the fitting has also been divided into two parts. In the first 30 s, the initial reaction rate method is used to calculate the kinetic constant, assuming order 1. From there, the rest of the data to the end of the experiment were fitted to pseudo-first order kinetics. The final time was 60 min for all cases, except for 10 mg Fe^{2+} /L and 150 mg H_2O_2 /L, where final time was 30 min due to DPH was totally removed at this time. The results obtained in the fittings are shown in Table 1. In addition, the fitting of data from Fig. 1 to pseudo-first order kinetics is shown in Figure S2 (supplementary information), for reaction times higher than 30 s.

Average Oxidation State (AOS), COD and TOC were also analyzed. Table 1 summarizes the obtained results. The calculation of AOS was performed according to Eq. (5), where TOC and COD are represented in mol/L of C and O_2 , respectively. As known, this indicator takes values between +4 (value for CO_2), state of maximum oxidation of carbon, and -4 (value for CH_4), state of maximum reduction (De la Cruz et al.,

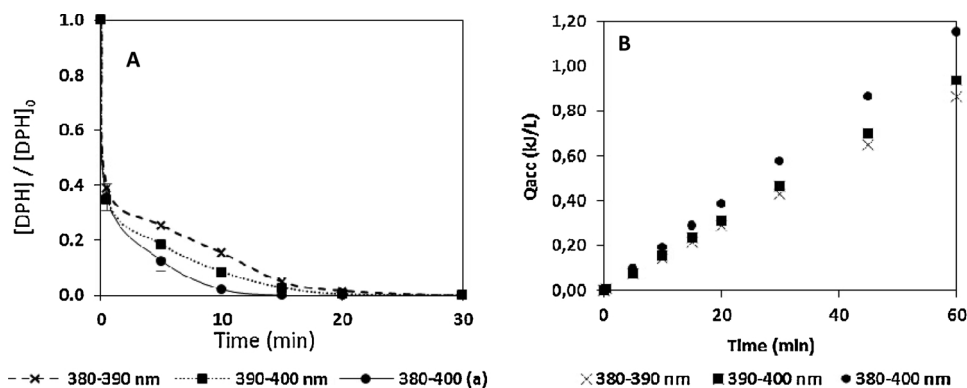


Fig. 3. (A) DPH degradation by photo-Fenton and (B) radiation accumulation with different LEDs wavelengths $[\text{DPH}]_0 = 50$ mg/L; $[\text{Fe}^{2+}] = 10$ mg/L; $[\text{H}_2\text{O}_2] = 150$ mg/L; Nominal power = 4.2 W.

Table 1

Values of the kinetic constants for different wavelengths and concentrations of Fe^{2+} and H_2O_2 . k_1 is the kinetic constant obtained during the first 30 s and k_2 is the kinetic constant for the rest of the experiment (fitting to pseudo first order kinetics).

Wavelength (nm)	$[\text{Fe}^{2+}]$ (mg/L)	$[\text{H}_2\text{O}_2]$ (mg/L)	k_1 (min^{-1})	k_2 (min^{-1})	R^2	AOS	COD (%)	TOC (%)
380-390	10	150	1.9	0.16	0.96	2.4	70.2	54.2
380-390	10	25	1.6	0.05	0.99	1.2	14.4	6.8
380-390	2.5	150	0.5	0.01	0.99	1.0	6.6	2.8
380-390	2.5	25	–	0.005	0.96	N/A	0.0	0.0
390-400	10	150	2.1	0.23	0.95	2.7	79.9	60.5
390-400	10	25	1.3	0.06	0.98	1.3	15.2	6.9
390-400	2.5	150	0.5	0.03	0.93	1.0	6.7	2.9
390-400	2.5	25	0.3	0.008	0.98	N/A	0.0	0.0
380-400	10	150	2.1	0.3	0.99	3.8	95.6	70.1

2013).

$$\text{AOS} = 4x \frac{\text{TOC} - \text{COD}}{\text{TOC}} \quad (6)$$

AOS started at a value of 1.0 (at initial time) and increased to the highest values using the highest concentrations of iron II and peroxide. The same trend was found in COD and TOC. A high degree of mineralization (54.2%) and oxidation (79.9%) were observed at 60 min, for the highest concentrations of peroxide and iron II. At this time, DPH has been completely degraded. This signified a rising oxidation and break of the DPH leading to more oxidized molecules. However, for 2.5 mg Fe^{2+} /L and 25 mg H_2O_2 /L mineralization and oxidation were not observed. These results show again that both the hydrogen peroxide and iron (II) concentrations play an important role in the photo-Fenton process.

From the data of Table 1, it is observed that the best results are obtained for 10 mg Fe^{2+} /L and 150 mg H_2O_2 /L, for all the wavelength ranges tested.

Concerning the values of k_1 , the wavelength of the radiation used does not have much influence. For instance, k_1 value is 0.5 min^{-1} for 380–390 nm and 390–400 nm, for 2.5 mg Fe^{2+} /L and 150 mg H_2O_2 /L. However, data show that iron and peroxide concentrations have large influence on the reaction rate. As an example, k_1 values are 2.1 min^{-1} , for 10 mg Fe^{2+} /L and 150 mg H_2O_2 /L, and 0.3 min^{-1} , for 2.5 mg Fe^{2+} /L and 25 mg H_2O_2 /L, in the range 390–400 nm. Results of Table 1 for k_1 confirm also that the concentration of Fe^{2+} has a higher influence than the concentration of H_2O_2 .

Once the initial moments (30 s) have passed, it can be observed a similar behavior of the system concerning the influence of Fe^{2+} and peroxide concentrations on the reaction rate. Thus, the highest values of k_2 are obtained for the concentrations of 10 mg Fe^{2+} /L and 150 mg H_2O_2 /L. This behavior appears as logical because Fe^{3+} slowly returns to Fe^{2+} and, therefore, the generation of hydroxyl radicals through the Eq. (3) is slower (see Fig. 3B). In addition, it seems that the wavelength can play a role, because, for the same concentration of iron and peroxide, k_2 is higher always for the experiments in the range 390–400 nm.

Comparing k_1 and k_2 values, it can be seen that k_2 is one order of magnitude lower than k_1 for all the tested concentrations of Fe^{2+} and peroxide and for all the wavelength ranges. This fact can be due to several factors and, among them, it could be mentioned that, after the initial instants, intermediates appear which compete with DPH for hydroxyl radicals. Hence, the degradation of DPH slows down. These results are in accordance with Eqs. (2), (3) and (4) if the reactions rates are considered. The reaction rate corresponding to Eq. (2) is 63 $\text{M}^{-1} \text{s}^{-1}$. However, the value for Eq. (4) is lower than Eq. (2) (10^{-3} – $10^{-2} \text{M}^{-1} \text{s}^{-1}$) (Buxton et al., 1988).

In order to study the synergy of wavelengths, as explained before, experiments were made using 4 LEDs at the top of the reactor, like explained just now, but in this case, 2 LEDs with 380–390 nm and 2 LEDs with 390–400 nm were combined. Experiments were done only for the best conditions (10 mg Fe^{2+} /L and 150 mg H_2O_2 /L). As has been

done when the two wavelength ranges were studied separately, the experimental data are fitted for two different periods of time: during the initial moments (up to 30 s) and from there to the end of the experiment. For the initial time (first 30 s), the value of the kinetic constant (k_1) was 2.1 min^{-1} (see Table 1). This value is very close to the values obtained for k_1 when LEDs of 380–390 nm or LEDs of 390–400 nm were used. As commented before, the reaction at this initial moment is very fast and it is strongly related to the Fe^{2+} concentration. It can be said that the generation of hydroxyl radicals is practically due to Fe^{2+} oxidation (Eq. (2)), meaning that the role of radiation is not so important (Fenton process). Thus, wavelength has not a large influence.

After the initial 30 s, the kinetic constant (k_2) obtained with the combined LEDs was 0.3 min^{-1} which is practically one order of magnitude lower than k_1 , as occurs with 380–390 nm and 390–400 nm studied separately (see Table 1). This k_2 value of 0.3 min^{-1} is higher than k_2 values obtained for the LEDs of 380–390 nm or 390–400 nm (see also Table 1) because, after the first 30 s, the reaction of Fe^{3+} reduction with H_2O_2 and light (Eq. (3)) is more important and photo-Fenton process is acting. This means that the role of the radiation is important after the initial period of 30 s, and explains that wavelength used has more influence. In addition, the effect of synergy could be explained from Eq. (7).

$$r = \sum_{\lambda} \varphi_{\lambda} \cdot \mu_{\lambda} \cdot I_{\lambda} \quad (7)$$

Where r is the reaction rate ($\text{mol} \cdot \text{cm}^{-3} \cdot \text{s}^{-1}$), φ_{λ} is the quantum yield ($\text{mol}/\text{Einstein}$), μ_{λ} is the absorbance (cm^{-1}) and I_{λ} is the photonic flow ($\text{Einstein} \cdot \text{cm}^{-2} \cdot \text{s}^{-1}$). According to Eq. (7), the reaction rate in any photochemical process depends on the absorbance, quantum yield and radiation intensity. These parameters can be considered a little different in the range of 380–390 nm or in the range 390–400 nm. For this reason, the results obtained for k_2 can change a little in these two ranges (see Table 1). In the range 380–400 nm, considering that r is the summation for all the wavelengths range (see Eq. (6)), it seems logical to expect that reaction rate increases. This is that we have observed experimentally and can explain that k_2 for the range 380–400 nm is higher than k_2 for the range 380–390 nm or for the range 390–400 nm. In fact, the consideration of k_2/Q_{acc} for each range of wavelength proves the synergy explained above. This calculation was done for 30 min (380–390 and 390–400 nm) and 15 min (380–400 nm), time at DPH was total removed. Values of 0.37, 0.49 and 1.04 correspond at 380–390, 390–400 and 380–400 nm. Thus, it is clear that 380–400 nm presents a value much higher confirming the synergistic effect of wavelength according to Eq. (7).

3.4. By-products and degradation pathways

As explained in Section 2, the intermediates of DPH were detected by LC/MS during the photo-Fenton process. Four intermediates were identified at the final of each experiment (60 min): $\text{C}_{17}\text{H}_{23}\text{NO}_5$, $\text{C}_{17}\text{H}_{21}\text{NO}_3$, $\text{C}_{17}\text{H}_{21}\text{NO}_2$ and $\text{C}_{13}\text{H}_{10}\text{O}$ (see table S1 in supplementary

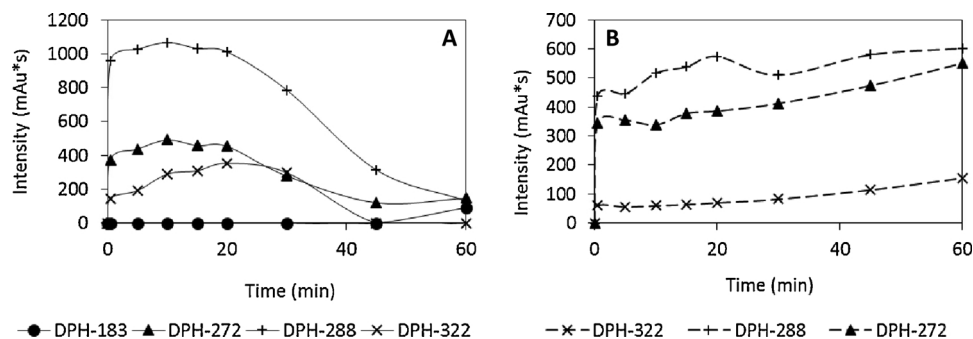


Fig. 4. Evolution of intermediates identified in different scenarios during the experiment. [DPH]₀ = 50 mg/L. Nominal power: 4.2 W. A) 10 mg Fe²⁺/L and 150 mg H₂O₂/L; B) 2.5 mg Fe²⁺/L and 25 mg H₂O₂/L.

material). Fig. 4 presents the evolution of the intermediates during one hour in different scenarios.

Fig. 4A and B represent intermediates identified in the best and the worst conditions regarding concentrations of iron (II) and hydrogen peroxide. The wavelength range used was 390–400 nm, but the same trend was observed for 380–390 nm and 380–400 nm. When 10 mg Fe²⁺/L and 150 mg H₂O₂/L were tested, the intermediates began to degrade at approximately 15 min. This time corresponds to the moment when there is a low concentration of DPH. In addition, DPH-183 was formed at 60 min due to the higher formation of hydroxyl radicals. This fact allows the degradation almost entirely of the first intermediates and formation of more oxidized intermediates.

However, when 2.5 mg Fe²⁺/L and 25 mg H₂O₂/L were tested, the intermediates formed did not degrade because DPH degradation reaction is not so fast (46.9% removal at 60 min). This means that the hydroxyl radicals are still mainly engaged in attacking the DPH. Thus, at 60 min the concentration of formed intermediates was higher than at the initial time because the intermediates have not yet begun to degrade. In addition, the intermediate DPH-183 does not appear because it comes from the degradation of DPH-272 (see Fig. S3) which has not started yet after 60 min of reaction (see Fig. 4B). It can be concluded that, as expected, the initial concentration of Fe²⁺ and H₂O₂ have a large influence on DPH degradation and, as a consequence, on the intermediates formation and degradation. Thus, the highest concentrations of Fe²⁺ and H₂O₂ give the fastest formation and degradation of intermediates (see Fig. 4A).

Figure S3 (supplementary material) presents a proposed DPH degradation pathway with the intermediates found. DPH-272, DPH-288 and DPH-322 could be formed from primary oxidation of the parent compound (DPH-256). The generation of DPH-272 appears to be due to the hydroxylation of the initial compound. DPH-322 might be formed by the opening of an aromatic ring in DPH-256. In addition, the hydroxylation and oxidation of one carbon from the initial compound could have led to the generation of DPH-288. Finally, DPH-183 could be produced by consecutive deamination/dihydroxylation reactions taking place in the DPH-272 structure.

4. Conclusions

UVA-LEDs (380–390 nm and 390–400 nm) are useful for DPH degradation. In addition, the combination of LEDs with 380–390 nm and 390–400 nm wavelength ranges produces synergistic effects on DPH removal.

The best results in DPH degradation were obtained for the highest concentrations of iron and peroxide (10 mg Fe²⁺/L and 150 mg H₂O₂/L).

Kinetic studies pointed out that the initial reaction rate (up to 30 s) is higher than the rate during the rest of the experiment, showing the influence of Fe²⁺ concentration. Thus, Fenton process prevails at the initial moments and photo-Fenton during the rest of the experiment.

Three intermediates (DPH-272, DPH-288 and DPH-322) were

generated from the oxidation of initial compound and DPH-183 was produced by subsequent reactions from DPH-272.

Acknowledgments

The authors are appreciative of the financing acquired by the Ministry of Science and Innovation of Spain (projects CTQ2014-52607-R and CTQ2017-86466-R), Ministry of Education, Culture and Sports (FPU research fellowship FPU-16/02101), Institute for Water Research (IdRA) of Universitat de Barcelona and AGAUR-Generalitat de Catalunya (project 20145GR245 and 2017SGR-131).

Appendix A. Supplementary data

Supplementary material related to this article can be found, in the online version, at doi:<https://doi.org/10.1016/j.jhazmat.2019.120882>.

References

- Verlicchi, P., Galletti, A., Petrovic, M., Barceló, D., 2010. Hospital effluents as a source of emerging pollutants: an overview of micropollutants and sustainable treatment options. *J. Hydrol.* 389, 416–428.
- Gebhardt, W., Schroder, H.F., 2007. Liquid chromatography–(tandem) mass spectrometry for the follow-up of the elimination of persistent pharmaceuticals during wastewater treatment and advanced oxidation. *J. Chromatogr. A* 1160, 34–43.
- Deo, R.P., 2007. Pharmaceuticals in the surface water of the USA: a review. *Current Environmental Health Reports* 1 (2014) 113–122. *J. Hazard. Mater.* 148, 751–755.
- Cominellis, C., Kapalka, A., Malato, S., Parsons, S.A., Poullos, I., Mantzavinos, D., 2008. *Advanced Oxidation Processes for water treatment: advances and trends for R&D.* *J. Chem. Technol. Biotechnol.* 83, 769–776.
- Kumar, J., Bansal, A., 2013. Photocatalysis by nanoparticles of Titanium Dioxide for drinking water purification: a conceptual and state-of art review. *Mater. Sci. Forum* 764, 130–150.
- Wankhade, A.V., Gaikwad, G.S., Dhonde, M.G., Khat, N.T., Thakare, S.R., 2013. Removal of organic pollutant from water by heterogeneous photocatalysis: a review. *Res. J. Chem. Environ.* 17, 84–94.
- Primo, O., Rivero, M.J., Ortiz, I., 2008a. Photo-Fenton process as an efficient alternative to the treatment landfill leachates. *J. Hazard. Mater.* 153, 834–842.
- Primo, O., Rueda, A., Rivero, M.J., Ortiz, I., 2008b. An integrated process, Fenton reaction-ultrafiltration, for the treatment of landfill leachate: pilot plant operation and analysis. *Ind. Eng. Chem. Res.* 47, 946–952.
- Lee, S.Y., Park, S.J., 2013. TiO₂ photocatalyst for water treatment applications. *J. Ind. Eng. Chem.* 19, 1761–1769.
- Pignatello, J.J., MacKay, A., 2006. Advanced oxidation processes for organic contaminant destruction based on the Fenton reaction and related chemistry. *Crit. Rev. Environ. Sci. Technol.* 36, 1–84.
- Carra, I., Sánchez Pérez, J.A., Malato, S., Autin, O., Jefferson, B., Jarvis, P., 2015. Application of high intensity UVC-LED for the removal of acetaminophen with the photo-Fenton process. *Chem. Eng. J.* 264, 690–696.
- Autin, O., Romelot, C., Rust, L., Hart, J., Jarvis, P., MacAdam, J., Parsons, S.A., Jefferson, B., 2013. Evaluation of a UV-light emitting diodes unit for the removal of micropollutants in water for low energy advanced oxidation processes. *Chemosphere* 92, 745–751.
- Xiong, P., Hu, J., 2012. Degradation of acetaminophen by UVA/LED/TiO₂ process. *Sep. Purif. Technol.* 91, 89–95.
- Verma, S., Sillanpää, M., 2015. Degradation of anatoxin-a by UV-C LED and UV-C LED/H₂O₂ advanced oxidation processes. *Chem. Eng. J.* 274, 274–281.
- Tayade, R.J., Natarajan, T.S., Bajaj, H.C., 2009. Photocatalytic degradation of methylene blue dye using ultraviolet light emitting diodes. *Ind. Eng. Chem. Res.* 48, 10262–10267.

- Würtele, M.A., Kolbe, T., Lipsz, M., Külbeg, A., Weyers, M., Kneissl, M., Jekel, M., 2011. Application of GaN-based ultraviolet-C light emitting diodes-UV-LEDs-for water disinfection. *Water Res.* 45, 1481–1489.
- Matafonova, G., Batoev, V., 2018. Recent advances in application of UV light-emitting diodes for degrading organic pollutants in water through advanced oxidation processes: a review. *Water Res.* 132, 177–189.
- De la Obra, I., Esteban García, B., García Sánchez, J.L., Casas López, J.L., Sánchez Pérez, J.A., 2017. Low cost UVA-LED as a radiation source for the photo-Fenton process: a new approach for micropollutant removal from urban wastewater. *Photochem. Photobiol. Sci.* 16, 72–78.
- Chevremont, A.C., Farnet, A.M., Sergent, M., Columb, B., 2012. Effect of coupled UV-A and UV-C LEDs on both microbiological and chemical pollution of urban wastewaters. *Sci. Total Environ.* 426, 304–310.
- Moreira, N.F.F., Sousa, J.M., Macebo, G., Ribeiro, A.T., Barrientos, L., Pedrosa, M., Faria, J.L., Pereira, F.R., Castro-Silva, S., Segundo, M.A., Manaia, C.M., Nunes, O.C., Silva, A.M.T., 2016. Photocatalytic ozonation of urban wastewater and surface water using immobilized TiO₂ with LEDs: micropollutants, antibiotic resistance genes and estrogenic activity. *Water Res.* 94, 10–22.
- Rasoulifard, M.H., Fazli, M., Eskandarian, M.R., 2015. Performance of the light-emitting diodes in a continuous photoreactor for degradation of Direct Red using UV-LED/S₂O₈²⁻ process. *J. Ind. Eng. Chem.* 24, 121–126.
- Hözl, K., Lietard, J., Somoza, M.M., 2017. High-Power 365 nm UV LED mercury Arc Lamp replacement for photochemistry and chemical photolithography. *ACS Sustain. Chem. Eng.* 5, 828–834.
- Joakim Larsson, D.G., De Pedro, C., Paxeus, N., 2007. Effluent from drug manufactures contains extremely high levels of pharmaceuticals. *J. Hazard. Mater.* 148, 751–755.
- Kuhn, H.J., Braslavsky, S.E., Schmidt, R., 2004. Chemical actinometry (IUPAC technical report). *Pure Appl. Chem.* 76, 2105–2146.
- Galbavy, E.S., Ram, K., Anastasio, C., 2010. 2-Nitrobenzaldehyde as a chemical actinometer for solution and ice photochemistry. *J. Photochem. Photobiol. A: Chem.* 209, 186–192.
- López, N., Plaza, S., Afkhami, A., Marco, P., Giménez, J., Esplugas, S., 2017. Treatment of Diphenhydramine with different AOPs including photo-Fenton at circumneutral pH. *Chem. Eng. J.* 318, 112–120.
- López, N., Marco, P., Giménez, J., Esplugas, S., 2018. Photocatalytic diphenhydramine degradation under different radiation sources: kinetic studies and energetic comparison. *Appl. Catal. B Environ.* 220, 497–505.
- Pupo Nogueira, R.F., Oliveira, M.C., Paterlini, W.C., 2005. Simple and fast spectrophotometric determination of H₂O₂ in photo-Fenton reactions using metavanadate. *Talanta* 66, 86–89.
- Eaton, A.D., Clesceri, L.S., Greenberg, A.E., Franson, M.A.H., 2005. *Standard Methodes for the Examination of Water and Wastewater*, twenty-first ed. APA-AWWA-WEE.
- De la Cruz, N., Dantas, R.F., Giménez, J., Esplugas, S., 2013. Photolysis and TiO₂ photocatalysis of the pharmaceutical propranolol: solar and artificial light. *Appl. Catal. B: Environ.* 249–256.
- Doumic, L.L., Houre, P.M., Cassanello, M.C., Ayude, M.A., 2013. Mineralization and efficiency in the homogeneous Fenton Orange G oxidation. *Appl. Catal. B: Environ.* 142–143, 214–221.
- Pulgarin, C., Invernizzi, M., Parra, S., Sarria, V., Polania, R., Péringier, P., 1999. Strategy for the coupling of photochemical and biological flow reactors useful in mineralization of biorecalcitrant industrial pollutants. *Catal. Today* 54, 341–352.
- Carra, I., Malato, S., Jiménez, M., Maldonado, M.I., Sánchez Pérez, J.A., 2014. Microcontaminant removal by solar photo-Fenton at natural pH run with sequential and continuous iron additions. *Chem. Eng. J.* 235, 132–140.
- Dogruel, S., Olmez-Hanci, T., Kartal, Z., Arslan-Alaton, I., Orhon, D., 2009. Effect of Fenton's oxidation on the particle size distribution of organic carbon in olive mill wastewater. *Water Res.* 43 (16), 3974–3983.
- Durán, A., Monteagudo, J.M., Carnicer, A., 2011. Photo-Fenton mineralization of synthetic apple-juice wastewater. *Chem. Eng. J.* 168 (1), 102–107.
- Cassano, D., Zapata, A., Brunetti, G., Del Moro, G., Di Iaconi, C., Oller, I., Malato, S., Mascolo, G., 2011. Comparison of several combined/integrated biological-AOPs setups for the treatment of municipal landfill leachate: minimization of operating costs and effluent toxicity. *Chem. Eng. J.* 172 (1), 250–257.
- Rodríguez-Chueca, J., Amor, C., Fernandes, J.R., Tavares, P.B., Lucas, M.S., Peres, J.A., 2016. Treatment of crystallized-fruit wastewater by UV-A LED photo-Fenton and coagulation-flocculation. *Chemosphere* 145, 351–359.
- Bolobajev, J., Kattel, E., Viisimaa, M., Goi, A., Trapido, M., Tenno, T., Dulova, N., 2014. Reuse of ferric sludge as an iron source for the Fenton-based process in wastewater treatment. *Chem. Eng. J.* 255, 8–13.
- Brink, A., Sheridan, C.M., Harding, K.G., 2017. The Fenton oxidation of biologically treated paper and pulp mill effluents: a performance and kinetic study. *Process. Saf. Environ. Prot.* 107, 206–215.
- Buxton, G.V., Greenstock, C.L., Helman, W.P., Ross, A.B., 1988. Critical review of rate constants for reactions of hydrated electrons, hydrogen atoms and hydroxyl radicals (OH^\cdot , O^\cdot) in aqueous solution. *J. Phys. Chem. Ref. Data* 17, 513–886.

Supplementary Information for

Synergies, radiation and kinetics in photo-Fenton process with UVA-LEDs

N. López-Vinent, A. Cruz-Alcalde, L.E. Romero, M.E. Chávez, P. Marco, J. Giménez*,
S. Esplugas

Department of Chemical Engineering and Analytical Chemistry, Faculty of Chemistry,
Universitat de Barcelona, C/Martí i Franqués 1, 08028 Barcelona, Spain.

*Corresponding author:

Jaime Giménez Farreras, phone: +34 934 02 01 54, e-mail: j.gimenez.fa@ub.edu

The SI includes the following 3 figures and 1 table:

Table of Contents

Figure S1. The schematic diagram of photoreactor with LEDs on the cover.....	p.2
Figure S2. Fitting of Fig. 2 data to pseudo-first order kinetics for reaction times higher than 30 s and A) wavelength range 380-390 nm, B) wavelength range 380-390 nm and C) wavelength range 380-400 nm	p.3
Figure S3. Suggested pathways for DPH degradation in the photo-Fenton experiments.....	p.4
Table S1. Intermediates detected and DPH as an initial compound in photo-Fenton experiments (Rt, retention time).....	p.5

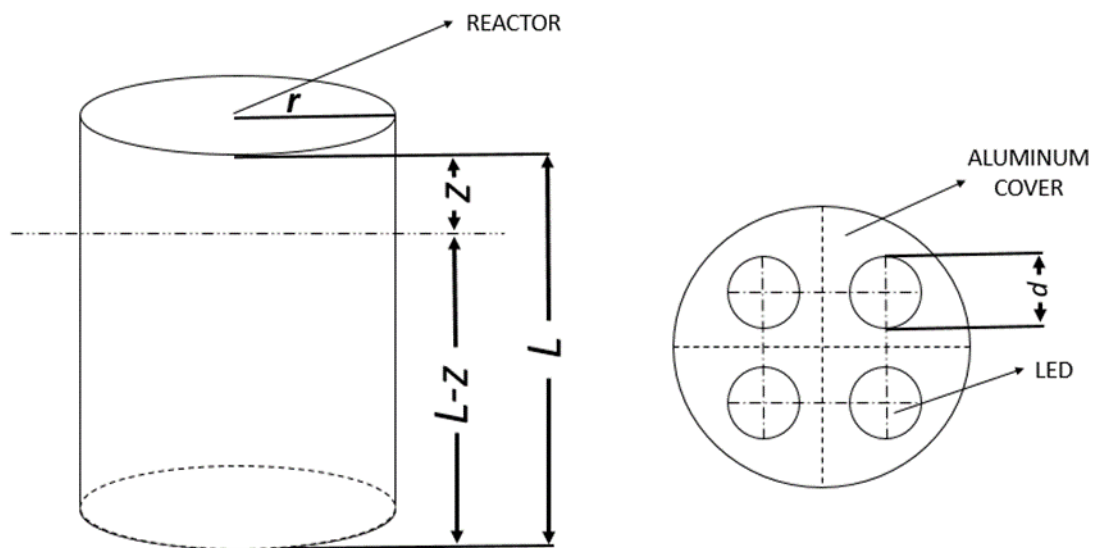


Figure S1. The schematic diagram of photoreactor with LEDs on the cover. $r = 4\text{cm}$, radius of the photoreactor; $L = 12\text{cm}$, photoreactor height; $z = 3\text{cm}$, height between aluminum cover and liquid layer; $d = 3\text{cm}$, LED diameter. When 380–400 nm were tested LEDs were located crossed.

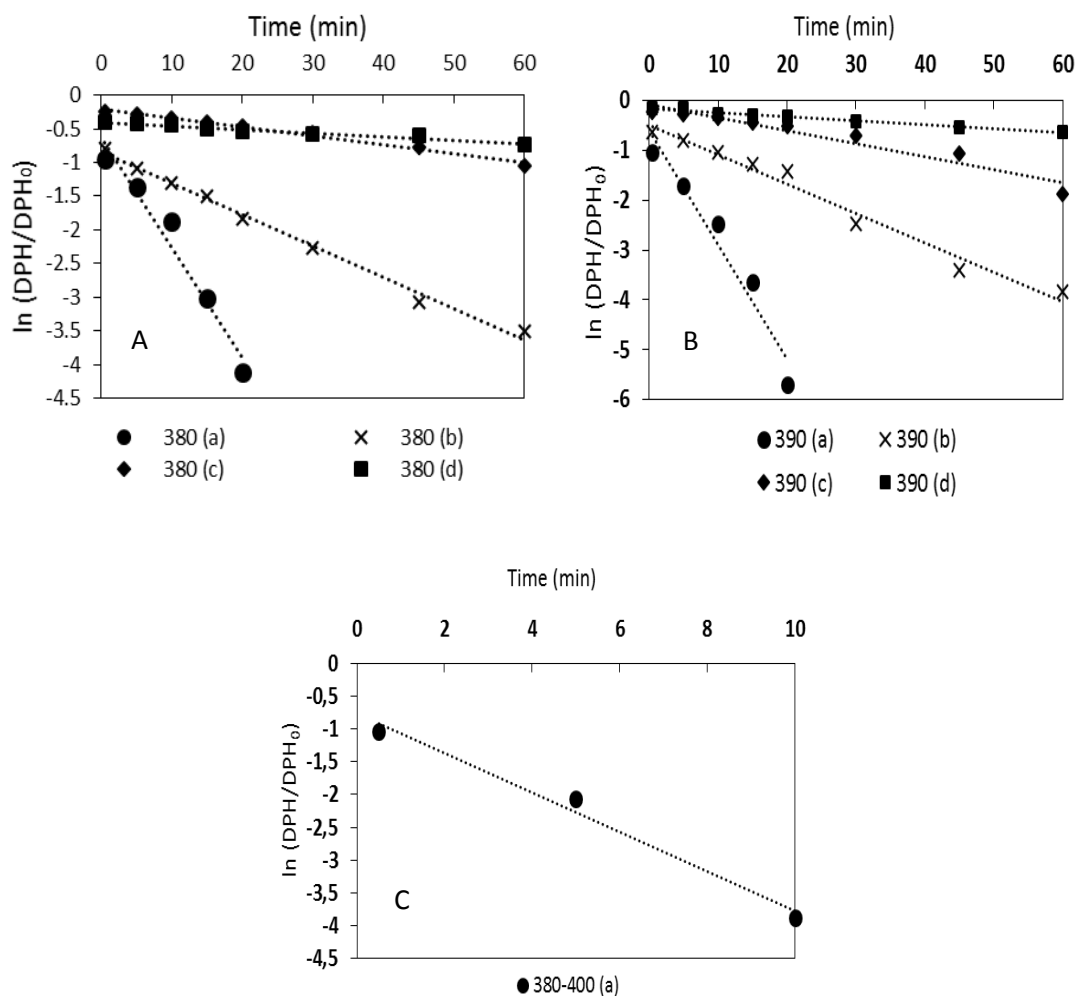


Figure S2. Fitting of Fig. 2 data to pseudo-first order kinetics for reaction times higher than 30 s and A) wavelength range 380-390 nm, B) wavelength range 380-390 nm and C) wavelength range 380-400 nm (a) 10 mg Fe^{2+}/L - 150 mg H_2O_2/L ; (b) 10 mg Fe^{2+}/L - 25 mg H_2O_2/L ; (c) 2.5 mg Fe^{2+}/L - 150 mg H_2O_2/L ; (d) 2.5 mg Fe^{2+}/L - 25 mg H_2O_2/L .

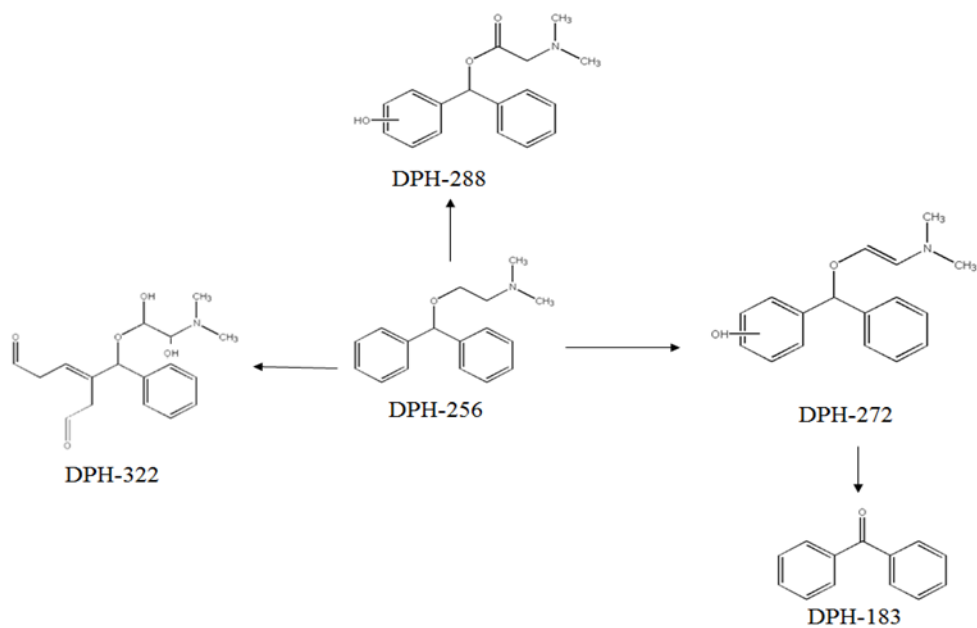


Figure S3. Suggested pathways for DPH degradation in the photo-Fenton experiments.

Table S1. Intermediates detected and DPH as an initial compound in photo-Fenton experiments (Rt, retention time)

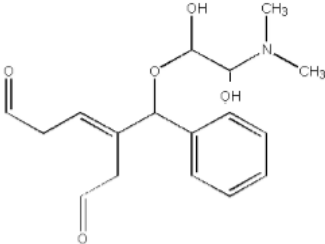
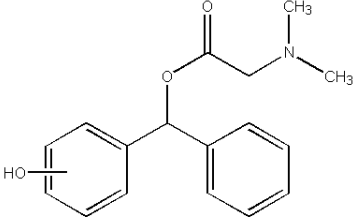
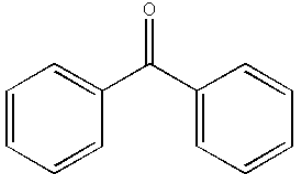
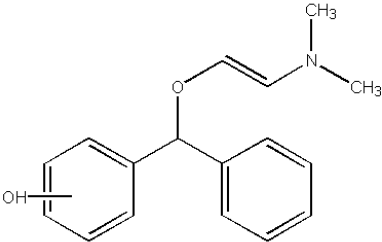
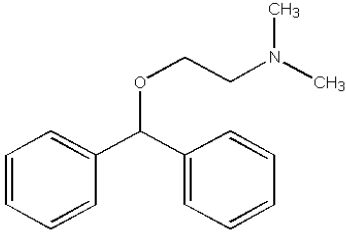
m/z (Da)	Rt [min]	Elemental composition	Proposed structure	
322 (m+1)	1.80	C ₁₇ H ₂₃ NO ₅		DPH-322
288 (m+1)	2.06	C ₁₇ H ₂₁ NO ₃		DPH-288
183 (m+1)	2.20	C ₁₃ H ₁₀ O		DPH-183
272 (m+1)	2.80	C ₁₇ H ₂₁ NO ₂		DPH-272

Table S1. (continued)

m/z (Da)	Rt [min]	Elemental composition	Proposed structure	
256 (m+1)	3.20	C ₁₇ H ₂₁ NO		DPH (initial compound)

4.2 Comparison of conventional BLB lamps and LEDs in photo-Fenton process for micropollutant abatement in real wastewater

A summary of the experiments displayed in Part II are detailed in Table 16, including the operational conditions, performance, as well as the figure within the publication where each experiment is located.

Table 16. Summary of the experiments presented in Part II.

Test	Target	[Reagents]	Irradiation	Matrix	pH	Performance	Figure in publication
BLB and LEDs comparison at acid pH							
B1	[PROP] = 50 mg L ⁻¹	[Fe ²⁺] = 10 mg L ⁻¹ [H ₂ O ₂] = 150 mg L ⁻¹	8 LEDs 365-370 nm on the center	Ultrapure water	2.8	Total PROP removal in 60 min	Figure 1A and 7C
B2	[PROP] = 50 mg L ⁻¹	[Fe ²⁺] = 10 mg L ⁻¹ [H ₂ O ₂] = 150 mg L ⁻¹	8 LEDs 365-370 nm on the center	MBR	2.8	52.1% PROP removal in 60 min	Figure 1A and 7A
B3	[PROP] = 50 mg L ⁻¹	[Fe ²⁺] = 10 mg L ⁻¹ [H ₂ O ₂] = 150 mg L ⁻¹	8 LEDs 365-370 nm on the center	CAS-NE	2.8	50.6% PROP removal in 60 min	Figure 1A and 7B
B4	[PROP] = 50 mg L ⁻¹	[Fe ²⁺] = 10 mg L ⁻¹ [H ₂ O ₂] = 150 mg L ⁻¹	8 LEDs 365-370 nm on the center	CAS	2.8	40.2% PROP removal in 60 min	Figure 1A and 7D
B5	[PROP] = 50 mg L ⁻¹	[Fe ²⁺] = 10 mg L ⁻¹ [H ₂ O ₂] = 150 mg L ⁻¹	8 LEDs 365-370 nm on the center	IFAS	2.8	32.9% PROP removal in 60 min	Figure 1A and 7E
B6	[PROP] = 50 mg L ⁻¹	[Fe ²⁺] = 10 mg L ⁻¹ [H ₂ O ₂] = 150 mg L ⁻¹	BLB	Ultrapure water	2.8	Total PROP removal in 60 min	Figure 1B
B7	[PROP] = 50 mg L ⁻¹	[Fe ²⁺] = 10 mg L ⁻¹ [H ₂ O ₂] = 150 mg L ⁻¹	BLB	MBR	2.8	95.3% PROP removal in 60 min	Figure 1B

Table 16. (continued)

Test	Target	[Reagents]	Irradiation	Matrix	pH	Performance	Figure in publication
B8	[PROP] = 50 mg L ⁻¹	[Fe ²⁺] = 10 mg L ⁻¹ [H ₂ O ₂] = 150 mg L ⁻¹	BLB	IFAS	2.8	68.8% PROP removal in 60 min	Figure 1B
Selection of chelating agent and molar ratio Ligand:Fe							
B9	[PROP] = 50 mg L ⁻¹	[Fe ²⁺] = 10 mg L ⁻¹ Molar ratio EDTA:Fe = 1:1 [H ₂ O ₂] = 150 mg L ⁻¹	8 LEDs 365-370 nm on the center	Ultrapure water	Natural	47.3% PROP removal in 60 min	Figure 3
B10	[PROP] = 50 mg L ⁻¹	[Fe ²⁺] = 10 mg L ⁻¹ Molar ratio EDTA:Fe = 1.5:1 [H ₂ O ₂] = 150 mg L ⁻¹	8 LEDs 365-370 nm on the center	Ultrapure water	Natural	47.3% PROP removal in 60 min	Figure 3
B11	[PROP] = 50 mg L ⁻¹	[Fe ²⁺] = 10 mg L ⁻¹ Molar ratio EDDS:Fe = 1.5:1 [H ₂ O ₂] = 150 mg L ⁻¹	8 LEDs 365-370 nm on the center	Ultrapure water	Natural	99.6% PROP removal in 60 min	Figure 3
B12	[PROP] = 50 mg L ⁻¹	[Fe ²⁺] = 10 mg L ⁻¹ Molar ratio EDDS:Fe = 1:1 [H ₂ O ₂] = 150 mg L ⁻¹	8 LEDs 365-370 nm on the center	Ultrapure water	Natural	99.6% PROP removal in 60 min	Figure 3, 5 and 7C
Natural pH using LEDs in WW							
B13	[PROP] = 50 mg L ⁻¹	[Fe ²⁺] = 10 mg L ⁻¹ Molar ratio EDDS:Fe = 1:1 [H ₂ O ₂] = 150 mg L ⁻¹	8 LEDs 365-370 nm on the center	MBR	Natural	62.7% PROP removal in 60 min	Figure 5 and 7A

Table 16. (continued)

Test	Target	[Reagents]	Irradiation	Matrix	pH	Performance	Figure in publication
B14	[PROP] = 50 mg L ⁻¹	[Fe ²⁺] = 10 mg L ⁻¹ Molar ratio EDDS:Fe = 1:1 [H ₂ O ₂] = 150 mg L ⁻¹	8 LEDs 365-370 nm on the center	CAS-NE	Natural	61.0% PROP removal in 60 min	Figure 5 and 7B
B15	[PROP] = 50 mg L ⁻¹	[Fe ²⁺] = 10 mg L ⁻¹ Molar ratio EDDS:Fe = 1:1 [H ₂ O ₂] = 150 mg L ⁻¹	8 LEDs 365-370 nm on the center	CAS	Natural	47.0% PROP removal in 60 min	Figure 5 and 7D
B16	[PROP] = 50 mg L ⁻¹	[Fe ²⁺] = 10 mg L ⁻¹ Molar ratio EDDS:Fe = 1:1 [H ₂ O ₂] = 150 mg L ⁻¹	8 LEDs 365-370 nm on the center	IFAS	Natural	14.3% PROP removal in 60 min	Figure 5 and 7E

4.2.1 Propranolol removal comparison using conventional lamps and LEDs

The economic and environmental problems, associated to conventional lamps in photo-Fenton process, lead to investigate alternative irradiation sources, such as LEDs. As LEDs are punctual sources of light, the photoreactor design is a key parameter to consider for a good distribution of light, avoiding dark zones. In this sense, photo-Fenton experiments were carried out in a photoreactor with BLB lamp (290-400 nm) or UV-A LEDs (365-370 nm), both located at the center of the photoreactor (irradiance: 6.7×10^{-7} and 5.4×10^{-7} Einstein s⁻¹, respectively). The comparison of two irradiation sources was performed by the efficiency in PROP removal in acidic conditions with different wastewater effluents and ultrapure water (B1-B8). Additionally, the results in PROP removal for different wastewater effluents were also compared due to their different physicochemical characteristics.

The results revealed the same tendency in PROP degradation by BLB and UV-A LEDs, for different wastewater effluents. Ultrapure water achieved the best PROP removals while IFAS the worst results. After 1 hour of treatment, 100%, 52.1%, 50.6%, 40.2% and 32.9% of PROP removal were achieved in Milli-Q, MBR, CAS-NE, CAS and IFAS, respectively

using UV-A LEDs (B1-B5). For BLB the results were 100%, 95.3% and 68.8% for Milli-Q, MBR and IFAS (B6-B8), respectively, obtaining higher results than UV-A LEDs. However, in the case of ultrapure water similar PROP results were achieved. The pseudo-first order kinetic constants were 0.15 min^{-1} and 0.14 min^{-1} , for BLB and UV-A LEDs, respectively. This result evidences that, when real matrices were used, the differences between two irradiation sources increase. This fact could be related to the radiation distribution inside the photoreactor, due to the scattering and absorption of light in the presence of organic matter. LEDs are punctual sources of light with an emission angle of 125° , in our case. This fact probably conducted to the formation of dark zones in the photoreactor, decreasing the efficiency in PROP removal. The emission angle of BLB lamp was 360° consequently, this effect was not so noticeable. In addition, the wider wavelength range in BLB can favor the removal of different types of organic matter in a complex system such as real matrix.

The influence of matrix on PROP degradation was investigated in experiments carried out with UV-A LEDs, testing 4 different wastewaters and ultrapure water. Real wastewaters compared with Milli-Q are complex systems (presence of organic matter and ions, alkalinity, turbidity...) which affect to the photo-Fenton efficiency. Regarding the results, IFAS and CAS effluents reached the lowest PROP degradations since they presented highest DOC and turbidity. Only 32.9% and 40.2% of PROP removal were achieved for IFAS and CAS, respectively at the end of the treatment. MBR and CAS-NE, with lower DOC and turbidity than IFAS and CAS, showed best performances. After 1 hour of treatment, 52.1% and 50.6% of PROP removal were achieved for MBR and CAS-NE, respectively. Comparing IFAS and MBR, approximately 20% more of PROP removal at the end of the experiment was reached with MBR. Comparing IFAS with ultrapure water, the degradation increases about 70% with the last one. This fact evidences the influence of dissolved organic matter on treatment efficiency since it also reacts with hydroxyl radicals decreasing the PROP degradation. The kinetic constant of DOM with HO^\bullet was estimated between 10^8 - $10^9 \text{ M}^{-1} \text{ s}^{-1}$, while PROP presents a kinetic of $1 \cdot 10^{10} \text{ M}^{-1} \text{ s}^{-1}$, which can explain the competition for hydroxyl radicals since the concentration of both was similar. Turbidity is other key parameter when photochemical treatments are employed due to the light scattering. IFAS and CAS presented 40 and 10 times higher turbidity than MBR and CAS-NE, respectively, which could affected in the generation of HO^\bullet and subsequent PROP removal. The influence of ions (Cl^- and N-NO_2^- , N-NO_3^-) was practically the same for the four wastewaters tested, due to the concentration of these compounds was similar in all of them. Nitrite reacts with a second-

order reaction rate of $1 \cdot 10^{10} \text{ M}^{-1} \text{ s}^{-1}$, which is very similar than the reaction rate of PROP. However, the concentration of nitrites was lower than PROP, probably acted as a scavenger in less extent than the other compounds. For its part, nitrates do not react with HO^\bullet . Chlorine ions probably acted as a scavenger of hydroxyl radicals in these experiments. The second-order reaction rate with HO^\bullet is $4.3 \cdot 10^9 \text{ M}^{-1} \text{ s}^{-1}$, which is lower than the reaction rate of PROP. However, the concentration of Cl^- was about 10 times higher than PROP, so the scavenging effect would be possible. The alkalinity is another parameter which could affect to process efficiency. Nevertheless, as the pH was 2.8 the alkalinity was neutralized.

4.2.2 Efficiency of EDDS:Fe(II) in different water matrices with LEDs

Conventional photo-Fenton needs to work at acidic conditions (pH = 2.8), to maintain the iron ions in solution, being an important drawback. This condition is a critical parameter when the aqueous solution to treat has a higher pH, such as in wastewater treatment. For this reason, it was investigated the performance of photo-Fenton at natural pH in four different wastewaters effluents and ultrapure water.

The selection of appropriate ligand and its molar ratio with iron is an important parameter to consider in this type of experiments. In this way, two chelating agents (EDTA and EDDS) and two molar ratios ligand : Fe(II) (1:1 and 1.5:1) were tested in ultrapure water to decide the best one (experiments B9-B12). In the selection it was considered the PROP degradation, the BOD_5 increase and the toxicity at the end of the treatment. From these results, EDDS was selected since the kinetic rate in PROP removal was 7 times higher than EDTA. The increase in BOD_5 was also higher in EDDS. Molar ratio 1:1 (EDDS:Fe) was also chosen as the experiments with two tested ratios achieved the same final PROP removal. Although the increase in BOD_5 in EDDS:Fe 1.5:1 was little higher than molar ratio 1:1, this last one was chosen since implies less amount of chelating agent, decreasing the cost and TOC's in the effluent. Finally, analyzing the toxicity with *Vibrio fishery*, EDTA was two times more toxic than EDDS.

The experiments using EDDS with molar ratio (ligand:Fe) 1:1 (B13-B16) followed the same trend than tests at acid pH. The efficiency in PROP removal decreased when the DOC of wastewater matrix increased. The percentages at the end of the treatment (60 min) were: 99.6, 62.7, 61.0, 47.0 and 14.3% for Milli-Q, MBR, CAS-NE, CAS and IFAS, respectively. An important parameter to follow is the dissolved iron, since the complexity of wastewaters (different type of compounds including ions) could be involved in the break of iron

complexes causing the iron precipitation and subsequent decrease in efficiency of PROP's removal. Additionally, hydroxyl radicals and irradiation could also provoke this breakage. This fact is one of the reasons why the degradation of PROP in ultrapure water is the highest, since only 30% of iron released at the end of the treatment. While in real effluents the precipitation was between 90 and 75%.

Photo-Fenton experiments at natural pH catalyzed by EDDS-Fe(II) were compared to conventional photo-Fenton. During the first 30 seconds, in conventional photo-Fenton fast PROP removal was reached while in photo-Fenton catalyzed by EDDS-Fe(II) the kinetic rates in all matrices were always lower. For instance, in Milli-Q water kinetic constants were 1.354 min^{-1} and 0.129 min^{-1} (for first 30 seconds of experiment) for conventional and natural photo-Fenton, respectively. This fact is related to the availability of iron in solution. As in the experiments with EDDS the iron was chelated, the reaction of iron with H_2O_2 was slower, resulting in a lower reaction rate in PROP degradation.

However, when all the time of experiment is considered, some things can change. At the end of the treatment, experiments carried out with Milli-Q water, in acidic conditions of pH, reached higher PROP removal than photo-Fenton catalyzed by EDDS-Fe(II). The same took place when experiments were performed in IFAS effluent. Curiously, with MBR, CAS-NE and CAS wastewaters, the opposite happened. In the case of experiments carried out with Milli-Q and EDDS, the PROP degradation in the first 30 seconds was about 50% and then it was continuously removed since there was no organic matter competing with PROP for HO^\bullet . Instead in the treatments performed with MBR, CAS-NE and CAS matrices, the degradation of PROP in 30 seconds was about 20-25% due to the presence of DOM. In that cases, probably a large part of iron (II) was oxidized to iron (III) and the subsequent reduction of iron (III) with irradiation was affected by the presence of organic matter. This fact, plus the competition of DOM and PROP for HO^\bullet , caused the reduction in the PROP removal. Thus, the possibility that photo-Fenton experiments at natural pH could reach higher PROP removals was more feasible. Nevertheless, at the end of the experiments, the degradation of PROP was similar in both treatments. For instance, in MBR, 62.7 and 52.1% of PROP abatements were achieved for natural and acid pH, respectively. As commented above, IFAS effluent did not present the same trend than other wastewaters. This fact could be related to the higher content of biopolymers and humic substances than other wastewaters. These substances could complex stronger the iron than EDDS, decreasing the process efficiency.

Part II

Micropollutant removal in real WW by photo-Fenton (circumneutral and acid pH) with BLB and LED lamps

Núria López-Vinent, Alberto Cruz-Alcalde, Coral Gutiérrez, Pilar Marco, Jaime Giménez,
Santiago Esplugas

Department of Chemical Engineering and Analytical Chemistry, Faculty of Chemistry,
University of Barcelona, C/Martí i Franqués 1, 08028 Barcelona, Spain.

Published in *Chemical Engineering Journal* 379 (2020) 122416



Micropollutant removal in real WW by photo-Fenton (circumneutral and acid pH) with BLB and LED lamps



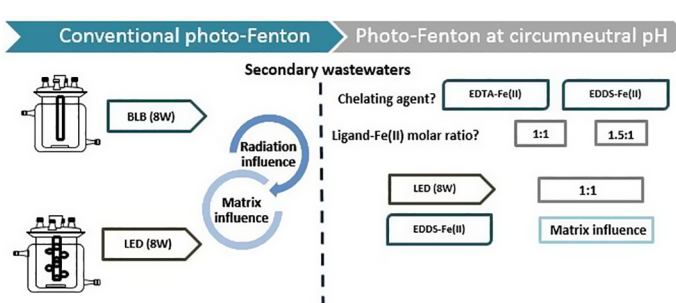
N. López-Vinent, A. Cruz-Alcalde, C. Gutiérrez, P. Marco, J. Giménez*, S. Esplugas

Department of Chemical Engineering and Analytical Chemistry, Faculty of Chemistry, Universitat de Barcelona, C/Martí i Franqués 1, 08028 Barcelona, Spain

HIGHLIGHTS

- BLB and LED radiation were compared in propranolol (PROP) removal by photo-Fenton.
- Chelating agent EDDS gives the best result in photo-Fenton at circumneutral pH.
- Four WW matrices were tested in conventional and circumneutral photo-Fenton.
- PROP degradation increases when TOC of WW decreases.
- Kinetic studies show that dark Fenton controls the initial reaction rate.

GRAPHICAL ABSTRACT



ARTICLE INFO

Keywords:
Photo-Fenton
Wastewater matrix
Circumneutral pH
UV-A LED
Propranolol

ABSTRACT

In this study, photo-Fenton treatment was performed to remove a target compound (propranolol, PROP) from wastewaters of secondary effluents coming from WWTP. Two different radiation sources were tested: BLB and UV-A LEDs, which implies low electrical power and no mercury content. The differences observed in the PROP removal with both lamps may be due to the different radiation distribution, absorption inside the reactor, emission angle and wavelength emission, which are key parameters in the radiation field of the photoreactor. Four wastewaters (IFAS, MBR, CAS and CAS-NE) and ultrapure water were tested to determine the influence of water matrix. Instead the propranolol degradation using UV-A LEDs was smaller than using BLB lamps, in ultrapure water the degradation was very similar. The matrices with more organic matter and turbidity achieved low propranolol removals due to the competition for hydroxyl radicals and the effect of the light scattering. In addition, photo-Fenton at neutral pH (to avoid the acidification/basification) was also carried out using two chelating agents (EDDS and EDTA). Two molar ratios ligand-Fe(II) were tested (1:1 and 1.5:1). EDDS with L:Fe(II) molar ratio 1:1 was selected based on studies of MP degradation, biodegradability and toxicity. Comparisons between conventional photo-Fenton and photo-Fenton with EDDS-Fe(II) were performed with UV-A LEDs. For Milli-Q and IFAS best results were achieved in conventional photo-Fenton (32.9% for IFAS instead of 14.3% in EDDS-Fe(II)). Contrary, for the MBR, CAS and CAS-NE the best results were shown for EDDS-Fe(II) photo-Fenton. In IFAS, biopolymers and humic substances were the responsible of the different behavior of IFAS than other WW. Finally, for conventional photo-Fenton, dark Fenton plays an important role during the first 30 s, then, photo-Fenton controls the process. For circumneutral photo-Fenton, dark Fenton is not so important during the initial time. These observations have been corroborated by different kinetic fittings for different reaction times.

* Corresponding author.

E-mail address: j.gimenez.fa@ub.edu (J. Giménez).

<https://doi.org/10.1016/j.cej.2019.122416>

Received 8 May 2019; Received in revised form 16 July 2019; Accepted 3 August 2019

Available online 06 August 2019

1385-8947/ © 2019 Elsevier B.V. All rights reserved.

1. Introduction

Nowadays, there is a concern on the occurrence of micropollutants (MPs) in effluents of municipal wastewater treatment plants (WWTP) [1–8]. For instance, in Athens (Greece) an important amount of medicines and antibiotics in WW effluents were detected [3], 79 different MPs were identified in WWTPs of Sweden [4] and pharmaceuticals in the surface were found in some places in USA [5]. These compounds can enter the environment causing untoward human health and ecological effects [6]. The potential for entering in the environment of these compounds is a consequence of their incomplete removal in conventional WWTPs [7,8].

Accordingly, with the future law requirements and to protect the ecosystems and water resources, additional treatments ought to be carried out [9]. Diverse works to remove MPs are based in Advanced Oxidation Processes (AOPs). Some authors indicated the efficiency of these treatments in the elimination of organic and recalcitrant compounds [6,9,19–25]. In this study, propranolol (PROP) was used as reference compound. This compound is used to treat cardiovascular diseases and is a non-selective β -blocker and it is the most frequent β -blocker found in aquatic environment [10]. PROP has been detected in the environment, for instance in wastewaters [11] or in rivers with a range of concentrations between 0.1 and 7.3 ng/L [12]. This compound was also detected by Deo in a surface waters with a concentration of 53 ng/L [5]. The occurrence in wastewaters includes private household, effluents from hospitals and retirement homes and pharmaceutical plant wastewater [13]. Propranolol has been detected in a different aquatic environments and countries, such as Spain, Croatia, France, Serbia, Bosnia and China [12,14–17]. Concerning ecotoxicology, some studies indicate that aquatic organisms present high sensitivity to PROP [18]. Among AOPs, the photo-Fenton treatment has been demonstrated its efficiency in the elimination of a variety of compounds: pesticides [19], dyes [20], insecticides [21], pharmaceuticals [22,23], humic acids [24] and PCBs [25], among others.

Nevertheless, there are some drawbacks related to the conventional photo-Fenton process. The costs associated with photo-reactor investment, electrical cost of lamps and reagents are the principal disadvantages for full-scale application for photo-Fenton [26,27]. Chemicals to adjust pH (to avoid iron precipitation) and subsequent neutralization and hydrogen peroxide (H_2O_2) consumption are the main costs related to reagents [28,29].

Several ligands for the iron complexation, to work at circumneutral pH, have been studied to overcome the drawbacks of photo-Fenton at acidic pH [29–31]. On the other hand, the costs associated to energy consumption could be decreased using light-emitting diodes (LEDs) as a source of radiation. In recent years, the studies with the use of LEDs in AOPs have increased [32,33] because LEDs show many advantages such as low power consumption, long lifetime (up to 26,000 h), no overheating and no mercury content [32–41].

Other important item to consider, due to the water scarcity, is the possibility of water reuse. In this way, more data are needed to know the behavior of different AOPs, with water matrices coming from WWTPs. In this way, four matrices of secondary effluents from WWTPs were used and compared with Milli-Q water: Integrated Fixed-Film Activated Sludge (IFAS), Membrane Bioreactor (MBR), Conventional Activated Sludge (CAS) and the same process with nutrient elimination (CAS-NE) with 70% elimination of nitrogen and phosphorus. IFAS and CAS showed high amount of organic matter and turbidity (see Table 1). However, MBR and CAS-NE, presented low values of these parameters. IFAS was the dirtiest matrix with values approximately of $52 \text{ mg C}\cdot\text{L}^{-1}$ of total organic carbon (TOC) followed by CAS presenting $38 \text{ mg C}\cdot\text{L}^{-1}$ of TOC. CAS-NE and MBR shown similar values of TOC (around $13 \text{ mg C}\cdot\text{L}^{-1}$) but different values of turbidity, which is an important parameter in this comparison.

Summarizing, this paper is focused on the study of the efficiency of the photo-Fenton treatment, using two different light sources (Black-

Table 1
Physicochemical parameters of secondary effluent samples.

Parameter	IFAS	MBR	CAS	CAS-NE
pH	7.8	7.7	8.0	7.5
Turbidity (NTU)	18.5	0.5	20.1	2.6
UV ₂₅₄ (cm^{-1})	50.3	17.4	48.9	24.6
TOC ($\text{mg C}\cdot\text{L}^{-1}$)	51.1	13.6	37.9	13.3
DOC ($\text{mg C}\cdot\text{L}^{-1}$)	21.7	13.3	18.7	13.2
Total alkalinity ($\text{mg CaCO}_3\cdot\text{L}^{-1}$)	469.4	208.3	449.1	275.0
Cl^- ($\text{mg}\cdot\text{L}^{-1}$)	543.0	565.2	486.0	464.4
SO_4^{2-} ($\text{mg}\cdot\text{L}^{-1}$)	196.8	187.8	175.2	199.5
N-NO_2^- ($\text{mg}\cdot\text{L}^{-1}$)	0.2	0.2	0.1	0.3
N-NO_3^- ($\text{mg}\cdot\text{L}^{-1}$)	0.3	8.4	0.3	8.3

light blue lamps (BLB) and LEDs), in the propranolol (PROP) degradation in four secondary wastewater matrices from two WWTPs. The effect of iron chelates (EDTA/EDDS) at different molar ratios (Fe(II)-Ligand) using UV-A LED was tested in the four wastewater matrices. Biodegradability and efficiency were also evaluated to determine the capability of the photo-Fenton process at circumneutral pH.

2. Methodology

2.1. Chemicals

Propranolol hydrochloride (PROP) from Sigma-Aldrich was used as a target compound. *S,S'*-ethylenediamine-*N,N'*-disuccinic acid trisodium salt (EDDS-Na) solution from Sigma-Aldrich and ethylenediaminetetraacetic acid (EDTA) from Panreac Quimica Inc. were used as a chelating agents. In photo-Fenton experiments hydrogen peroxide (30% w/w) from Sigma-Aldrich and ferrous sulfate ($\text{FeSO}_4\cdot 7\text{H}_2\text{O}$) from Panreac Quimica were used. Acetonitrile and orthophosphoric acid (Panreac Quimica) were used as a mobile phase for HPLC. Sodium hydroxide (NaOH) and sulphuric acid (H_2SO_4) (both from Panreac Quimica Inc) were employed for the initial pH adjustments and subsequently neutralization, respectively.

2.2. Secondary effluents samples

Two secondary effluents (after the biological treatment) from two different Wastewater Treatment Plants (WWTPs) of Catalonia (Spain) were tested in this study. The characteristics of these wastewaters (WW) are shown in Table 1. The samples of the secondary effluent, were filtered with conventional laboratory paper to remove the largest particles. One WWTP has two parallel secondary treatments which include IFAS and MBR. The second one includes CAS and CAS-NE.

2.3. Photo-Fenton experiments

All experiments were performed in a 2L Pyrex-jacketed thermostatic photoreactor (inner diameter 11 cm; height 23 cm). A BLB lamp (Philips TL 8W, 08 FAM, wavelength range 290–400 nm with a maximum at 365 nm), covered with a quartz glass tube, was located at the center of the reactor. A hand-made lamp with eight LEDs (Intelligent LED solutions) arranged on an aluminum bar forming a spiral (to minimize the dark zones in the photoreactor) was also employed. The nominal power of each LED was 1.00 W, with 350 mA, irradiance angle of 125° and emission wavelength at 365 nm. The temperature of the solution was kept constant at 25°C with a thermostatic bath (Haake C-40) and the solutions were magnetically stirred into the photoreactor.

To carry out the conventional photo-Fenton experiments, a solution of 0.18 mM of Fe(II) was prepared in water acidified at $\text{pH } 2.8 \pm 0.2$ with H_2SO_4 . Then, PROP (0.19 mM = 50 mg/L) was added (this concentration was selected to assure accurate measurements of concentrations) and, finally, hydrogen peroxide (4.41 mM = 150 mg/L)

was added just before to run the experiment. These concentrations were selected because they achieved the best efficiency in PROP removal, according to previous experiments done in our laboratory. In the experiments at circumneutral pH, iron chelates (EDTA or EDDS) at two molar ratios (1:1 and 1:1.5) of L-Fe(II) were tested. Then, the pH of the EDTA solution was adjusted around 8.0 with NaOH 0.2 M to allow their dissolution due to the low solubility of this compound at acid pH. After the chelates were totally dissolved, Fe(II), H₂O₂ and PROP were added to the solution using the same concentrations listed above. Samples were taken from the photoreactor at fixed times during one hour.

2.4. Analytical methods

HPLC (Infinity Series from Agilent) was used to determine the concentration of PROP. Acetonitrile and Milli-Q water adjusted at pH = 3 by orthophosphoric acid (25:75) were employed. UV detector at 214 nm and a flow of 0.7 mL min⁻¹ were applied. The column used was SEA18 Teknokroma (250 × 4.6 mm i.d; 5 μm particle size). Hydrogen peroxide (H₂O₂) consumption was followed by the metavanadate spectrophotometric method [42]. Total iron was determined by the o-phenantroline standardized procedure (ISO 6332) at 510 nm. Biochemical Oxygen Demand (BOD) was evaluated according to the 5210-standard method (see [Supplementary material](#) for more information in section: Biochemical Oxygen Demand: Brief explanation of the process). The analysis of COD was done according to the ASTM D1252-06 Standard Test Methods, consisting in the sample oxidation with potassium dichromate in excess, in an acid medium, with catalysts and at 150 °C for 2 h [43]. Toxicity assays were performed in Microtox M500 toxicity analyzer (Modern Water, UK) [43]. Size Exclusion Chromatography combined with Organic Carbon Detection (SEC-OCD) was used to detect and quantify the different effluent organic matter (EfOM) present in the WW matrices tested [44] (more information can be found in [Table S1 in supplementary information](#)).

3. Results and discussion

3.1. Light sources comparison and effect of the matrix

The degradation of PROP by conventional photo-Fenton (pH = 2.8 ± 0.2) with BLB and UV-A LED is shown in [Fig. 1](#). Four wastewater matrices were tested with UV-A LED (MBR, CAS-NE, CAS, IFAS). The experiments achieving the best and the worst results in PROP degradation with UV-A LED were also performed with BLB lamps. In addition, Milli-Q water was also tested to evaluate more

accurately the influence of water matrix.

In the presence of UV-A LED, PROP degradation at 60 min was 100%, 52.1%, 50.6%, 40.2% and 32.9% for Milli-Q, MBR, CAS-NE, CAS and IFAS, respectively. While in the presence of BLB light source, PROP degradations reached were 100%, 95.3% and 68.8% for Milli-Q, MBR and IFAS, respectively. Thus, the same trend was followed with the two radiation sources and PROP removal decreases when TOC of water matrix increases. The percentage of standard deviation in photo-Fenton experiments did not exceed 5%. As can be observed in [Fig. 1](#), in the case of Milli-Q water similar PROP removal was achieved at 60 min for both, BLB and UV-A LED. Moreover, the kinetic constants obtained were very close (0.15 min⁻¹ for BLB and 0.14 min⁻¹ for LEDs, after first 30 s and assuming first order kinetics). When real matrices were used, the differences between BLB and LEDs were higher. This can be related to radiation distribution and absorption inside the reactor. Thus, the emission angle for BLB is 360° and only 125° for LEDs, which implies different distribution of radiation and probably dark zones in the case of LEDs. This last hypothesis can be strengthened because LEDs are punctual sources of light (see [Fig. S1 in the supplementary information](#)). In addition, although BLB presents the maximum peak at 365 nm, the emission range (290–400 nm) is wider than in LEDs (365–370 nm). Thus, depending on the absorption of different compounds in the real matrix their photolysis could be higher when BLB or LEDs are used. Probably in a complex system, such as a real matrix, the use of a light source with wider emission range favours the removal of different types of organic matter.

Real wastewaters compared with ultrapure water are complex systems due to different physico-chemical parameters (turbidity, high Total Organic Carbon (TOC), colour, presence of ions, etc.). Thus, WW matrices do not favor the photolysis and there is a highest competition for hydroxyl radicals [45] due to the presence of organic compounds different of target compound. [Fig. 1](#) shows the influence of different matrices with UV-A LED. Thus, ultrapure water, which achieved the best results, presents a TOC of 2 μg/L and obviously does not present ions or turbidity. Consequently, hydroxyl radicals only degrade the target pollutant and the byproducts of reaction, but no competition was detected with other compounds of the matrix. Regarding the values of TOC, these decrease following the order IFAS, CAS, CAS-NE and MBR. Thus, less competition is provided for the radicals produced and higher removal of the target compound was achieved when values of TOC were lower. As obvious, the composition of each WW is different but several authors have determined the kinetic constants for the reaction between hydroxyl radicals and dissolved organic matter (DOM). These values are in the order 10⁸–10⁹ L·mol⁻¹·s⁻¹ [46–51], which can

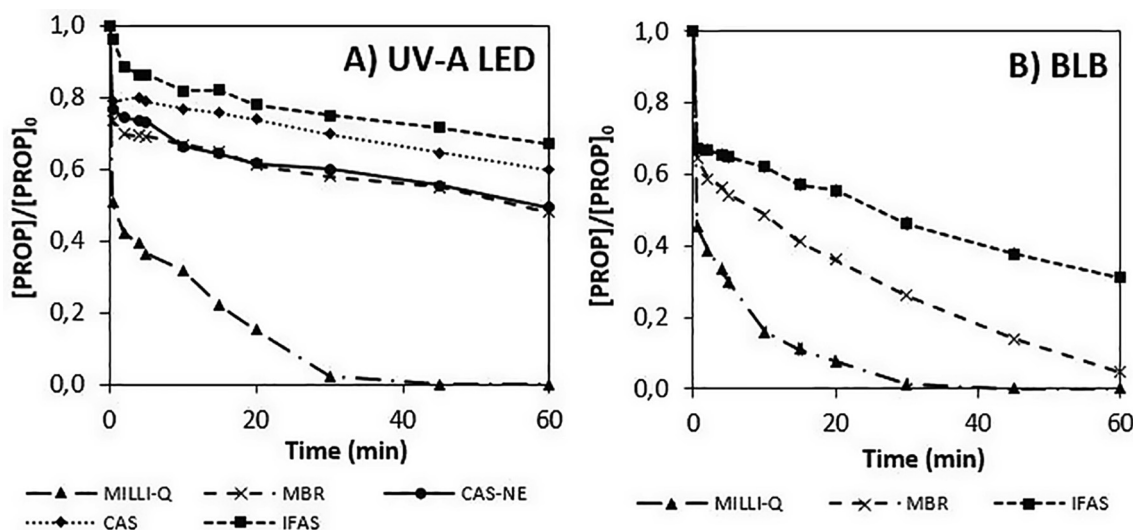


Fig. 1. PROP degradation in different light sources by conventional photo-Fenton process. [PROP]₀ = 0.19 mM; [Fe(II)]₀ = 0.18 mM; [H₂O₂]₀ = 4.41 mM.

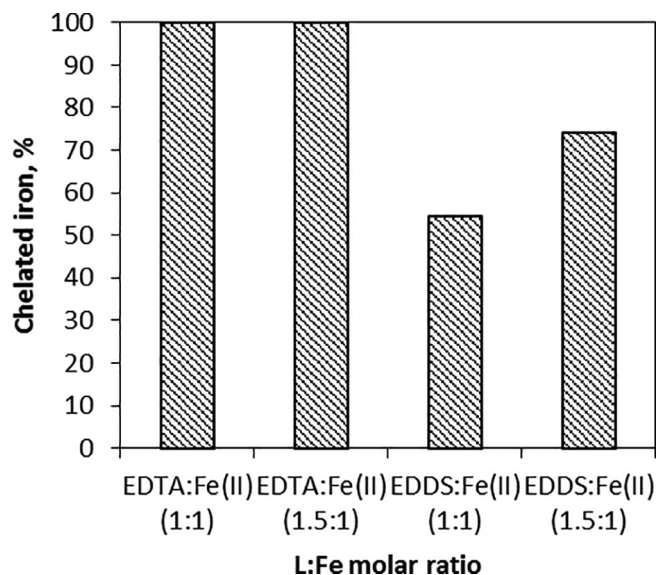


Fig. 2. Percentage of iron chelates formed with two L:Fe(II) molar ratios tested. Calculated by absorbance at 258 nm.

explain again the strong competition between organic matter present in WW and target compound for the hydroxyl radicals. Other important parameter influencing on PROP removal was turbidity due to light scattering. In this way, IFAS presents high turbidity and the highest TOC and, as a consequence, the lowest PROP removal. However, MBR and CAS-NE presented very close results in PROP degradation, achieving the highest removals of PROP, regarding wastewaters. In that case, their values of TOC and turbidity were the lowest. In the same way as the TOC, the dissolved organic carbon (DOC) influences on micropollutant degradation. The presence of an organic matter in solution can compete with target compound for hydroxyl radicals reducing the removal efficiency of the micropollutant. In addition, UV_{254} is a spectroscopic property related to the presence of organic matter, particularly aromatic and unsaturated moieties which can also readily react with hydroxyl radicals. IFAS, which achieved lower PROP degradation, also showed the highest values of DOC and UV_{254} and MBR, which shown the best PROP removal, the lowest. Finally, the effect of ions (Cl^- , SO_4^{2-} , $N-NO_2^-$) was not significant, because their concentrations were similar in all treated WW. Nevertheless, when ultrapure water and wastewater were compared the effect of ions can appear. Alkalinity is an important indicator of (bi)carbonates concentration in WW. However, in conventional photo-Fenton, the alkalinity of the solution was neutralized when the matrix was acidified and then mixed. Other inorganic ions can act as a scavenger of $\cdot OH$. The nitrite reacts with the hydroxyl radicals, producing nitrite radicals, with a second-order reaction rate of $1.0 \cdot 10^{10} M^{-1} s^{-1}$ [52]. According to Benner and coworkers, the reaction rate of propranolol is $1.0 \cdot 10^{10} M^{-1} s^{-1}$ [53]. Thus, the reaction rate for PROP and nitrite with $\cdot OH$ is practically the same. However, as the nitrite concentration is lower than PROP the nitrite probably acts as a scavenger to a lesser extent in these experiments. Moreover, nitrite can produce hydroxyl radicals by photolysis (Eqs. (1) and (2)).



Nitrite absorbs radiation in the UV-A range (around 355 nm) [54] but its concentration in the four WW tested is very low. Thus, the equilibrium between generation and scavenging of hydroxyl radicals produces a stationary state in hydroxyl radicals concentration [54]. Regarding nitrates, in accordance with Buxton *et al.* [52] NO_3^- does not react with hydroxyl radicals. The photolysis of nitrates, giving $\cdot OH$

radicals, has been studied in various works [55,56,57]. They mostly absorb in the UV-B (absorption maximum around 305 nm). However, LEDs used in this work emit in 365–370 nm range. Thus, the photolysis of nitrate is not possible. Finally, Cl^- reacts with hydroxyl radicals with a second-order reaction rate of $4.3 \cdot 10^9 M^{-1} s^{-1}$ [52]. As mentioned above, the reaction rate of propranolol is $1.0 \cdot 10^{10} M^{-1} s^{-1}$, being higher than this one of chloride. Nevertheless, the concentration of chloride is 10 times higher than propranolol in the tested WW. Thus, the ion chloride probably acts as a scavenger of hydroxyl radicals. Thus, when ultrapure water and wastewaters were compared the results achieved presented significant differences due, in part, to the presence of ions in WW. However, according to Table 1 data, the ions concentrations are very close for the different WW tested. Consequently, ions concentrations do not imply significant differences in the influence of the different WW matrices on PROP removal.

3.2. photo-Fenton at circumneutral pH with LEDs

3.2.1. Iron chelates

An important parameter in photo-Fenton process when ligands (L) are used is the L-Fe molar ratio. A ratio L-Fe higher than stoichiometric, is required experimentally to ensure a satisfactory chelation process [28]. Two ligands were tested (EDTA and EDDS) at two molar ratios L-Fe (1:1 and 1.5:1). The percentage of chelated iron with each condition was determined at 258 nm [28] with ultrapure water to avoid any interference. The results are shown in Fig. 2.

Regarding Fig. 2, EDTA presents the 100% of chelated iron for both molar ratios 1:1 and 1.5:1. However, for EDDS the percentage of chelated iron is always lower than 100% and that percentage increases with 1.5:1 M ratio (54.4% and 74.0% for 1:1 and 1.5:1, respectively).

The decision on the best chelating agent and the best molar ratio L-Fe (II) also depends on the efficiency in the target compound degradation and the increase in the biodegradability. In this way, the results of PROP degradation are showed in Fig. 3. All the experiments presented in this section were performed in ultrapure water to avoid any interference.

For both EDDS and EDTA, the same PROP degradation results were observed when two ratios were tested (Fig. 3). The pseudo-first order kinetic constants for EDDS-Fe(II) were 0.07 and 0.06 min^{-1} for L-Fe(II) molar ratio of 1:1 and 1.5:1, respectively. For EDTA-Fe(II), the kinetic constant was 0.01 min^{-1} for the two L-Fe molar ratios. Thus, EDDS runs

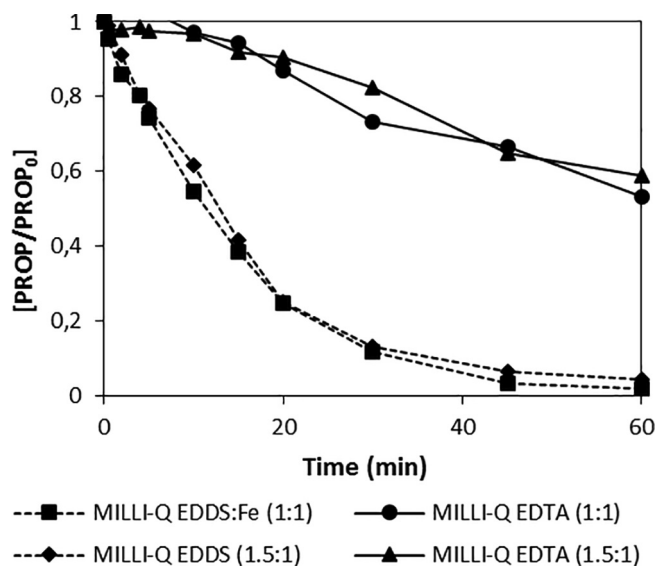


Fig. 3. PROP degradation with EDTA and EDDS and two molar ratio L:Fe(II) (1:1 and 1.5:1) in ultrapure water. $[PROP]_0 = 0.19 \text{ mM}$; $[Fe(II)]_0 = 0.18 \text{ mM}$; $[H_2O_2]_0 = 4.41 \text{ mM}$. Radiation source: LEDs.

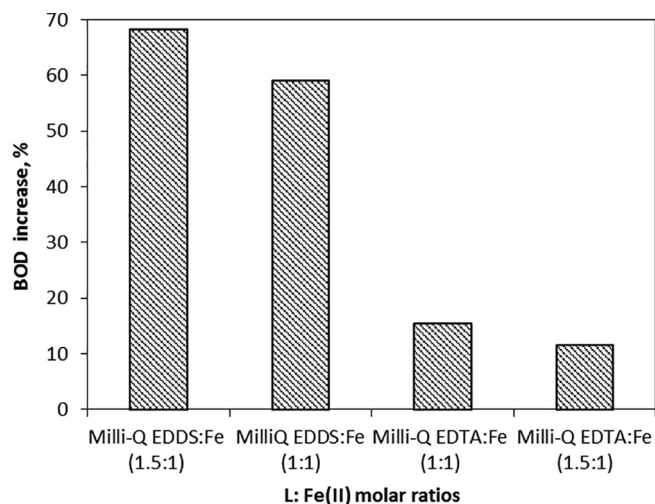


Fig. 4. Percentage of BOD increase after treatment of EDTA and EDDS with 1:1 and 1.5:1 L-Fe(II) molar ratios. $[\text{PROP}]_0 = 0.19 \text{ mM}$; $[\text{Fe(II)}]_0 = 0.18 \text{ mM}$; $[\text{H}_2\text{O}_2]_0 = 4.41 \text{ mM}$.

better than EDTA in PROP degradation: 99.6% for EDDS and 47.3% for EDTA after 60 min (molar ratio L-Fe(II) 1:1). The best molar ratio L-Fe(II) is 1:1, implying that less amount of chelating agent has to be used, which represents a decrease in effluent's TOC and in the cost associated at chelating agent. Moreover, PROP and chelates compete for hydroxyl radicals and this fact explains the efficiency decrease when L-Fe(II) ratio increases.

Other properties to take into account to select the best chelate are biodegradability and toxicity. Fig. 4 shows that the biodegradability increase is higher for EDDS than EDTA. The results agree with the research works of different authors who investigated the replacement of EDTA to EDDS [29,31]. Thus, EDDS is a more appropriate chelating agent than EDTA, because it is environmentally friendly, easily biodegradable and stable at neutral pH [38]. Finally, regarding to hazardousness, toxicity (*Vibrio fischeri*) was assessed for both EDTA and EDDS (molar ratio L-Fe(II) 1:1). The results were expressed with $1/\text{EC}_{50}$, being EC_{50} the value of sample dilution that kills 50% of bioluminescent bacteria population. The values obtained were 0.008 and 0.016 for EDDS and EDTA, respectively, indicating that EDTA is about 2 times more toxic than EDDS.

3.2.2. Efficiency of EDDS-Fe(II) in different water matrices with LEDs

The efficiency of EDDS-Fe(II) complex was compared in the PROP degradation by photo-Fenton in the different water matrices previously used (see Fig. 5). The initial pH was the corresponding to each wastewater, around 7.5–8.0 (Table 1), and remained stable during the experiment.

Regarding the percentages of PROP eliminated (60 min), they were 99.6, 62.7, 61.0, 47.0 and 14.3% for Milli-Q, MBR, CAS-NE, CAS and IFAS, respectively. As commented before, the PROP removal decreases when the TOC of WW increases. Thus, IFAS, with the highest TOC (see Table 1), shows the lowest degradation with only a 10% after 1 h of experiment. This behavior points out the competition of the organic matter present in WW for the hydroxyl radicals and light.

During the reaction, an important parameter to follow is the total dissolved iron, because hydroxyl radicals attack PROP and organic matter of wastewaters but also the EDDS-Fe(II) complex. Fig. 6 shows the total iron dissolved remaining in solution for each wastewater during the experiment.

As it can be observed in the Fig. 6, the iron remaining at the end of the treatment was lower when wastewaters were used. The values of total iron in solution at 60 min were between 10 and 25% of the total initial iron in solution in different wastewaters. However, when Milli-Q

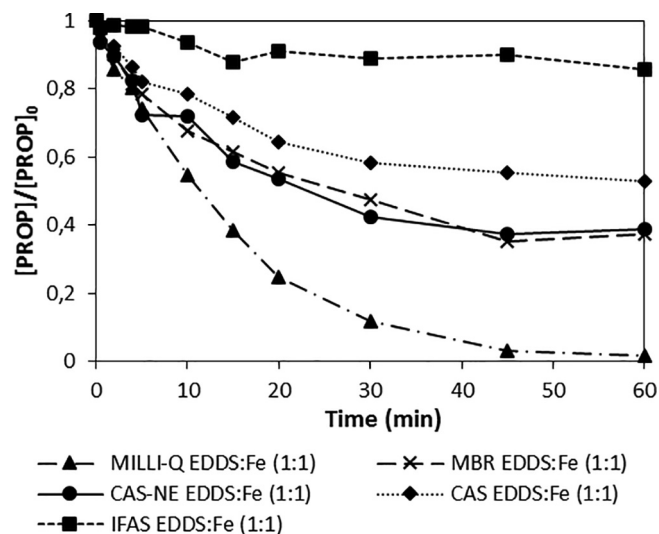


Fig. 5. PROP degradation in different matrices by photo-Fenton, with LEDs, at circumneutral pH. EDDS:Fe(II) (1:1); $[\text{PROP}]_0 = 0.19 \text{ mM}$; $[\text{Fe(II)}]_0 = 0.18 \text{ mM}$; $[\text{H}_2\text{O}_2]_0 = 4.41 \text{ mM}$.

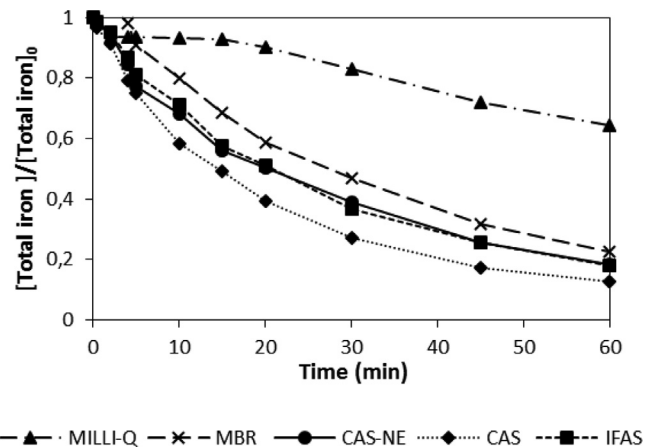


Fig. 6. Total dissolved iron during the reaction of photo-Fenton catalyzed by EDDS-Fe(II) for each wastewater. EDDS:Fe(II) (1:1); $[\text{PROP}]_0 = 0.19 \text{ mM}$; $[\text{Fe(II)}]_0 = 0.18 \text{ mM}$; $[\text{H}_2\text{O}_2]_0 = 4.41 \text{ mM}$.

water was tested around 70% of total initial dissolved iron remained at the end of the experiment. The stability of the complexes can be affected by many parameters. In this sense, in Milli-Q water only target compound, their respective intermediates and chelating agent are present in the solution. Nevertheless, wastewater matrices are a complex system with different types of organic matter and other dissolved species. All this decreases the stability of the complexes making them more vulnerable to hydroxyl radicals.

In the same way that total dissolved iron was analyzed, the concentrations of H_2O_2 for different wastewaters were monitored during the reaction. In Supplementary material can be found a figure (Fig. S2) with hydrogen peroxide curves for each wastewater in conventional photo-Fenton and photo-Fenton catalyzed by EDDS-Fe(II) with LEDs.

The PROP removal at conventional photo-Fenton and photo-Fenton catalyzed by EDDS-Fe(II) is reported in Fig. 7 in order to establish comparisons between the two systems.

In Fig. 7 it is observed that, for all tested water matrices, there is a common trend, with lower TOC and DOC, higher conversion. Therefore, Milli-Q gives the best results and IFAS the worst ones. This happens for both conventional photo-Fenton and photo-Fenton at circumneutral pH.

For a better comparison, different fittings were done and results are

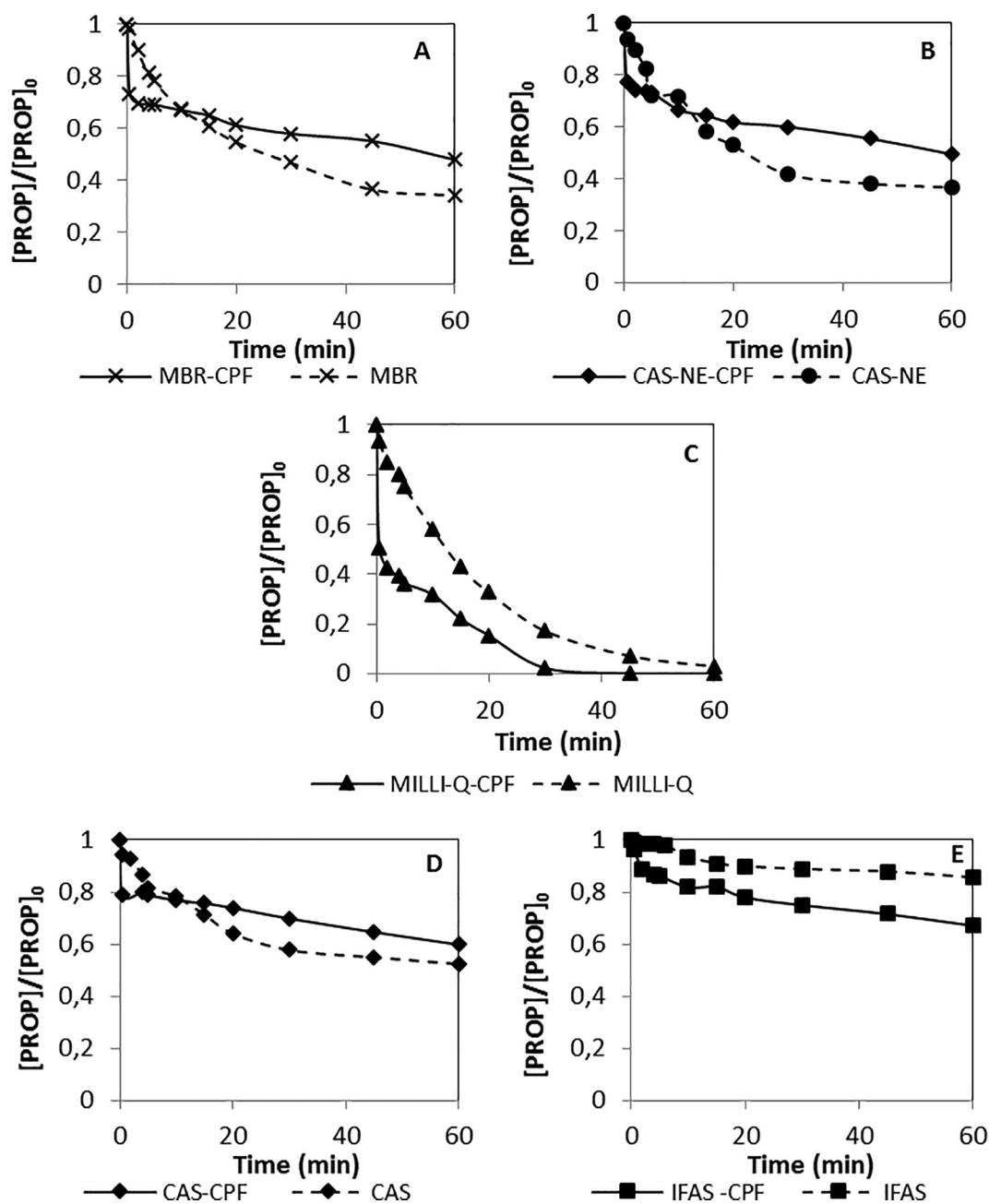


Fig. 7. Degradation of PROP by conventional photo-Fenton (CPF) and photo-Fenton, with LEDs, catalyzed by EDDS-Fe(II) in different wastewaters. EDDS:Fe(II) (1:1); [PROP]₀ = 0.19 mM; [Fe(II)]₀ = 0.18 mM; [H₂O₂]₀ = 4.41 mM.

Table 2

Values of kinetic constants for conventional photo-Fenton and photo-Fenton catalyzed by EDDS (k_1 , k_2 , k_3 fitting to pseudo first order kinetics, k_4 to zero order kinetic).

Kinetic constants	k_1 (min ⁻¹)	k_2 (min ⁻¹)	R ² k_2	k_3 (min ⁻¹)	R ² k_3	k_4 (ppm/min)
MILLI-Q-CPF	1.354	0.135 ± 0.040	0.92	0.136 ± 0.030	0.92	0.022
MBR-CPF	0.621	0.006 ± 0.001	0.96	0.0085 ± 0.006	0.60	0.010
CAS-NE-CPF	0.525	0.007 ± 0.001	0.92	0.0093 ± 0.005	0.68	0.010
CAS-CPF	0.477	0.005 ± 0.001	0.98	0.0065 ± 0.004	0.68	0.008
IFAS-CPF	0.073	0.006 ± 0.002	0.87	0.0064 ± 0.002	0.82	0.006
MILLI-Q EDDS	0.129	0.058 ± 0.002	0.99	0.0220 ± 0.002	0.99	0.021
MBR-EDDS	0.038	0.021 ± 0.004	0.96	0.0219 ± 0.004	0.96	0.014
CAS-NE-EDDS	0.129	0.021 ± 0.005	0.93	0.0220 ± 0.005	0.93	0.014
CAS-EDDS	0.120	0.013 ± 0.003	0.92	0.0135 ± 0.003	0.91	0.010
IFAS-EDDS	0.025	0.003 ± 0.001	0.83	0.0031 ± 0.001	0.84	0.003

Table 3
EfOM compositions for MBR and IFAS wastewater samples.

Compounds [$\mu\text{g}\cdot\text{L}^{-1}$]	MBR	IFAS	CAS
Biopolymers	51	3392	1611
Humic substances	3319	5217	3916
Building Blocks	1139	1622	1701
Neutrals	1667	3205	3318
Acids	350	789	1140

shown in Table 2. The used data are these ones of the experiments presented in Fig. 7.

The kinetic constant k_1 corresponds to the initial reaction rate and has been calculated for the initial 30 s of the experiment. k_2 and k_3 were calculated assuming pseudo-first order kinetics, according to Eq. (3). For the fitting of k_2 only the concentration-time data from 30 s to the end of the experiment have been used. While, for k_3 fitting, the concentration-time data from time zero to the end of the experiment have been considered. In both cases, 45 min has been taken as the final time, because at this time the 100% of PROP degradation is achieved in Milli-Q water and conventional photo-Fenton.

$$\ln\left(\frac{C_f}{C_0}\right) = k \cdot t \quad (3)$$

On the other hand, k_4 indicates an average rate of PROP removal (would be equivalent to assume zero-order kinetics) and it has been estimated according to Eq. (4).

$$k_4 = \frac{C_0 - C_f}{t} \quad (4)$$

where c_0 is the initial PROP concentration (ppm), c_f is the final PROP concentration (ppm) and t is the time (min).

It should be noted that the kinetic constants that appear in Table 2 will be used qualitatively trying to explain the shape of the graphs in Fig. 7. Their absolute values do not matter as much as the comparison between them. Likewise, all these constants have been indicated to show the importance of choosing well the type of fitting and the intervals used.

From Fig. 7, it can be seen that, in conventional photo-Fenton and WW matrices, the concentration of PROP decreases quickly at the beginning of the experiment, during the first 30 s, and then decreases very slowly. From there it could be deduced that, in the initial 30 s, dark-Fenton controls the reaction rate. In addition it can be said that k_1 decreases when TOC of WW increases. After this period, since the Fe^{2+} has already passed practically everything to Fe^{3+} , photo-Fenton would be the controlling mechanism and the reaction rate becomes much slower. In fact, it is also observed in Table 2 that k_1 is much higher than k_2 (in the case of MBR, CAS-NE and CAS is almost 100 times higher). In the case of IFAS, it is only 10 times higher for different reasons that will be discussed later.

In circumneutral photo-Fenton, one could say that the behavior is similar to a certain extent. In this case, the initial drop in the concentration of PROP is lower because Fe^{2+} is chelated. In fact, the k_1 values in Table 2, for the same water matrix, are lower for circumneutral photo-Fenton. However, it is also observed that at the end of the experiment the curves flatten because the iron has already largely precipitated (see Fig. 6) and the photo-Fenton slows down a lot.

In any case, the composition of WW is very important because the experiments done with IFAS present a behavior something different than the experiments carried out with the other WW as a matrix. In IFAS it is even more pronounced that dark Fenton, at circumneutral pH, has less weight. In such a way that it lowers very little and then flattens out and therefore does not get to cross with the photo-Fenton at normal pH. In fact, in experiments done with another sample of IFAS, similar behavior was observed but the initial drop was a little more pronounced. In that experiment, which lasted up to 180 min, the great

slowdown after the initial drop was also observed, when there is a chelating agent. In fact, it was observed that between 30 and 180 min, the concentration of PROP was only reduced by 10% (more information can be found in Fig. S3 in Supplementary information). The behavior seems geometrically similar to Milli-Q but it is the opposite. In Milli-Q, the curves (Fig. 7) corresponding to conventional photo-Fenton and photo-Fenton at circumneutral pH do not cross each other because in normal photo-Fenton the dark Fenton is very important and the concentration drops a lot. In fact, for conventional photo-Fenton, the value of k_1 with Milli-Q was 1.35 min^{-1} , this is the highest value for different matrices and approximately 10 times higher than the value for circumneutral pH. The value of k_2 was also the highest. Thus, the reaction rate was very high and the possibility of circumneutral photo-Fenton process to achieve better kinetics was low.

Concerning to the kinetic constants presented in Table 2, another observation can be made. k_2 obtained at circumneutral pH is higher than this one at conventional photo-Fenton for MBR, CAS-NE and CAS, but the contrary occurs with IFAS. Probably, this fact was due to the presence of different organic matter constituents which were not present in MBR sample, even though both came from the same WWTP. Table 3 presents the EfOM composition corresponding to MBR and IFAS samples, analysed by SEC-OCD methodology. In Table 3, it can also be observed EfOM composition corresponding to CAS, which present high organic content (like IFAS) but gives better performance in both photo-Fenton at neutral pH and conventional photo-Fenton. As it can be observed, in all compounds, IFAS presents higher concentrations than MBR and CAS.

IFAS has an approximately 70 times higher concentration of biopolymers than MBR, and almost 2 times more of humic substances. Biopolymers and humic substances can chelate the iron present in solution. Thus, probably the explanation of the different trend in IFAS than other WW in circumneutral photo-Fenton could be that iron in solution was also chelated by biopolymers or humic substances. This fact could make the efficiency of the process decrease. In addition, IFAS has an approximately 2 times higher concentration of biopolymers than CAS, and 1.3 times more of humic substances. Compared to MBR, the highest difference is in biopolymers since the concentration of humic substances is similar. MBR and CAS showed better results for PROP removal in photo-Fenton catalyzed by EDDS-Fe(II). However, IFAS achieved better PROP degradation in conventional photo-Fenton. Thus, it could be deduced that probably the highest influence on iron chelates is due to humic substances and in a lesser extent to biopolymers.

Coming back again to the different kinetic constants used, it can be seen that, when the matrix is WW and for a given matrix, the values of k_2 , k_3 and k_4 are not very different from each other. However, k_3 and k_4 show a much worse interpretation of what happens since they do not distinguish the fast initial decrease in PROP concentration due to dark Fenton. On the other hand, k_3 and k_4 allow an easy global approximation to determine the process that allows the highest rate in the global reduction of the PROP concentration.

To conclude this section the results of biodegradability for photo-Fenton catalyzed by EDDS-Fe(II) are shown in Fig. 8. These results are presented as a percentage of BOD increase after the photo-Fenton treatment.

As it can be observed in Fig. 8, all matrices demonstrated an increase of BOD after the treatment. Moreover, in Supplementary material (Table S2) they can be found the initial values of BOD, COD and biodegradability. Milli-Q water shows the best results (near 70%) and IFAS the worst ones (approximately 30%). CAS, MBR and CAS-NE gave close results (approximately 50%).

In Milli-Q water the solution is the most biodegradable due to almost all the PROP was removed (99.6%). Thus, the intermediates formed could be oxidized during the photo-Fenton treatment. Therefore, the structures of remaining intermediates at 60 min probably were more simples than in the other matrices increasing the BOD. In addition, as it can be seen in Fig. 6, the iron remaining in solution is

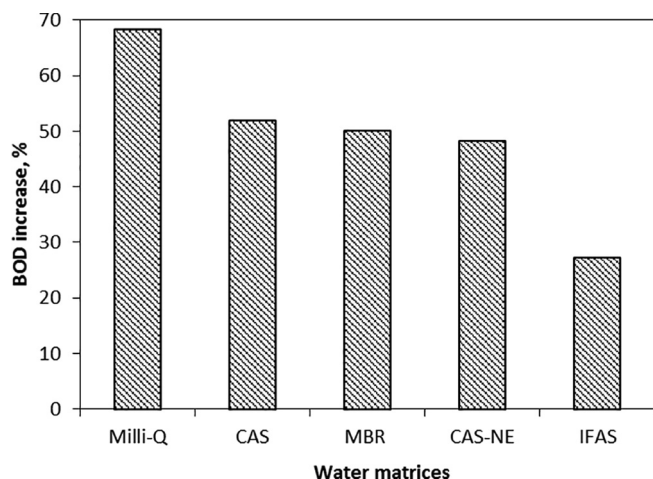


Fig. 8. Percentage of BOD increase after treatment of different matrices with a ratio of 1:1 L-Fe(II). $[\text{PROP}]_0 = 0.19 \text{ mM}$; $[\text{Fe(II)}]_0 = 0.18 \text{ mM}$; $[\text{H}_2\text{O}_2]_0 = 4.41 \text{ mM}$.

higher in Milli-Q than other matrices. Thus, there is more chelating agent (EDDS) in solution and, as EDDS is considered biodegradable, this could also increase the biodegradability. Regarding CAS and CAS-NE the results were very close. On the other hand, MBR showed similar results than CAS-NE because both present a similar PROP degradation (62.7% for MBR and 61.0% for CAS-NE). The two wastewaters present values of TOC very close too. So that, the organic matter to oxidize in the BOD analysis is probably the same in the two WW. Finally, IFAS presented a lower percentage of increase of biodegradability, because only a 14.3% of PROP removal was achieved. In addition, IFAS is an effluent of secondary treatment and its content on biodegradable organic matter is lower.

The increase in biodegradability suggests that the oxidation intermediates are becoming simpler structures. In this work the main oxidation intermediates of propranolol were not analyzed. However, some articles in the literature and previous works in our laboratory detected the main intermediates of propranolol and its pathways [11,58–62]. Moreover, in Table S3 in supplementary material the structures of main oxidation intermediates of propranolol detected in our previous works can be found [61,62].

4. Conclusions

In this study, the degradation of PROP by conventional photo-Fenton with BLB and UV-A LED radiation was compared. The results indicated that, using ultrapure water, the differences were not significant. However, with WW matrices the differences increase mainly due to the presence of different organic matter which absorbs part of radiation and also competes with PROP for hydroxyl radicals. Turbidity also influences on the radiation transfer through the photoreactor. In addition, PROP removal decreases when TOC of WW increases. Thus, ultrapure water achieved the best PROP degradation while IFAS presented the worst PROP removal.

Two molar ratios L-Fe (1:1 and 1.5:1) and two chelating agents (EDDS and EDTA) were tested. EDDS as a chelating agent with 1:1 L-Fe molar ratio gave the best results in PROP degradation, biodegradability and toxicity.

Concerning the efficiency in PROP degradation, experiments of photo-Fenton at circumneutral pH showed the same trend than experiments of conventional photo-Fenton for the different matrices. Comparing photo-Fenton at acid pH and circumneutral pH, IFAS and ultrapure water achieved higher PROP removals with conventional photo-Fenton but MBR, CAS and CAS-NE showed the highest PROP degradations for photo-Fenton catalyzed by EDDS-Fe(II). In the case of

IFAS the presence of biopolymers and more humic substances, which can chelate with iron, probably affected the PROP degradation and changing the trend of degradation than other WWs.

Dark Fenton is very important during the initial time (30 s) of the experiments. For instance, with Milli-Q water, 50% of PROP is degraded in 30 s. For the other WW matrices, the trend is similar. After the initial 30 s, photo-Fenton controls the process and reaction rate slows down. In the case of photo-Fenton at circumneutral pH, the effect of dark Fenton during the initial 30 s is not so important due to the chelation of Fe^{2+} .

Acknowledgments

The authors are appreciative with the Ministry of Science and Innovation of Spain (projects CTQ2014-52607-R and CTQ2017-86466-R), Ministry of Education, Culture and Sports (FPU research fellowship FPU-16/02101), Institute for Water Research (IdRA) of Universitat de Barcelona and AGAUR-Generalitat de Catalunya (project 2014SGR245 and 2017SGR-131) for providing funds for this study.

Appendix A. Supplementary data

Supplementary data to this article can be found online at <https://doi.org/10.1016/j.cej.2019.122416>.

References

- [1] T.A. Ternes, A. Joss, Human Pharmaceuticals Hormones and Fragrances. The Challenge of Micropollutants in Urban Water Management, IWA Publishing, London, New York, 2006.
- [2] Y. Lee, U. von Gunten, Oxidative transformation of micropollutants during municipal wastewater treatment: Comparison of kinetic aspects of selective chlorine, (chlorine dioxide, ferrate VI, and ozone) and non-selective oxidants (hydroxyl radical), *Water Res.* 44 (2010) 555–566.
- [3] M. Ibáñez, V. Borova, C. Boix, R. Aalizadeh, R. Bade, N.S. Thomaidis, F. Hernández, UHPLC-QTOF MS screening of pharmaceuticals and their metabolites in treated wastewater samples from Athens, *J. Hazard. Mater.* 323 (Part A) (2017) 26–35.
- [4] M. Gros, K.M. Blum, H. Jernstedt, G. Renman, S. Rodríguez-Mozaz, P. Haglund, P.L. Andersson, K. Wiberg, L. Ahrens, Screening and prioritization of micropollutants in wastewaters from on-site sewage treatment facilities, *J. Hazard. Mater.* 328 (2017) 37–45.
- [5] R.P. Deo, Pharmaceuticals in the surface water of the USA: a review, *Curr. Environ. Health Rep.* 1 (2014) 113–122.
- [6] N. De la Cruz, J. Giménez, S. Esplugas, D. Grandjean, L.F. de Alencastro, C. Pulgarin, Degradation of 32 emergent contaminants by UV and neutral photo-Fenton in domestic wastewater effluent previously treated by activated sludge, *Water Res.* 46 (2012) 1947–1957.
- [7] A. Pal, K.Y.H. Gin, A.Y.C. Lin, M. Reinhard, Impacts of emerging organic contaminants on freshwater resources: review of recent occurrences, sources, fate and effects, *Sci. Total Environ.* 408 (2010) 6062–6069.
- [8] L.H.M.L.M. Santos, A.N. Araujo, A. Fachini, A. Pena, C. Delerue-Matos, M.C.B.S.M. Montenegro, Ecotoxicological aspects related to the presence of pharmaceuticals in the aquatic environment, *J. Hazard. Mater.* 175 (2010) 45–95.
- [9] N. De la Cruz, L. Esquiú, D. Grandjean, A. Magnet, A. Tungler, L.F. de Alencastro, C. Pulgarin, Degradation of emergent contaminants by UV, UV/ H_2O_2 and neutral photo-Fenton at pilot scale in a domestic wastewater treatment plant, *Water Res.* 47 (2013) 5836–5845.
- [10] J. Maszkowska, S. Stolte, J. Kumirska, P. Łukaszewicz, K. Mioduszevska, A. Puckowski, M. Caban, M. Wagil, P. Stepnowski, A. Białk-Bielinska, Beta-blockers in the environment: part I. Mobility and hydrolysis study, *Sci. Total Environ.* 493 (2014) 1112–1121.
- [11] S.O. Ganiyu, N. Oturan, S. Raffy, G. Esposito, E.D. van Hullebusch, M. Cretin, M.A. Oturan, Use of sub-stoichiometric titanium oxide as a ceramic electrode in anodic oxidation and electro-fenton degradation of the beta-blocker propranolol: degradation kinetics and mineralization pathway, *Electrochim. Acta* 242 (2017) 344–354.
- [12] C. Fernández, M. González-Doncel, J. Pro, G. Carbonell, J.V. Tarazona, Occurrence of pharmaceutically active compounds in surface waters of the henares-jarama-tajo river system (madrid, spain) and a potential risk and characterization, *Sci. Total Environ.* 408 (2010) 543–551.
- [13] K. Kümmerer, Drugs in the environment: emission of drugs, diagnostic aids and disinfectants into wastewater by hospitals in relation to other sources: a review, *Chemosphere* 45 (2001) 957–969.
- [14] M. Gros, M. Petrovic, D. Barceló, Development of a multi-residue analytical methodology based on liquid chromatography-tandem mass spectrometry (LC-MS/MS) for screening and trace level determination of pharmaceuticals in surface and wastewaters, *Talanta* 70 (2006) 678–690.

- [15] V. Gabet-Giraud, C. Miège, J.M. Choubert, S.M. Ruel, M. Coquery, Occurrence and removal of estrogens and beta blockers by various processes in wastewater treatment plants, *Sci. Total Environ.* 408 (2010) 4257–4269.
- [16] S. Terzić, I. Senta, M. Ahel, M. Gros, M. Petrovic, D. Barceló, J. Müller, T. Knepper, I. Martić, F. Ventura, P. Jovancic, D. Jabucar, Occurrence and fate of emerging wastewater contaminants in Western Balkan Region, *Sci. Total Environ.* 399 (2009) 66–77.
- [17] Y. Yang, J. Fu, H. Peng, L. Hou, M. Liu, J.L. Zhou, Occurrence and phase distribution of selected pharmaceuticals in Yangtze Estuary and its costal zone, *J. Hazard. Mater.* 190 (2011) 588–596.
- [18] D.B. Huggett, B.W. Brooks, B. Peterson, C.M. Foran, D. Schlenk, Toxicity of select beta adrenergic receptor-blocking pharmaceuticals (b-blockers) on aquatic organisms, *Arch. Environ. Contam. Toxicol.* 43 (2002) 229–235.
- [19] J.J. Pignatello, Y. Sun, Complete oxidation of metolachlor and methyl parathion in water by the photoassisted Fenton reaction, *Water Res.* 29 (1995) 1837–1844.
- [20] J.M. Monteagudo, A. Duran, C. Lopez-Almodovar, Homogeneous ferrioxalate assisted solar photo-Fenton degradation of Orange II aqueous solutions, *Appl. Catal. B* 83 (2008) 46–55.
- [21] E. Evgenidou, I. Konstantinou, K. Fytianos, I. Poulous, Oxidation of two organophosphorus insecticides by the photo-assisted Fenton reaction, *Water Res.* 41 (2007) 2015–2027.
- [22] F. Méndez-Arriaga, S. Esplugas, J. Giménez, Degradation of the emerging contaminant ibuprofen in water by photo-Fenton, *Water Res.* 44 (2010) 589–595.
- [23] R.G. Zepp, B.C. Faust, J. Hoigné, Hydroxyl radical formation in aqueous reactions (pH 3–8) of iron(II) with hydrogen peroxide: the photo-Fenton reaction, *Environ. Sci. Technol.* 26 (1992) 313–319.
- [24] M. Fukushima, K. Tatsumi, S. Nagao, Degradation characteristics of humic acid during photo-Fenton processes, *Environ. Sci. Technol.* 35 (2001) 3683–3690.
- [25] J.J. Pignatello, G. Chapa, Degradation of PCBs by ferric ion, hydrogen peroxide and UV light, *Environ. Toxicol. Chem.* 13 (1994) 423–427.
- [26] S. Miralles-Cuevas, D. Darowna, A. Wanag, S. Mozia, S. Malato, I. Oller, Comparison of UV/H₂O₂, UV/S₂O₈²⁻, solar/Fe(II)/H₂O₂ and solar/Fe(II)/S₂O₈²⁻ at pilot plant scale for the elimination of micro-contaminants in natural water, *Chem. Eng. J.* 310 (2017) 514–524.
- [27] I. De la Obra, L. Ponce-Robles, S. Miralles-Cuevas, I. Oller, S. Malato, J.A. Sánchez Pérez, Microcontaminant removal in secondary effluents by solar photo-Fenton at circumneutral pH in raceway pond reactors, *Catal. Today* 287 (2017) 10–14.
- [28] J.J. Pignatello, E. Oliveros, A. McKay, Advanced oxidation processes for organic contaminant destruction based on the Fenton reaction and related chemistry, *Crit. Rev. Environ. Sci. Technol.* 36 (2006) 1–84.
- [29] S. Miralles-Cuevas, I. Oller, A. Ruiz-Delgado, A. Cabrera-Reina, L. Cornejo-Ponce, S. Malato, EDDS as complexing agent for enhancing solar advanced oxidation processes in natural water: effect of iron species and different oxidants, *J. Hazard. Mater.* (2019), <https://doi.org/10.1016/j.jhazmat.2018.03.018>.
- [30] A. De Luca, R.F. Dantas, S. Esplugas, Assessment of iron chelates efficiency for photo-Fenton at neutral pH, *Water Res.* 61 (2014) 232–242.
- [31] W. Huang, M. Brigante, F. Wu, K. Hanna, G. Mailhot, Development of a new homogeneous photo-Fenton process using Fe(II)-EDDS complexes, *J. Photochem. Photobiol. A: Chem.* 239 (2012) 17–23.
- [32] I. De la Obra, B. Esteban García, J.L. García Sánchez, J.L. Casas López, J.A. Sánchez Pérez, Low cost UVA-LED as a radiation source for the photo-Fenton process: a new approach for micropollutant removal from urban wastewater, *Photochem. Photobiol. Sci.* 16 (2017) 72–78.
- [33] A.C. Chevremont, A.M. Farnet, M. Sergent, B. Columb, Effect of coupled UV-A and UV-C LEDs on both microbiological and chemical pollution of urban wastewaters, *Sci. Total Environ.* 426 (2012) 304–310.
- [34] O. Autin, C. Romelot, L. Rust, J. Hart, P. Jarvis, J. MacAdam, S.A. Parsons, B. Jefferson, Evaluation of a UV-light emitting diodes unit for the removal of micropollutants in water for low energy advanced oxidation processes, *Chemosphere* 92 (2013) 745–751.
- [35] P. Xiong, J. Hu, Degradation of acetaminophen by UVA/LED/TiO₂ process, *Sep. Purif. Technol.* 91 (2012) 89–95.
- [36] S. Verma, M. Sillanpää, Degradation of anatoxin-a by UV-C LED and UV-C LED/H₂O₂ advanced oxidation processes, *Chem. Eng. J.* 274 (2015) 274–281.
- [37] R.J. Tayade, T.S. Natarajan, H.C. Bajaj, Photocatalytic degradation of methylene blue dye using ultraviolet light emitting diodes, *Ind. Eng. Chem. Res.* 48 (2009) 10262–10267.
- [38] M.A. Würtele, T. Kolbe, M. Lipsz, A. Külberg, M. Weyers, M. Kneissl, M. Jekel, Application of GaN-based ultraviolet-C light emitting diodes-UV-LEDs-for water disinfection, *Water Res.* 45 (2011) 1481–1489.
- [39] G. Matafonova, V. Batoev, Recent advances in application of UV light-emitting diodes for degrading organic pollutants in water through advanced oxidation processes: a review, *Water Res.* 132 (2018) 177–189.
- [40] N.F.F. Moreira, J.M. Sousa, G. Macebo, A.T. Ribeiro, L. Barrientos, M. Pedrosa, J.L. Faria, F.R. Pereira, S. Castro-Silva, M.A. Segundo, C.M. Manaia, O.C. Nunes, A.M.T. Silva, Photocatalytic ozonation of urban wastewater and surface water using immobilized TiO₂ with LEDs: micropollutants, antibiotic resistance genes and estrogenic activity, *Water Res.* 94 (2016) 10–22.
- [41] M.H. Rasoulifard, M. Fazli, M.R. Eskandarian, Performance of the light-emitting diodes in a continuous photoreactor for degradation of Direct Red using UV-LED/S₂O₈²⁻ process, *J. Ind. Eng. Chem.* 24 (2015) 121–126.
- [42] R.F. Pupo Nogueira, M.C. Oliveira, W.C. Paterlini, Simple and fast spectrophotometric determination of H₂O₂ in photo-Fenton reactions using metavanadate, *Talanta* 66 (2005) 86–89.
- [43] A.D. Eaton, L.S. Clesceri, A.E. Greenberg, M.A.H. Franson, Standard Methods for the Examination of Water and Wastewater, twenty-first ed., APA-AWWA-WEE, 2005.
- [44] S.A. Huber, A. Balz, M. Abert, W. Pronk, Characterization of aquatic humic and non-humic matter with size-exclusion chromatography-organic carbon detection-organic nitrogen detection (LC-OCD-OND), *Water Res.* 45 (2011) 879–885.
- [45] S. Giannakis, F.A. Gamarra Vives, D. Grandjean, A. Magnet, L.F. De Alencastro, C. Pulgarin, Effect of advanced oxidation processes on the micropollutants and the effluent organic matter contained in municipal wastewater previously treated by three different secondary methods, *Water Res.* 84 (2015) 295–306.
- [46] B. Schowanek, T.C.J. Feijtel, C.M. Perkins, F.A. Hartman, T.W. Federle, R.J. Larson, Biodegradation of [S, S], [R, R] and mixed stereoisomers of ethylene diamine disuccinic acid (EDDS), a transition metal chelator, *Chemosphere* 34 (11) (1997) 2375–2391.
- [47] J.D. Englehardt, D.E. Meeroff, L. Echegoyen, Y. Deng, F.M. Raymo, T. Shibata, Oxidation of aqueous EDTA and associated organics and coprecipitation of inorganics by ambient iron-mediated aeration, *Environ. Sci. Technol.* 41 (2006) 270–276.
- [48] S. Metsarinen, T. Tuhkanen, R. Aksela, Photodegradation of ethylenediaminetetraacetic acid (EDTA) and ethylenediamine disuccinic acid (EDDS) within natural UV radiation range, *Chemosphere* 45 (2001) 949–955.
- [49] J. Li, 17β-Estradiol Degradation Photoinduced by Iron Complex, Clay and Iron Oxide Minerals: Effect of the Iron Complexing Agent Ethylenediamine-Ethylenediamine-N, N- Disuccinic Acid, PhD Thesis University Blaise Pascal, Aubière, 2010.
- [50] W. Huang, M. Brigante, F. Wu, C. Mousty, K. Hanna, G. Mailhot, Assessment of the Fe(III)-EDDS complex in Fenton-Like process: from the radical formation to the degradation of bisphenol A, *Environ. Sci. Technol.* 47 (2013) 1952–1959.
- [51] B.H.J. Bielski, D.E. Cabelli, R.L. Arudi, A.B. Ross, Reactivity of HO₂/O₂⁻ radicals in aqueous solution, *J. Phys. Chem. Ref. Data* 14 (1985) 1041–1100.
- [52] G.V. Buxton, C.L. Greenstock, W.P. Helman, A.B. Ross, Critical review of rate constants for reactions of hydrated electrons, hydrogen atoms and hydroxyl radicals (OH/O⁻) in aqueous solution, *J. Phys. Chem. Ref. Data* 17 (2) (1988) 513–883.
- [53] J. Benner, E. Salhi, T. Termes, U. von Gunten, ozonation of reverse osmosis concentrate: kinetics and efficiency of beta blocker oxidation, *Water Res.* 42 (2008) 3003–3012.
- [54] D. Vione, M. Minella, V. Maurino, C. Minero, Indirect photochemistry in sunlit surface waters: photoinduced production of reactive transient species, *Chem.: Eur. J.* 20 (2014) 10590–10606.
- [55] J. Mack, J.R. Bolton, Photochemistry of nitrite and nitrate in aqueous solution: a review, *J. Photochem. Photobiol. A: Chem.* 128 (1–3) (1999) 1–13.
- [56] S. Goldstein, J. Rabani, Polychromatic UV photon irradiance measurements using chemical actinometers based on NO₃⁻ and H₂O₂ excitation: applications for industrial photoreactors, *Environ. Sci. Technol.* 42 (9) (2008) 3248–3253.
- [57] Y.F. Ji, C. Zeng, C. Ferronato, J.M. Chovelon, X. Yang, Nitrate-induced photodegradation of atenolol in aqueous solution: kinetics, toxicity and degradation pathways, *Chemosphere* 88 (2012) 644–649.
- [58] T. Chen, J. Ma, Q. Zhang, Z. Xie, Y. Zeng, R. Li, H. Liu, Y. Liu, W. Lv, G. Liu, Degradation of propranolol by UV-activated persulfate oxidation: reaction kinetics, mechanisms, reactive sites, transformation pathways and Gaussian calculation, *Sci. Total Environ.* 690 (2019) 878–890.
- [59] E. Marco-Urrea, J. Radjenovic, G. Caminal, M. Petrovic, T. Vicent, D. Barceló, Oxidation of atenolol, propranolol, carbamazepine, and clofibrate by biological Fenton-like system mediated by the white-rot fungus *Trametes versicolor*, *Water Res.* 44 (2010) 521–532.
- [60] E. Cuervo Lumbaque, R.M. Cardoso, A. Dallegrave, L.O. dos Santos, M. Ibáñez, F. Hernández, C. Sirtori, Pharmaceutical removal from different water matrices by Fenton process at near-neutral pH: Doehler design and transformation products identification by UHPLC-QTOF MS using a purpose-built database, *J. Environ. Chem. Eng.* 6 (2018) 3951–3961.
- [61] N. De la Cruz, Estudio de la eliminación de contaminantes emergentes en aguas mediante procesos de oxidación avanzados, Doctoral Thesis, University of Barcelona, 2013 http://diposit.ub.edu/dspace/bitstream/2445/66864/1/NDLCC_TESIS.pdf and <http://hdl.handle.net/2445/66864>.
- [62] V. Romero, N. De la Cruz, R.F. Dantas, P. Marco, J. Giménez, S. Esplugas, Photocatalytic treatment of metoprolol and propranolol, *Catal. Today* 161 (2011) 115–120.

Supplementary Information for

Micropollutants removal in real WW by photo-Fenton (circumneutral and acid pH) with BLB and LED lamps

N. López-Vinent, A. Cruz-Alcalde, C. Gutiérrez, P. Marco, J. Giménez*, S. Esplugas

Department of Chemical Engineering and Analytical Chemistry, Faculty of Chemistry, Universitat de Barcelona, C/Martí i Franqués 1, 08028 Barcelona, Spain.

*Corresponding author:

Jaime Giménez Farreras, phone: +34 934021293 e-mail: j.gimenez.fa@ub.edu

Table of Contents

Biological Oxygen Demand	p.2
Figure S1. Reactor illumination with two radiation sources.....	p.2
Figure S2. Hydrogen peroxide monitoring for different WW in conventional photo-Fenton and photo-Fenton catalyzed by EDDS-Fe(II) using LEDs.....	p.2
Figure S3. Degradation of PROP by conventional photo-Fenton (CPF) and photo-Fenton catalyzed with EDDS with another sample of IFAS.....	p.3
Table S1. Description of dissolved effluent organic matter (EfOM) fractions.....	p.4
Table S2. Initial values of BOD, COD and biodegradability for different wastewaters and Milli-Q.....	p.4
Table S3. Main oxidation intermediates of propranolol identified by N. de la Cruz [61].....	p.5

Biological Oxygen Demand: Brief explanation of the process.

The biodegradability was evaluated according to the 5210-standard method. This method consists on filling with seeded and nourished sample an airtight bottle of specified size, which is incubated it at the specified temperature for 5 days.

The measurement was done by OxyTop whose mechanism is based on variation the pressure in a closed system. The microorganisms that are in the sample consume oxygen and generate CO₂ because of their metabolic activity. This CO₂ is absorbed with NaOH and then a pressure decrease is produced, which is related to oxygen concentration and BOD.

The calculations of biodegradability were performed following equations S1 and S2. Equation S1 was calculate at initial and at the end of the experiment. Where “*f*” is at the end of the experiment and “*i*” is the biodegradability at initial time.

$$\text{Biodegradability} = \frac{DBO}{COD} \quad (\text{S1})$$

$$\% \text{ increase biodegradability} = \left(\frac{\text{Biodegradability}_f - \text{Biodegradability}_i}{\text{Biodegradability}_f} \right) \times 100 \quad (\text{S2})$$

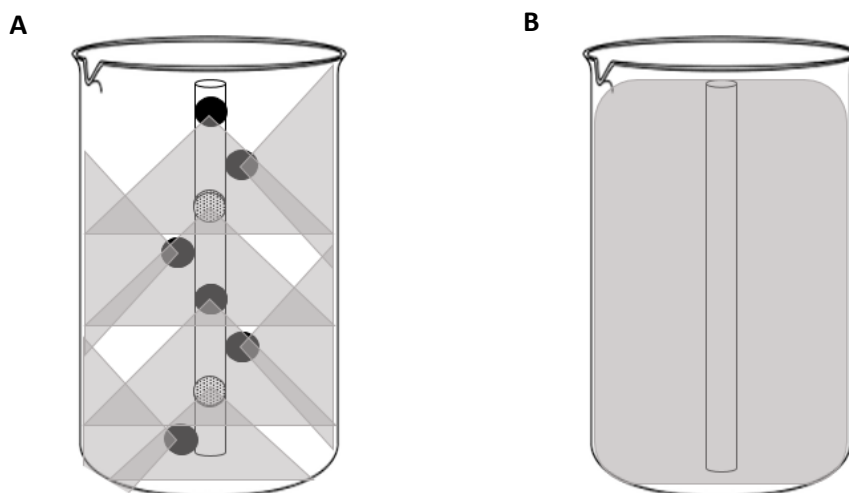


Figure S1. Reactor illumination with two radiation sources. A) UV-A LED 8W; B) BLB 8W.

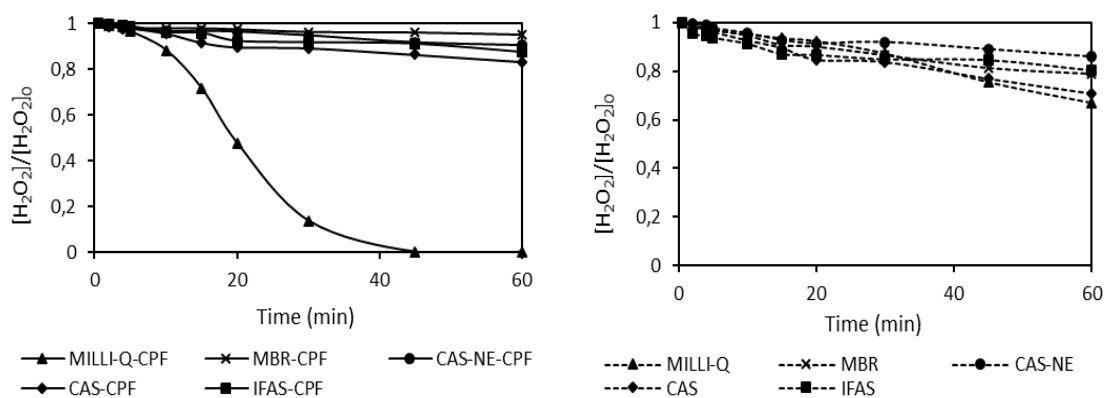


Figure S2. Hydrogen peroxide monitoring for different WW in conventional photo-Fenton (CPF) and photo-Fenton catalyzed by EDDS-Fe(II) using LEDs.

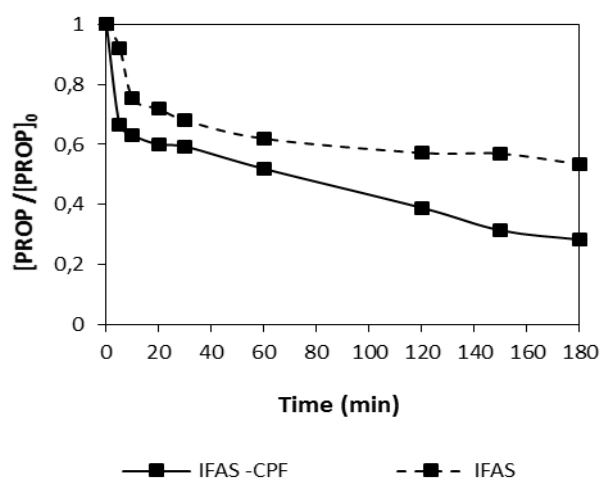


Figure S3. Degradation of PROP by conventional photo-Fenton (CPF) and photo-Fenton catalyzed with EDDS with another sample of IFAS.

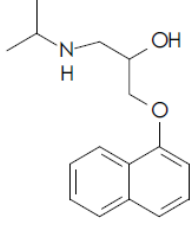
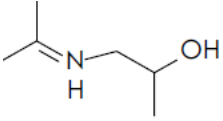
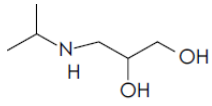
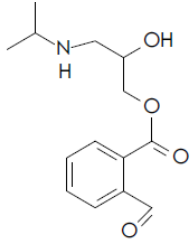
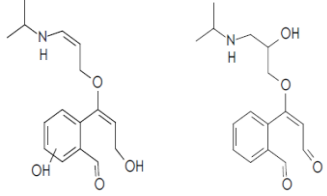
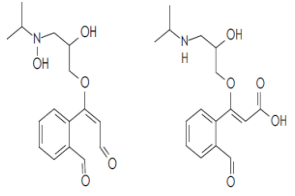
Table S1. Description of dissolved effluent organic matter (EfOM) fractions.

EfOM fractions	Description
Biopolymers	Amino acids and proteins
Humic substances	Humic/fluvic acids and hydrophobic humics
Building Blocks	Intermediates of humic substances
Low molecular weight neutrals	Non-acidic intermediates (alcohols, ketones..)
Low molecular weight acids	Intermediates of organics

Table S2. Initial values of BOD, COD and biodegradability for different wastewaters and Milli-Q.

Matrix	BOD (mg O₂ · L⁻¹)	COD (mg O₂ · L⁻¹)	Biodegradability
Milli-Q	6.4	105.0	0.061
MBR	10.6	100.2	0.106
CAS-NE	16.5	100.0	0.165
CAS	16.0	125.3	0.128
IFAS	13.6	127	0.107

Table S3. Main oxidation intermediates of propranolol identified by N. de la Cruz [61].

Compound	m/z (+)	Molecular formula	Structure
Propranolol	260	C ₁₆ H ₂₁ NO ₂	
PROP _I	116	C ₆ H ₁₃ NO	
PROP _{II}	134	C ₆ H ₁₅ NO ₂	
PROP _{III}	266	C ₁₄ H ₁₉ NO ₄	
PROP _{IV}	292	C ₁₆ H ₂₁ NO ₄	
PROP _V	308	C ₁₆ H ₂₁ NO ₅	

[61] N. De la Cruz, Estudio de la eliminación de contaminantes emergentes en aguas mediante procesos de oxidación avanzados, *Doctoral Thesis*, University of Barcelona, 2013.

4.3 Assessment of organic fertilizers as an iron source in photo-Fenton at circumneutral pH for wastewater treatment and its potential application in agriculture

A summary of the experiments displayed in Part III-VI are detailed in Table 17. It was decided to collect all data in a single table due to the experiments of this subsection are related to the use of organic fertilizers as an iron source in photo-Fenton.

Table 17. Summary of the experiments presented in Part III-VI.

Test	Target	[Reagents]	Irradiation	Matrix	pH	Performance	Figure in publication
Part III							
DTPA-Fe as an iron source to treat different WW							
C1	[PROP] = 0.5 mg L ⁻¹ Total coliforms = 1.7x10 ² CFU mL ⁻¹	[Fe ²⁺] = 10 mg L ⁻¹ Molar ratio DTPA:Fe = 1:1 [H ₂ O ₂] = 150 mg L ⁻¹	8 LEDs 365-370 nm tubular photoreactor	MBR	Natural	94% removal at 120 min. Total inactivation of Total coliforms at 90 min (2-log reduction).	Figure 1, 2, 4 and 5
C2	[PROP] = 0.5 mg L ⁻¹ Total coliforms = 1.8x10 ² CFU mL ⁻¹	[Fe ²⁺] = 10 mg L ⁻¹ Molar ratio DTPA:Fe = 1:1 [H ₂ O ₂] = 150 mg L ⁻¹	8 LEDs 365-370 nm tubular photoreactor	CAS-NE	Natural	75.4% removal at 120 min. Total inactivation of Total coliforms at 120 min (2-log reduction).	Figure 1 and 4
C3	[PROP] = 0.5 mg L ⁻¹ Total coliforms = 3.8x10 ² CFU mL ⁻¹ <i>E. coli</i> = 3x10 ¹ CFU mL ⁻¹	[Fe ²⁺] = 10 mg L ⁻¹ Molar ratio DTPA:Fe = 1:1 [H ₂ O ₂] = 150 mg L ⁻¹	8 LEDs 365-370 nm tubular photoreactor	CAS	Natural	62.5% removal at 120 min. 2-log reduction of Total coliforms and total inactivation of <i>E. coli</i> at 90 min (1.5 log-reduction)	Figure 1, 2, 4 and 5
C4	[PROP]= 0.5 mg L ⁻¹ Total coliforms = 9.8x10 ³ CFU mL ⁻¹ <i>E. coli</i> = 9x10 ² CFU mL ⁻¹	[Fe ²⁺] = 10 mg L ⁻¹ Molar ratio DTPA:Fe = 1:1 [H ₂ O ₂] = 150 mg L ⁻¹	8 LEDs 365-370 nm tubular photoreactor	IFAS	Natural	63.2% removal at 120 min. 2-log reduction for Total coliforms and <i>E. coli</i> at 120 min.	Figure 1 and 4

Table 17. (continued)

Test	Target	[Reagents]	Irradiation	Matrix	pH	Performance	Figure in publication
Part III							
EDDS-Fe and EDTA-Fe as an iron source to treat MBR and CAS effluents							
C5	[PROP] = 0.5 mg L ⁻¹ Total coliforms = 1.7x10 ² CFU mL ⁻¹	[Fe ²⁺] = 10 mg L ⁻¹ Molar ratio EDDS:Fe = 2:1 [H ₂ O ₂] = 150 mg L ⁻¹	8 LEDs 365-370 nm tubular photoreactor	MBR	Natural	91.3% removal at 120 min. Total inactivation of Total coliforms at 90 min (2-log reduction).	Figure 2 and 5
C6	[PROP] = 0.5 mg L ⁻¹ Total coliforms = 3.8x10 ² CFU mL ⁻¹ <i>E.coli</i> = 3x10 ¹ CFU mL ⁻¹	[Fe ²⁺] = 10 mg L ⁻¹ Molar ratio EDDS:Fe = 2:1 [H ₂ O ₂] = 150 mg L ⁻¹	8 LEDs 365-370 nm tubular photoreactor	CAS	Natural	51.9% removal at 120 min. 1 log-reduction of Total coliforms and <i>E.coli</i> at 120 min.	Figure 2 and 5
C7	[PROP] = 0.5 mg L ⁻¹ Total coliforms = 1.7x10 ² CFU mL ⁻¹	[Fe ²⁺] = 10 mg L ⁻¹ Molar ratio EDTA:Fe = 1:1 [H ₂ O ₂] = 150 mg L ⁻¹	8 LEDs 365-370 nm tubular photoreactor	MBR	Natural	Total removal at 120 min. Total inactivation of Total coliforms at 90 min (2-log reduction).	Figure 2 and 5
C8	[PROP] = 0.5 mg L ⁻¹ Total coliforms = 3.8x10 ² CFU mL ⁻¹ <i>E.coli</i> = 3x10 ¹ CFU mL ⁻¹	[Fe ²⁺] = 10 mg L ⁻¹ Molar ratio EDTA:Fe = 1:1 [H ₂ O ₂] = 150 mg L ⁻¹	8 LEDs 365-370 nm tubular photoreactor	CAS	Natural	68.7% removal at 120 min. 1.5 log-reduction of Total coliforms and total inactivation of <i>E.coli</i> at 120 min (1.5-log reduction).	Figure 2 and 5
Part IV							
Five organic fertilizers assessment							
D1	[PROP] = 0.25 mg L ⁻¹ [ACMP] = 0.25 mg L ⁻¹ [SMX] = 0.25 mg L ⁻¹	[Fe ²⁺] = 5 mg L ⁻¹ DTPA-Fe (7% of iron) [H ₂ O ₂] = 50 mg L ⁻¹	Simulated solar light	MBR	Natural	89.0%, 67.6% and 31.0% for PROP, SMX and ACMP, respectively, at 180 min.	Figure 2, 5, 6 and 9

Table 17. (continued)

Test	Target	[Reagents]	Irradiation	Matrix	pH	Performance	Figure in publication
Part IV							
D2	[PROP] = 0.25 mg L ⁻¹ [ACMP] = 0.25 mg L ⁻¹ [SMX] = 0.25 mg L ⁻¹	[Fe ²⁺] = 5 mg L ⁻¹ EDTA-Fe (13.3% of iron) [H ₂ O ₂] = 50 mg L ⁻¹	Simulated solar light	MBR	Natural	100% for PROP and SMX at 90 and 120 min, respectively. 67.6% for ACMP, at 180 min.	Figure 2, 4, 6 and 8
D3	[PROP] = 0.25 mg L ⁻¹ [ACMP] = 0.25 mg L ⁻¹ [SMX] = 0.25 mg L ⁻¹	[Fe ²⁺] = 5 mg L ⁻¹ HEDTA- Fe (13.0% of iron) [H ₂ O ₂] = 50 mg L ⁻¹	Simulated solar light	MBR	Natural	91.1%, 67.8% and 31.0% for PROP, SMX and ACMP, respectively, at 180 min.	Figure 2
D4	[PROP] = 0.25 mg L ⁻¹ [ACMP] = 0.25 mg L ⁻¹ [SMX] = 0.25 mg L ⁻¹	[Fe ²⁺] = 5 mg L ⁻¹ EDDHA- Fe (6.0% of iron) [H ₂ O ₂] = 50 mg L ⁻¹	Simulated solar light	MBR	Natural	23.3%, 29.3% and 15.0% for PROP, SMX and ACMP, respectively, at 180 min.	Figure 2
D5	[PROP] = 0.25 mg L ⁻¹ [ACMP] = 0.25 mg L ⁻¹ [SMX] = 0.25 mg L ⁻¹	[Fe ²⁺] = 5 mg L ⁻¹ Molar ratio EDDS:Fe = 1:1 [H ₂ O ₂] = 50 mg L ⁻¹	Simulated solar light	MBR	Natural	94.8%, 79.9% and 38.5% for PROP, SMX and ACMP, respectively, at 180 min.	Figure 2, 4, 5, 8 and 9
Mixtures of three organic fertilizers at 50%-50%							
D6	[PROP] = 0.25 mg L ⁻¹ [ACMP] = 0.25 mg L ⁻¹ [SMX] = 0.25 mg L ⁻¹	[Fe ²⁺] = 5 mg L ⁻¹ Mix of EDDS- EDTA (50%- 50%) [H ₂ O ₂] = 50 mg L ⁻¹	Simulated solar light	MBR	Natural	100% for PROP and SMX at 30 and 90 min, respectively. 70.0% for ACMP, at 180 min.	Figure 4 and 8

Table 17. (continued)

Test	Target	[Reagents]	Irradiation	Matrix	pH	Performance	Figure in publication
Part IV							
D7	[PROP] = 0.25 mg L ⁻¹ [ACMP] = 0.25 mg L ⁻¹ [SMX] = 0.25 mg L ⁻¹	[Fe ²⁺] = 5 mg L ⁻¹ Mix of EDDS- DTPA (50%-50%) [H ₂ O ₂] = 50 mg L ⁻¹	Simulated solar light	MBR	Natural	95.0%, 77.4% and 39.4% for PROP, SMX and ACMP, respectively, at 180 min.	Figure 5 and 9
D8	[PROP] = 0.25 mg L ⁻¹ [ACMP] = 0.25 mg L ⁻¹ [SMX] = 0.25 mg L ⁻¹	[Fe ²⁺] = 5 mg L ⁻¹ Mix of EDTA- DTPA (50%-50%) [H ₂ O ₂] = 50 mg L ⁻¹	Simulated solar light	MBR	Natural	100% for PROP and SMX at 90 and 120 min, respectively. 63.7% for ACMP at 180 min.	Figure 6
Mixtures of three organic fertilizers at 25%-75%							
D9	[PROP] = 0.25 mg L ⁻¹ [ACMP] = 0.25 mg L ⁻¹ [SMX] = 0.25 mg L ⁻¹	[Fe ²⁺] = 5 mg L ⁻¹ Mix of EDDS- EDTA (25%-75%) [H ₂ O ₂] = 50 mg L ⁻¹	Simulated solar light	MBR	Natural	100% of PROP and SMX at 120 and 180 min, respectively. 51.9% of ACMP at 180 min.	Figure 8
D10	[PROP] = 0.25 mg L ⁻¹ [ACMP] = 0.25 mg L ⁻¹ [SMX] = 0.25 mg L ⁻¹	[Fe ²⁺] = 5 mg L ⁻¹ Mix of EDDS- DTPA (25%-75%) [H ₂ O ₂] = 50 mg L ⁻¹	Simulated solar light	MBR	Natural	90.9%, 66.4% and 29.3% for PROP, SMX and ACMP, respectively at 180 min.	Figure 9
Part V							
Mixtures of organic fertilizers in CAS effluent							
E1	[PROP] = 0.25 mg L ⁻¹ [ACMP] = 0.25 mg L ⁻¹ [SMX] = 0.25 mg L ⁻¹ Total coliforms = 10 ³ -10 ⁴ CFU mL ⁻¹	[Fe ²⁺] = 5 mg L ⁻¹ Mix of EDDS- EDTA (50%-50%) [H ₂ O ₂] = 50 mg L ⁻¹	Simulated solar light	CAS	Natural	85.7%, 59.5% and 30.6% for PROP, SMX and ACMP, respectively, at 180 min. 2.1 log- reduction of Total coliforms at 180 min.	Figure 1

Table 17. (continued)

Test	Target	[Reagents]	Irradiation	Matrix	pH	Performance	Figure in publication
Part V							
E2	[PROP] = 0.25 mg L ⁻¹ [ACMP] = 0.25 mg L ⁻¹ [SMX] = 0.25 mg L ⁻¹ Total coliforms = 10 ³ -10 ⁴ CFU mL ⁻¹	[Fe ²⁺] = 5 mg L ⁻¹ Mix of EDDS- DTPA (50%- 50%) [H ₂ O ₂] = 50 mg L ⁻¹	Simulated solar light	CAS	Natural	60.4% 34.4% and 12.4% for PROP, SMX and ACMP respectively, at 180 min. 2.1 log-reduction of Total coliforms at 180 min.	Figure 3
E3	[PROP] = 0.25 mg L ⁻¹ [ACMP] = 0.25 mg L ⁻¹ [SMX] = 0.25 mg L ⁻¹ Total coliforms = 10 ³ -10 ⁴ CFU mL ⁻¹	[Fe ²⁺] = 5 mg L ⁻¹ Mix of EDTA- DTPA (50%- 50%) [H ₂ O ₂] = 50 mg L ⁻¹	Simulated solar light	CAS	Natural	86.8% 61.2% and 28.3% for PROP, SMX and ACMP respectively, at 180 min. 1.5 log-reduction of Total coliforms at 180 min.	Figure 4
E4	[PROP] = 0.25 mg L ⁻¹ [ACMP] = 0.25 mg L ⁻¹ [SMX] = 0.25 mg L ⁻¹ Total coliforms = 10 ³ -10 ⁴ CFU mL ⁻¹	[Fe ²⁺] = 5 mg L ⁻¹ Molar ratio EDDS:Fe = 1:1 [H ₂ O ₂] = 50 mg L ⁻¹	Simulated solar light	CAS	Natural	46.8% 30.0% and 10.5% for PROP, SMX and ACMP respectively, at 180 min. 1.8 log-reduction of Total coliforms at 180 min.	Figure 1, 3
E5	[PROP] = 0.25 mg L ⁻¹ [ACMP] = 0.25 mg L ⁻¹ [SMX] = 0.25 mg L ⁻¹ Total coliforms = 10 ³ -10 ⁴ CFU mL ⁻¹	[Fe ²⁺] = 5 mg L ⁻¹ EDTA-Fe (13.3% of iron) [H ₂ O ₂] = 50 mg L ⁻¹	Simulated solar light	CAS	Natural	88.8% 72.5% and 35.8% for PROP, SMX and ACMP respectively, at 180 min. 1.3 log-reduction of Total coliforms at 180 min.	Figure 1 and 4

Table 17. (continued)

Test	Target	[Reagents]	Irradiation	Matrix	pH	Performance	Figure in publication
Part V							
E6	[PROP] = 0.25 mg L ⁻¹ [ACMP] = 0.25 mg L ⁻¹ [SMX] = 0.25 mg L ⁻¹ Total coliforms = 10 ³ -10 ⁴ CFU mL ⁻¹	[Fe ²⁺] = 5 mg L ⁻¹ DTPA-Fe (7% of iron) [H ₂ O ₂] = 50 mg L ⁻¹	Simulated solar light	CAS	Natural	60.5% 38.0% and 18.3% for PROP, SMX and ACMP respectively, at 180 min. 1.5 log-reduction of Total coliforms at 180 min.	Figure 3 and 4
Mixtures of organic fertilizers in MBR effluent							
E7	[PROP] = 0.25 mg L ⁻¹ [ACMP] = 0.25 mg L ⁻¹ [SMX] = 0.25 mg L ⁻¹	[Fe ²⁺] = 5 mg L ⁻¹ Mix of EDDS- EDTA (50%- 50%) [H ₂ O ₂] = 50 mg L ⁻¹	Simulated solar light	MBR	Natural	100% for PROP and SMX at 30 and 90 min, respectively. 70.0% for ACMP, at 180 min.	Figure 1
E8	[PROP] = 0.25 mg L ⁻¹ [ACMP] = 0.25 mg L ⁻¹ [SMX] = 0.25 mg L ⁻¹	[Fe ²⁺] = 5 mg L ⁻¹ Mix of EDDS- DTPA (50%- 50%) [H ₂ O ₂] = 50 mg L ⁻¹	Simulated solar light	MBR	Natural	95.0%, 77.4% and 39.4% for PROP, SMX and ACMP, respectively, at 180 min.	Figure 3
E9	[PROP] = 0.25 mg L ⁻¹ [ACMP] = 0.25 mg L ⁻¹ [SMX] = 0.25 mg L ⁻¹	[Fe ²⁺] = 5 mg L ⁻¹ Mix of EDTA- DTPA (50%- 50%) [H ₂ O ₂] =50 mg L ⁻¹	Simulated solar light	MBR	Natural	100% for PROP and SMX at 90 and 120 min, respectively. 63.7% for ACMP at 180 min.	Figure 4
E10	[PROP] = 0.25 mg L ⁻¹ [ACMP] = 0.25 mg L ⁻¹ [SMX] = 0.25 mg L ⁻¹	[Fe ²⁺] = 5 mg L ⁻¹ DTPA-Fe (7% of iron) [H ₂ O ₂] = 50 mg L ⁻¹	Simulated solar light	MBR	Natural	89.0%, 67.6% and 31.0% for PROP, SMX and ACMP, respectively, at 180 min.	Figure 3 and 4

Table 17. (continued)

Test	Target	[Reagents]	Irradiation	Matrix	pH	Performance	Figure in publication
Part V							
E11	[PROP] = 0.25 mg L ⁻¹ [ACMP] = 0.25 mg L ⁻¹ [SMX] = 0.25 mg L ⁻¹	[Fe ²⁺] = 5 mg L ⁻¹ Molar ratio EDDS:Fe = 1:1 [H ₂ O ₂] = 50 mg L ⁻¹	Simulated solar light	MBR	Natural	94.8%, 79.9% and 38.5% for PROP, SMX and ACMP, respectively, at 180 min.	Figure 1, 3
E12	[PROP] = 0.25 mg L ⁻¹ [ACMP] = 0.25 mg L ⁻¹ [SMX] = 0.25 mg L ⁻¹	[Fe ²⁺] = 5 mg L ⁻¹ EDTA-Fe (13.3% of iron) [H ₂ O ₂] = 50 mg L ⁻¹	Simulated solar light	MBR	Natural	100% for PROP and SMX at 90 and 120 min, respectively. 67.6% for ACMP, at 180 min.	Figure 1 and 4
Part VI							
Photo-Fenton using organic fertilizers in ultrapure water							
F1	[SMX] = 1 mg L ⁻¹	[Fe ²⁺] = 5 mg L ⁻¹ DTPA-Fe (7% of iron) [H ₂ O ₂] = 50 mg L ⁻¹	Simulated solar light	Ultrapure water	7.5	91.0% removal at 120 min.	Figure 2
F2	[SMX] = 1 mg L ⁻¹	[Fe ²⁺] = 5 mg L ⁻¹ EDTA-Fe (13.3% of iron) [H ₂ O ₂] = 50 mg L ⁻¹	Simulated solar light	Ultrapure water	7.5	Total removal at 120 min.	Figure 2
F3	[SMX] = 1 mg L ⁻¹	[Fe ²⁺] = 5 mg L ⁻¹ HEDTA- Fe (13% of iron) [H ₂ O ₂] = 50 mg L ⁻¹	Simulated solar light	Ultrapure water	7.5	90.2% removal at 120 min.	Figure 2
F4	[SMX] = 1 mg L ⁻¹	[Fe ²⁺] = 5 mg L ⁻¹ EDDHA- Fe (6% of iron) [H ₂ O ₂] = 50 mg L ⁻¹	Simulated solar light	Ultrapure water	7.5	17.8% removal at 120 min.	Figure 2

Table 17. (continued)

Test	Target	[Reagents]	Irradiation	Matrix	pH	Performance	Figure in publication
Part VI							
F5	[SMX] = 1 mg L ⁻¹	[Fe ²⁺] = 5 mg L ⁻¹ Molar ratio EDDS:Fe = 1:1 [H ₂ O ₂] = 50 mg L ⁻¹	Simulated solar light	Ultrapure water	7.5	93.3% removal at 120 min.	Figure 2
Fenton process							
F6	[SMX] = 1 mg L ⁻¹	[Fe ²⁺] = 5 mg L ⁻¹ DTPA-Fe (7% of iron) [H ₂ O ₂] = 50 mg L ⁻¹	No	Ultrapure water	7.5	66.9% removal at 120 min	Figure 3
F7	[SMX] = 1 mg L ⁻¹	[Fe ²⁺] = 5 mg L ⁻¹ EDTA-Fe (13.3% of iron) [H ₂ O ₂] = 50 mg L ⁻¹	No	Ultrapure water	7.5	56.8% removal at 120 min	Figure 3
F8	[SMX] = 1 mg L ⁻¹	[Fe ²⁺] = 5 mg L ⁻¹ HEDTA-Fe (13% of iron) [H ₂ O ₂] = 50 mg L ⁻¹	No	Ultrapure water	7.5	60.6% removal at 120 min	Figure 3
F9	[SMX] = 1 mg L ⁻¹	[Fe ²⁺] = 5 mg L ⁻¹ Molar ratio EDDS:Fe = 1:1 [H ₂ O ₂] = 50 mg L ⁻¹	No	Ultrapure water	7.5	47.5% removal at 120 min	Figure 3
Irradiated experiments without H₂O₂							
F10	[SMX] = 1 mg L ⁻¹	[Fe ²⁺] = 5 mg L ⁻¹ DTPA-Fe (7% of iron) No H ₂ O ₂	Simulated solar light	Ultrapure water	7.5	30.0% removal at 120 min	Figure 4

Table 17. (continued)

Test	Target	[Reagents]	Irradiation	Matrix	pH	Performance	Figure in publication
Part VI							
F11	[SMX] = 1 mg L ⁻¹	[Fe ²⁺] = 5 mg L ⁻¹ EDTA-Fe (13.3% of iron) No H ₂ O ₂	Simulated solar light	Ultrapure water	7.5	6.0% removal at 120 min	Figure 4
F12	[SMX] = 1 mg L ⁻¹	[Fe ²⁺] = 5 mg L ⁻¹ HEDTA-Fe (13% of iron) No H ₂ O ₂	Simulated solar light	Ultrapure water	7.5	6.0% removal at 120 min	Figure 4
F13	[SMX] = 1 mg L ⁻¹	[Fe ²⁺] = 5 mg L ⁻¹ EDDHA- Fe (6% of iron) No H ₂ O ₂	Simulated solar light	Ultrapure water	7.5	No degradation	Figure 4
F14	[SMX] = 1 mg L ⁻¹	[Fe ²⁺] = 5 mg L ⁻¹ Molar ratio EDDS:Fe = 1:1 No H ₂ O ₂	Simulated solar light	Ultrapure water	7.5	43.5% removal at 120 min	Figure 4
Photo-Fenton experiments with tBuOH							
F15	[SMX] = 1 mg L ⁻¹	[Fe ²⁺] = 5 mg L ⁻¹ DTPA-Fe (7% of iron) [H ₂ O ₂] = 50 mg L ⁻¹ [tBuOH] = 25 mM	Simulated solar light	Ultrapure water	7.5	5% removal at 120 min	Figure 5
F16	[SMX] = 1 mg L ⁻¹	[Fe ²⁺] = 5 mg L ⁻¹ EDTA-Fe (13.3% of iron) [H ₂ O ₂] = 50 mg L ⁻¹ [tBuOH] = 25 mM	Simulated solar light	Ultrapure water	7.5	5% removal at 120 min	Figure 5

Table 17. (continued)

Test	Target	[Reagents]	Irradiation	Matrix	pH	Performance	Figure in publication
Part VI							
F17	[SMX] = 1 mg L ⁻¹	[Fe ²⁺] = 5 mg L ⁻¹ HEDTA-Fe (13% of iron) [H ₂ O ₂] = 50 mg L ⁻¹ [tBuOH] = 25 mM	Simulated solar light	Ultrapure water	7.5	5% removal at 120 min	Figure 5
F18	[SMX] = 1 mg L ⁻¹	[Fe ²⁺] = 5 mg L ⁻¹ Molar ratio EDDS:Fe = 1:1 [H ₂ O ₂] = 50 mg L ⁻¹ [tBuOH] = 25 mM	Simulated solar light	Ultrapure water	7.5	9.2% removal at 120 min	Figure 5
Photo-Fenton experiments without chelating agent and dosing Fe²⁺							
F19	[SMX] = 1 mg L ⁻¹	[Fe ²⁺] added = 2.2 mg L ⁻¹ [H ₂ O ₂] = 50 mg L ⁻¹	Simulated solar light	Ultrapure water	7.5	16.6% removal at 120 min	Figure 6
F20	[SMX] = 1 mg L ⁻¹	[Fe ²⁺] added = 0.4 mg L ⁻¹ [H ₂ O ₂] = 50 mg L ⁻¹	Simulated solar light	Ultrapure water	7.5	13.7% removal at 120 min	Figure 6
Photo-Fenton experiments without O₂							
F21	[SMX] = 1 mg L ⁻¹	[Fe ²⁺] = 5 mg L ⁻¹ DTPA-Fe (6% of iron) [H ₂ O ₂] = 50 mg L ⁻¹ Bubbling N ₂	Simulated solar light	Ultrapure water	7.5	69.2% removal at 120 min	Figure 7
F22	[SMX] = 1 mg L ⁻¹	[Fe ²⁺] = 5 mg L ⁻¹ EDTA-Fe (13.3% of iron) [H ₂ O ₂] = 50 mg L ⁻¹ Bubbling N ₂	Simulated solar light	Ultrapure water	7.5	88.8% removal at 120 min	Figure 7

Table 17. (continued)

Test	Target	[Reagents]	Irradiation	Matrix	pH	Performance	Figure in publication
Part VI							
F23	[SMX] = 1 mg L ⁻¹	[Fe ²⁺] = 5 mg L ⁻¹ HEDTA-Fe (13% of iron) [H ₂ O ₂] = 50 mg L ⁻¹ Bubbling N ₂	Simulated solar light	Ultrapure water	7.5	64.0% removal at 120 min	Figure 7
F24	[SMX] = 1 mg L ⁻¹	[Fe ²⁺] = 5 mg L ⁻¹ Molar ratio EDDS:Fe = 1:1 [H ₂ O ₂] = 50 mg L ⁻¹ Bubbling N ₂	Simulated solar light	Ultrapure water	7.5	79.8% removal at 120 min	Figure 7
Irradiated experiments without O₂ or H₂O₂							
F25	[SMX] = 1 mg L ⁻¹	[Fe ²⁺] = 5 mg L ⁻¹ DTPA-Fe (7% of iron) No H ₂ O ₂ Bubbling N ₂	Simulated solar light	Ultrapure water	7.5	11.0% removal at 120 min	Figure 7
F26	[SMX] = 1 mg L ⁻¹	[Fe ²⁺] = 5 mg L ⁻¹ Molar ratio EDDS:Fe = 1:1 No H ₂ O ₂ Bubbling N ₂	Simulated solar light	Ultrapure water	7.5	7.8% removal at 120 min	Figure 4

4.3.1 Micropollutant abatement and bacterial inactivation using DTPA-Fe

In a water scarcity scenario, the reused wastewater could be an important source of irrigation, considering that freshwater demand for agriculture is about 70% of the total one. In this sense, the efficiency of an organic fertilizer DTPA was investigated as a complexing agent of iron for photo-Fenton process at circumneutral pH. This iron chelate had not investigated in the literature in this field. The results obtained from this work were compared with EDDS

and EDTA, which are the most investigated chelating agents. These experiments were gathered in Part III and they were carried out in a tubular photoreactor with 8 LEDs (365 nm, irradiance: $2.7 \cdot 10^{-7}$ Einstein s^{-1}). Reagent's concentrations were 10 mg L^{-1} and 150 mg L^{-1} of iron and H_2O_2 .

The results suggested that DTPA was effective on MP abatement and bacterial inactivation at natural pH in different secondary effluents. Higher performance was obtained in MBR matrix with 94% of PROP' removal after 2 hours of treatment. Nevertheless, conversions of 75.4, 63.2 and 62.5% were reached in CAS-NE, IFAS and CAS matrices, respectively (C1-C4). As explained in section 4.2.1, the presence of turbidity and organic matter in the matrix affects negatively in the process efficiency.

The comparison of DTPA with EDDS and EDTA was carried out in MBR and CAS (C1, C3, C5-C8). In that case, the ligand:Fe(II) molar ratios used were 1:1 for EDTA and DTPA and 2:1 for EDDS. These ratios were selected to ensure the total chelation of iron. As observed in the results, the highest reaction rate was achieved by EDTA in MBR, presenting total PROP removal in only 15 min. For the same time, EDDS also showed fast PROP removal. However, then the degradation was flattened and not reaching the total conversion (94.0% at 2 hours). DTPA had slowest kinetic rate but reached similar PROP degradation (91.3%) than EDDS at the end of the treatment. The differences between these chelating agents were regarding their stability constant with iron. The stability constants (k_{stab}) of each chelating agent with iron are specific for the iron species (k_{stab} DTPA-Fe(III) = 28.60, k_{stab} EDTA-Fe(III) = 25.10, k_{stab} EDDS-Fe(III) = 22.0, k_{stab} DTPA-Fe(II) = 16.55, k_{stab} EDTA-Fe(II) = 14.33). There were not available data about k_{stab} for EDDS-Fe(II). As observed DTPA presents the highest constant so the availability of iron to react with H_2O_2 is lower, decreasing the efficiency of the process. Total iron in solution is a key parameter to consider in experiments at circumneutral pH. As EDDS presents lowest stability constant with iron, the precipitation of this one was almost 100% at the end of the treatment. Additionally, at 30 minutes, the iron release was about 75%, reason why the efficiency decreased a lot in PROP removal. For EDTA, the iron precipitation was about 70% at 2 hours. However, this fact not affected to degradation efficiency since total PROP was removed at 15 min. When DTPA was used, only 10% of iron precipitated during the experiment. This fact is beneficial for wastewater reuse in agriculture since plants can absorb chelated iron but not iron hydroxides. In CAS effluent the differences between three chelating agents were lower. The

presence of higher organic matter, turbidity and alkalinity, influenced on PROP removal's efficiency. At the end of the experiment, 68.7, 62.5 and 51.9% of PROP degradation was reached by EDTA, DTPA and EDDS. This fact was related to the precipitation of iron, which influence was more noticeable due to the decrease in kinetic rates.

The efficiency of three organic fertilizers was also tested on bacterial inactivation (*E. coli* and *total coliforms*). Using DTPA as a chelating agent, total reduction of *total coliforms* was achieved in 90 and 120 min in MBR and CAS-NE (2-log reduction), respectively. In CAS and IFAS effluents, also 2-log inactivation was reached at 120 min. However, no total inactivation was achieved due to the higher number of *total coliforms* at initial time. *E. coli* was total inactivated at 90 min in CAS effluent, while in IFAS 2-log reduction was reached at the end of the treatment, observing 7 CFU mL⁻¹ at 120 min. In both cases good reductions were observed since in IFAS the amount of *E. coli* at initial time was about 1.5 log higher than CAS.

Comparing the efficiency on bacterial inactivation of different chelating agents, similar trends were observed in *E. coli* and total coliforms reduction using EDTA and EDDS. However, with DTPA, although the differences were not large, best results were reached at the end of the treatment. For instance, total inactivation of total coliforms in MBR were achieved at 90 min with DPTA and at 120 min with EDDS and EDTA. The results suggested that the stability of ligand with iron is also important in bacterial inactivation. The growth-on-the-plate was also investigated at the end of the treatment for different chelating agents and effluents for 48 and 72 hours. Experiments performed with DTPA showed lowest bacterial regrowth while using EDDS highest regrowth was observed. This fact could be related to the chemical and biochemical properties of the chelating agent. EDDS is the most biodegradable, so the microorganisms could degrade this molecule causing better conditions to growth. Comparing effluents, in MBR was observed lower regrowth than CAS with three chelating agents.

Finally, BOD₅, phytotoxicity and acute toxicity (*Vibrio fishery*) were also investigated to determine the suitability of treated effluents to be reused in agriculture. For all treatments, no phytotoxicity nor toxicity at the end of the treatment were observed. Regarding BOD₅, EDDS was the chelating agent with highest value at the end of the treatment with about 33 and 42 mg O₂ L⁻¹ for MBR and CAS. While EDTA and DTPA presented close values and always lower than 15 mg O₂ L⁻¹.

Comparing the results at the end of the treatments for all conditions with the parameters included in *Proposal of minimum requirements for agricultural reuse*, different levels of reuse can be established. For DTPA the final effluents accomplished the requirements of category A and B for CAS and MBR, respectively. For EDTA, both effluents were included in category C. Thus, for DTPA and EDTA, the effluents satisfied the quality requirements for agricultural reuse. However, for EDDS, as the BOD₅ was very high, the final effluent was not suitable for water reuse in agriculture.

4.3.2 Potential improvement on photo-Fenton at circumneutral pH

From the results included in Part III, it was observed that high stability constant of chelating agent with iron caused low kinetic constants on MPs removal but presented high iron in solution at the end of the treatment. This fact is important in the field of water reuse in agriculture. However, chelating agents presenting low stability constant gave highest kinetic rates on MPs abatement at initial times but then the efficiency of the process decreased due to the high iron precipitation. On that purpose, the efficiency of organic fertilizers mixtures was investigated, considering the ability of keeping iron in solution and available for catalytic reactions generating HO[•]. To select the appropriate mixtures of chelating agents, two new organic fertilizers (HEDTA and EDDHA) were studied besides to chelating agents already investigated. This investigation was carried out using solar simulated irradiation (290-400 nm, irradiance: $6.6 \cdot 10^{-7}$ Einstein s⁻¹), looking for a more efficient and eco-friendlier photo-Fenton process. The experiments were conducted in two real effluents (MBR and CAS) and the target MPs selected were: ACMP, SMX and PROP. In CAS matrix, *E. coli* inactivation was also investigated. The concentration of reagents was 5 mg L⁻¹ and 50 mg L⁻¹ of iron and H₂O₂, respectively.

Concerning the differences in MPs, the efficiency on PROP removal was the best followed by SMX, while ACMP presented the lowest degradations (D1-D5). The trend was the same in five different chelating agents. This fact was in accordance to the kinetic rates of each compound with hydroxyl radicals ($k_{\text{PROP,HO}} = 1.0 \cdot 10^{10} \text{ M}^{-1} \text{ s}^{-1}$, $k_{\text{SMX,HO}} = 5.5 \cdot 10^9 \text{ M}^{-1} \text{ s}^{-1}$, $k_{\text{ACMP,HO}} = 2.1 \cdot 10^9 \text{ M}^{-1} \text{ s}^{-1}$). At the end of the treatment, more than 90% of PROP removal was reached for different chelating agents except EDDHA. While the best abatement of ACMP was achieved by EDTA with a final degradation about 70%.

Concerning chelating agents (D1-D5), EDTA showed the highest kinetic rates for three MPs during the treatment. However, at initial times (until 30 min), experiments with EDDS gave

the best MPs abatement. After this time, the degradation curves were flattened, not reaching the complete removal of MPs. With DTPA and HEDTA, close results were observed during the treatment. Finally, with experiments carried out with EDDHA, poor MPs degradations were observed.

In this type of experiments, the precipitation of iron is a key parameter in the process efficiency, which is linked to the stability constant of ligand and iron. For instance, EDDHA has a highest stability constant and only 10% of iron was released during the experiment. However, EDDS presents the lowest stability, and the iron precipitation was about 90% at the end of the treatment. This fact was beneficial at initial times since the availability of H_2O_2 and light to interact with iron was greater, increasing the hydroxyl radical's generation. However, no total degradation of MPs was achieved due to the higher iron precipitation. Approximately, percentages of 50%, 30% and 20% of iron release were observed for EDTA, HEDTA and DTPA, respectively.

From these results, three organic fertilizers combinations were tested (D6-D8): mixtures EDDS+EDTA, EDDS+DTPA and EDTA+DTPA with 50% of each chelating agent. An improvement of the photo-Fenton efficiency was observed. The combination of EDDS+EDTA reached the best results comparing to the experiments with 100% of EDDS or 100% of EDTA. For instance, with the mixture, total removal of PROP was achieved at 30 min, while with EDTA (which presented the best removal), total degradation was at 90 min. Additionally, with the EDDS+EDTA, the total iron in solution at the end of the treatment was 5.5 times higher than EDDS. Different results were obtained with the mixture EDDS+DTPA, and the MPs degradation at the end of the treatment was the same than EDDS. However, the iron in solution was higher than experiments with 100% EDDS due to the influence of DTPA. Finally, with EDTA+DTPA the degradation curves for three MPs were identical to tests with 100% EDTA and the iron remaining in solution at the end of the treatment like DTPA. These results are advantageous for water reuse in agriculture since good MPs removals were reached and an appropriate amount of iron was kept in solution at the end of the treatment. These combinations were also tested in CAS effluent (E1-E6) which presents higher turbidity, organic matter and alkalinity than MBR. This comparison was carried out to study the role of the matrix in iron precipitation. It was observed that the iron release was higher in CAS effluent than in MBR for all experiments. This behavior could be related to the highest complexity of the CAS. The different compounds contained in wastewaters, such as ions, can be involved in the breakdown of the iron complex since they

could build new complexes with the complexing agent if the stability constant is higher than the iron. This fact is one of the reasons why MPs removal is lower in CAS than in MBR, since the catalytic activity to generate hydroxyl radicals decreased. Moreover, the higher organic matter, which could compete with MPs for hydroxyl radicals, was another reason of these low efficiencies.

EDDS was the chelating agent more affected since is the ligand with lower stability with iron. For instance, only about 40% of PROP removal was achieved at the end of the treatment (180 min) in CAS while in MBR about 90% was reached in 30 min. Using EDTA, which presents greater stability with iron, the differences between two effluents were lower. Total PROP removal was observed at 90 min, in MBR, and 90% at the end of the experiment with CAS. Regarding the mixtures, the same trend was followed than MBR. However, in CAS effluent, the combinations comprising EDDS were more effective than MBR, since the experiments with only EDDS reached lower MPs degradations and higher iron release. Comparing the efficiency on MPs degradation of the mixture (EDDS+EDTA) with experiments with only EDTA, it was observed only a small improvement. However, the application of the mixture to the crops is a more sustainable measure since EDDS presents a biodegradable character and EDTA was more recalcitrant, negatively affecting the soils when the plants do not absorb all amount of fertilizer.

Additionally, other proportions of chelating agents in the mixtures were investigated. Combinations with 25% of EDDS and 75% of EDTA or DTPA were also tested in MBR effluent (D9 and D10). In two combinations, the efficiency on MPs removal was lower than 50%-50% mixtures. In the case of 25%EDDS+75%DTPA, the MPs removal and iron release were similar to experiments with only DTPA (which implied lower efficiencies than only EDDS). However, with the mixture of 25%EDDS+75%EDTA, better performances (MPs removal and iron release) were achieved than only EDDS, but lower efficiencies compared to tests with only EDTA. Thus, in general, the proportion 50%+50% achieved better yields.

Finally, the inactivation of *E. coli*, BOD₅ and phytotoxicity were evaluated to determine if the final treated effluents could be used for agricultural purposes. Values of *E. coli* and BOD₅ were compared with the maximum values listed in the *Regulation of the European Parliament and of the Council on minimum requirements for agricultural wastewater reuse*. The results suggested that all treated MBR effluents accomplish with the minimum requirements for their reuse. Nevertheless, in the case of CAS, high reaction time was

required to achieve better performances in *E. coli* inactivation, since the final CFU mL⁻¹ exceeded the maximum value proposed in the Regulation.

4.3.3 Potential reactivity of organic fertilizers in the aquatic environment and the mainly involved reaction mechanisms

The additional potential reactions involved in micropollutants degradation when iron chelates are used in photo-Fenton process at circumneutral pH were also investigated. In the literature, there is evidence of the reactivity of chelating agents with ultraviolet radiation and dissolved oxygen, generating reactive oxygen species (ROS). These reactions and the photoredox cycle of iron (III) complexes may be important to the environment, contributing to the self-depuration of the aquatic compartments by oxidation of some persistent organic pollutants.

EDDS has been the chelating agent more studied in this field. However, each ligand has a certain stability constant with iron and each iron complex presents different quantum yields. Thus, the additional mechanisms involved, when EDDS is tested, probably are not the same than other chelating agents are employed. The results derived from this investigation were included in Part VI. SMX was the target compound spiked in ultrapure water. Solar simulator was used to carry out the experiments.

Firstly, Fenton experiments at circumneutral pH were compared with photo-Fenton tests to evaluate the contribution of irradiation in the MPs abatement (F1-F9). From these results, it was observed the photoredox cycle like in acidic conditions, since the SMX removal in all cases was higher in photo-Fenton than Fenton. However, it seems that the irradiation affects differently depending on the iron chelate. Chelating agents with high stability constant with iron, such as DTPA and HEDTA, gave reaction rates 2.2 and 2.5 times higher in photo-Fenton than Fenton process. However, the iron chelates with low stability constant, like EDDS and EDTA, presented kinetic rates 11.0 and 8.4 times greater. This fact could be related to the stability of the iron complex. In photo-Fenton, higher kinetic rates were observed at higher iron precipitation. It seems that the lower stability of iron chelate eases its reaction with light, favoring the cycle of iron and leading the generation of more hydroxyl radicals. Another parameter to consider is the iron in solution. Thus, in photo-Fenton experiments the iron release was always higher than Fenton tests. Again, the highest differences were observed in EDDS and EDTA. Iron chelates are organic compounds which

could be attacked by light and hydroxyl radicals causing the breakdown of the complex and posterior decrease in MPs removal efficiency.

Research studies related on the use of EDDS revealed that the photoreduction of Fe(III) complex, induced by light by the ligand-to-metal charge transfer, produces the excitation of the iron complex and its subsequent breakage, leading to a reduction of Fe(III) to Fe(II) and EDDS radical (EDDS[•]). This radical tends to reach its stable oxidation state requiring a second electron transfer through reaction with dissolved oxygen, generating superoxide radical, which can take part in additional reactions as a precursor of hydroxyl radicals. Since the breakage of the iron complexes was different in photo-Fenton experiments, the formation of ligand radical and additional mechanisms could be different in other iron chelates. In this way, irradiation experiments were carried out without H₂O₂.

The results suggested that the experiments carried out with EDDS and DTPA achieved 43.5 and 30.0% of SMX abatement. While tests performed with HEDTA, EDDHA and EDTA obtained only 6.0%. Curiously, when DTPA was used, only 6.0% of iron was precipitated while in experiments with EDTA a percentage of 30.7% of iron release was observed. Additionally, when HEDTA was employed, 15.8% of iron precipitation was observed but no higher SMX degradation than DTPA. These results evidenced the differences between iron chelates, so the mechanisms cannot be generalized. The formation of H₂O₂ during these reactions was evaluated and the results obtained with DTPA-Fe suggested the generation of small amounts of H₂O₂, with maximum observed concentrations of 0.7 mg L⁻¹. Thus, in the experiments without initial H₂O₂, its generation could produce HO[•] by photo-Fenton reactions, a fact which agreed with the little hydrogen peroxide consumed during the experiments.

Photo-Fenton experiments were also carried out with tBuOH to understand the role of superoxide radical, probably formed in the above reaction mechanisms. The results indicated that HO[•] generated directly by photo-Fenton reactions and by the photoexcitation of Fe-complexes (EDDS-Fe and DTPA-Fe) was the final specie involved in the degradation of SMX.

Experiments with non-chelated iron were also investigated in an attempt of elucidating the possible involvement of free iron in solution in the formation of hydroxyl radicals. As observed, when organic fertilizers complexed with iron were used, the greater iron release was followed by higher reaction rate in SMX. This fact can lead to confusion in the

degradation mechanisms. Thus, two experiments with different iron dosage during the reaction were tested. Total Fe(II) addition was 2.2 and 0.4 mg L⁻¹, which corresponded to 16.6 and 13.7% of SMX removal, respectively. This fact evidenced that, at the studied conditions, iron chelates were involved in the photo-Fenton reactions. A small part of the SMX degradation could be caused by dissolved iron before precipitating as Fe(III) oxyhydroxides. However, it was not the main path through which the generation of HO[•] took place.

Finally, experiments without O₂ (bubbling N₂) were also performed in photo-Fenton experiments to study its contribution in MPs removal. In all cases, in the presence of O₂ better performances on SMX degradation were reached. This fact confirmed the potential reaction of this specie with excited iron chelates or ligand radicals to generate superoxide radical and final hydroxyl radical production. Additionally, the superoxide radical generated, could react with Fe(III) and accelerate the Fe(III)/Fe(II) cycle, which in photo-Fenton process is an additional way to produce hydroxyl radicals

Part III

Organic fertilizer as a chelating agent in photo-Fenton at neutral pH with LEDs for agricultural wastewater reuse: Micropollutant abatement and bacterial inactivation

Núria López-Vinent, Alberto Cruz-Alcalde, Jacqueline Aparecida Malvestiti, Pilar Marco, Jaime Giménez, Santiago Esplugas

Department of Chemical Engineering and Analytical Chemistry, Faculty of Chemistry, University of Barcelona, C/Martí i Franqués 1, 08028 Barcelona, Spain.

Published in *Chemical Engineering Journal* 388 (2020) 124246



Organic fertilizer as a chelating agent in photo-Fenton at neutral pH with LEDs for agricultural wastewater reuse: Micropollutant abatement and bacterial inactivation



N. López-Vinent^a, A. Cruz-Alcalde^a, J.A. Malvestiti^b, P. Marco^a, J. Giménez^{a,*}, S. Esplugas^a

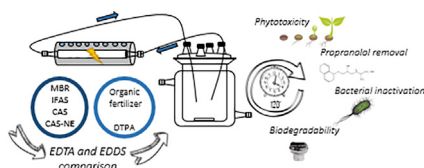
^a Department of Chemical Engineering and Analytical Chemistry, Faculty of Chemistry, Universitat de Barcelona, C/Martí i Franqués 1, 08028 Barcelona, Spain

^b School of Technology, University of Campinas – UNICAMP, Paschoal Marmo, 1888, 13484332 Limeira, SP, Brazil

HIGHLIGHTS

- Organic fertilizer DTPA as new chelating agent used in photo-Fenton at neutral pH.
- Simultaneous propranolol abatement and bacterial inactivation can be achieved.
- The influence of four WW matrices was tested in DTPA - photo Fenton.
- DTPA chelate presents higher stability than EDTA and EDDS chelates.
- Effluents treated with DTPA:Fe²⁺ satisfy the requirements for agricultural reuse.

GRAPHICAL ABSTRACT



ARTICLE INFO

Keywords:

DTPA
Photo-Fenton
Wastewater
Circumneutral pH
UV-A LED

ABSTRACT

In a water scarcity scenario, the reused wastewater could be an essential source for agricultural irrigation considering that 60% of fresh water is destined to this area. In this study, an organic fertilizer (Diethylene triamine pentaacetic acid, DTPA) was used as a new chelating agent of iron for photo-Fenton's application at neutral pH using LEDs. Secondary effluents with different characteristics were tested for propranolol removal and bacterial inactivation. With DTPA, the best results were achieved with MBR matrix: 94.0% of propranolol removal and total bacterial inactivation after 120 min. IFAS matrix showed the worst results: 63.2% of propranolol removal and only 2-log reduction for Total Coliforms. The performance of DTPA as chelating agent was compared with EDTA and EDDS with two matrices. In MBR matrix, propranolol removal with EDTA was 100% in 15 min, while DTPA and EDDS reached similar results at 120 min (94.0 and 91.3%), respectively. The iron precipitation was evaluated, and DTPA showed high stability with Fe²⁺ (only 10.4% of iron reduction instead 97.3% for EDDS). In addition, it looks like that the stability of iron chelates plays an important role in bacterial inactivation. Thus, the experiments with DTPA showed the lowest bacterial growth-on-the-plate after 72 h of the end of the experiment. Biodegradability and phytotoxicity were also evaluated and the experiments with DTPA had the lowest toxicity. The results of the experiments performed with DTPA were compared with the values in *Proposal for agricultural water reuse* suggesting that treated effluent accomplish the requirements for agriculture.

* Corresponding author.

E-mail address: j.gimenez.fa@ub.edu (J. Giménez).

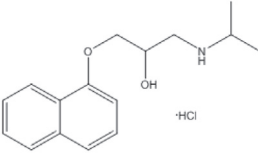
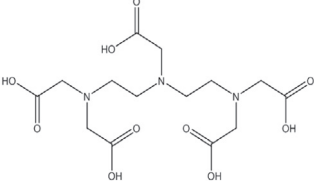
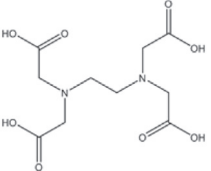
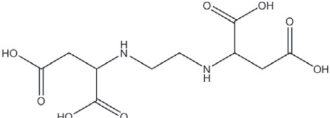
<https://doi.org/10.1016/j.cej.2020.124246>

Received 25 October 2019; Received in revised form 21 January 2020; Accepted 26 January 2020

Available online 29 January 2020

1385-8947/ © 2020 Elsevier B.V. All rights reserved.

Table 1
Properties of propranolol and three chelating agents tested in this study.

Compound	Molecular formula	Chemical structure	Molecular weight (g/mol)
PROP	$C_{16}H_{12}NO_2 \cdot HCl$		295.81
DTPA	$C_{14}H_{23}N_3O_{10}$		393.35
EDTA	$C_{10}H_{16}N_2O_8$		292.24
EDDS	$C_{10}H_{16}N_2O_8$		292.24

1. Introduction

The World Wildlife Fund (WWF) estimates that two-thirds of the world's population may face water shortage by 2025 at the current water consumption rate. Many of the water systems, which maintain ecosystems flourishing and provide water for human population, have changed into stressed [1]. All of that have forced to scientific community to investigate more efficient technologies for wastewater (WW) treatment and reuse [2]. Reused WW could be an important source of irrigation in the scarcity water scenario. According to UNESCO (The United Nations Educational, Scientific and Cultural Organization), the water consumed by agriculture is between 60 and 70% of fresh water, and this amount can increase up to 89% by 2025. Nevertheless, the quality of the reused WW must ensure the maintenance of an adequate level of public health and environmental protection. The key parameters can be found in the Proposal for a Regulation of the European Parliament and of the Council on minimum requirements for water reuse. This proposal establishes key parameters concerning pathogens [3]. However, in view of future WW reuse laws, micropollutants (MPs) probably will be regulated. So far, in the field of water policy, two regulations have been released in order to identify priority substances in water: Directive 2013/39/UE, which establish a list of priority compounds and environmental quality standards for these substances and other compounds [4], and Decision (EU) 2018/840, establishing a watch list of substances for monitoring in the field of water policy [5].

In the last decades, Advanced Oxidation Processes (AOPs) have proven to be efficient in the removal of large amount of non-biodegradable and recalcitrant compounds [6–9], which are not removed in conventional Wastewater Treatment Plants (WWTPs) [10–13]. In addition, there are some disadvantages related to conventional methods used for disinfection of WW, for instance chlorination [14]. The generation of disinfection by-products (DBPs), like trihalomethanes, is risky to human health and aquatic ecosystems [15]. Among AOPs, the photo-Fenton process is one of the most effective for disinfection and MPs abatement [16–18]. However, the optimal conditions of this process (acid pH) can make it unattractive for its application at full scale

[19,20]. In this way, several chelating agents have been tested in order to operate at neutral pH. Citrate, oxalate, EDTA (Ethylenedinitrilotetraacetic acid) and EDDS (Ethylenediamine-N, N'-disuccinic acid) are the most common chelating agents used in photo-Fenton process [21]. However, there are no data, as far as we have been able to investigate, in the assessment of DTPA (Diethylene triamine pentaacetic acid) as chelating agent in photo-Fenton process. This compound is used in different processes, mainly in agriculture and horticulture as an organic fertilizer. For instance, DTPA is included in the register of fertilizer products of the Ministry of Agriculture, Fisheries and Food of the Spanish Government [22]. Thereby, if DTPA was used as chelating agent, the treated WW could be employed in agriculture without needing to separate. The costs associated to electrical consumption by lamps are other disadvantage for the large-scale application of photo-Fenton process. These costs can be reduced when light emitting diodes (LEDs) are used in comparison with conventional lamps. No mercury content, low power consumption, long lifetime and no overheating are the main advantages in the replacement of conventional lamps by LEDs.

Therefore, the focus of this work is to test the efficiency of DTPA as a chelating agent in photo-Fenton at neutral pH using LEDs. Four different WW of secondary effluents from two WWTPs (located in Barcelona, Spain) were used with different characteristics. In addition, EDTA and EDDS (two of the most used chelating agents) were compared with DTPA in the MPs removal. In this case, propranolol (PROP) was selected as a target compound. This compound is a type of non-selective drug called beta-blocker and it is the one with the greatest presence in the aquatic environments [23]. Their occurrence in rivers or wastewaters was detected in concentrations ranging from 0.1 to 7.3 ng·L⁻¹ [24,25]. In surface waters was found in concentration of 53 ng·L⁻¹ [26]. In addition, their presence was found in different countries: Spain, Croatia, France, Serbian, Bosnian and China [24,27–30]. Bacterial disinfection (*E. coli* and Total coliforms) was also evaluated. The changes of biodegradability and toxicity (*Vibrio Fishery* and phytotoxicity) of the treated effluents are also important to know if the treated water satisfy the requirements for agricultural use [3].

Table 2

Parameters of the tested effluents before spike target compound. N/A: below the detection level.

Parameters	IFAS	MBR	CAS	CAS-NE
pH	7.9	7.8	8.0	7.6
Turbidity (NTU)	13.9	1.0	8.9	4.0
UV ₂₅₄ (m ⁻¹)	48	0.3	29	13
TOC (mg C · L ⁻¹)	29.5	5.3	24.1	7.9
DOC (mg C · L ⁻¹)	22.2	4.7	20.9	5.1
Total alkalinity (mg CaCO ₃ ·L ⁻¹)	545	312	457	304
Cl ⁻¹ (mg·L ⁻¹)	507	470	519	482
SO ₄ ²⁻ (mg·L ⁻¹)	152	125	242	236
N-NO ₂ ⁻ (mg·L ⁻¹)	N/A	N/A	N/A	N/A
N-NO ₃ ⁻ (mg·L ⁻¹)	N/A	9.9	24.8	31.7

2. Material and methods

2.1. Chemicals

Propranolol hydrochloride, EDDS-Na solution, DTPA (99%), hydrogen peroxide (H₂O₂) (30% w/v), Chromocult® Coliform Agar and catalase from bovine liver were obtained from Sigma-Aldrich. Ferrous sulfate (FeSO₄·7H₂O), EDTA, acetonitrile and orthophosphoric acid were purchased from Panreac Quimica. Buffered peptone water was acquired from Labkem. The following table (Table 1) shows the properties of target compound and different chelating agents used in this work.

2.2. Real WW effluents

The experiments were performed with four different WW. The effluents were acquired from the Gavà and El Prat de Llobregat WWTPs (province of Barcelona, Spain) after the biological treatment. Table 2 shows the main parameters of these WW.

Each WWTP presents two secondary treatments in parallel. WWTP of Gavà has Membrane Bioreactor (MBR) and Integrated Fixed-Film Activated Sludge (IFAS). WWTP of El Prat de Llobregat includes Conventional Activated Sludge (CAS) and the same treatment with nutrients elimination (CAS-NE) where the removal of 70% of phosphorus and nitrogen takes place.

2.3. Experimental procedure

All experiments were performed with real WW and carried out in a UV-A LED tubular photoreactor composed with 8 LEDs (wavelength 365 nm; irradiance: 2.66·10⁻⁷ Einstein · L⁻¹·s⁻¹). More information about the installation can be found in the supplementary material in Fig. S1. Each LED has 1.05 W of nominal power and 125° of irradiance angle. The 1 L of solution to be treated arrived to photoreactor from a feeding tank and it was continuously recirculated to the tank, where it was magnetically stirred. The temperature was maintained constant at 25° (Haake C-40) during all the experiment.

Real WW was taken out of the fridge a few hours before the experiment started for bacterial acclimation. To prepare the solutions, the respective chelating agent (EDDS, EDTA or DTPA) in each experiment was added to real WW. When this was dissolved, Fe(II) (0.18 mM) was put into the solution to form the complex. The molar ratios chelating agent:Fe(II) were 1:1 for EDTA and DTPA and 2:1 for EDDS, based on previous experiments. Finally, PROP (1.9 μM) was spiked to the solution. This concentration was selected to perform the study more realistic comparing with the PROP concentrations detected in the aquatic ecosystems. At the same time, this concentration allows a good monitoring of PROP. Hydrogen peroxide (4.41 mM) was added just before to start the experiment. Samples were withdrawn from the photoreactor at different times for 120 min. To stop the Fenton reaction, 10 μL of bovine catalase solution (200 mg·L⁻¹) was added to 5 mL of each

sample to decompose H₂O₂.

2.4. Analytical measurements

Hydrogen peroxide concentration was determined by colorimetric method based on the use of metavanadate [31] which forms a stable yellow complex with H₂O₂ and absorbs at 410 nm. Total iron in solution was measured at 510 nm by the o-phenatroline procedure (ISO 6332). The concentration of target compound at each time was monitored by HPLC Infinity Series (Agilent) and C-18 column (Tecknokrroma) (250 × 4.6 mm i.d; 5 μm particle size). According to the absorbance of PROP the UV detector worked at 214 nm. Acetonitrile and orthophosphoric water solution (pH = 3) were used as a mobile phase (25:75, respectively). An injection volume of 100 μL and 0.7 mL·min⁻¹ of flux were fixed. Biochemical Oxygen Demand (BOD) was performed following the 5210-standard method. Phytotoxicity was determined according Tam and Tiquia [32] using *Lactuca sativa* (lettuce) seeds. More information can be found in Table S1 in supplementary information. Acute toxicity was performed with Microtox M500 (*Vibrio Fishery*). Bacterial inactivation analyses were performed with 1 mL of each sample, where catalase was added to remove residual H₂O₂. This volume was plated on Chromocult® Coliform Agar before prepared in the laboratory. When a dilution was needed, buffered peptone water was used. Standard plated counted method was employed after an incubation period of 24 h at 35°. Growth-on-the-plate was determined for 48 and 72 h in the same plates of 120 min incubated at 35°.

3. Results and discussion

3.1. Effect of DTPA on photo-Fenton process

The efficiency of organic fertilizer (DTPA) as chelating agent was studied in the PROP abatement by neutral photo-Fenton with UV-A LEDs (Fig. 1). Due to the novelty in the use of DTPA as chelating agent in photo-Fenton process, some preliminary tests were performed to determine the optimum molar ratio Ligand:Fe(II) (Supplementary material Fig.S2 and Table S2). At the beginning of the experiment, total iron was chelated using 1:1 L:Fe(II) molar ratio and PROP degradation was faster. Thus, this L:Fe(II) molar ratio was employed in the rest of experiments with DTPA. Evaluation was performed in four wastewaters, which characteristics differ considerably (see Table 2), implying different behaviors in the MP removal. The photo-Fenton experiments were carried out at the natural pH of the effluents (between 7.6 and 8.0, according to Table 2).

Among different WWs, MBR showed higher degradation compared

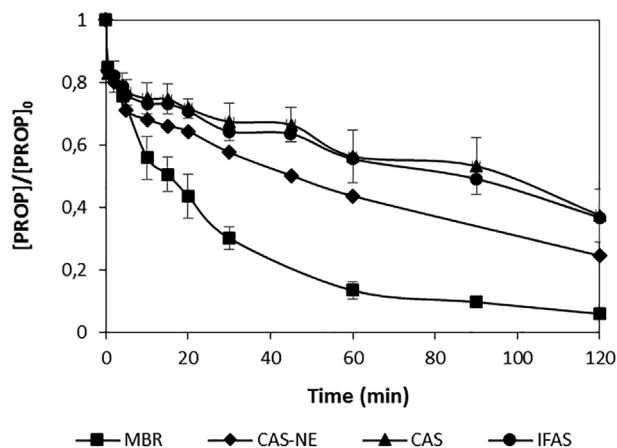


Fig. 1. Propranolol removal by UV-A LEDs circumneutral photo-Fenton process catalyzed by DTPA:Fe(II) in four different WWs. [PROP]₀ = 1.9 μM; [Fe(II)]₀ = 0.18 mM; [H₂O₂] = 4.41 mM; L:Fe(II) molar ratio = 1:1.

Table 3

Kinetic constants obtained for photo-Fenton catalyzed by DTPA:Fe(II) in different wastewaters at initial time (0–30 s) and between 30 s and 120 min (fitting to a first order kinetics). Values of R^2 of k_1 are not shown due to only two points were used..

Wastewaters	k_1 (min^{-1})	k_2 (min^{-1})	R^2 k_2
MBR	0.324	0.022	0.97
CAS-NE	0.350	0.009	0.99
CAS	0.375	0.006	0.96
IFAS	0.321	0.004	0.97

to other three wastewaters, achieving 94.0% PROP removal after 120 min ($0.63 \text{ kJ}\cdot\text{L}^{-1}$). However, only 63.2% and 62.5% were removed in 120 min for IFAS and CAS, respectively, being the worst. PROP abatement in CAS-NE was 75.4% at the end of the experiment. As known, real wastewaters are complicated matrix because of the different compounds present. As it can be observed in Table 2, MBR presents low TOC (Total Organic Carbon) and turbidity. Nevertheless, the same parameters in IFAS were the highest. The PROP removal is related to TOC values and decreases when TOC increases. The kinetic constants of the reaction between hydroxyl radical and DOM depend largely on the type of organic matter present in the matrix. However, some authors have quantified the kinetic constants between 10^8 and $10^9 \text{ L}\cdot\text{mol}^{-1}\cdot\text{s}^{-1}$ [33–38]. In this way, less organic matter produces less competition for hydroxyl radicals. The turbidity is also important in terms of the light scattering. CAS-NE presents approximately 2 times and 3 times lower turbidity than CAS and IFAS, respectively. In MBR the turbidity was approximately 9 times lower than in CAS and 14 times lower than in IFAS.

In order to better explain the results of MP abatement in different wastewaters two different fittings to a first order kinetics (Table 3) were performed for the different WW effluents. The kinetic constant k_1 represents the fitting in the first 30 s and it is strongly related to the initial reaction rate. While k_2 is the fitting from 30 s until 120 min. A first order kinetics was assumed according to Eq. (1).

$$\ln\left(\frac{C_f}{C_0}\right) = k \cdot t \quad (1)$$

As it can be observed in Table 3, the values of k_1 were practically the same in the four WWs even presenting different values of TOC and turbidity. In addition, k_1 was higher than k_2 in all WWs. This fact evidences that the dark Fenton process controls the reaction rate in first 30 s, as explained in previous works [17]. The differences due to the matrix were appreciated when k_2 was calculated. The values of k_2 decrease when TOC and turbidity increase (see Table 2). Thus, MBR presents the highest rate and IFAS the lowest. These facts seem to indicate that photo-Fenton controls the reaction rate after the first 30 s. This means that light plays an important role which can explain that k_2 decreases when turbidity and TOC increase, because light scattering or light absorption can increase. Thus, as it can be seen in Table 2, the turbidity of MBR is by the far the lowest and these differences were highlighted in the values of k_2 .

3.2. Comparison with conventional chelating agents

Several authors have been proved the efficiency of different chelating agents in the photo-Fenton process at circumneutral pH: nitrilotriacetic acid (NTA) [39–41], oxalic acid (OA) [42–44], citric acid (Cit) [45–47], ethylenedinitrilotetraacetic acid (EDTA) [39,48,49], ethylenediamine-N,N'-disuccinic acid (EDDS) [20,21,37,50–52] and DL-tartaric acid (TA) [39]. A problem related to the use of chelating agents is linked to the fact that the hydroxyl radicals generated in the Fenton's reaction also attack the complex of iron and chelating agent leaving iron in solution at neutral pH [39], producing the catalytic

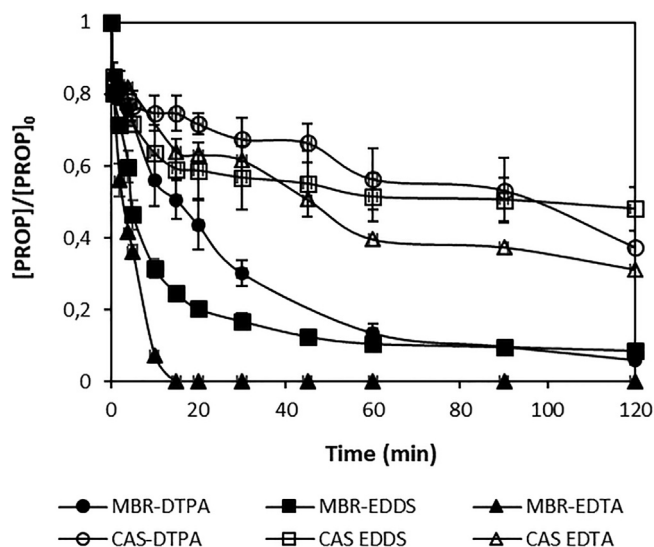


Fig. 2. Propranolol removal by UV-A LEDs circumneutral photo-Fenton in CAS (open symbols) and MBR (closed symbols). $[\text{PROP}]_0 = 1.9 \mu\text{M}$; $[\text{Fe}(\text{II})]_0 = 0.18 \text{ mM}$; $[\text{H}_2\text{O}_2] = 4.41 \text{ mM}$; $\text{EDTA}:\text{Fe}(\text{II}) = 1:1$; $\text{DTPA}:\text{Fe}(\text{II}) = 1:1$; $\text{EDDS}:\text{Fe}(\text{II}) = 2:1$.

activity decrease due to the subsequent iron precipitation and chelating degradation. DTPA can help to address this problem. Thus, the next step is to compare the DTPA behavior with two of the most used chelating agents, such as EDTA and EDDS. The target compound was also PROP, in two WWs: CAS and MBR, dirty and clean WW, respectively. The L:Fe (II) molar ratios used were 1:1 for EDTA and DTPA and 2:1 for EDDS. These values were necessary to ensure the complete iron chelation at the beginning of the experiment. Figs. 2 and 3 show the obtained results.

As obvious, when MBR was tested, the three chelating agents presented better results than CAS, due to the highest TOC and turbidity of CAS, as explained above (section 3.1). Regarding the efficiency on PROP removal, the percentages reached in MBR at the end of the experiment (120 min, $0.63 \text{ kJ}\cdot\text{L}^{-1}$) were 100%, 94.0% and 91.3% for EDTA, DTPA and EDDS, respectively. In CAS the removals were 68.7%, 62.5% and 51.9% in the same order.

In MBR matrix, EDTA presented the total PROP removal at 15 min of treatment ($0.08 \text{ kJ}\cdot\text{L}^{-1}$). However, for DTPA and EDDS at the same

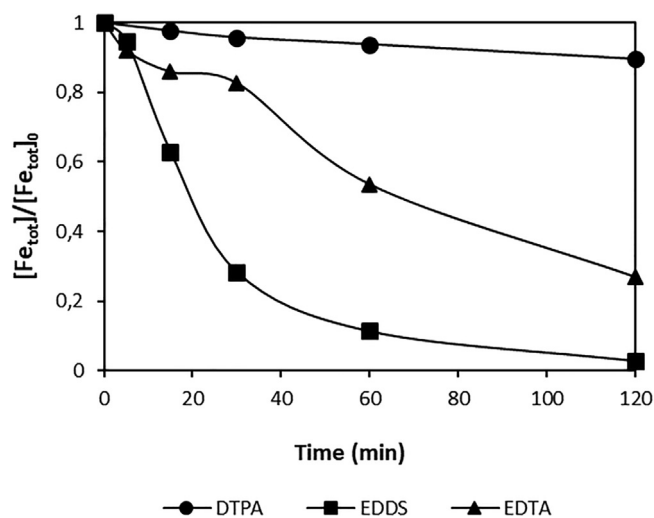


Fig. 3. Trend of total dissolved iron during the reaction for EDTA, DTPA and EDDS in MBR matrix. $[\text{PROP}]_0 = 1.9 \mu\text{M}$; $[\text{Fe}(\text{II})]_0 = 0.18 \text{ mM}$; $[\text{H}_2\text{O}_2] = 4.41 \text{ mM}$; $\text{EDTA}:\text{Fe}(\text{II}) = 1:1$; $\text{DTPA}:\text{Fe}(\text{II}) = 1:1$; $\text{EDDS}:\text{Fe}(\text{II}) = 2:1$.

time (15 min), the removal percentages were: 49.4% and 75.4%, respectively. EDDS presents a good removal at this time but then slows down a lot, achieving only 15.9% of degradation between 15 and 120 min. The explanation of this behavior can be related to iron precipitation. Iron content was monitored during each experiment, as represented in Fig. 3. In the course of the reaction, hydroxyl radicals attack PROP and the iron complex. This fact implies the breaking of the complexes and subsequent iron precipitation, due to the neutral pH, provoking a decrease in the catalytic activity, as commented before.

As observed in Fig. 3, complex destruction started at 5 min of reaction for EDDS. After this, a gradual reduction of total dissolved iron was observed, with a reduction of 97.3% at the end of the experiment (120 min). Nevertheless, at 15 min of the experiment, 37.3% had already been decreased. This fact is in agreement with the high percentage of PROP removal achieved in 15 min with EDDS in MBR (see Fig. 2). After this, the degradation slowed down a lot (see also Fig. 2), due to the precipitation of iron (see Fig. 3), which reduces the catalytic activity. For EDTA, a great amount of total dissolved iron was precipitated at the end of the experiment (72.9% of iron reduction). However, in this case, the precipitated iron at 15 min was only 14.1% (Fig. 3), which is in agreement with the fact that PROP was totally removed at 15 min (see Fig. 2), and this minimum reduction of total dissolved iron did not seem to be so important in the decrease of catalytic activity. Concerning DTPA, it is important to consider that only 10.4% of total dissolved iron precipitated after 120 min of the reaction. This fact shows the higher stability of the chelate and its resistance against hydroxyl radicals and radiation when DTPA is used. The stability constants (k_{stab}) of each chelating agent and iron are specific for the iron species ($k_{\text{stab}} \text{DTPA-Fe(III)} = 28.60$, $k_{\text{stab}} \text{EDTA-Fe(III)} = 25.10$, $k_{\text{stab}} \text{EDDS-Fe(III)} = 22.0$, $k_{\text{stab}} \text{DTPA-Fe(II)} = 16.55$, $k_{\text{stab}} \text{EDTA-Fe(II)} = 14.33$) [53]. Data were not found about k_{stab} for EDDS-Fe(II). Nevertheless, always DTPA presents a high stability constant with iron. Thus, in DTPA the degradation was slower than with EDTA and EDDS, due to the high stability in chelation of iron, but a gradual PROP reduction was observed achieving even a higher PROP removal than EDDS at the end of the experiment (see Fig. 2). The stability of the metal chelates appears to be influenced by their chemical structure, mainly the number and strength of the Fe-ligand interactions. According to this, the additional amino group in the chemical structure of DTPA provides its complex with iron with a coordination number of 7 instead of 6, as is the case of EDTA and EDDS. Therefore, this results in a higher stability of the DTPA complex. The observed differences in the stability of EDTA and EDDS complexes are caused by the larger distance from the amino groups to the carboxylic extremes of the EDDS molecule compared to EDTA. This causes a weaker interaction between these groups and iron, leading thus to a lower overall stability of the resulting complex.

Concerning CAS, the differences between three chelating agents were not so significant than in MBR. In this case, the effect of iron precipitation was more pronounced for EDTA. As it can be observed in Fig. 3, in first 45 min ($0.32 \text{ kJ}\cdot\text{L}^{-1}$) of the experiment the degradation curves for EDTA and EDDS were very similar and removals obtained were 44.9% and 49.3% for EDDS and EDTA, respectively. When EDDS was used (between 15 and 120 min of the treatment) the degradation was very low due to the iron precipitation, as observed with MBR matrix. However, in EDTA system the iron precipitation was lower and approximately 70% of iron remains in solution at 45 min. After that time, the PROP removal continued to increase in EDTA system until 60 min ($0.47 \text{ kJ}\cdot\text{L}^{-1}$). Values of 48.6% and 60.4% of PROP removal were achieved at 60 min for EDDS and EDTA, respectively, proving that the iron precipitation is so important for the catalytic activity. However, at 60 min the iron leaching gradually increased in EDTA until the end of the experiment, decreasing the PROP removal (between these times of the reaction, the degradation curve significantly slowed down). When the organic fertilizer (DTPA) was used, the PROP degradation came down more slowly than EDTA and EDDS during the experiment.

However, at the end of the treatment, the PROP removals achieved for different chelating agents were: 68.7%, 62.5% and 51.9% for EDTA, DTPA and EDDS, respectively. The high biodegradability of EDDS and low stability constant with iron caused the iron precipitation, generating low catalytic activity. Moreover, in EDDS the molar ratio L:Fe (II) was 2:1, but for EDTA and DTPA this ratio was 1:1. This increase in TOC, due to the presence of more EDDS, can also decrease the catalytic activity. For EDTA, degradation in CAS was slower than in MBR, because CAS has high TOC than MBR and, therefore, more influence of iron leaching was observed. Nevertheless, the high stability of DTPA with iron was essential to achieve close degradation than EDTA.

Summarizing, as it can be observed in Fig. 2, the reaction rate is very high at the beginning of the process (first 30 s) and similar for the two WW and the three chelating agents tested. This fact was due to the dark Fenton controls the reaction at first 30 s. Details of this behavior can be found in previous works [17,54].

After this initial period, the reaction rate is strongly determined by the iron precipitation and therefore for the complex stability. DTPA forms a more stable chelate with iron, as seen in Fig. 3. This explains a slower profile in the reaction rate, as shown in Fig. 2. However, EDTA and EDDS form less stable chelates, especially EDDS (see Fig. 3). Hence, between 30 s and 15 min, the break of the chelate allows more iron to be dissolved in the solution for a time and this would explain that the reaction rate is higher for EDTA and EDDS than for DTPA. However, in the last part of the experiment, between 15 and 120 min and according to Fig. 3, for EDDS practically no iron remains in solution and this implies that the reaction rate is drastically reduced. Thus, the iron in solution (Fig. 3), or the stability of the chelate, strongly determine the degradation rate of PROP (Fig. 2). Table S3 in the supplementary material shows a pseudo-quantitative explanation of all that. This commented behavior was observed for the two matrices tested (MBR and CAS) but reaction rates are little lower in CAS due to its high TOC and turbidity.

From this perspective, to rise the stability of iron chelates is advantageous to perform photo-Fenton at neutral pH, but the efficiency is also important [55]. It could be added that with EDTA and EDDS, due to iron precipitation, some mud is formed, which also interferes with the action of light and could help to explain, for example, the decrease of reaction rate for the EDDS.

3.3. Disinfection tests

Along with micropollutants, an efficient wastewater disinfection processes is important to improve public health, mainly when the reuse is aimed [56]. Therefore, it is important to find a process capable to eliminate both pathogens and MPs. The quantification of total coliforms (TC) in the four WWs revealed the presence of 1.7×10^2 , 1.8×10^2 , 3.8×10^2 and 9.8×10^3 colony-forming units per 1 mL ($\text{CFU}\cdot\text{mL}^{-1}$) at initial time for MBR, CAS-NE, CAS and IFAS, respectively. Initial concentrations of *E. coli* were 3×10^1 and 9×10^2 ($\text{CFU}\cdot\text{mL}^{-1}$) for CAS and IFAS, respectively. In MBR and CAS-NE, *E. coli* was not found. Fig. 4A shows the TC inactivation and Fig. 4B the *E. coli* inactivation with photo-Fenton process catalyzed by DTPA:Fe(II). According to Ortega-Gómez et al, the recirculation system (pump and flow) had no effect on cell viability [1]. Blank tests with only iron or hydrogen peroxide were performed and no inactivation was achieved with these concentrations.

According to Fig. 4, the circumneutral photo-Fenton using DTPA as a chelating agent was effective for the disinfection of total coliforms in different water matrices. MBR and CAS-NE reached the total coliform disinfection at the end of the treatment. Concerning CAS and IFAS, total coliforms decreased 2 order of magnitude at 120 min. As it can be seen in Fig. 4A, the inactivation curves for MBR and CAS-NE were overlapped in the first 30 min. In addition, MBR, which is the cleanest matrix, presented a high reduction, arriving at $1 \text{ CFU}\cdot\text{mL}^{-1}$ at 90 min ($0.47 \text{ kJ}\cdot\text{L}^{-1}$). However, in CAS-NE fewer reductions were observed in

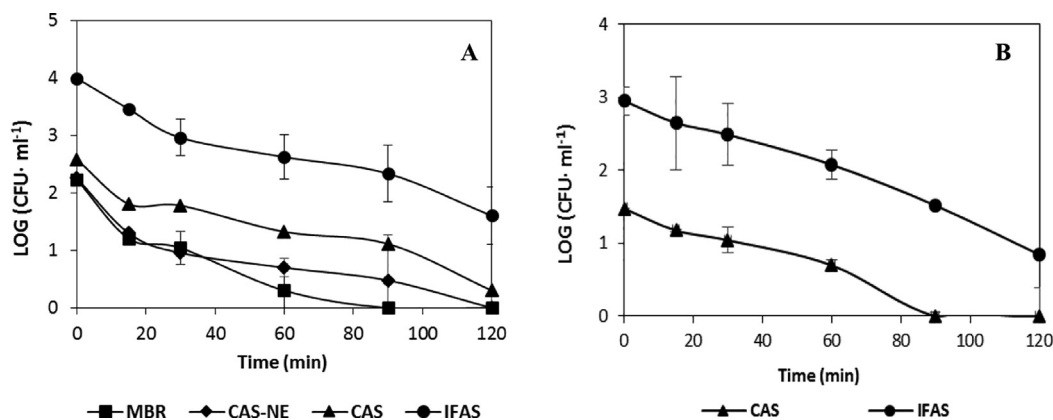


Fig. 4. TC inactivation in four WWs (A) and *E. coli* inactivation in IFAS and CAS (B) with photo-Fenton process catalyzed by DTPA:Fe(II). [PROP]₀ = 1.9 μM; [Fe(II)]₀ = 0.18 mM; [H₂O₂] = 4.41 mM; L:Fe(II) molar ratio = 1:1.

the next minutes (presenting 3 CFU·mL⁻¹ at 90 min). CAS and IFAS presented the worst results in terms of CFU·mL⁻¹. To compare with the other matrices, at 90 min values of 1.3×10^1 and 2.16×10^2 CFU·mL⁻¹ were obtained for CAS and IFAS, respectively. Obviously, IFAS is the one with the highest decrease in TC in absolute value, which is logical since it also has the highest initial value in TC. However, when representing log TC versus time, as shown in Fig. 4A, the disappearance rate is lower in IFAS. It was tried to make different kinetic fittings to be able to compare the data mathematically but none of them offered good correlations. This is also logical considering that TC are living beings whose behavior has nothing to do with that of inert chemical compounds. However, it is observed that, at the beginning, the disappearance rate is much higher in MBR and CAS-NE than in IFAS. This could be related to the fact that the higher TOC and turbidity of IFAS also represents a greater competition for hydroxyl radicals, reducing efficiency in the elimination of TC in IFAS.

Initial concentrations of *E. coli* were 3×10^1 and 9×10^2 CFU·mL⁻¹ for CAS and IFAS, respectively. *E. coli* inactivation (Fig. 4B) followed similar trend than TC. At 90 min, 0 CFU·mL⁻¹ was reached in CAS. However, in IFAS 2 orders of magnitude of inactivation were achieved at the end of the treatment. Nevertheless, 7 CFU·mL⁻¹ were counted at 120 min. Again, the influence of the water matrix was present, leading to a significant difference in the inactivation time.

The disinfection activity of DTPA was also compared with EDTA and EDDS. In this case, CAS and MBR were selected for the chelating agents comparison (TC: 1.7×10^2 and 3.8×10^2 CFU·mL⁻¹ at initial time for MBR and CAS, respectively; *E. Coli*: 3×10^1 CFU·mL⁻¹ for CAS). Fig. 5

shows the bacterial inactivation for different chelating agents in CAS and MBR.

As it can be seen, the photo-Fenton treatment reduced the bacterial concentration in TC (Fig. 5A) and *E. coli* (Fig. 5B). MBR matrix achieved the best results arriving until 0 CFU·mL⁻¹ at the end of the treatment for the three chelating agents. During the first 30 min of the treatment, EDDS showed higher reduction than EDTA and DTPA, followed by a slight reduction of TC the next 60 min (until 90 min of the experiment). DTPA and EDTA presented similar inactivation curves during the first 45 min. After this, DTPA showed a high inactivation rate, achieving the total TC inactivation at 90 min. After 60 min of the experiment the inactivation curves for EDTA and EDDS were very similar. The iron precipitation plays again an important role in hydroxyl radical formation, achieving DTPA good results due to the stability of the chelate (see Fig. 3). When CAS is used as water matrix, things change because the inactivation efficiency is deeply dependent on the characteristics of the matrix. At 120 min of the experiment, reductions of 2.3, 1.7 and 1.2 orders were achieved for DTPA, EDTA and EDDS, respectively. However, during the first hour the inactivation curves for the three chelating agents were similar. For EDDS slight reduction of TC was observed from 30 min until the end of the experiment. DTPA and EDTA followed the same trend than in MBR, achieving good results at the end of the experiment. The influence of chelate stability is pointed out again, according to Fig. 3. Fig. 5 shows also that, depending on the effluent properties, the irradiation needed to achieve complete inactivation differ greatly. For instance, when DTPA was tested in MBR, total TC inactivation was achieved at 90 min, with an energy consumption of

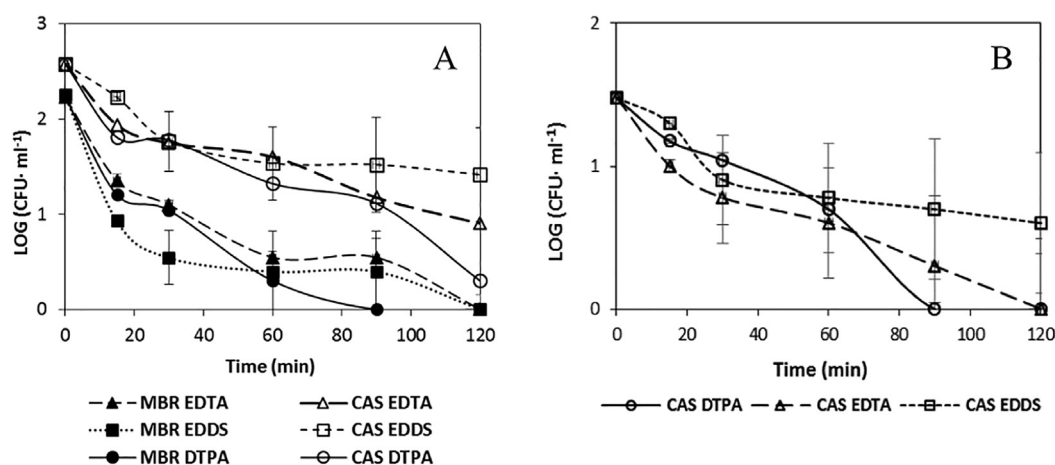


Fig. 5. (A) TC inactivation in CAS and MBR for EDTA, EDDS and DTPA and (B) *E. coli* inactivation in CAS for EDTA, EDDS and DTPA with photo-Fenton process at circumneutral pH. [PROP]₀ = 1.9 μM; [Fe(II)]₀ = 0.18 mM; [H₂O₂] = 4.41 mM; EDTA:Fe(II) = 1:1; DTPA:Fe(II) = 1:1; EDDS:Fe(II) = 2:1.

0.47 kJ·L⁻¹. However, in CAS, at 120 min of the treatment and an energy consumption of 0.63 kJ·L⁻¹, the total inactivation had not been achieved. Turbidity and TOC of wastewater matrices can play an important role in these different behaviors.

It has been reported that the hydroxyl radicals formed in the photo-Fenton process can generate reactions affecting DNA, lipids and proteins, producing bacteria mortality [57,58]. In addition, the bacterial inactivation can be explained by Fe(II) intracellular diffusion, where hydroxyl radicals can be generated during internal Fenton reactions [59,60]. However, in photo-Fenton at neutral pH, using chelating agents, the presence of Fe(II) in solution is almost null, due to the fast formation of iron oxohydroxides and posterior precipitation. In addition, the diffusion of chelated iron (Ligand-Fe(II)) not likely to occur because of the high molecular weight. Concerning the action of iron oxohydroxides, controversy exists related to bacterial inactivation [61]. The formation of iron oxohydroxides due to the attack of hydroxyl radicals or the photo-degradation of the complex drives to a dissolution with high turbidity, which can scatter the light. Similar results were found by Samira and coworkers [62]. Apart from that, there is less dissolved iron in solution, which reduces the catalytic activity, generating less hydroxyl radicals. These facts can explain the differences between three iron complexes tested in this study. The iron complexes formed by EDDS and EDTA show the highest precipitation of iron and the lowest bacterial inactivation at the end of the treatment. However, with DTPA-Fe(II) complex good results were found due to the less precipitation of iron.

Regarding *E. coli*, the efficiency of three chelating agents was the same than TC: DTPA > EDTA > EDDS. At the end of the experiment, EDTA and DTPA achieved total *E. coli* inactivation, being DTPA the best due to the total inactivation was reached at 90 min of the treatment.

An important parameter to take into account in wastewater reuse is the bacterial growth-on-the-plate. There are some pathogens, like *E. Coli*, that can manifest a “dormancy” mechanism during the treatment of WWs [63] and could turn into reactive under special conditions [64]. *E. Coli* and Total coliforms growth-on-the-plate was tested at the end of the experiment for EDTA, EDDS and DTPA and after 24, 48 and 72 h from the accomplishment of the treatment. In Fig. 6, the bacterial growth-on-the-plates values are represented for TC (Fig. 6A) and *E. Coli* (Fig. 6B) in CAS and MBR matrices.

The efficiency in bacterial growth-on-the-plates also depends on the quality of treated effluent. This was clearly seen in Fig. 6A where bacterial growth-on-the-plates of TC in CAS was higher than in MBR in all tested conditions. The introduction of DTPA as a chelating agent seems to be an enhancement for bacterial inactivation, as can be shown above. When DTPA was used in CAS, total coliforms were increased two times and three times at 48 and 72 h, respectively. After 72 h a value of 6 CFU·mL⁻¹ was obtained, whilst in MBR after 72 h 2 CFU·mL⁻¹ were quantified. The differences between the distinct WW matrices were also clearly observed when EDTA and EDDS were tested. The highest growth-on-the-plate was observed for EDDS in CAS, achieving 80 CFU·mL⁻¹ after 72 h. Concluding, the growth-on-the-plate increases in the order: DTPA < EDTA < EDDS and, concerning WW matrix, CAS presents higher growth-on-the-plate than MBR.

Concerning *E. Coli* (Fig. 6B), no bacterial growth-on-the-plate was observed for DTPA. With EDTA, the bacterial growth-on-the-plate was observed from 24 to 48 h. After this, no bacterial growth-on-the-plate was found. For EDDS, the bacterial growth-on-the-plate appears before 24 h and remains constant until 72 h. At 72 h after the finalization of the photo-Fenton treatment the values for different chelating agents were 0, 2 and 4 CFU·mL⁻¹, for DTPA, EDTA and EDDS, respectively.

The differences observed for the chelating agents lie in the different chemical and biochemical properties of each ligand. EDDS is more biodegradable than EDTA or DTPA. Thus, the microorganisms in the effluent can degrade this molecule causing better conditions for growth-on-the-plate. As a consequence, the lowest CFU·mL⁻¹ at the end of the experiment was obtained with DTPA. Thus, it is normal that the

growth-on-the-plate was lower.

3.4. Biodegradability and toxicity assessments

Depending on the final purpose of reused water, the requirements for water quality can be different. As explained above, agriculture consumption reaches to 60–70% of the total fresh water in the world. The minimum requirements for agricultural wastewater reuse can be found in the Proposal for a Regulation of the European Parliament and of the Council, Annex I [3]. *E. coli* (CFU·100 mL⁻¹) and BOD₅ (mg O₂·L⁻¹) are two important parameters listed in the Regulation. Thus, in this study biodegradability assays and disinfection (section 3.2) were performed in different experimental conditions where toxicity assessments (*Vibrio Fishery* and Phytotoxicity) were carried out.

For phytotoxicity tests, *L. sativa* (lettuce) seeds, acquired at a market, were used according to standardized protocols [32,65]. The values were expressed in percentage of germination index (GI) according to equations 2–4 [32]. These tests were performed for three chelating agents in MBR and CAS (Fig. 7). The control tests were carried out in deionized water.

$$\% \text{ seed germination} = \frac{\text{germination \% in the sample}}{\text{germination \% in the control}} \times 100 \quad (2)$$

$$\% \text{ root growth} = \frac{\text{mean root lenght in the sample}}{\text{mean root lenght in the control}} \times 100 \quad (3)$$

$$\text{Germination index} = \frac{\% \text{ seed germination} \times \% \text{ root growth}}{100} \quad (4)$$

Fig. 7A shows that, at initial time, the effluent stimulated a root elongation only in EDTA with a germination index of 136%. For DTPA and EDDS the germination index at initial time was 93 and 69%, respectively, being DTPA similar to control test (which corresponds to 100% of germination index). Zucconi and co-workers explained that germination index above 80–85% indicates the disappearance of phytotoxicity and values above 50–60% of GI do not cause significant injury to the plant growth. However, GI lower than 20% indicates the inhibition of seed germination and root elongation. Values between 20 and 50% of GI indicates presence of phytotoxicity [66,67]. At 30 min of the treatment, the germination indexes were the lowest in the three chelating agents (64.9, 51.9 and 11.9% for DTPA, EDTA and EDDS, respectively) indicating high phytotoxicity in EDDS. At the end of the treatment (120 min) for MBR the GI values of DTPA revealed stimulation of root elongation (GI = 109.3%). However, for EDTA and EDDS values of 58.2 and 75.8% of GI were achieved. Although these values were higher than these ones at 30 min, total disappearance of phytotoxicity were not observed. These results are in accordance with other studies where the toxicity increases in the middle of the treatment and at the end of the photo-Fenton process the toxicity decreases [68]. The phytotoxicity increase, achieved at 30 min of the treatment, could be associated to the formation of by-products more toxic than initial compound. Then, these by-products could be removed decreasing the toxicity. In addition, when DTPA was used and more toxic substances were removed, a favourable effect was observed at the end of the treatment. Concerning CAS, the same trend than in MBR was observed for the three chelating agents during the experiment. However, the changes in the phytotoxicity were less marked in CAS than in MBR for EDTA and EDDS. When DTPA was used, the values of germination index were similar to EDTA and EDDS during the first 60 min. Nevertheless, at the end of the experiment with DTPA, root elongation achieved a value of 291.4% of GI. The fact that the changes in germination index were higher in CAS than in MBR could be the presence of compounds that in low concentrations can act as a micronutrient leading to the stimulation of the root elongation. Real photos of measurements of *L.Sativa* can be found in supplementary material (Figs. S3 and S4). In addition, values of number of germination seeds and mean

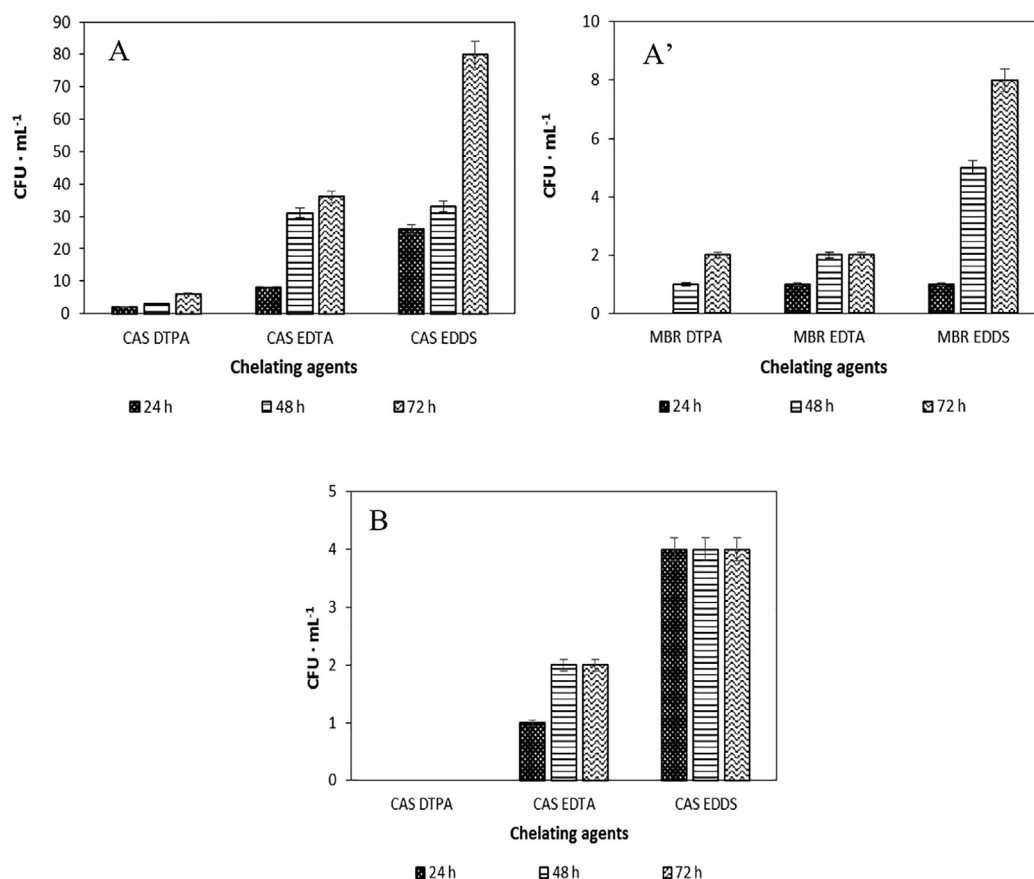


Fig. 6. Bacterial regrowth after 120 min of treatment for (A) Total Coliforms in CAS, (A') Total Coliforms in MBR and (B) *E. Coli* in CAS. [PROP]₀ = 1.9 μM; [Fe(II)]₀ = 0.18 mM; [H₂O₂] = 4.41 mM; EDTA:Fe(II) = 1:1; DTPA:Fe(II) = 1:1; EDDS:Fe(II) = 2:1.

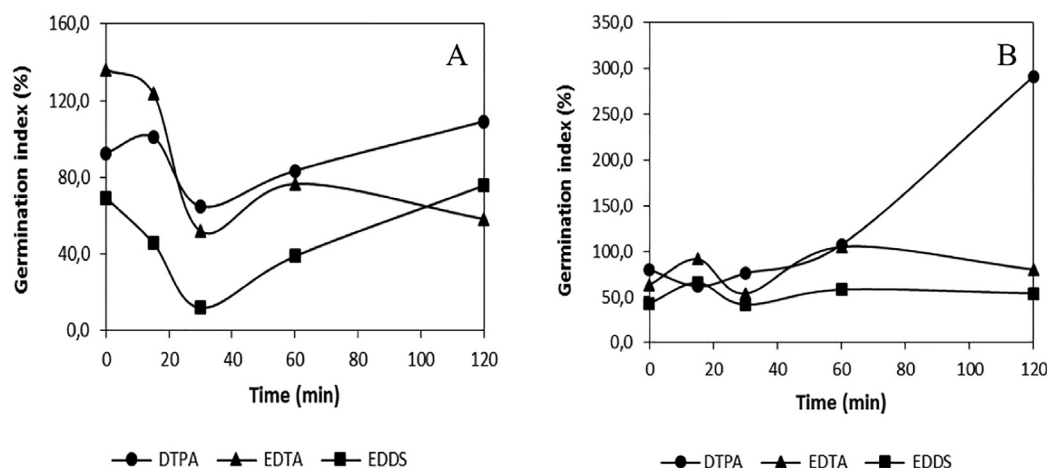


Fig. 7. Percentage of germination index of *L. sativa* for different chelating agents (A) in MBR and (B) in CAS. [PROP]₀ = 1.9 μM; [Fe(II)]₀ = 0.18 mM; [H₂O₂] = 4.41 mM; EDTA:Fe(II) = 1:1; DTPA:Fe(II) = 1:1; EDDS:Fe(II) = 2:1.

root length (mm) for each condition tested were also included in [supplementary material](#) (Table S4).

Acute toxicity was studied with Microtox bioassay (*Vibrio Fishery*). In these experiments, same treatment times than for phytotoxicity were selected in order to establish comparisons. The two organisms showed different sensibilities during the experiment. Thus, no response was observed during the experiment with MBR or CAS for the three chelating agents when *Vibrio Fishery* was tested. In this way, *Lactuca sativa* demonstrated that was more sensitive than *Vibrio Fishery* in the evaluation of the effluent ecotoxicity.

Finally, the biodegradability was also evaluated since it is a

parameter included in the Proposal for minimum requirements for agricultural water reuse. Fig. 8 shows the BOD₅ in MBR and CAS for the three chelating agents.

As it can be observed in Fig. 8, the biodegradability for EDDS was the highest in two WWs, being 32.8 and 41.8 mg O₂ · L⁻¹ for MBR and CAS, respectively. EDTA and DTPA presented close values and always lower than 15 mg O₂ · L⁻¹. The high biodegradability and the high L:Fe(II) molar ratio, when EDDS was employed, probably were two factors that influenced in these values.

The Proposal for agricultural water reuse [3] lists four reclaimed water qualities classes (A, B, C and D). Category A establishes a level

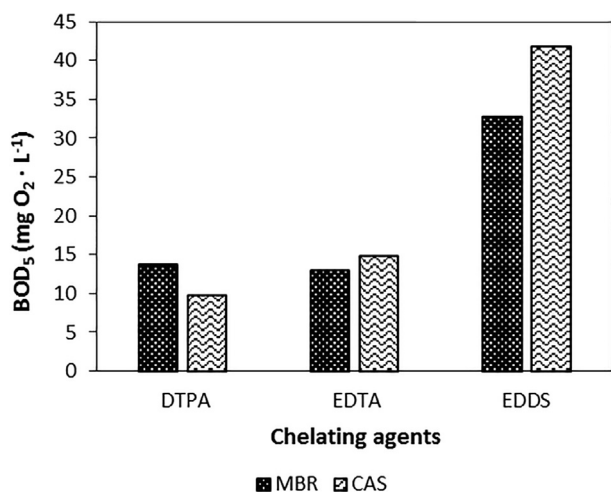


Fig. 8. Biodegradability evaluation for EDTA, EDDS and DTPA in two WW (MBR and CAS). [PROP]₀ = 1.9 μM; [Fe(II)]₀ = 0.18 mM; [H₂O₂] = 4.41 mM; EDTA:Fe(II) = 1:1; DTPA:Fe(II) = 1:1; EDDS:Fe(II) = 2:1.

≤ 10 mg O₂ · L⁻¹ of BOD₅. Categories from B to D establish a level ≤ 25 mg O₂ · L⁻¹ of BOD₅. For *E. Coli*, the established levels are ≤ 10 CFU·100 mL⁻¹, ≤ 100 CFU·100 mL⁻¹, ≤ 1,000 CFU·100 mL⁻¹ and ≤ 10,000 CFU·100 mL⁻¹ for categories A, B, C and D, respectively (more information about the categories can be found in Table S5 of supplementary material). The values of *E. Coli* selected to discuss the categories, were at 72 h after the end of the treatment. Therefore, when DTPA was used in CAS, at the end of the treatment the effluent satisfied the quality requirements of category A. In MBR matrix with DTPA, the effluent at the end of the treatment was included in category B. Finally, when EDTA was employed, the final effluent accomplished the requirements for the category C. In the case of EDDS, although the values for *E. Coli* satisfied the requirements for category C, the BOD₅ of the final effluent was higher than the level for water reuse for both wastewaters MBR and CAS. Thus, this effluent could not be reused for agriculture.

4. Conclusions

In this study, an organic fertilizer (DTPA) as a chelating agent of Fe²⁺ for neutral photo-Fenton was proven to be effective in simultaneous propranolol abatement and bacterial inactivation. MBR effluent (which is the cleanest matrix) showed higher propranolol degradation (94% of removal after 120 min) compared to other three wastewaters. Neutral photo-Fenton using DTPA was also effective for the disinfection of total coliforms and *E. Coli* in the different water matrices tested. Concerning wastewaters, the same trend was followed in bacterial inactivation than in propranolol removal.

Regarding the comparison of organic fertilizer with conventional chelating agents (EDTA and EDDS), EDTA showed better results in propranolol degradation (100% at 15 min) in MBR matrix but EDDS and DTPA show also good results (> 90% at 120 min). In CAS matrix, the PROP removal was very similar for DTPA and EDTA. The observed differences are mainly related to the iron precipitation and the stability of the formed complex, being the complex DTPA:Fe(II) the more stable. In bacterial inactivation, DTPA showed the best results compared with the other chelating agents due to the stability of iron complexes. In addition, DTPA presented the lowest bacterial growth-on-the-plate for all conditions due to the internal damages that the complex produces.

The biodegradability for EDDS was the highest in two wastewaters and EDTA and DTPA presented close values. Regarding phytotoxicity, this increases in the middle of the treatment and at the end of the photo-Fenton process the toxicity decreases for three chelating agents, achieving DTPA the best germination index and the lower

phytotoxicity.

Finally, when DTPA was used, at the end of the treatment, the effluent satisfied the quality requirements for agricultural reuse.

Acknowledgments

This study was funded by the Ministry of Science and Innovation of Spain (project CTQ2017-86466-R), AGAUR-Generalitat de Catalunya (project 2017SGR-131), Ministry of Education, Culture and Sports (FPU research fellowship FPU-16/02101) and Institute for Water Research (IdRA) of Universitat de Barcelona.

Appendix A. Supplementary data

Supplementary data to this article can be found online at <https://doi.org/10.1016/j.cej.2020.124246>.

References

- [1] E. Ortega-Gómez, B. Esteban García, M.M. Ballesteros Martín, P. Fernández Ibáñez, J.A. Sánchez Pérez, Inactivation of natural enteric bacteria in real municipal wastewater by solar photo-Fenton at neutral pH, *Water Res.* 63 (2014) 316–324.
- [2] A. Rastogi, S.R. Al-Abed, D.D. Dionysiou, Effect of inorganic, synthetic and naturally occurring chelating agents on Fe(II) mediated advanced oxidation chlorophenols, *Water Res.* 43 (2009) 684–694.
- [3] European Commission, Proposal for a Regulation of the European Parliament and of the Council of 28 May 2018 establishing the minimum requirements for water reuse, *Off. J. Eur. Communities.* 337 (2018) (2018) 1–27.
- [4] European Commission, Directive 2013/39/EU of the European Parliament and of the Council of 12 August 2013 amending Directives 2000/60/EC and 2008/105/EC as regards priority substances in the field of water policy, *Off. J. Eur. Union.* 226 (2013) (2013) 1–17.
- [5] European Commission, Decision 2018/840/EU of 5 June establishing a watch list of substances for Union-wide monitoring in the field of water policy pursuant to Directive 2008/105/EC of the European Parliament and of the Council and repealing Decision 2015/495/EU, *Off. J. Eur. Union.* 141 (2018) 9–12.
- [6] F.C. Moreira, R.A.R. Boaventura, E. Brillas, V.J. Vilar, Degradation of trimethoprim antibiotic by UVA photoelectron-Fenton process mediated by Fe(III)-carboxylate complexes, *Appl. Catal. B: Environ.* 162 (2015) 34–44.
- [7] R. Andreozzi, V. Caprio, A. Insola, R. Marotta, Advanced oxidation processes (AOP) for water purification and recovery, *Catal. Today* 53 (1999) 51–59.
- [8] B. Kasprzyk-Hordern, R.M. Dindsale, A.J. Guwy, The occurrence of pharmaceuticals personal care products, endocrine disruptors and illicit drugs in surface water in South Wales, UK, *Water Res.* 42 (2008) 3498–3518.
- [9] S.D. Kim, J. Cho, I.S. Kim, B.J. Vanderford, S.A. Snyder, Occurrence and removal of pharmaceuticals and endocrine disruptors in South Korean surface drinking, and waste waters, *Water Res.* 41 (2007) 1013–1021.
- [10] P. Soriano-Molina, J.L. García Sánchez, O.M. Alfano, L.O. Conte, S. Malato, J.A. Sánchez Pérez, Mechanistic modeling of solar photo-Fenton process with Fe³⁺-EDDS at neutral pH, *Appl. Catal. B: Environ.* 233 (2018) 234–242.
- [11] B. Quinn, F. Gagné, C. Blaise, An investigation into the acute and chronic toxicity of eleven pharmaceuticals (and their solvents) found in wastewater effluent on the cnidarian, *Hydra attenuata*, *Sci. Total Environ.* 389 (2008) 306–314.
- [12] M.M. Schultz, E.T. Furlong, D.W. Kolpin, S.L. Werner, H.L. Schoenfuss, L.B. Barber, V.S. Blazer, D.O. Norris, A.M. Vajda, Antidepressant pharmaceuticals in two US effluent-impacted streams: occurrence and fate in water and sediment and selective uptake in fish neural tissue, *Environ. Sci. Technol.* 44 (2010) 1918–1925.
- [13] L. Clarizia, D. Russo, I. Di Somma, R. Marotta, R. Andreozzi, Homogeneous photo-Fenton processes at near neutral pH: A review, *Appl. Catal. B* 209 (2017) 358–371.
- [14] J.A. Lima Perini, A.L. Tonetti, C. Vidal, C.C. Montagner, R.F. Pupo Nogueira, Simultaneous degradation of ciprofloxacin, amoxicillin, sulfathiazole and sulfamethazine, and disinfection of hospital effluent after biological treatment via photo-Fenton process under ultraviolet germicidal irradiation, *Appl. Catal. B* 224 (2018) 761–771.
- [15] A. Fiorentino, R. Cucciniello, A. Di Cesare, D. Fontaneto, P. Prete, L. Rizzo, G. Corno, A. Proto, Disinfection of urban wastewater by a new photo-Fenton like process using Cu-iminodisuccinic acid complex as catalyst at neutral pH, *Water Res.* 146 (2018) 206–215.
- [16] M. Català, N. Domínguez-Moruco, A. Migens, R. Molina, F. Martínez, Y. Valcárcel, N. Mastroianni, M. López de Alda, D. Barceló, Y. Segura, Elimination of drugs of abuse and their toxicity from natural Waters by photo-Fenton treatment, *Sci. Total Environ.* 520 (2015) 198–205.
- [17] N. López-Vinent, A. Cruz-Alcalde, L.E. Romero, M.E. Chávez, P. Marco, J. Giménez, S. Esplugas, Synergies, radiation and kinetics in photo-Fenton process with UVA-LEDs, *J. Hazard. Mater.* 380 (2019) 120882.
- [18] S. Giannakis, M. Voumard, S. Rtimi, C. Pulgarin, Bacterial disinfection by the photo-Fenton process: Extracellular oxidation or intracellular photo-catalysis? *Appl. Catal. B* 227 (2018) 285–295.
- [19] S. Miralles-Cuevas, D. Darowna, A. Wanag, S. Mozia, S. Malato, I. Oller, Comparison of UV/H₂O₂, UV/S₂O₈²⁻, solar/Fe(II)/H₂O₂ and solar/Fe(II)/S₂O₈²⁻ at pilot plant

- scale for the elimination of micro-contaminants in natural water, *Chem. Eng. J.* 310 (2017) 514–524.
- [20] I. De la Obra, L. Ponce-Robles, S. Miralles-Cuevas, I. Oller, S. Malato, J.A. Sánchez Pérez, Microcontaminant removal in secondary effluents by solar photo-Fenton at circumneutral pH in raceway pond reactors, *Catal. Today* 287 (2017) 10–14.
- [21] W. Huang, M. Brigante, F. Wu, K. Hanna, G. Mailhot, Development of a new homogeneous photo-Fenton process using Fe(III)-EDDS complexes, *J. Photochem. Photobiology A: Chem.* 239 (2012) 17–23.
- [22] Ministry of Agriculture, Fisheries and Food, Fertilizer products, (2019). <https://www.mapa.gob.es/app/consultafertilizante/DetalleFertilizante.aspx?clave=1435#> (accessed May 20, 2019).
- [23] J. Maszkowska, S. Stolte, J. Kumirska, P. Lukaszewicz, K. Mioduszewska, A. Puckowski, M. Caban, M. Wagil, P. Stepnowski, A. Białk-Bielinska, Beta-blockers in the environment: Part I. Mobility and hydrolysis study, *Sci. Total Environ.* 493 (2014) 1112–1121.
- [24] C. Fernández, M. González-Doncel, J. Pro, G. Carbonell, J.V. Tarazona, Occurrence of pharmaceutically active compounds in surface waters of the Henares-Jarama-Tajo river system (Madrid, Spain) and a potential risk and characterization, *Sci. Total Environ.* 408 (2010) 543–551.
- [25] S.O. Ganiyu, N. Oturan, S. Raffy, G. Esposito, E.D. van Hullesbusch, M. Cretin, M.A. Oturan, Use of sub-stoichiometric titanium oxide as a ceramic electrode in anodic oxidation and electro-fenton degradation of the beta-blocker propranolol: degradation kinetics and mineralization pathway, *Electrochim. Acta* 242 (2017) 344–354.
- [26] R.P. Deo, Pharmaceuticals in the surface water of the USA: A review, *Current Environ. Health Rep.* 1 (2014) 113–122.
- [27] M. Gros, M. Petrović, D. Barceló, Development of a multi-residue analytical methodology based on liquid chromatography-tandem mass spectrometry (LC-MS/MS) for screening and trace level determination of pharmaceuticals in surface and wastewaters, *Talanta* 70 (2006) 678–690.
- [28] V. Gabet-Giraud, C. Miège, J.M. Choubert, S.M. Ruel, M. Coquery, Occurrence and removal of estrogens and beta blockers by various processes in wastewater treatment plants, *Sci. Total Environ.* 408 (2010) 4257–4269.
- [29] S. Terzić, I. Senta, M. Ahel, M. Gros, M. Petrović, D. Barceló, J. Müller, T. Knepper, I. Martí, F. Ventura, P. Jovancic, D. Jabucar, Occurrence and fate of emerging wastewater contaminants in Western Balkan Region, *Sci. Total Environ.* 399 (2009) 66–77.
- [30] Y. Yang, J. Fu, H. Peng, L. Hou, M. Liu, J.L. Zhou, Occurrence and phase distribution of selected pharmaceuticals in Yangtze Estuary and its coastal zone, *J. Hazard. Mater.* 190 (2011) 588–596.
- [31] R.F. Pupo Nogueira, M.C. Oliveira, W.C. Paterlini, Simple and fast spectrophotometric determination of H₂O₂ in photo-Fenton reactions using metavanadate, *Talanta* 66 (2005) 86–89.
- [32] N.F.Y. Tam, S. Tiquia, Assessing toxicity of spent pig litter using a seed germination technique, *Resour. Conserv. Recycl.* 11 (1994) 261–274.
- [33] D. Schowanek, T.C.J. Fejtel, C.M. Perkins, F.A. Hartman, T.W. Federle, R.J. Larson, Biodegradation of [S, S], [R, R] and mixed stereoisomers of ethylene diamine disuccinic acid (EDDS), a transition metal chelator, *Chemosphere* 34 (11) (1997) 2375–2391.
- [34] J.D. Englehardt, D.E. Meeroff, L. Echegoyen, Y. Deng, F.M. Raymo, T. Shibata, Oxidation of aqueous EDTA and associated organics and coprecipitation of inorganics by ambient iron-mediated aeration, *Environ. Sci. Technol.* 41 (2006) 270–276.
- [35] S. Metsarinne, T. Tuhkanen, R. Aksela, Photodegradation of ethylenediaminetetraacetic acid (EDTA) and ethylenediamine disuccinic acid (EDDS) within natural UV radiation range, *Chemosphere* 45 (2001) 949–955.
- [36] J. Li, 17β-Estradiol Degradation Photoinduced by Iron Complex, Clay and Iron Oxide Minerals: Effect of the Iron Complexing Agent Ethylenediamine-Ethylenediamine-N, N-Disuccinic Acid, University Blaise Pascal, Aubière, 2010, PhD Thesis.
- [37] W. Huang, M. Brigante, F. Wu, C. Mousty, K. Hanna, G. Mailhot, Assessment of the Fe(III)-EDDS complex in Fenton-Like process: from the radical formation to the degradation of bisphenol A, *Environ. Sci. Technol.* 47 (2013) 1952–1959.
- [38] B.H.J. Bielski, D.E. Cabelli, R.L. Arudi, A.B. Ross, Reactivity of HO₂/O₂⁻ radicals in aqueous solution, *J. Phys. Chem. Ref. Data* 14 (1985) 1041–1100.
- [39] A. De Luca, R.F. Dantas, S. Esplugas, Assessment of iron chelates efficiency for photo-Fenton at neutral pH, *Water Res.* 61 (2014) 232–242.
- [40] O. Abida, G. Mailhot, M. Litter, M. Bolte, Impact of iron-complex (Fe(III)-NTA) on photoinduced degradation of 4-chlorophenol in aqueous solution, *Photochem. Photobiol. Sci.* 5 (2006) 395–402.
- [41] S.-P. Sun, X. Zeng, A.T. Lemley, Kinetics and mechanism of carbamazepine degradation by a modified Fenton-like reaction with ferric-nitilotriacetate complexes, *J. Hazard. Mater.* 252–253 (2013) 155–165.
- [42] L.I. Doumic, P.A. Soares, M.A. Ayude, M. Cassanello, R.A.R. Boaventura, V.J.P. Vilar, Enhancement of a solar photo-Fenton reaction by using ferrioxalate complexes for the treatment of a synthetic cotton-textile dyeing wastewater, *Chem. Eng. J.* 277 (2015) 86–96.
- [43] I.N. Dias, B.S. Souza, J.H.O.S. Pereira, F.C. Moreira, M. Dezotti, R.A.R. Boaventura, V.J.P. Vilar, Enhancement of the photo-Fenton reaction at near neutral pH through the use of ferrioxalate complexes: a case study on trimethoprim and sulfamethoxazole antibiotics removal from aqueous solutions, *Chem. Eng. J.* 247 (2014) 302–313.
- [44] N. Klammerth, S. Malato, M.I. Maldonado, A. Agüera, A.R. Fernandez-Alba, Modified photoFenton for degradation of emerging contaminants in municipal wastewater effluents, *Catal. Today* 161 (2011) 241–246.
- [45] X. Ou, X. Quan, S. Chen, F. Zhang, Y. Zhao, Photocatalytic reaction by Fe(III)-citrate complex and its effect on the photodegradation of atrazine in aqueous solution, *J. Photochem. Photobiol. A* 197 (2008) 382–388.
- [46] M.R.A. Silva, A.G. Trovo, R.F.P. Nogueira, Degradation of the herbicide tebutiuron using solar photo-Fenton process and ferric citrate complex at circumneutral pH, *J. Photochem. Photobiol. A* 191 (2007) 187–192.
- [47] H. Katsumata, S. Kaneco, T. Suzuki, K. Ohta, Y. Yobiko, Photo-Fenton degradation of alachlor in the presence of citrate solution, *J. Photochem. Photobiol. A* 180 (2006) 38–45.
- [48] P. Kocot, A. Karocki, Z. Stasicka, Photochemistry of the Fe(III)-EDTA complexes A mechanistic study, *J. Photochem. Photobiol. A* 179 (2006) 176–183.
- [49] J.J. Pignatello, E. Oliveros, A. MacKay, Advanced oxidation processes for organic contaminant destruction based on the Fenton reaction and related chemistry, *Critical Rev. Environ. Sci. Technol.* 36 (1) (2006) 1–84.
- [50] J. Li, G. Mailhot, F. Wu, N. Deng, Photochemical efficiency of Fe(III)-EDDS complex: OH radical production and 17_β-estradiol degradation, *J. Photochem. Photobiol. A* 212 (2010) 1–7.
- [51] N. Klammerth, S. Malato, A. Agüera, A.R. Fernandez-Alba, G. Mailhot, Treatment of municipal wastewater treatment plant effluents with modified photo-Fenton as a tertiary treatment for the degradation of micro pollutants and disinfection, *Environ. Sci. Technol.* 46 (2012) 2885–2892.
- [52] S. Miralles-Cuevas, I. Oller, J.A.S. Perez, S. Malato, Removal of pharmaceuticals from MWTP effluent by nanofiltration and solar photo-Fenton using two different iron complexes at neutral pH, *Water Res.* 64 (2014) 23–31.
- [53] Dojindo Molecular Technologies, Inc, Table of Stability Constants, (2020). https://www.dojindo.com/images/Product%20Photo/Chelate_Table_of_Stability_Constants.pdf (accessed January 15, 2019).
- [54] N. López-Vinent, A. Cruz-Alcalde, C. Gutiérrez, P. Marco, J. Giménez, S. Esplugas, Micropollutant removal in WW by photo-Fenton (circumneutral and acid pH) with BLB and LED lamps, *Chem. Eng. J.* 379 (2020) 122416.
- [55] K. Davididou, E. Chatzisyseon, L. Pérez-Estrada, I. Oller, S. Malato, Photo-Fenton treatment of saccharin in a solar pilot compound parabolic collector: Use of olive mill wastewater as iron chelating agent, preliminary results, *J. Hazard. Mater.* 372 (2019) 137–144.
- [56] M.C. Collivignarelli, A. Abba, I. Benigna, S. Sorlini, V. Torretta, Overview of the main disinfection processes for wastewater and drinking water treatment plants, *Sustainability* 10 (1) (2018) 86.
- [57] D. Spuhler, A.J. Rengifo-Herrera, C. Pulgarin, The effect of Fe²⁺, Fe³⁺, H₂O₂ and the photo-Fenton reagent at near neutral pH on the solar disinfection (SODIS) at low temperatures of water containing *Escherichia coli* K12, *Appl. Catal. B* 96 (2010) 126–141.
- [58] I. García-Fernández, M. Polo-López, I. Oller, P. Fernández-Ibáñez, Bacteria and fungi inactivation using Fe³⁺/sunlight, H₂O₂/sunlight and near neutral photo-Fenton: a comparative study, *Appl. Catal. B* 121–122 (2012) 20–29.
- [59] B. Halliwell, J. Gutteridge, Oxygen toxicity, oxygen radicals, transition metals and disease, *Biochem. J.* 219 (1984) 1–14.
- [60] M.I. Polo-López, I. Oller, P. Fernández-Ibáñez, Benefits of photo-Fenton at low concentrations for solar disinfection of distilled water. A case study: Phytophthora capsici, *Catal. Today* 209 (2013) 181–187.
- [61] J. Rodríguez-Chueca, M. Polo-López, R. Mosteo, M. Ormad, P. Fernández-Ibáñez, Disinfection of real and simulated urban wastewater effluents using a mild solar photo-Fenton, *Appl. Catal. B* 150 (2014) 619–629.
- [62] S. Nahim-Granados, I. Oller, S. Malato, J.A. Sánchez Pérez, M.I. Polo-López, Commercial fertilizer as effective iron chelate (Fe³⁺+EDDHA) for wastewater disinfection under natural sunlight for reusing in irrigation, *Appl. Catal. B* 253 (2019) 286–292.
- [63] A.R. Grupte, C.L.E. de Rezende, S.W. Joseph, Irrigation and resuscitation of viable but nonculturable *Salmonella enterica* serovar typhimurium DT104, *Appl. Environ. Microbiol.* 69 (11) (2003) 6669–6675.
- [64] J.D. Oliver, The viable but nonculturable state in bacteria, *J. Microbiol.* 43 (S) (2005) 93–100.
- [65] US EPA, Protocols for short term toxicity screening of hazardous waste sites. A. 8.7, Lettuce root elongation (*Lactuca sativa*). EUA, Chicago (1989).
- [66] F. Zucconi, A. Pera, M. Forte, Evaluating toxicity of immature compost, *Biocycle* (1981) 54–57.
- [67] F. Zucconi, M. Forte, A. Monaco, Biological evaluation of compost maturity, *Biocycle* (1981) 27–29.
- [68] A.M. Freitas, G. Rivas, M.C. Campos-Mañas, J.L. Casas López, A. Agüera, J.A. Sánchez Pérez, Ecotoxicity evaluation of a WWTP effluent treated by solar photo-Fenton at neutral pH in a raceway pond reactor, *Environ. Sci. Poll. Res.* 24 (2017) 1093–1104.

Supplementary Information for

Organic fertilizer as a chelating agent in photo-Fenton at neutral pH for agricultural wastewater reuse: micropollutant abatement and bacterial inactivation

N. López-Vinent, A. Cruz-Alcalde, Jacqueline A. Malvestiti, P. Marco, J. Giménez*, S.
Esplugas

Department of Chemical Engineering and Analytical Chemistry, Faculty of Chemistry,
Universitat de Barcelona, C/Martí i Franqués 1, 08028 Barcelona, Spain.

*Corresponding author:

Jaime Giménez Farreras, phone: +34 934 02 01 54, e-mail: j.gimenez.fa@ub.edu

Table of Contents

Figure S1. Experimental setup.....	p.2
Figure S2. Percentage of chelated iron for six DTPA-Fe(II) molar ratios tested.....	p.2
Table S1. Conditions for the determination of the phytotoxicity with <i>Lactuca sativa</i>	p. 3
Table S2. Degradation of propranolol by photo-Fenton at neutral pH with different Ligand-Fe(II) molar ratios.....	p.3
Table S3. Kinetic constants obtained for photo-Fenton at circumneutral pH	p. 5
Figure S3. Measurement of root growth of <i>L. Sativa</i> to calculate the germination index.....	p.5
Figure S4. Evaluation the number of <i>L. Sativa</i> seeds germination.....	p.6
Table S4. Number of seed germination and mean root length (mm) of 10 seeds of <i>L. Sativa</i> ...	p.6
Table S5. Classes of reclaimed water quality and allowed agricultural use and irrigation method.....	p.7

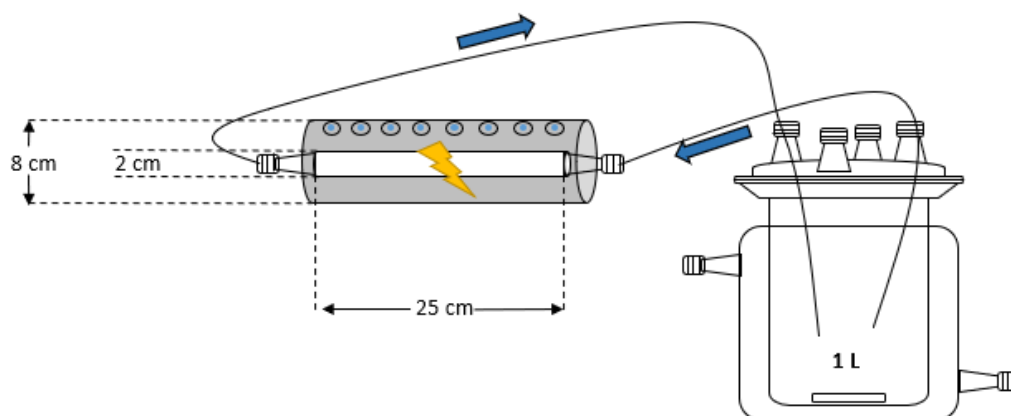


Figure S1. Experimental setup

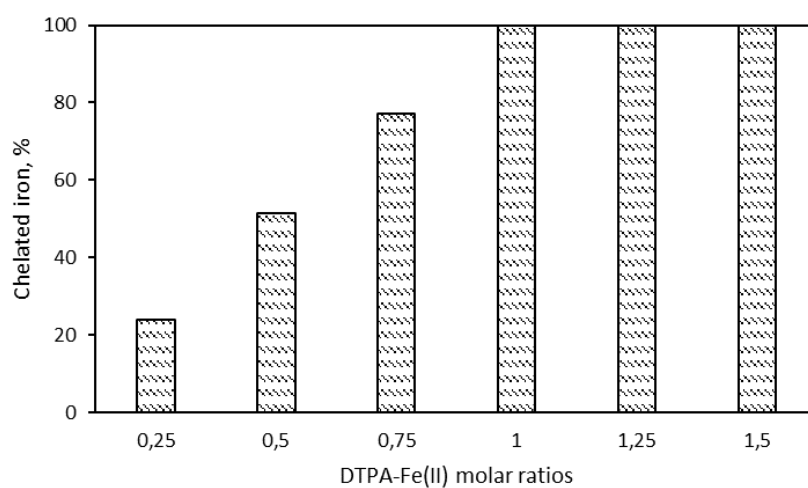


Figure S2. Percentage of chelated iron for six DTPA-Fe(II) molar ratios tested.

Table S1. Conditions for the determination of the phytotoxicity with *Lactuca sativa* [1]

Parameters	Conditions
Temperature	22.0 °C
Light	No
Test volume	4 mL per plate
Control	Distilled water
Number of seeds	10 seeds
Test duration	5 days
Test vessel	100 x 10 mm culture plate with 1 filter paper

Table S2. Degradation of propranolol by photo-Fenton at neutral pH with different Ligand-Fe(II) molar ratios. [PROP]= 0.19 mM; [H₂O₂]= 4.41 mM; [Fe(II)]= 0.18 mM.

DTPA:Fe(II) molar ratio	PROP removal (%) at 120
	minutes
0.25:1	27.58
0.50:1	31.79
0.75:1	36.40
1:1	48.11
1.25:1	25.51
1.50:1	21.37

In that case, as a preliminary tests, the experiments, shown in Figure S2 and Table S2, were performed with 0.19 mM of target compound in order to see better the differences between different Ligand:Fe(II) molar ratios.

Table S3. Kinetic constants obtained for photo-Fenton at circumneutral pH. Values of R^2 of k_1 are not shown due to only two points were selected ($R^2= 1$).

WW	Chelating agent	k_1	k_2	R^2	k_3	R^2
		(min^{-1})	(min^{-1})	k_2	(min^{-1})	k_3
MBR	EDTA	0.397	0.252	0.97	-	-
	EDDS	0.438	0.085	0.97	0.009	0.84
	DTPA	0.324	0.038	0.97	0.020	0.97
CAS	EDTA	0.339	0.020	0.98	0.007	0.94
	EDDS	0.331	0.025	0.96	0.002	0.95
	DTPA	0.375	0.007	0.82	0.006	0.95

Table S3 shows the different kinetic constants for each chelating agent in MBR and CAS. These kinetics constants were performed in order to evidence the importance of the complex stability as explained above. The first order kinetic constants were calculated according to equation 1. Three kinetics were performed: k_1 is the kinetic constant at first 30 seconds of the treatment, k_2 is the kinetic constant from 30 seconds until 15 minutes (from this time the PROP degradation significantly slowed down in EDDS) and k_3 is the kinetic constant between 15 and 120 minutes.

Obviously, the fact of making three different fittings for each experiment comes out of what is a classical kinetic fitting. In this case, more than obtaining rigorous kinetic constants, it was intended to quantify the different behaviors observed throughout the same experiment. In this way, the influence on the MP degradation rate of the light, the type of chelating agent, the precipitation of the iron and the type of residual water can be explained in a pseudo-quantitative manner. Therefore, it has simply been tried to explain in a pseudo-quantitative way the shape of the graphs of figures 2 and 3 of the paper and the relationships among them.

References

- [1] N.F.Y. Tam, S. Tiquia, Assessing toxicity of spent pig litter using a seed germination technique, *Resources, Conservation and Recycling* 11 (1994) 261-274.
- [2] European Commission, Proposal for a Regulation of the European Parliament and of the Council of 28 May 2018 establishing the minimum requirements for water reuse, *Off. J. Eur. Communities*. 337 (2018) 1-27.

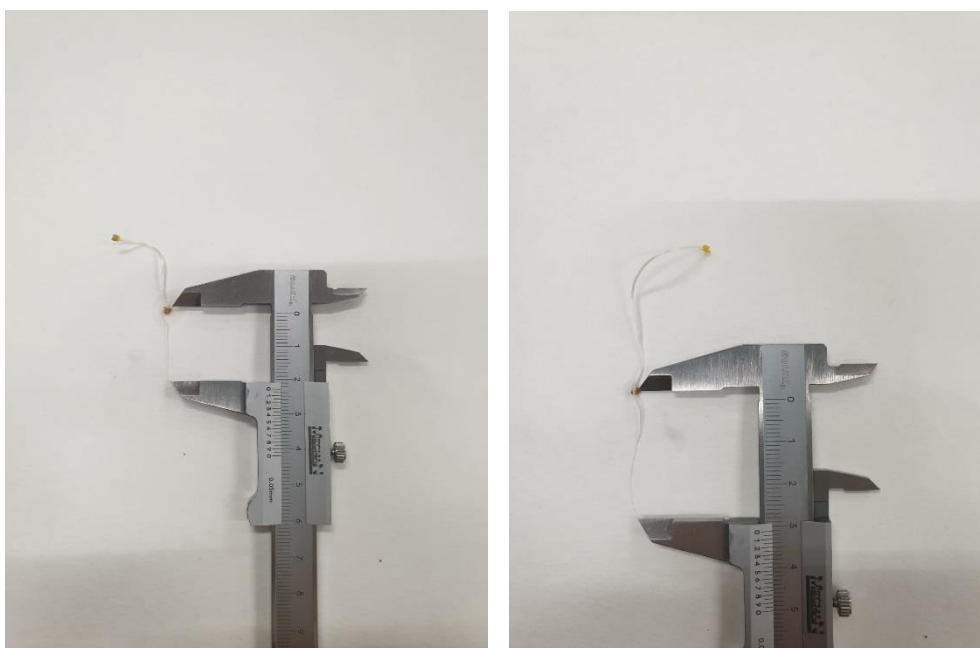


Figure S3. Measurement of root growth of *L. Sativa* to calculate the germination index

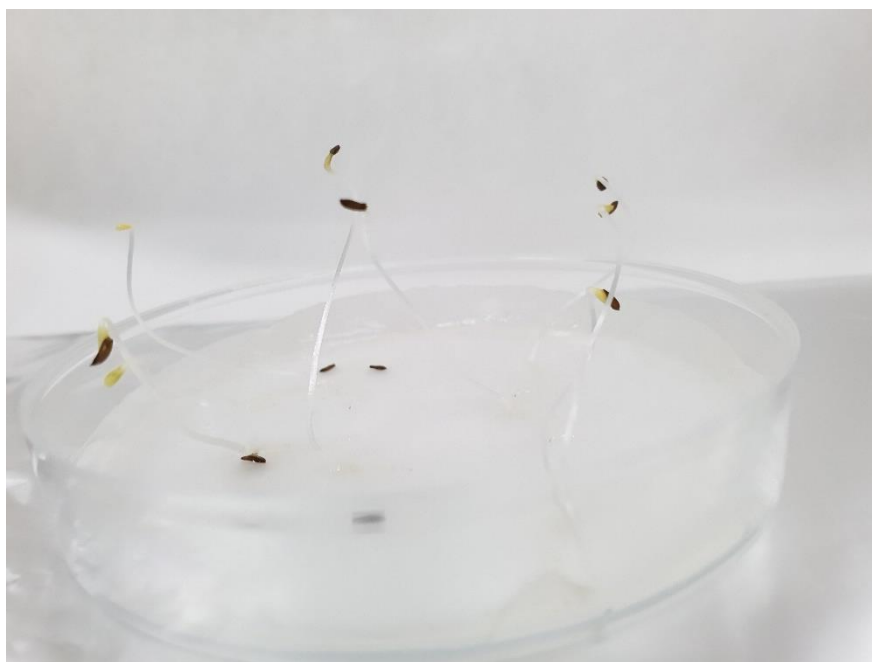


Figure S4. Evaluation the number of *L. Sativa* seeds germination

Table S4. Number of seed germination and mean root length (mm) of 10 seeds of *L. Sativa*

		Time (min)					Time (min)				
		0	15	30	60	120	0	15	30	60	120
		Number of seed germination (0/10)					Mean root length (mm)				
MBR	DTPA	10	10	8	9	10	8.9	9.7	7.8	8.9	10.5
	EDTA	10	9	6	8	8	13.1	13.2	8.3	9.2	7.0
	EDDS	7	6	3	6	8	9.5	7.3	3.8	6.2	9.1
CAS	DTPA	8	6	9	10	10	9.6	9.9	8.1	10.3	28.0
	EDTA	8	8	7	9	7	7.6	11.0	7.4	11.2	11.0
	EDDS	9	10	8	8	8	4.6	6.3	5.0	7.1	6.5
Control (mean)		8.5					11.3				

Table S5. Classes of reclaimed water quality and allowed agricultural use and irrigation method [2]

Minimum reclaimed water quality class	Crop category	Irrigation method
A	Food crops, including root crops consumed raw and food crops where the edible part is in direct contact with reclaimed water	All
B	Food crops consumed raw where the edible part is produced above ground and is not in direct contact with reclaimed water, processed food crops and non-	All
C	food crops including crops to feed milk- or meat-producing animals	Drip *
D	Industrial, energy, and seeded crops	All

(*) Drip irrigation (also called trickle irrigation) is a micro-irrigation system capable of delivering water drops or tiny streams to the plants and involves dripping water onto the soil or directly under its surface at very low rates (2-20 liters/hour) from a system of small diameter plastic pipes fitted with outlets called emitters or drippers.

Part IV

Improvement of the photo-Fenton at natural condition of pH using organic fertilizers mixtures: potential application to agricultural reuse of wastewater

Núria López-Vinent, Alberto Cruz-Alcalde, Jaime Giménez, Santiago Esplugas, Carmen Sans

Department of Chemical Engineering and Analytical Chemistry, Faculty of Chemistry,
University of Barcelona, C/Martí i Franqués 1, 08028 Barcelona, Spain.

Published in *Applied Catalysis B: Environmental* 290 (2021) 120066



Improvement of the photo-Fenton process at natural condition of pH using organic fertilizers mixtures: Potential application to agricultural reuse of wastewater

N. López-Vinent ^{*}, A. Cruz-Alcalde, J. Giménez, S. Esplugas, C. Sans

Department of Chemical Engineering and Analytical Chemistry, Faculty of Chemistry, Universitat de Barcelona, C/Martí i Franqués 1, 08028, Barcelona, Spain

ARTICLE INFO

Keywords:

Organic fertilizers
Wastewater reuse
Iron chelates mixtures
Photo-Fenton

ABSTRACT

Five organic fertilizers (DTPA, EDDHA, HEDTA, EDTA and EDDS) were studied as iron sources for photo-Fenton process at natural pH to remove micropollutants (MPs) from wastewater for its reuse in irrigation. The results demonstrated that the stability constant of iron chelates is a key parameter for optimal micropollutants removal and it is linked to the structure of chelator. Mixtures of organic fertilizers were also tested to overcome excessive iron loose and to optimize MPs abatement kinetics. An improvement of photo-Fenton process occurred when using chelating mixtures. For instance, with 50 %EDDS + 50 %EDTA total removal of propranolol (PROP) was achieved at 30 min while EDTA needed up to 90 min of reaction and with EDDS total degradation was not achieved. In addition, the availability of dissolved iron of the mixture at the end of the treatment was 5.5 times higher than EDDS, increasing its suitability as reuse water for irrigation.

1. Introduction

Water scarcity is a growing environmental problem that the world's population must confront. According to the World Wildlife Fund (WWF) and UNESCO (The United Nations Educational, Scientific and Cultural Organization), a large part of the aquatic ecosystems has changed into a stress situation during the last decades [1]. Under the current water consumption pattern, moreover, these organizations have estimated that two-thirds of the world population could suffer from water shortages by 2025 [2]. In front of this critical scenario, the reuse of wastewater (WW) is expected to be necessary to ensure the coverage of the water demand in a near future.

The water destined to agriculture is around 70 % of the total freshwater demand and this percentage accounts for 90 % in some developing countries. Thus, different measures are required to address the acute water challenges in agriculture for the next few years [2]. In this sense, the WW reuse in agriculture seems a good strategy to reduce the percentage of fresh water destined to this sector. However, the quality of this reclaimed WW has to accomplish some minimum requirements to ensure a safe use of this alternative resource in crop irrigation. These requisites are currently established in the Proposal for a Regulation of the European Parliament and of the Council on minimum requirements

for water reuse [3], where Biochemical Oxygen Demand (BOD), turbidity and pathogens are defined as the main parameters to be controlled. Nevertheless, wastewater can also contain micropollutants (MPs), which are not completely regulated yet. However, as the presence of these substances in water can be harmful for ecosystems and human health [4–7], and the inclusion of new quality criteria in water reuse regulations concerning this kind of pollution is expected shortly.

Most MPs are only efficiently degraded by hydroxyl radicals (HO·), which can be generated by Advanced Oxidation Processes (AOPs). Among these techniques, photo-Fenton process has demonstrated its efficiency in the removal of several organic compounds and pathogens [8–11]. Nevertheless, acidic conditions under which this treatment is effective make the process economically unattractive for full-scale application [12,13]. To solve this inconvenience and work at natural pH, several chelating agents have been studied to keep iron complexed and avoid its precipitation at pH above 2.8 (i.e., the optimal working conditions for photo-Fenton process). Compounds such as EDTA (Ethylenedinitrilotetraacetic acid) and EDDS (Ethylenediamine-N, N'-disuccinic acid), as well as citric and oxalic acids have been the most investigated [14–17]. However, the low stability of the corresponding iron complexes eventually provokes the precipitation of iron during the treatment, consequently decreasing the removal efficiency of MPs.

^{*} Corresponding author.

E-mail address: nuria.lopez@ub.edu (N. López-Vinent).

<https://doi.org/10.1016/j.apcatb.2021.120066>

Received 8 September 2020; Received in revised form 19 January 2021; Accepted 14 February 2021

Available online 28 February 2021

0926-3373/© 2021 Elsevier B.V. All rights reserved.

Recently, studies with other chelating agents such as DTPA (Diethylene triamine pentaacetic acid) and EDDHA (Ethylenediamine-*N,N'*-bis (2-hydroxyphenylacetic acid)) have also demonstrated their efficiency in abatement of organic micropollutants and bacterial inactivation [18, 19]. All of these iron chelates are approved by the European Commission for their agricultural use [20] as these can be applied in the form of ferric chelates to provide the crops with the iron required to produce chlorophyll and some enzymatic functions involved in respiration and metabolism. In this sense, an investigation on new organic fertilizers more sustainable with the environment studied the EDDS as a fertilizer to avoid the chlorosis in plants. The results revealed that EDDS is suitable for the correct development of the plants [21] and it is more biodegradable in soils than DTPA or EDTA, which are also commonly employed in agriculture as organic fertilizers.

Unlike the most common chelating agents, DTPA and EDDHA iron complexes present very high stability. Consequently, degradation rates of MPs are slow, although their use can involve advantages such as having a higher amount of chelated iron at the end of the treatment [18]. To improve the process, an equilibrium between iron availability and complexes stability in solution is needed to ensure a sustained production of hydroxyl radicals during the entire treatment and, consequently, a good treatment efficiency.

The aim of this work is to test the performance of different iron chelates in the treatment of secondary wastewater effluent by photo-Fenton, for their subsequent reutilization in agriculture. The selected endpoints for assessment of the treatment efficiency were the abatement of three representative micropollutants: acetamiprid (ACMP), propranolol (PROP) and sulfamethoxazole (SMX). For the first time, as far as we have been able to know, five different organic fertilizers (EDTA, EDDS, DTPA, EDDHA and HEDTA (2-Hydroxyethyl ethylenediamine-*N,N'*-triacetic acid)) were compared in the same study under similar and feasible operational conditions, showing the potential applicability of each compound. Moreover, some of the best performing chelates were combined and tested in additional photo-Fenton experiment. The aim of this part was to explore possible performance increase of the process with the use of chelates mixtures, taking advantage of the particular properties of each compound concerning the ability of keeping iron complexed and available for catalytic reactions conducting to HO-generation. Apart from MPs abatement, BOD₅ after treatment was evaluated to compare the results of treated wastewater with the legislation for agricultural water reuse.

2. Material and methods

2.1. Chemicals

Propranolol hydrochloride (PROP), acetamiprid (ACMP), sulfamethoxazole (SMX), EDDS-Na solution and liver bovine catalase from bovine liver were acquired from Sigma-Aldrich. Organic fertilizers (bought with iron chelated) DTPA-Fe (7% of iron), EDTA-Fe (13.3 % of iron) and HEDTA-Fe (13.0 % of iron), used as iron chelates, were purchased from Phygenera, Germany. EDDHA-Fe (6.0 % of iron) was obtained from Fertiberia. Acetonitrile, orthophosphoric acid, ferrous sulfate (FeSO₄·7H₂O) hydrogen peroxide (H₂O₂, 30 % w/v), o-Nitrobenzaldehyde (98 %) and ethanol (96 %, v/v) were acquired from Panreac Quimica.

2.2. WWTP effluent

Secondary effluent from a membrane bioreactor (MBR) of a wastewater treatment plant (WWTP) located in Barcelona, Spain (plant of Gavà-Viladecans; 384,000 population equivalent (PE); DF (design flow): 64,000 m³ d⁻¹) was chosen to perform the experiments. The MBR is a combination of conventional activated sludge (CAS) and external membrane post-treatment by ultrafiltration. Table 1 lists the principal parameters of the WW.

Table 1
Physic-chemical parameters of wastewater.

Parameters	MBR
pH	7.8
Turbidity (NTU)	0.3
UV ₂₅₄ (m ⁻¹)	19.1
TOC (mg C L ⁻¹)	7.0
DOC (mg C L ⁻¹)	6.7
Total alkalinity (mg CaCO ₃ L ⁻¹)	233.2
HCO ₃ ⁻ (mg HCO ₃ ⁻ L ⁻¹)	279.8
Cl ⁻ (mg L ⁻¹)	591.6
SO ₄ ²⁻ (mg L ⁻¹)	168.8
N-NO ₂ ⁻ (mg L ⁻¹)	0.4
N-NO ₃ ⁻ (mg L ⁻¹)	N/A
PO ₄ ³⁻ (mg L ⁻¹)	N/A

N/A: below the detection level.

2.3. Experimental procedure

All experiments were carried out in a solar simulator (Xenonterm-1500RF.CCI) with a Xenon lamp (1.5 kW) (wavelength range: 290–400 nm; irradiance: 6.6·10⁻⁷ Einstein·L⁻¹ s⁻¹ (13.9 W m⁻²) obtained by o-Nitrobenzaldehyde actinometry. The methodology to prepare the solutions to carry out the actinometry was extracted from De la Cruz et al. 2013 [22]. The emission spectrum can be found in Fig. S1 of supplementary information. The tubular photoreactor (25 cm length x2 cm diameter) was located on the axis of a parabolic mirror made of reflective aluminum (*reflectivity between 0.8 and 0.9*), at the bottom of solar simulator. The total volume of each experiment was 1 L and the solution was continuously recirculated from the feeding tank (magnetically stirred) to the tubular photoreactor. The temperature was controlled by Haake C-40 bath and keep constant at 25 °C. More information about the experimental set-up can be found in Fig. 1.

To prepare the dissolutions with iron chelates, an appropriate amount of each organic fertilizer was added to WW. The concentration of each one was calculated according to the percentage of iron content (information in section 2.1) in order to obtain a concentration of 5 mg L⁻¹ of iron in solution (which is the maximum concentration in irrigation water permitted by international regulations) [23,24]. To perform the experiments with two iron chelates an appropriate amount of each organic fertilizer, according to the iron content of each one, was added to solution also to achieve a total concentration of 5 mg L⁻¹ of iron. In the mixtures with EDDS, which was the only one that was not acquired as an iron chelate, a molar ratio of 1:1 (EDDS: Fe(II)) was selected based on previous studies [25]. In these cases, the EDDS was firstly added to the solution and then the iron, to ensure a good chelation. After this, the corresponding organic fertilizer was added to obtain the total iron concentration. A concentration of 0.25 mg L⁻¹ of PROP, ACMP and SMX was spiked to the WW (total concentration of 0.75 mg L⁻¹). Finally, hydrogen peroxide (50 mg L⁻¹) was added just before the reaction began. Samples were retired periodically from the tank during 180 min and liver bovine catalase was employed to stop the reaction (10 µL of liver bovine catalase at a concentration of 200 mg L⁻¹ to 5 mL of each sample). Samples to analyze the total iron content were filtered with 0.20 µm PVDF filter to ensure a good read of soluble (chelated and not) iron. In addition, ascorbic acid was added to the sample to have the total soluble iron.

The degradation of MPs was plotted considering the accumulated energy (Q_{acc}, kJ L⁻¹), which was calculated according to Eq.1 [22,26].

$$Q_{acc} = \sum_{i=1}^n \frac{I \cdot \Delta t_i}{V} \quad (1)$$

I is the irradiation entering the photoreactor (kJ s⁻¹), Δt_i is the increment of the time of reaction (s) and V is the reaction volume (L).

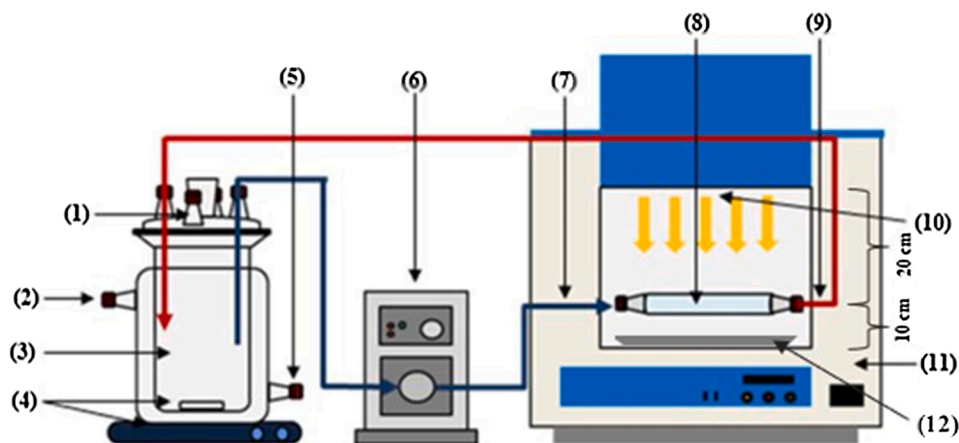


Fig. 1. Experimental setup. (1) Sampling orifice; (2) Thermostatic bath-IN; (3) Feeding tank; (4) Magnetic stirrer; (5) Thermostatic bath-OUT; (6) Peristaltic pump; (7) Recirculation IN; (8) Tubular photoreactor; (9) Recirculation OUT; (10) Xenon lamp; (11) Solar simulator chamber; (12) Parabolic mirror.

2.4. Analytical measurements

The concentration of MPs (PROP, ACMP and SMX) was followed by High Performance Liquid Chromatography (HPLC Infinity Series, Agilent Technologies), using a C-18 Tecknokroma column (250 × 4.6 mm i. d; 5 μm particle size). Acetonitrile (20 %) and water acidified with orthophosphoric acid (pH = 3) (80 %) were employed as mobile phases. The flowrate was 1 mL min⁻¹ and the injection volume was set to 100 μL. Three wavelengths were fixed according to absorbance of each

compound: 214, 250 and 270 nm for PROP, ACMP and SMX, respectively. Equal than MPs, the concentration of o-Nitrobenzaldehyde was measured by HPLC with the column aforementioned. The mobile phases were acetonitrile and water (pH = 3) (60:40, respectively), UV detection was set to 258 nm and 0.6 mL min⁻¹ was fixed as a flow rate. The monitoring of H₂O₂ and total iron in solution was performed by colorimetric method of metavanadate [27] and o-phenantroline procedure (ISO 6332), respectively. The BOD₅ was carried out using the 5210-standard method.

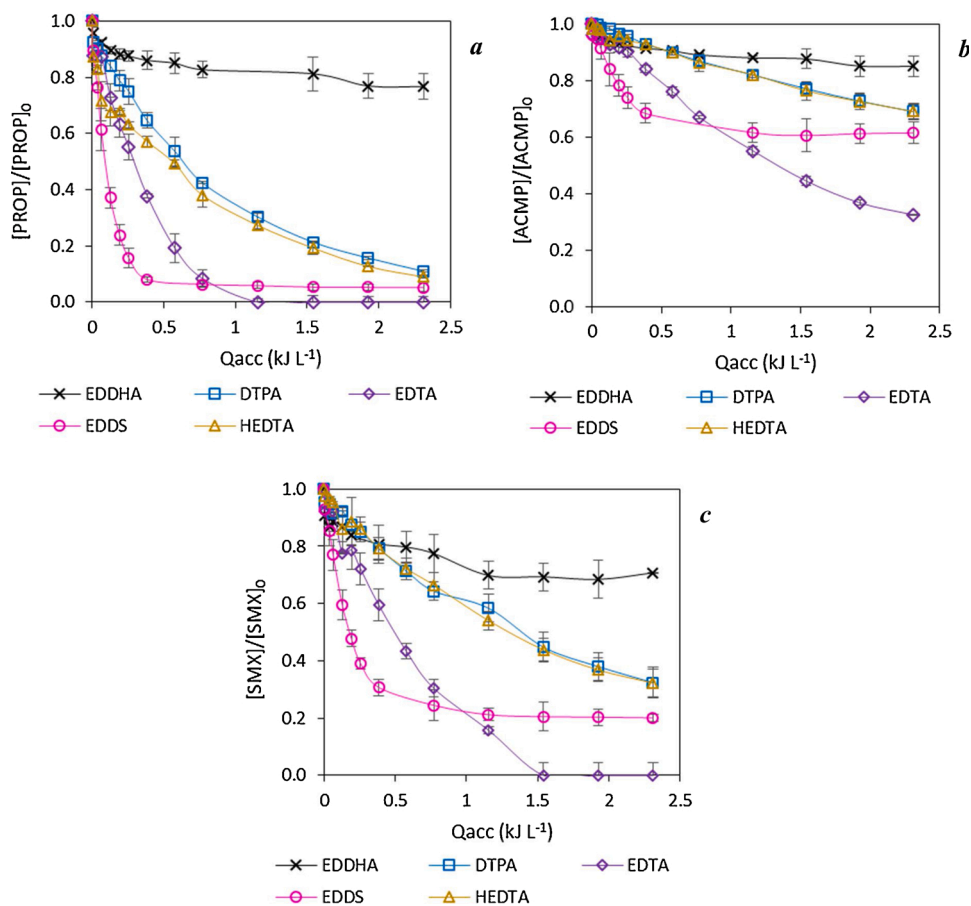


Fig. 2. a) PROP b) ACMP and c) SMX degradation as a function of the accumulated energy for experiments with different organic fertilizers as chelating agents in photo-Fenton in MBR secondary effluent (pH = 7.8). [PROP]₀ = [ACMP]₀ = [SMX]₀ = 0.25 mg L⁻¹; [Fe]₀ = 5 mg L⁻¹; [H₂O₂]₀ = 50 mg L⁻¹. Total treatment time: 180 min, Qacc = 2.31 kJ L⁻¹.

3. Results and discussion

3.1. Efficiency of organic fertilizers in photo-Fenton process

First of all, 3 new organic fertilizers (EDDHA, HEDTA and DTPA) and EDDS and

EDTA, as a conventional fertilizers used in photo-Fenton, were tested and compared as iron chelates in the abatement of three MPs (PROP, ACMP, SMX) by photo-Fenton at natural pH. These MPs were selected, as model compounds, due to their different kinetic constants with hydroxyl radicals ($k_{\text{PROP},\text{HO}} = 1.0 \cdot 10^{10} \text{ M}^{-1} \text{ s}^{-1}$ [28], $k_{\text{SMX},\text{HO}} = 5.5 \cdot 10^9 \text{ M}^{-1} \text{ s}^{-1}$ [29], $k_{\text{ACMP},\text{HO}} = 2.1 \cdot 10^9 \text{ M}^{-1} \text{ s}^{-1}$ [30]). Many research works are mainly focused on the use of one or two chelating agents [31–35]. However, to the best of our knowledge, in this study 5 chelating agents were tested and compared between them, for a first time. All experiments were carried out in real secondary WW (MBR) using 5 mg L^{-1} of iron and 50 mg L^{-1} of H_2O_2 . The results are given in Fig. 2a–c (PROP, ACMP and SMX respectively). In addition, the photolysis of three MPs in MBR matrix was previously evaluated as a control test and the results at the end of the treatment ($Q_{\text{acc}} = 2.31 \text{ kJ L}^{-1}$; 180 min) were 12.4, 5.3 and 2.4 % of depletion for PROP, SMX and ACMP, respectively.

Among different micropollutants, PROP achieved the best degradations with the five chelating agents followed by SMX, while ACMP presented the lowest removals in all conditions. This fact is in accordance with the kinetic constant of each micropollutant with hydroxyl radicals, being PROP the highest and ACMP the lowest, as commented before.

Regarding the chelating agents, the best removals were achieved for EDTA (100 % for PROP and SMX and 67.6 % for ACMP) and the worst degradations were presented for EDDHA (23.3, 29.3 and 15 % for PROP, SMX and ACMP, respectively) at the end of the treatment ($Q_{\text{acc}} = 2.31 \text{ kJ L}^{-1}$; 180 min). The removals of the MPs when using DTPA and HEDTA were very similar (89 and 91.1 % for PROP, 67.6 and 67.8 % for SMX and 31 % for ACMP, respectively). However, a distinct behavior was observed for EDDS. As can be seen in Fig. 2a–c, the degradation of three MPs was faster until 0.39 kJ L^{-1} (30 min). Then, the removal dropped significantly, failing to reach the complete degradation. Results for EDDS at the end of the treatment ($Q_{\text{acc}} = 2.31 \text{ kJ L}^{-1}$, 180 min) were 94.8, 79.9 and 38.5 % for PROP, SMX and ACMP, respectively, close to the removals at 0.39 kJ L^{-1} (30 min), 89.9, 69.3 and 31.7 % for PROP, SMX and ACMP, respectively.

Removal kinetics are closely linked to the release and subsequent precipitation of iron during the treatments. Fig. 3 shows the evolution of total iron in solution along the performed photo-Fenton experiments. As it can be observed, faster MPs removal kinetics corresponds to EDDS which presented higher iron release and precipitation compared with the other chelating agents, already from the beginning of the experiment. On the contrary, EDDHA with the lower iron loss kinetics obtained the worse MPs removal. In the particular case of EDDS, after 30 min of reaction (0.39 kJ L^{-1}) and at the highest MPs removal kinetics, the available iron was still about 60 % of the initial chelated iron that is about 3 mg L^{-1} . The abrupt efficiency removal drop from that point could be related with the generation of insoluble species of iron with by-products of the chelate agent and/or the organic matter present in the wastewater, degrading the performance of the photo-Fenton reaction. Thus, soluble iron dropped to 25 % (less than 1 ppm of soluble iron) at 60 min of reaction (0.39 kJ L^{-1}) and it was almost completely precipitated by the end of the experiment.

MPs removal and iron availability are related to the stability constant (k_{stab}) of the complexes with iron (See Table 2). Among studied chelates, EDDS presents one of the lowest constants, which is in accordance with high iron precipitation during the experiment. No data were found for the stability constant of EDDS-Fe(II). However, it is expected that the constant with iron (II) would be lower than stability constant with iron (III), as it happens with other chelating agents (see Table 2). On the other hand, EDDHA and DTPA, which present high stability constants

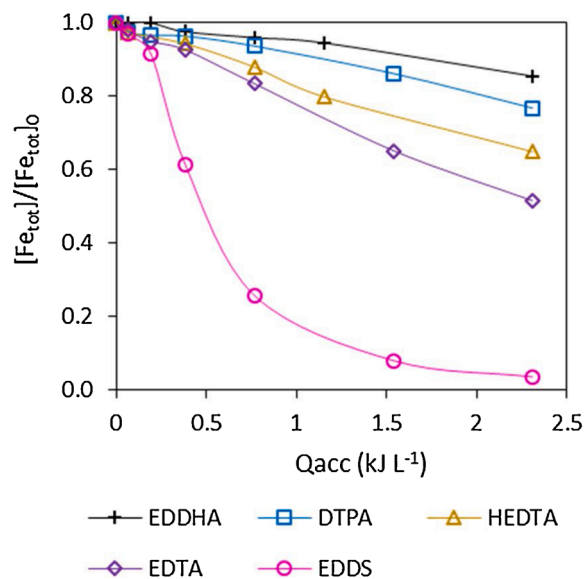


Fig. 3. Evolution of total iron in solution as a function of the accumulated energy for experiments with different organic fertilizers as a chelating agents in photo-Fenton process of MBR secondary effluent. $[\text{PROP}]_0 = [\text{ACMP}]_0 = [\text{SMX}]_0 = 0.25 \text{ mg L}^{-1}$; $[\text{Fe}]_0 = 5 \text{ mg L}^{-1}$; $[\text{H}_2\text{O}_2]_0 = 50 \text{ mg L}^{-1}$. Total treatment time: 180 min, $Q_{\text{acc}} = 2.31 \text{ kJ L}^{-1}$.

with iron, revealed low kinetic removal rates with the three MPs.

The stability constant of the chelates with iron is linked to their chemical structure, particularly the strength, functional groups, number of the chelates interactions and pH [18,39]. Chemical structures of five complexes can be seen in Table 3.

For EDDHA, the phenolate groups with hydroxyl in ortho position forming two bonds with iron (III) together with the octahedral geometry (coordination number = 6) give to the chelate greater stability [39]. In addition, the low MPs degradations could probably be related to the brown color of the iron complex, affecting light absorption capacity. In the case of DTPA, the complex presents a coordination number of 7 forming a pentagonal bipyramidal geometry which results in a higher stability than octahedral geometry. However, no phenolate groups in the structure makes overall DTPA stability lower than EDDHA. These higher stabilities protect the iron from oxidants resulting in a lower iron leakage and lower MPs kinetic removal rates [39].

Different behavior was observed for HEDTA, which presents low stability constant, even lower than EDTA, but iron precipitation and MPs degradation were also significantly lower. Both chelates present octahedral geometry but EDTA presents 4 carboxylate groups while HEDTA only 3 (see Table 3). Most probably EDTA complex undergoes higher photodegradation [39], increasing iron leakage and precipitation. In addition, the competition of Ca^{2+} and Zn^{2+} with Fe^{3+} for EDTA is increased at pH higher than 6.2 (secondary effluent pH = 7.8), which would favor the iron precipitation [39]. DTPA also has 4 carboxylate groups but the additional coordination number, which implies a higher stability than HEDTA, balanced the photodegradation.

EDDS contains four carboxylate groups and the iron is not so structurally protected by the chelator from oxidants. Consequently, the iron can react more easily with H_2O_2 , increasing hydroxyl radical kinetic generation, obtaining high MPs removal rates at initial times compared with the other complexes with higher stability constants. However, this lower iron protection by the chelator causes the rapid precipitation of iron, failing to reach the total degradation of MPs. According to obtained data presented in Table 2, the kinetic rate (k_t) of PROP degradation by EDTA was 2.6 times lower than EDDS during the first 30 min of reaction, in accordance with the higher stability EDTA with iron. However, this high stability constant of EDTA allowed to keep more iron in solution after 30 min of the experiment and around 50 % of iron remained in

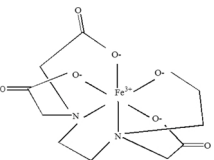
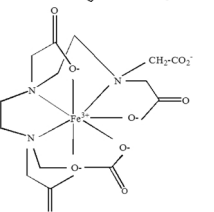
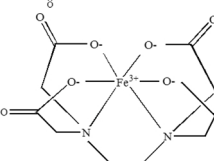
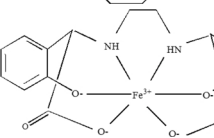
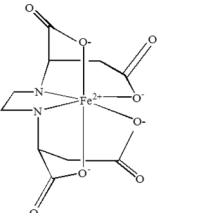
Table 2

Principal parameters of different chelating agents for their comparison. Total degradation of PROP and iron in solution were the values at the end of the treatment (2.31 kJ L⁻¹; 180 min). k_1 is the kinetic constant at initial time (0-0.39 kJ L⁻¹, 30 min) and k_2 is the kinetic from 30 min to 90 % of PROP degradation. (1) Total degradation not reached 90 %; (2) Total degradation at 0.39 kJ L⁻¹. Values of K_{stab} were retrieved from references [36–38].

	Total PROP removal (%)	k_1 (kJ ⁻¹)	R^2 (k_1)	k_2 (kJ ⁻¹)	R^2 (k_2)	Iron in solution (%)	K_{stab} (Ligand-Fe(III))	K_{stab} (Ligand-Fe(II))
EDTA	100	2.36	0.98	3.91	0.99	52.0	25.10	14.33
EDDS	94.8	6.21	0.98	0.21	0.83	4.0	22.0	–
HEDTA	91.1	1.00	0.81	0.90	0.99	64.9	19.80	12.20
DTPA	89.0	1.09	0.97	1.00	0.99	77.0	28.60	16.55
EDDHA	23.3	0.35	0.80	(1)	(1)	85.5	35.09	–
EDDS-EDTA	100	6.97	0.99	(2)	(2)	78.2	–	–
EDDS-DTPA	74.6	3.54	0.99	1.06	0.98	70.0	–	–
EDTA-DTPA	100	3.14	0.94	2.53	0.96	56.3	–	–

Table 3

Properties of different iron complexes employed in this study.

Compound	Molecular formula	Chemical structure	Molecular weight (g/mol)
HEDTA-Fe	C ₁₀ H ₁₈ FeN ₂ O ₇ ·5H ₂ O		424.11
DTPA-Fe	C ₁₄ H ₁₈ N ₃ O ₁₀ FeNa ₂		490.20
EDTA-Fe	C ₁₀ H ₁₂ N ₂ O ₈ FeNa·3H ₂ O		421.10
EDDHA-Fe	C ₁₈ H ₁₆ N ₂ O ₆ FeNa		435.20
EDDS-Fe	C ₁₀ H ₆ N ₂ FeNa ₃ O ₈		409.85

solution at the end of the treatment. Thus, photo-Fenton reactions can go further, achieving the total degradation in the case of PROP and SMX. In that case, the kinetic rate after 30 min of reaction (k_2) of EDTA was 18.6 times higher than EDDS. The same fact was observed between DTPA, HEDTA and EDDS. After 30 min, the kinetic rates (k_2) were 4.8 and 4.3 times higher for HEDTA and DTPA than EDDS. More information about the kinetic rates can be found in Fig. S2 of supplementary material.

3.2. Organic fertilizers mixtures

The results explained in section 3.1 highlight the necessity to find the equilibrium between keeping the iron in solution and achieving high abatement rates for MPs. Mixtures of chelating agents with different stability with iron could be formulated towards this objective. In this section, EDDS, EDTA and DTPA were selected to perform the mixtures,

according to the results of previous experiments. EDDS was included due to the high kinetic rates for MPs degradation at the beginning of the reaction and its good properties as a fertilizer in agriculture [21]. EDTA obtained total degradation of PROP and SMX and the best removal of ACMP. Finally, DTPA was chosen due to its high stability constant with iron, assuring the disposal of iron during all the experimentation, and its extended employment in agriculture compared with HEDTA. EDDHA was discarded due to the low degradations reached for three MPs. The mixtures assayed were EDDS-EDTA, EDDS-DTPA and EDTA-DTPA. Each combination was performed with 50 % of the total iron content of each chelator achieving 5 mg L⁻¹ of total dissolved iron. For comparison purposes, the experiments were carried out in the same MBR secondary effluent.

The Figs. 4, 5 and 6 present the degradation curves of PROP, ACMP and SMX, in MBR matrix, using EDDS-EDTA, EDDS-DTPA and EDTA-

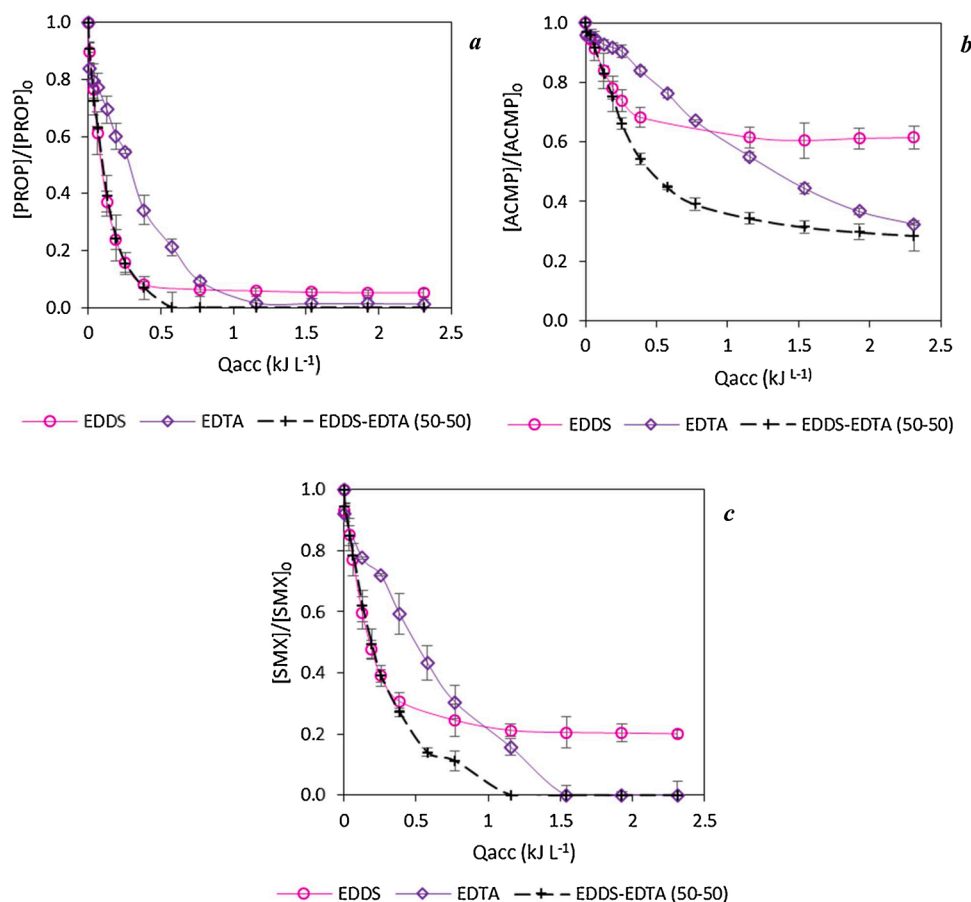


Fig. 4. Profile of a) PROP b) ACMP and c) SMX degradation as a function of the accumulated energy for experiments with EDDS, EDTA and a mixture of both (50 % EDDS + 50 % EDTA) in photo-Fenton at natural pH in MBR secondary effluent. $[\text{PROP}]_0 = [\text{ACMP}]_0 = [\text{SMX}]_0 = 0.25 \text{ mg L}^{-1}$; $[\text{Fe}]_0 = 5 \text{ mg L}^{-1}$; $[\text{H}_2\text{O}_2]_0 = 50 \text{ mg L}^{-1}$. Total treatment time: 180 min, $Q_{\text{acc}} = 2.31 \text{ kJ L}^{-1}$.

DTPA mixtures, respectively.

The mixture of EDDS and EDTA (Fig. 4) showed the best results compared with the same chelates working alone since it maintained (see Table 2 for kinetic of PROP and SMX) or even improved (ACMP) the high kinetic rate during the first minutes of the reaction. Moreover, the total degradation of PROP and SMX was reached in less irradiation time. For instance, total removal of PROP was achieved at 0.39 kJ L^{-1} (30 min) for the mixture EDDS-EDTA but at 1.16 kJ L^{-1} (90 min) for EDTA alone. This fact can be linked again with the evolution of total iron in solution, shown in Fig. 7. The overall iron precipitation for the EDDS-EDTA mixture was slower than for EDDS alone. At 0.77 kJ L^{-1} (60 min), 50 % of iron was in solution with the mixture of chelating agents, while in EDDS only 25 % was kept in solution. At the end of the treatment, EDDS-EDTA mixture had 22 % of the total iron in solution while EDDS only 4%. These results confirm that the chelates mixture EDDS-EDTA significantly improved the kinetics and the overall removals reached by the chelates used alone.

Different results were obtained with the mixture EDDS-DTPA, as can be observed in Fig. 5. MPs degradation kinetics was placed between the ones obtained with EDDS (higher) and DTPA (lower) alone. For example, at 0.39 kJ L^{-1} (30 min) the mixture obtained 75 % of PROP removal, being a significant enhancement compared to DTPA (only 35.5 % of degradation), and little lower than the degradation obtained with EDDS. However, the iron remaining in solution was 86 % for the combination EDDS-DTPA and only 61 % for EDDS alone (see Fig. 7). Thus, with the combination of the two chelating agents an equilibrium between high kinetic rates and a higher iron in solution disposal was achieved. In fact, at the end of experiment the level of MP degradation is practically the same.

When a combination of EDTA and DTPA was tested (Fig. 6), the kinetic rate for the three MPs studied was very similar to the results with only EDTA. This fact is due to the kinetic rates for experiments with only one chelating agent (EDTA and DTPA) were more similar between them than experiments with only EDDS or DTPA (see Table 2). Thus, in Fig. 6a an enhancement of PROP removal was observed (like Fig. 5a) compared to experiment with only DTPA. With the combination EDTA-DTPA a 90 % of PROP degradation was achieved at 0.77 kJ L^{-1} (60 min) equal than experiments with only EDTA. However, experiments with only DTPA reached 90 % of PROP degradation at the end of the experiment (180 min, see Fig. 1) which implies a difference of 120 min more than the combination with EDTA. Although no kinetic rates and overall efficiency improvement was obtained, the EDTA-DTPA mixture retained higher iron content at the end of the photo-Fenton process, (75 % of the initial value) compared with EDTA (about 50 %). This fact represents an improvement since more soluble iron will arrive to the plants with the water effluent reuse to avoid ferric chlorosis.

3.3. Mixtures with different chelating agents' proportions

In order to optimize the combinations of chelating agents, mixtures using 25 % of EDDS and 75 % of EDTA or DTPA were also tested. These percentages would bring information about the proper combination of chelates to reach high removal rates, minimizing iron precipitation during the photo-Fenton treatment. Fig. 8 shows the degradation curves of PROP, ACMP and SMX for the combination of 25 % EDDS + 75 % EDTA and the evolution of total iron in solution.

As can see in Fig. 8, when a mixture of 25 % EDDS and 75 % of EDTA was performed the degradation curves for each MP are between the

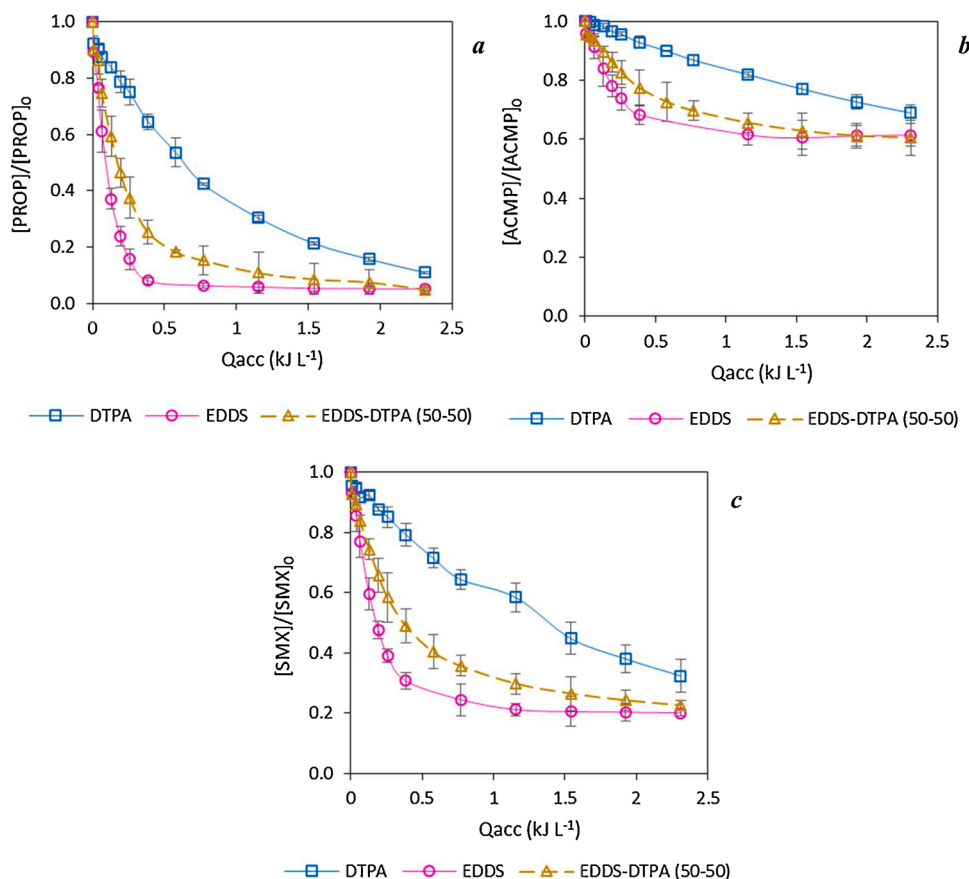


Fig. 5. Profile of a) PROP b) ACMP and c) SMX degradation as a function of the accumulated energy for experiments with EDDS, DTPA and a mixture of both (50 % EDDS + 50 % DTPA) in photo-Fenton at natural pH in MBR secondary effluent. $[\text{PROP}]_0 = [\text{ACMP}]_0 = [\text{SMX}]_0 = 0.25 \text{ mg L}^{-1}$; $[\text{Fe}]_0 = 5 \text{ mg L}^{-1}$; $[\text{H}_2\text{O}_2]_0 = 50 \text{ mg L}^{-1}$. Total treatment time: 180 min, $Q_{\text{acc}} = 2.31 \text{ kJ L}^{-1}$.

removal curves of two chelating agents tested alone until 0.77 kJ L^{-1} (60 min). Since this time, the degradation rate was lower than this one with EDTA alone but higher than the one obtained with EDDS alone. With the mixture 25 % EDDS + 75 % EDTA, a total degradation was achieved at 1.5 kJ L^{-1} (120 min) for PROP and at the end of the experiment for SMX (180 min). With 100 % EDDS the complete degradation was not achieved for any micro-pollutant (see Fig. 8a–c). In the case of ACMP, a removal of 51.9 % was reached with the mixture, at the end of the experiment, compared to only 38.5 % achieved with EDDS alone. Moreover, iron evolution was similar to EDTA (see Fig. 8d), with 40 % less of iron precipitation than experiments with 100 % EDDS. These results are logical since 75 % of iron is chelated with EDTA which present high stability constant. In that case, the tendency is closer to experiments with 100 % EDTA than 100 % EDDS compared with the combination of 50 % EDDS + 50 % EDTA, which was the other way around. In addition, the shape of the curves is also strongly related to the percentage of chelating agents. Thus 50 % EDDS + 50 % EDTA shows a degradation curve with a shape very similar to that of the EDDS alone. On the contrary, experiments with 25 % EDDS + 75 % EDTA show curves with a shape very close to this corresponding to EDTA alone. The same occurs with the experiments with 25 % EDDS + 75 % DTPA, where the degradation curves are very close to these ones corresponding to DTPA alone (see Fig. 9).

As can be observed in Fig. 9, the degradation lines for the two percentages tested for mixtures were between experiments with only EDDS and only DTPA. When 50 %-50 % combination was tested the tendency was more similar to EDDS. However, with 25 % EDDS + 75 % DTPA the trend was comparable to DTPA, as happened with EDDS-EDTA combination. Since the 50 %-50 % mixture presented this behavior it was reflected that EDDS had an important weight in the experiment.

The MPs removals obtained at the end of the treatment were only a little different for the two percentages tested. The results for 25 % EDDS + 75 % DTPA were: 90.9, 66.4 and 29.3 % for PROP, SMX and ACMP, respectively. While the removals for 50 % EDDS + 50 % DTPA were: 95, 77.4 and 39.4 % in the same order. It was observed that more close results were achieved for PROP. That fact is related to the highest kinetic rate with hydroxyl radicals for this compound. Although at the end of the treatment the different mixtures presented similar results, different kinetic rates were observed during the experiment. For instance, 74.6 and 56.2 % were obtained for PROP with 50–50 and 25–75 at 30 min, respectively. That behavior was related to iron in solution and their availability. With 50 %-50 % more iron was chelated with EDDS which avoid higher kinetic rates at initial time. But, at the same time, the iron precipitation was higher than 25–75. That fact caused the degradation of MPs to slow down. Conversely, with 50–50 mixture the degradation was slower but steady. Thus, at the end of the treatment the difference of MPs degradation between two percentages of mixtures was lower than at first time of the experiment.

Comparing Figs. 8 and 9, different behavior was observed with the mixtures in both cases 50 %-50 % and 25 %-75 %. These differences are related to the stability constant of DTPA and EDTA. DTPA presents higher stability constant, making the reaction with peroxide more difficult. In the case of EDTA, the lower stability constant with iron and the medium stability constant of EDTA-Fe permits the faster degradation of MPs with the mixture performed with 50 % EDDS + 50 % EDTA. In addition, better MPs removals than only EDDS and close results than EDTA were achieved with 25 % EDDS + 75 % EDTA combination.

Moreover, the quantity of iron chelated is an important think to consider. If less iron is chelated the precipitation of this one will be slower (due to non-chelated iron remain in solution more time before to

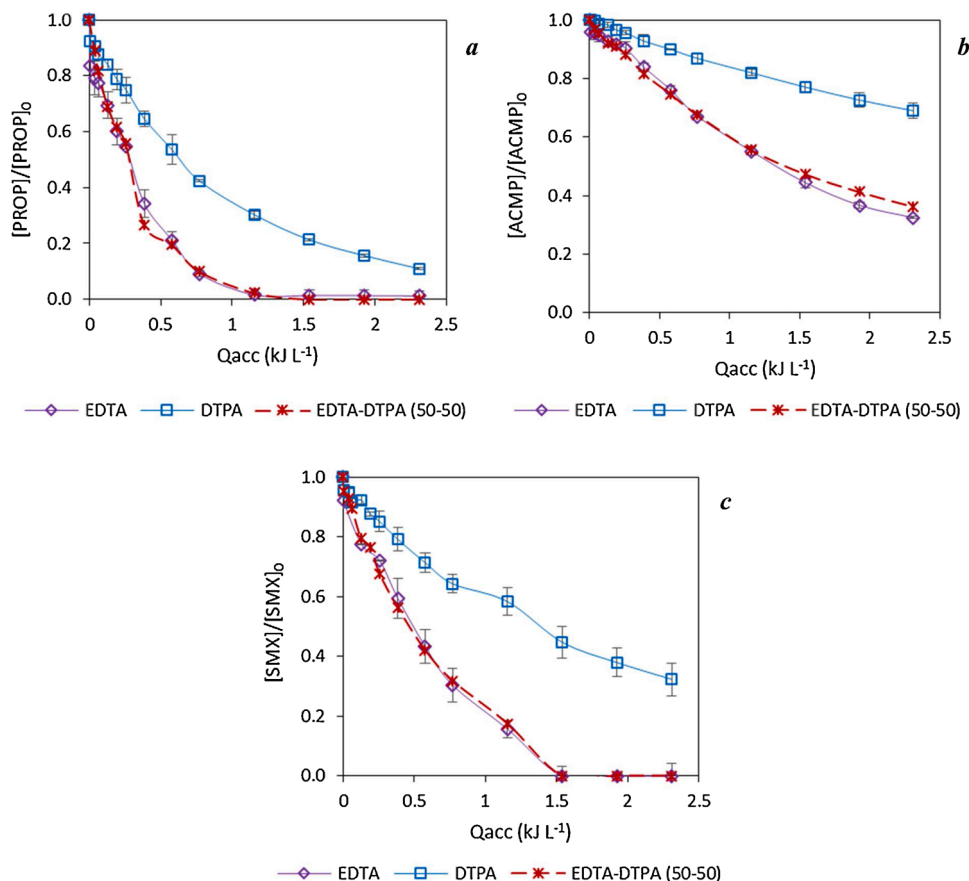


Fig. 6. Profile of a) PROP b) ACMP and c) SMX degradation as a function of the accumulated energy for experiments with EDTA, DTPA and a mixture of both (50 % EDTA + 50 % DTPA) in photo-Fenton at natural pH in MBR secondary effluent. $[PROP]_0 = [ACMP]_0 = [SMX]_0 = 0.25 \text{ mg L}^{-1}$; $[Fe]_0 = 5 \text{ mg L}^{-1}$; $[H_2O_2]_0 = 50 \text{ mg L}^{-1}$. Total treatment time: 180 min, $Q_{acc} = 2.31 \text{ kJ L}^{-1}$.

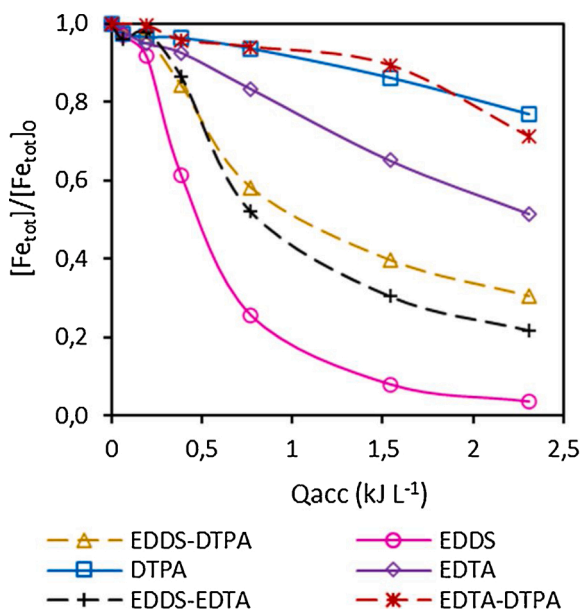


Fig. 7. Evolution of total iron in solution as a function of the accumulated energy for experiments with different mixtures of chelating agents in photo-Fenton at natural pH in MBR secondary effluent. $[PROP]_0 = [ACMP]_0 = [SMX]_0 = 0.25 \text{ mg L}^{-1}$; $[Fe]_0 = 5 \text{ mg L}^{-1}$; $[H_2O_2]_0 = 50 \text{ mg L}^{-1}$. Total treatment time: 180 min, $Q_{acc} = 2.31 \text{ kJ L}^{-1}$.

precipitate), being able to continue generating hydroxyl radicals. This fact influences on the mixtures using 50 % EDDS + 50 % EDTA, where 2.5 mg L^{-1} of iron is chelated with EDDS as long as the experiments with 100 % of EDDS 5 mg L^{-1} of iron is chelated. Part of the yield increase is due to less iron precipitation with EDDS adding only 2.5 mg L^{-1} is chelated with EDTA, which maintain the iron chelated to produce more hydroxyl radicals. In the case of mixture 25%–75% only 1.25 mg L^{-1} is chelated with EDDS and 3.5 mg L^{-1} chelated with EDTA. More iron is chelated with a chelating agent which present high stability constant so that the kinetic rate is similar to this one. Otherwise, the iron precipitation will be slower but the quantity of iron chelated is also important in the photo-Fenton reactions. With only 1.25 mg L^{-1} of iron (25 % EDDS) is not enough to achieve close kinetic than 5 mg L^{-1} (100 % EDDS).

3.4. Biochemical oxygen demand at 5 days tests

The Proposal for a Regulation of the European Parliament and of the Council lists the minimum requirements for agricultural wastewater reuse [3] where BOD_5 ($\text{mgO}_2 \text{ L}^{-1}$) is an important parameter to take into account. Fig. 10 shows the values of BOD_5 after the photo-Fenton treatment with the chelates or mixture of chelates in MBR effluents. Process catalyzed by EDDS presented highest value of BOD_5 at the end of the treatment, reaching $19.6 \text{ mg O}_2 \text{ L}^{-1}$ while the combination of EDTA-DTPA achieved the lowest: $3.6 \text{ mgO}_2 \text{ L}^{-1}$. The BOD_5 values of the treated effluent with combinations of 50 % EDDS with EDTA or DTPA were placed between 13.6 and $9.6 \text{ mg O}_2 \text{ L}^{-1}$, respectively. This fact represents an advantage compared to EDDS since the EU regulation for agricultural water reuse establishes four categories (A, B, C and D)

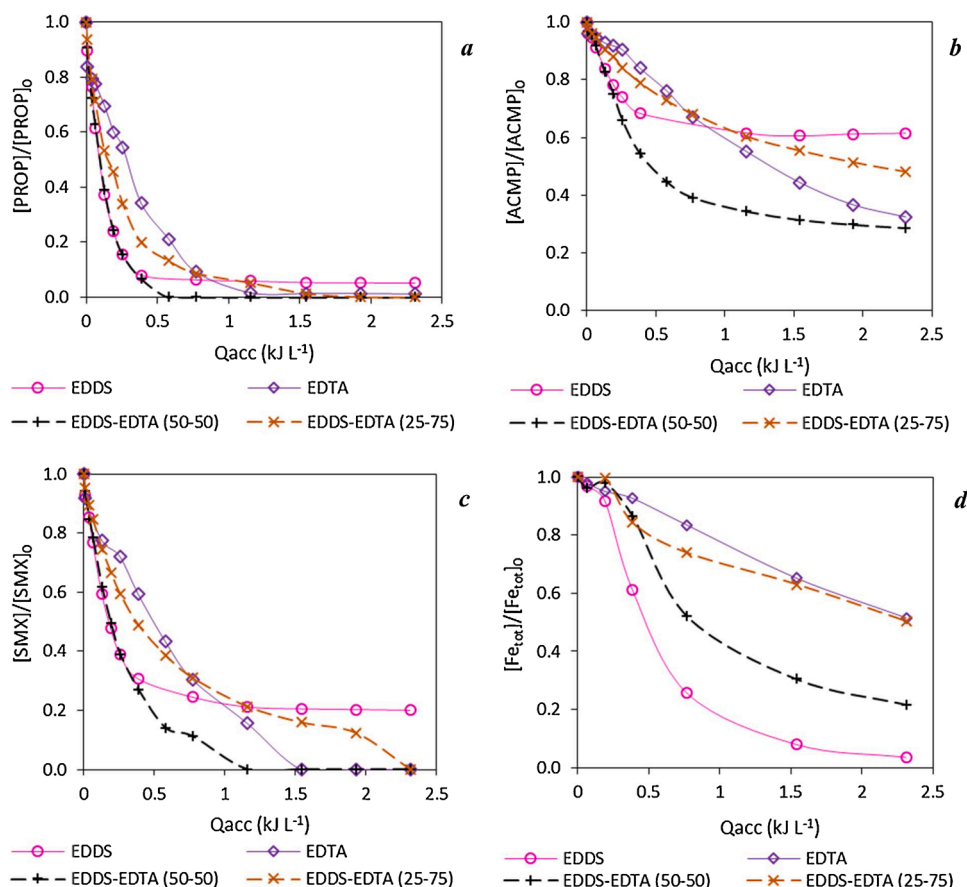


Fig. 8. Profile of a) PROP b) ACMP and c) SMX degradation as a function of the accumulated energy for experiments with EDDS, EDTA and a mixture of both (25 % EDDS + 75 % EDTA) in photo-Fenton at natural pH in MBR secondary effluent. d) Evolution of total dissolved iron during different treatments. $[PROP]_0 = [ACMP]_0 = [SMX]_0 = 0.25 \text{ mg L}^{-1}$; $[Fe]_0 = 5 \text{ mg L}^{-1}$; $[H_2O_2]_0 = 50 \text{ mg L}^{-1}$. Total treatment time: 180 min, $Q_{acc} = 2.31 \text{ kJ L}^{-1}$.

depending on the quality of treated water. Category A fixes a value of $BOD_5 \leq 10 \text{ mg O}_2 \text{ L}^{-1}$ and categories from B to D a level of $BOD_5 \leq 25 \text{ mg O}_2 \text{ L}^{-1}$ [3]. Thus, when mixture of EDDS-DTPA was employed the treated effluent goes from category B to A (Table S1 and S2 in supplementary information explains different categories and quality requirements). Treated effluents using EDTA, DTPA and a mixture of EDTA-DTPA were also classified in category A.

Finally, Fig. 11 was performed to obtain an overview of how the chelating agents and their mixtures respond to important parameters like MPs removal, iron stability, BOD_5 and chelating agent cost. The values of each parameter were normalized in the scale from 0 to 10, being the value of 10 the best conditions and 0 the worst. In supplementary material (Table S3) can be found the rules followed to normalize the different parameters.

As can be observed in Fig. 11, the experiments carried out with one chelating agent presented some deficiencies. For instance, EDDS show high price and low iron stability. EDTA presented medium iron stability. While DTPA displays high price and low removal at first 30 min. Nevertheless, with the combinations of these chelating agents an improvement was seen in all parameters. For example, the mixture composed by EDTA-DTPA (50 %-50 %) exhibited good enhancements in almost all parameters compared with single EDTA or DTPA. Only in the price was the second best under EDTA (price of mixture: 0.004€/experiment and 0.002 €/experiment for EDTA). In addition, the combination of EDTA-EDDS also reached good improvements in all parameters compared with EDDS: better removal at first 30 min and price (0.008 €/experiment for EDDS and 0.005 €/experiment for the mixture) were the enhancements more highlighted. Compared to EDTA, better removal at first 30 min was the improvement.

4. Conclusions

The organic fertilizers tested in this study were effective in removing the three selected micropollutants throughout photo-Fenton at natural pH. In the case of DTPA and HEDTA similar results were achieved in the MPs removal (about 90 % for PROP, 70 % for SMX and 30 % for ACMP) reaching worst results for ACMP because of its poor reactivity with hydroxyl radicals. EDDHA achieved the poor results (23.3, 29.3 and 15 % for PROP, SMX and ACMP, respectively) due to its high stability constant with iron which affects its availability for Fenton reaction. EDTA and EDDS both presented good removals for PROP and SMX. However, only EDTA reached about 70 % of ACMP. Removal kinetics and soluble iron availability resulted closely linked to the stability constant (k_{stab}) of the chelating agents. EDDS showed low stability constant with iron allowing high removal rates at initial times. However, the rapid iron precipitation decreased the overall efficiency of the process failing to reach total degradation for the three MPs. On the contrary, EDDHA with the highest stability constant showed the lower iron release and overall MPs removal efficiencies. Nevertheless, for the other 3 chelating agents studied with high stability constant, the iron precipitation was slower achieving less, but constant, hydroxyl radicals formation so that good MPs removals were observed at the end of the treatment.

For all this, assuring the process effectivity requires an equilibrium between to keep iron in solution and to achieve fast kinetic constants for MPs abatement. The three mixtures of different chelating agents tested (EDDS-EDTA, EDDS-DTPA and EDTA-DTPA, 50 %-50 %) show yields improvement. The EDDS-EDTA combination reached higher kinetic rates in the MPs abatement and final soluble iron availability, compared

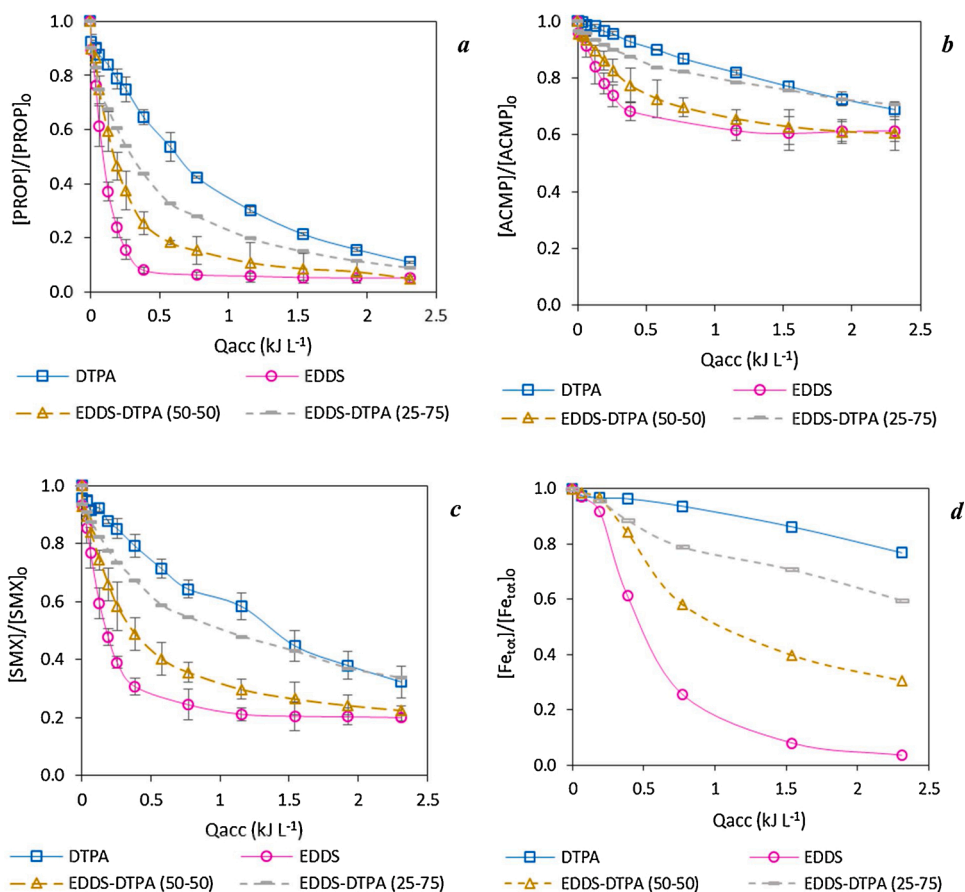


Fig. 9. Degradation curves of a) PROP b) ACMP and c) SMX degradation as a function of the accumulated energy for experiments with EDDS, DTPA and a mixture of both (25 % EDDS + 75 % DTPA) in photo-Fenton at natural pH in MBR secondary effluent. d) Evolution of total dissolved iron during different treatments. $[PROP]_0 = [ACMP]_0 = [SMX]_0 = 0.25 \text{ mg L}^{-1}$; $[Fe]_0 = 5 \text{ mg L}^{-1}$; $[H_2O_2]_0 = 50 \text{ mg L}^{-1}$. Total treatment time: 180 min, $Q_{acc} = 2.31 \text{ kJ L}^{-1}$.

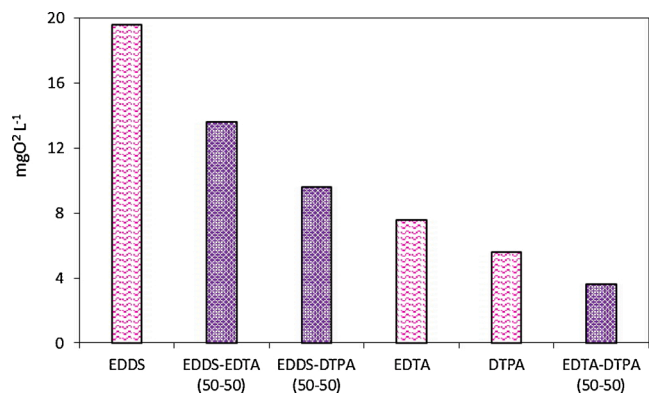


Fig. 10. Biochemical Oxygen Demand at 5 days evaluation in MBR with photo-Fenton process at natural pH catalyzed by DTPA, EDTA, EDDS and three different combinations of these chelating agents at the end of the treatment. $[Fe]_0 = 5 \text{ mg L}^{-1}$; $[H_2O_2]_0 = 50 \text{ mg L}^{-1}$.

to the treatment using the chelates separately.

Tests of Biochemical Oxygen Demand at 5 days at the end of the treatment obtained that all effluents could reuse in agriculture according to current European legislation (Proposal for water reuse in agriculture [3]).

Finally, an evaluation of the most significant parameters of treated wastewater (low BOD₅, iron stability, MPs removal first 30 min, final MPs abatement and price of chelating agent) revealed that solar photo-Fenton using organic fertilizers can be applied in agriculture reuse of

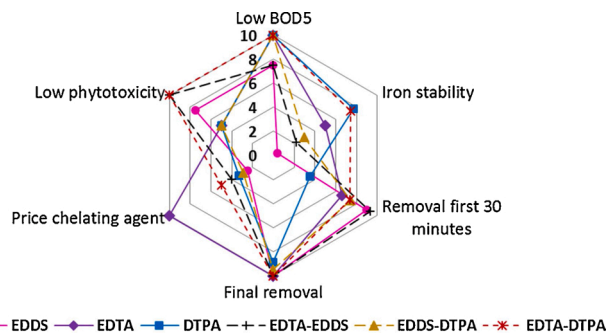


Fig. 11. Overview of the response of different chelating agents and their mixtures for different parameters normalized from 0 to 10, being 10 the best conditions and 0 the worst.

wastewater, being EDTA-EDDS mixture the most suitable among the chelating agents studied.

CRediT authorship contribution statement

N. López-Vinent: Conceptualization, Investigation, Data curation, Writing - original draft, Writing - review & editing, Visualization, Project administration. **A. Cruz-Alcalde:** Conceptualization, Investigation, Data curation, Writing - original draft, Writing - review & editing, Visualization, Project administration. **J. Giménez:** Writing - review & editing, Supervision, Project administration. **S. Esplugas:** Writing - review & editing, Supervision, Project administration. **C. Sans:** Writing - review &

editing, Supervision, Project administration.

Declaration of Competing Interest

The authors report no declarations of interest.

Acknowledgments

The authors wish to thank the Ministry of Economy and Competitiveness (project CTQ2017-86466-R, MINECO/FEDER, UE), AGAUR-Generalitat de Catalunya (project 2017SGR-131) and Nuria López FPU research fellowship (FPU-16/02101) financed by Ministry of Science, Innovation and Universities.

Appendix A. Supplementary data

Supplementary material related to this article can be found, in the online version, at doi:<https://doi.org/10.1016/j.apcatb.2021.120066>.

References

- Ortega-Gómez, B., Esteban García, M.M., Ballesteros Martín, P., Fernández Ibáñez, J.A., Sánchez Pérez, Inactivation of natural enteric bacteria in real municipal wastewater by solar photo-Fenton at natural pH, *Water Res.* 63 (2014) 316–324.
- Food and Agriculture Organization of the United Nations, Land & Water: Water Scarcity, Consulted at, 2021 <http://www.fao.org/land-water/world-water-day-2021/water-scarcity/en/>.
- European Commission, Proposal for a regulation of the European Parliament and of the Council of 28 May 2018 establishing the minimum requirements for water reuse, *Off. J. Eur. Commun.* 337 (2018) 1–27.
- N. De la Cruz, J. Giménez, S. Esplugas, D. Grandjean, L.F. de Alencastro, C. Pulgarin, Degradation of 32 emergent contaminants by UV and neutral photo-Fenton in domestic wastewater effluent previously treated by activated sludge, *Water Res.* 46 (2012) 1947–1957.
- D. Bertagna Silva, A. Cruz-Alcalde, C. Sans, J. Giménez, S. Esplugas, Performance and kinetic modelling of photolytic and photocatalytic ozonation for enhanced micropollutants removal in municipal wastewaters, *Appl. Catal. B: Environ.* 249 (2019) 211–217.
- N. López-Vinent, A. Cruz-Alcalde, L.E. Romero, M.E. Chávez, P. Marco, J. Giménez, S. Esplugas, Synergies, radiation and kinetics in photo-Fenton process with UVA-LEDs, *J. Hazard. Mater.* 380 (2019) 120882.
- N. López, S. Plaza, A. Afkhami, P. Marco, J. Giménez, Treatment of diphenyldramine with different AOPs including photo-Fenton at neutral pH, *Chem. Eng. J.* 318 (2017) 112–120.
- I. Carra, J.A. Pérez Sánchez, S. Malato, O. Autin, B. Jefferson, P. Jarvis, Application of high intensity UVC-LED for the removal of acetamiprid with the photo-Fenton process, *Chem. Eng. J.* 264 (2015) 690–696.
- Y. Aguas, M. Hincapie, P. Fernández-Ibáñez, M.I. Polo-López, Solar photocatalytic disinfection of agricultural pathogenic fungi (*Curvularia sp.*) in real urban wastewater, *Sci. Total Environ.* 607–608 (2017) 1213–1224.
- A. Serra-Clusellas, L. De Angelis, C.H. Lin, P. Vo, M. Bayati, L. Sumner, Z. Lei, N. B. Amaral, L.M. Bertini, J. Mazza, L.R. Pizzio, J.D. Stripeikis, J.A. Rengifo-Herrera, M.M. Fidalgo de Cortalezzi, Abatement of 2,4-D by H₂O₂ solar photolysis and solar photo-Fenton-like process with minute Fe(III) concentrations, *Water Res.* 144 (2018) 572–580.
- S. Miralles-Cuevas, D. Darowna, A. Wanag, S. Mozia, S. Malato, I. Oller, Comparison of UV/H₂O₂, UV/S₂O₈²⁻, solar/Fe(II)/H₂O₂ and solar/Fe(II)/S₂O₈²⁻ at pilot plant scale for the elimination of micro-contaminants in natural water, *Chem. Eng. J.* 310 (2017) 514–524.
- I. De la Olla, L. Ponce-Robles, S. Miralles-Cuevas, I. Oller, S. Malato, J.A. Sánchez Pérez, Microcontaminant removal in secondary effluents by solar photo-Fenton at circumneutral pH in raceway pond reactors, *Catal. Today* 287 (2017) 10–14.
- B. Esteban García, G. Rivas, S.J.A. Sánchez Pérez, Wild bacteria inactivation in WWTP secondary effluents by solar photo-Fenton at neutral pH in raceway pond reactors, *Catal. Today* 313 (2018) 72–78.
- L. Clarizia, D. Russo, I. Di Somma, R. Marotta, R. Andreozzi, Homogeneous photo-Fenton processes at near neutral pH: a review, *Appl. Catal. B: Environ.* 209 (2017) 358–371.
- A. De Luca, R.F. Dantas, S. Esplugas, Study of Fe(III)-NTA chelates stability for applicability in photo-Fenton at neutral pH, *Appl. Catal. B: Environ.* 179 (2015) 372–379.
- I. García-Fernández, S. Miralles-Cuevas, I. Oller, S. Malato, P. Fernández-Ibáñez, M. I. Polo-López, Inactivation of *E. coli* and *E. faecalis* by solar photo-Fenton with EDDS complex at neutral pH in municipal wastewater effluents, *J. Hazard. Mater.* 372 (2019) 85–93.
- S. Miralles-Cuevas, I. Oller, J.A. Sánchez Pérez, S. Malato, Removal of pharmaceuticals from MWTP effluent by nanofiltration and solar photo-Fenton using two different iron complexes at neutral pH, *Water Res.* 64 (2014) 23–31.
- N. López-Vinent, A. Cruz-Alcalde, J.A. Malvestiti, P. Marco, J. Giménez, S. Esplugas, Organic fertilizer as a chelating agent in photo-Fenton at neutral pH with LEDs for agricultural wastewater reuse: micropollutant abatement and bacterial inactivation, *Chem. Eng. J.* 388 (2020) 124246.
- S. Nahim-Granados, I. Oller, S. Malato, J.A. Sánchez Pérez, M.I. Polo-López, Commercial fertilizer as effective iron chelate (Fe³⁺-EDDHA) for wastewater disinfection under natural sunlight for reusing in irrigation, *Appl. Catal. B: Environ.* 253 (2019) 286–292.
- European Commission, Regulation (EC) No 2003/2003 of the European Parliament and of the Council of 13 October 2003 relating to fertilizers, *Off. J. Eur. Commun.* (2003).
- S. López-Rayó, P. Nadal, J.J. Lucena, Novel chelating agents for iron, manganese, zinc and copper mixed fertilization in high pH soil-less cultures, *J. Sci. Food Agric.* 96 (2016) 1111–1120.
- N. De la Cruz, V. Romero, R.F. Dantas, P. Marco, B. Bayarri, J. Giménez, S. Esplugas, O-Nitrobenzaldehyde actinometry in the presence of suspended TiO₂ for photocatalytic reactors, *Catal. Today* 209 (2013) 209–214.
- Guidelines for Water Reuse 600/R-12/618, Environmental Protection Agency: Washington, DC, USA, 2012.
- R.S. Ayers, D.W. Westcot, *Water Quality for Agriculture, Food and Agriculture Organization of the United Nations*, Rome, Italy, 1985.
- N. López-Vinent, A. Cruz-Alcalde, C. Gutiérrez, P. Marco, J. Giménez, S. Esplugas, Micropollutant removal in WW by photo-Fenton (circumneutral and acid pH) with BLB and LED lamps, *Chem. Eng. J.* 379 (2020) 122416.
- L.I. Doumic, P.M. Houe, M.C. Cassanello, M.A. Ayude, Mineralization and efficiency in the homogeneous Fenton Orange G oxidation, *Appl. Catal. B: Environ.* 142–143 (2013) 214–221.
- R.F. Pupo Nogueira, M.C. Oliveira, W.C. Paterlini, Simple and fast spectrophotometric determination of H₂O₂ in photo-Fenton reactions using metavanadate, *Talanta* 66 (2005) 86–89.
- J. Benner, E. Salhi, T. Ternes, U. von Gunten, Ozonation of reverse osmosis concentrate: kinetics and efficiency of beta blocker oxidation, *Water Res.* 42 (2008) 3003–3012.
- M.M. Huber, S. Canonica, G.Y. Park, U. Von Gunten, Oxidation of pharmaceuticals during ozonation and advanced oxidation processes, *Environ. Sci. Technol.* 37 (2003) 1016–1024.
- A. Cruz-Alcalde, C. Sans, S. Esplugas, Priority pesticides abatement by advanced oxidation water technologies: the case of acetamiprid removal by ozonation, *Sci. Total Environ.* 599–600 (2017) 1454–1461.
- S. Arzate, M.C. Campos-Mañas, S. Miralles-Cuevas, A. Agüera, J.L. García Sánchez, J.A. Sánchez Pérez, Removal of contaminants of emerging concern by continuous flow solar photo-Fenton process at neutral pH in open reactors, *J. Environ. Manage.* 261 (2020) 110265.
- S. Miralles-Cuevas, F. Audino, I. Oller, R. Sánchez-Moreno, J.A. Sánchez Pérez, S. Malato, Pharmaceuticals removal from natural water by nanofiltration combined with advanced tertiary treatments (solar photo-Fenton, photo-Fenton-like Fe(II)-EDDS complex and ozonation), *Sep. Purif. Technol.* 122 (2014) 515–522.
- P. Soriano-Molina, S. Miralles-Cuevas, B. Esteban-García, P. Plaza-Bolaños, J. A. Sánchez Pérez, Two strategies of solar photo-Fenton at neutral pH for the simultaneous disinfection and removal contaminants of emerging concern. Comparative assessment in raceway pond reactors, *Catal. Today* (2021) article in press.
- K. Davididou, E. Chatzisydney, L. Pérez-Estrada, I. Oller, S. Malato, Photo-Fenton treatment of saccharin in a solar pilot compound parabolic collector: use of olive mill wastewater as iron chelating agent, preliminary results, *J. Hazard. Mater.* 372 (2019) 137–144.
- A. De Luca, R.F. Dantas, S. Esplugas, Study of Fe(III)-NTA chelates stability for applicability in photo-Fenton at neutral pH, *Appl. Catal. B: Environ.* 179 (2015) 372–379.
- Dojindo Molecular Technologies, Inc, Table of Stability Constants, 2020 (Accessed March 24, 2020), <https://www.dojindo.com/images/Product%20Photo/ChelateTableofStabilityConstants.pdf>.
- A.E. Martell, R.J. Motekaitis, D. Chen, R.D. Hancock, D. McManus, Selection of new Fe(III)/Fe(II) chelating agents as catalysts for the oxidation of hydrogen sulphide to sulfur by air, *Can. J. Chem.* 74 (1996) 1872–1879.
- M.A. Sierra, M. Gómez-Gallego, R. Alcázar, J.J. Lucena, F. Yunta, S. García-Marco, Effect of the tether on the Mg(II), Ca(II), Cu(II) and Fe(II) stability constants and pM values of chelating agents related to EDDHA, *Dalton Trans.* 21 (2004) 3741–3747.
- A. Sánchez, Mejora de la eficacia de los quelatos de hierro sintéticos a través de sustancias húmicas y aminoácidos (Tesis Doctoral), Universidad de Alicante, España, 2002.

Supplementary Information for

Improvement of the photo-Fenton process at natural condition of pH using organic fertilizers mixtures: potential application to agricultural reuse of wastewater

N. López-Vinent*, A. Cruz-Alcalde, J. Giménez, S. Esplugas, C. Sans

Department of Chemical Engineering and Analytical Chemistry, Faculty of Chemistry, Universitat de Barcelona, C/Martí i Franqués 1, 08028 Barcelona, Spain.

*Corresponding author:

Núria López Vinent, phone: +34 934 02 01 54, e-mail: nuria.lopez@ub.edu

Table of Contents

Figure S1. Emission spectrum of solar simulator.....	p.2
Figure S2. Fitting of Figure 1 data to pseudo-first order kinetics using different chelating agents in photo-Fenton at natural pH.....	p.2
Table S1. Classes of reclaimed water quality and allowed agricultural use and irrigation method.....	p.3
Table S2. Reclaimed water quality requirements for agricultural irrigation.....	p.3
Table S3. Normalization in the scale from 0 to 10 of different parameters. Used to elaborate Figure 9.....	p.4

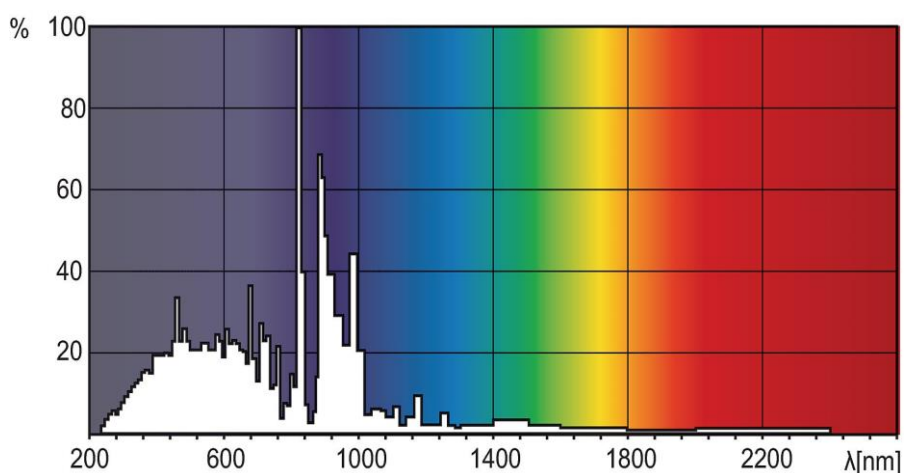


Figure S1. Emission spectrum of solar simulator

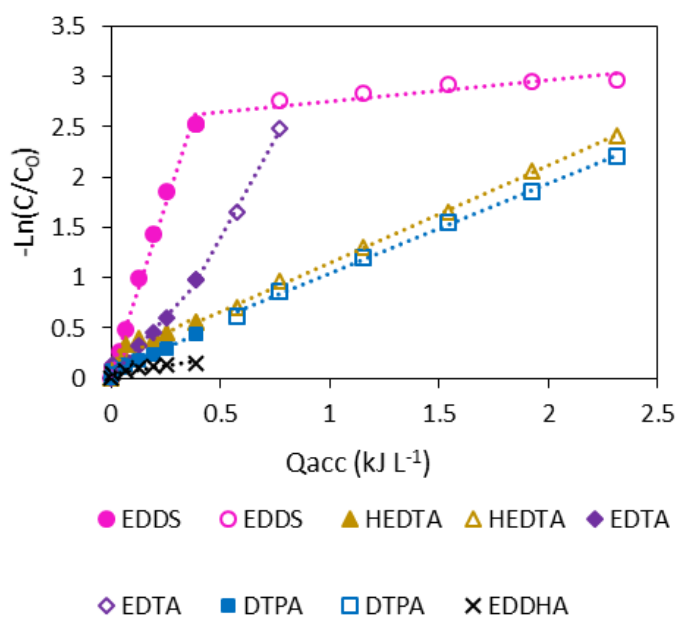


Figure S2. Fitting of Figure 1a data to pseudo-first order kinetics using different chelating agents in photo-Fenton at natural pH in MBR at initial accumulated energy (0-0.39 kJ L⁻¹, 30 min) (close symbols) and from 30 min to 90% of PROP degradation (open symbols). [PROP]₀ = [ACMP]₀ = [SMX]₀ = 0.25 mg L⁻¹; [Fe]₀ = 5 mg L⁻¹; [H₂O₂]₀ = 50 mg L⁻¹.

Table S1. Classes of reclaimed water quality and allowed agricultural use and irrigation method [3].

Minimum reclaimed water quality class	Crop category	Irrigation method
A	Food crops, including root crops consumed raw and food crops where the edible part is in direct contact with reclaimed water	All
B	Food crops consumed raw where the edible part is produced above ground and is not in direct contact with reclaimed water, processed food crops and non-food crops including crops to feed milk- or meat-producing animals	All
C		Drip *
D	Industrial, energy, and seeded crops	All

(*) Drip irrigation (also called trickle irrigation) is a micro-irrigation system capable of delivering water drops or tiny streams to the plants and involves dripping water onto the soil or directly under its surface at very low rates (2-20 liters/hour) from a system of small diameter plastic pipes fitted with outlets called emitters or drippers.

Table S2. Reclaimed water quality requirements for agricultural irrigation [3].

Reclaimed water quality class	Quality requirements				
	<i>E. coli</i> (CFU/100 mL)	BOD ₅ (mg/L)	TSS (mg/L)	Turbidity (NTU)	Other
A	≤ 10 Or below detection limit	≤ 10	≤ 10	≤ 5	Legionella spp.: <1000 CFU/L where there is risk of aerosolization in greenhouses
B	≤ 100			-	Intestinal nematodes (helminth eggs): ≤1 egg/L for irrigation of pastures or forage
C	≤ 1000	≤ 25	≤ 35	-	
D	≤ 10000			-	

Table S3. Normalization in the scale from 0 to 10 of different parameters. Used to elaborate Figure 9.

Parameters	Normalization
Low BOD ₅ (1)	Category A: 10. Category B: 7.5. Category C: 5. Category D: 2.5. If WW is not able to reuse in agriculture: 0.
Iron stability	10 for 0% of iron precipitation at the end of the treatment.
Removal first 30 minutes	10: 100% of PROP removal
Final removal	10: 100% of PROP removal
Price chelating agents (2)	10: cheaper chelating agent

(1) According to Proposal for water reuse in agriculture, which establishes different classes of reclaimed water quality [3].

(2) Prices from Phygenera (Germany) and Sigma-Aldrich.

Part V

Mixtures of chelating agents to enhance photo-Fenton process at natural pH: influence of wastewater matrix on micropollutant removal and bacterial inactivation

Núria López-Vinent, Alberto Cruz-Alcalde, Jaime Giménez, Santiago Esplugas,

Department of Chemical Engineering and Analytical Chemistry, Faculty of Chemistry,
University of Barcelona, C/Martí i Franqués 1, 08028 Barcelona, Spain.

Published in *Science of the Total Environment* 786 (2021) 147416



Mixtures of chelating agents to enhance photo-Fenton process at natural pH: Influence of wastewater matrix on micropollutant removal and bacterial inactivation



N. López-Vinent^{a,*}, A. Cruz-Alcalde^{a,b}, J. Giménez^a, S. Esplugas^a

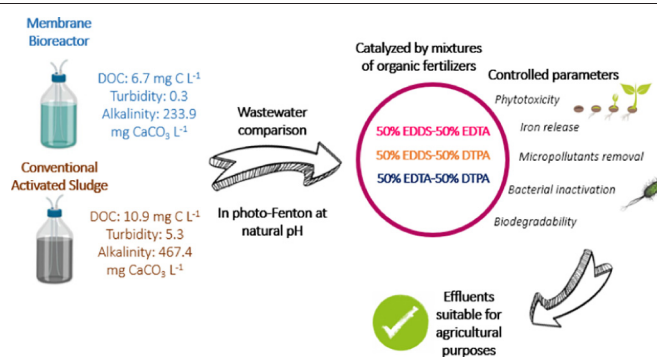
^a Department of Chemical Engineering and Analytical Chemistry, Faculty of Chemistry, Universitat de Barcelona, C/Martí i Franqués 1, 08028 Barcelona, Spain

^b Institute of Environmental Assessment and Water Research, Spanish National Research Council (IDAEA-CSIC), C/Jordi Girona 18-26, 08034 Barcelona, Spain

HIGHLIGHTS

- Mixtures of fertilizers as complexing agents are effective in photo-Fenton process.
- Process efficiency improvements are observed with organic fertilizers mixtures.
- More than 70% of micropollutants abatement is achieved in MBR matrix with mixtures.
- Higher iron release is observed in CAS matrix decreasing the process efficiency.
- Suitability of treated effluents for their reuse in agriculture is reached.

GRAPHICAL ABSTRACT



ARTICLE INFO

Article history:

Received 7 March 2021

Received in revised form 22 April 2021

Accepted 24 April 2021

Available online 29 April 2021

Editor: Damia Barcelo

Keywords:

Iron chelates
Photo-Fenton
Bacterial inactivation
Micropollutants
Wastewater

ABSTRACT

Three organic fertilizers (EDTA (**E**thyl**e**nedi**n**itri**l**o**t**etra**a**cetic acid), EDDS (Ethylenediamine-N, N'-disuccinic acid) and DTPA (Diethylene triamine pentaacetic acid)) were tested as Fe-complexes in photo-Fenton process at natural pH for micropollutants (MPs) abatement and simultaneous *E.coli* inactivation. Less stable Fe-complexes show high iron precipitation, stopping MPs degradation. On the contrary, stable Fe-complexes imply low kinetic rates for MPs removal. To solve these inconveniences, three mixtures of organic fertilizers were also tested, trying to improve the kinetic rates of micropollutants oxidation and overcome iron precipitation. Three different pollutants (propranolol (PROP), acetamiprid (ACMP) and sulfamethoxazole (SMX)) were used as the target compounds. As the iron release is, in part, linked to the hardness of water, two water matrices from two different secondary wastewaters (Membrane Bioreactor (MBR) and Conventional Activated Sludge (CAS)) were tested. The best performance in micropollutant degradation and *E.coli* inactivation was achieved with the combination of EDDS + EDTA, accomplishing a good equilibrium between iron precipitation and rate of MPs removal. For instance, total removal of propranolol was achieved at 45 min in MBR, while it was only 85.7% in CAS, being an improvement of the process comparing with that obtained using single organic fertilizers. At the end of the treatment, 2.1 log-inactivation for *E.coli* was reached in CAS. The differences observed between both wastewaters were related to CAS' higher DOC, turbidity, and hardness. Finally, from the physicochemical characterization conducted, including Biochemical Oxygen Demand at 5 days and phytotoxicity, it is possible to highlight the suitability of these treated effluents for its reuse in irrigation, as long as in CAS matrix the final values of *E. coli* are within the legal limit.

© 2021 Elsevier B.V. All rights reserved.

* Corresponding author.

E-mail address: nuria.lopez@ub.edu (N. López-Vinent).

1. Introduction

The rapid growth of the population has caused fast global socio-economic changes, involving important environmental problems, such as water scarcity (Iglesias et al., 2007). At the current water consumption rate, in 2025 two-thirds of the world population could face water shortage, according to estimations of the World Wildlife Fund (WWF) (Ortega-Gómez et al., 2014). In front of this scenario, the development of suitable water reuse technologies is fundamental to confront water scarcity. The reuse of wastewater (WW) seems a good strategy for an efficient use of water, crucial for a sustainable development. In accordance with UNESCO (The United Nations Educational, Scientific and Cultural Organization), the agricultural sector represents about 70% of the total fresh water demand. The use of treated wastewater in this sector could guarantee agricultural production, mainly in areas with water deficit, reducing the water footprint. Nevertheless, the reuse of wastewater must negatively impact the public health. Thus, Regulation of the European Parliament and of the Council on minimum requirements for water reuse (European Commission, 2020) establishes the key parameters to be controlled for the agricultural reuse, such as *E. coli*. Conventional methods used for wastewater disinfection are based on chlorinated compounds (Iglesias et al., 2007; Nahim-Granados et al., 2019; Lima Perini et al., 2018). However, the formation of unhealthy and toxic substances, like halogenated disinfection by-products (DBPs), results to be dangerous for aquatic ecosystems and human health (Meireles et al., 2016). Sometimes it can be hard to simultaneously meet the limit for *E. coli* and residual chlorine ($< 1 \text{ mg L}^{-1}$), making impossible the reuse of wastewater treated in this way for agricultural purposes (Nahim-Granados et al., 2019; ISO-16075-2). Consequently, the evaluation of less conventional technologies has gained importance in the last decades. Different studies have proven the efficiency of homogeneous Advanced Oxidation Processes (AOPs) on bacterial inactivation (Fiorentino et al., 2019; Malvestiti et al., 2019a; Malvestiti et al., 2019b) and micropollutants (MPs) abatement (Rodríguez-Chueca et al., 2018; López et al., 2018; Cruz-Alcalde et al., 2020). Additionally, studies with iron-based materials in heterogeneous AOPs suggested that these can play an important role in a large-scale wastewater treatment (Luo et al., 2021). Among AOPs, the use of solar driven processes seems a good strategy, being an ecofriendly option, which allow important reductions of electric costs. In this sense, solar photo-Fenton has gained importance among these alternatives due to its capabilities for water purification (Soriano-Molina et al., 2021; Ahile et al., 2021; López-Vinent et al., 2019). However, the required acidic conditions for photo-Fenton constitute the most serious drawback for its full-scale application (López-Vinent et al., 2020a). In that case, some authors proposed different chelating agents to work at natural pH. EDTA (**Ethylenedinitrilotetraacetic acid**), EDDS (Ethylenediamine-*N,N'*-disuccinic acid), citric acid and oxalic acid are, among others, the most investigated compounds (Huang et al., 2012; García-Fernández et al., 2019; Miralles-Cuevas et al., 2014; de Luca et al., 2014). Recently, organic fertilizers such as DTPA (Diethylene triamine pentaacetic acid) (López-Vinent et al., 2020b) and EDDHA (Ethylenediamine-*N,N'*-bis(2-hydroxyphenylacetic acid)) (Nahim-Granados et al., 2019) were also studied as the chelating agents to perform photo-Fenton process at natural pH.

As observed in previous studies, EDDS displays low stability with iron, which results in higher kinetic rates of MPs degradation at the first minutes of the treatment. Then, the efficiency decreases presenting a plateau and failing to reach the complete MPs removal (López-Vinent et al., 2020a, 2020b). However, other chelating agents, like DTPA, which presents high stability with iron, shows low kinetic rates in MPs abatement. However, in such case, continuous MPs degradation was observed, achieving good removals at the end of the treatment. In a previous work, the behavior of EDDS, EDTA and DTPA was studied in different wastewater effluents (López-Vinent et al., 2020b) and was discussed regarding the evolution of iron during the experiment.

These results displayed the necessity to search for chelating agents whose use could avoid high iron precipitation and lead to fast kinetic rates in MPs degradation. For this reason, mixtures of EDDS, EDTA and DTPA were used in this study. These combinations should lead to a mix of both unstable iron complexes providing high rates for MPs removal and iron-stable complexes allowing the continuous formation of hydroxyl radical, thus avoiding the efficiency decrease. Furthermore, these combinations could prevent additional treatments to remove iron hydroxides, because of a lower iron precipitation compared to that observed in treatments using EDDS only. Moreover, the treatment time should decrease compared to that in treatments employing more stable iron chelates. Another advantage is related to the reuse of wastewater for agricultural purposes: all three chelating agents are fertilizers approved by the European Commission (European Commission, 2003).

Different type of wastewaters effluents can be found in WWTPs due to different treatments and wastewaters used. The physicochemical parameters of wastewater greatly influence the efficiency of micropollutants abatement with AOPs (López-Vinent et al., 2020a, 2020b; Maniakova et al., 2021). The turbidity, DOC and alkalinity can affect the photo-chemical reactions due to light scattering, competition for hydroxyl radicals due to the organic matter present in the matrix and hydroxyl radicals scavenging due to the presence of carbonate and bicarbonate.

Summarizing and according all the commented in the last paragraphs, the aim of this study is to evaluate the efficiency of organic fertilizers mixtures on micropollutants abatement and *E.coli* inactivation by photo-Fenton at natural pH, in two different wastewaters. Three micropollutants were selected as model compounds: propranolol hydrochloride (PROP), acetamiprid (ACMP) and sulfamethoxazole (SMX). The selected matrices correspond to two secondary effluents, from membrane bioreactor (MBR) and Conventional Activated Sludge (CAS) treatments with distinct physicochemical characteristics, especially in organic matter, turbidity, and alkalinity. The performance of organic fertilizers mixtures will be compared to single compounds usage, being one of the main goals, along with wastewater comparison to determine the role of WW properties on iron precipitation and subsequent slowdown of degradation kinetics. Linked to this, another endpoint in this work is to identify the organic fertilizers combinations which are more suitable for each type of wastewater and relate it to their relative stability with iron. Finally, the feasibility of reusing these treated effluents for agricultural purposes was assessed through Biochemical Oxygen Demand (BOD₅) analyses. The results of each condition at the end of the treatment were compared with the maximum limit in the legislation for its reuse. Additionally, phytotoxicity was evaluated during the treatment by *E.sativa* seeds.

2. Material and methods

2.1. Chemicals

Three micropollutants were selected as model compounds: propranolol hydrochloride (PROP), acetamiprid (ACMP) and sulfamethoxazole (SMX), all of them acquired from Sigma-Aldrich. EDDS-Na solution (purchased from Sigma-Aldrich), DTPA-Fe (7% of iron) and EDTA-Fe (13.3% of iron), both obtained from Phygenera (Germany), were selected as chelating agents for photo-Fenton experiments. Catalase from bovine liver and Chormocult® Coliform Agar were acquired from Sigma-Aldrich. Hydrogen peroxide (H₂O₂, 30% w/v), ferrous sulfate (FeSO₄•7H₂O), orthophosphoric acid and acetonitrile were purchased from Panreac Química.

2.2. Wastewater matrices

Two secondary effluents from two different wastewater treatment plants (WWTPs) located in Barcelona (Spain) were selected to perform photo-Fenton experiments. They were collected from the outlet of a

Membrane Bioreactor and a Conventional Activated Sludge. They present markedly different physicochemical characteristics (see Table 1) mainly related to TOC (total organic carbon) and turbidity, which are expected to have an impact in photochemical experiments.

2.3. Photo-Fenton at natural pH experiments

A solar simulator (Xenonterm-1500RF, CCI) equipped with a Xenon lamp (1.5 kW) was used to perform the photo-Fenton experiments. Irradiance was determined by *o*-nitrobenzaldehyde actinometry (De la Cruz et al., 2013) obtaining a value of 13.9 W m^{-2} in the wavelength range between 290 and 400 nm. A tubular photoreactor was placed inside of the simulator (25 cm length x 2 cm diameter). During the assays, the solution was continuously recirculated from the feeding tank (1 L) to the tubular photoreactor. The medium temperature was kept constant at 25° by means of a Haake C-40 bath. A schematic design can be found in the supplementary material (Fig. S1).

Total iron in solution was 5 mg L^{-1} (corresponding to the maximum concentration allowed for water irrigation) (Guidelines 600/R-12/618; Ayers and Westcot, 1985) so that an appropriate amount of EDTA-Fe or DTPA-Fe was added to corresponding wastewater, previously acclimated. The calculations were performed according to the percentage of iron chelated in each case (see Section 2.1). In the case of EDDS, this was first dissolved and then the iron (5 mg L^{-1}) added to ensure the chelation and avoid iron precipitation. A molar ratio (Chelating agent: Fe) of 1:1 was selected according to our previous study (López-Vinent et al., 2020b). To prepare the solution with mixtures of chelating agents, the same total iron in solution than that used in experiments with a single chelating agent was employed (5 mg L^{-1}). In that case, 50% of chelated iron was added from one chelating agent and 50% from the other. Three mixtures were tested: EDDS + EDTA, EDDS + DTPA and EDTA + DTPA. A concentration of 0.25 mg L^{-1} of each micropollutant (PROP, ACMP and SMX) was added to the solution. The selection of these MPs was devised due to different kinetic constant values for reactions with hydroxyl radical ($k_{\text{PROP,HO}} = 1.0 \cdot 10^{10} \text{ M}^{-1} \text{ s}^{-1}$ (Benner et al., 2008) $k_{\text{SMX,HO}} = 5.5 \cdot 10^9 \text{ M}^{-1} \text{ s}^{-1}$ (Huber et al., 2003), $k_{\text{ACMP,HO}} = 2.1 \cdot 10^9 \text{ M}^{-1} \text{ s}^{-1}$ (Cruz-Alcalde et al., 2017)). Finally, just before the experiment started, a concentration of 50 mg L^{-1} of H_2O_2 was added. During the experiment, samples were continuously withdrawn, and the reaction was stopped with catalase (200 mg L^{-1}). To evaluate the total iron in solution, the samples were filtered with $0.20 \mu\text{m}$ syringe filters and ascorbic acid in excess was added to the sample to reduce iron (III) to iron (II), which then reacts with *o*-phenanthroline.

All plots were performed considering the accumulated energy (Q_{acc} , kJ L^{-1}), calculated according to Eq. (1) (Romero Olarte, 2015).

$$Q_{\text{acc}} = \sum_{i=1}^n \frac{I \cdot \Delta t_i}{V} \quad (1)$$

where I is the irradiation entering the photoreactor (kJ s^{-1}), Δt_i is the increment in the time of reaction (s) and V is the reaction volume (L).

Table 1
Principal parameters of two wastewaters characterization. N/A: below the detection level.

Parameters	MBR	CAS
pH	7.8	8.2
Turbidity (NTU)	0.3	5.3
UV_{254} (m^{-1})	19.1	28.8
TOC (mg C L^{-1})	7.0	16.6
DOC (mg C L^{-1})	6.7	10.9
Total alkalinity ($\text{mg CaCO}_3 \text{ L}^{-1}$)	233.2	467.4
Cl^{-1} (mg L^{-1})	591.6	406.4
SO_4^{2-} (mg L^{-1})	168.8	206
N-NO_2^- (mg L^{-1})	0.4	0.4
N-NO_3^- (mg L^{-1})	N/A	1.6

2.4. Analytical techniques

High Performance Liquid Chromatography (Agilent Technologies) was used to measure the concentrations of all three micropollutants (PROP, ACMP and SMX). An isocratic method was employed for simultaneous MPs detection with a C-18 column (Tecknokroma, $200 \times 4.6 \text{ mm i.d.}$; $5 \mu\text{m}$ particle size). The wavelengths were fixed at 214, 250 and 270 nm for PROP, ACMP and SMX, respectively. The mobile phases selected were acetonitrile and water acidified with orthophosphoric acid ($\text{pH} = 3$) (20:80, respectively). The flux was set to 1 mL min^{-1} and an injection volume of $100 \mu\text{L}$ was used. Hydrogen peroxide (H_2O_2) concentrations were followed during the reaction by the metavanadate colorimetric method (Pupo Nogueira et al., 2005). Total dissolved iron was also monitored by the *o*-phenanthroline procedure (ISO 6332). The BOD_5 analyses were performed following the 5210-standard method (detection limit $1 \text{ mg O}_2 \text{ L}^{-1}$). Seeds of *Eruca sativa* (arugula) were employed to determine the phytotoxicity (Tam and Tiquia, 1994) (further information can be found in the supplementary material Table S1). To perform the disinfection tests, 1 mL of each sample was plated on Chromocult® Coliform Agar (*E. coli* selective agar). Buffered peptone was used when dilution was needed. The plates were incubated at 35°C for 24, 48 and 72 h. The standard plated count method was used to determine the colony-forming units per 1 mL (CFU mL^{-1}).

3. Results and discussion

3.1. Comparison of chelating agents' mixtures in two different wastewaters

Chelating agents have different efficiencies on MPs removal and bacterial inactivation due to their different chemical structure, which implies distinct stability constants with iron. In general terms, a low stability of iron chelates causes a fast abatement of MPs but, at the same time, quick iron precipitation causing a decrease in the process efficiency. Nevertheless, in the case of iron chelates with a higher stability, the opposite happens resulting in a low but continued rate of MPs removal (López-Vinent et al., 2020b). Thus, an equilibrium between high degradation rates and low iron precipitation is necessary for the process to be efficient.

Despite this, the performance on MPs abatement and bacterial inactivation are related to the complexity of the effluent. For these reasons, it is important to study the process with effluents presenting different physicochemical parameters to have a global vision of the process behavior in different systems. To study this influence, the process performance on two different WWTPs effluents, CAS and MBR, was compared in this work.

With the aim of comparing the efficiency of two wastewater matrices, the same combinations of chelating agents and concentrations of reagents were used (5 mg L^{-1} of iron and 50 mg L^{-1} of H_2O_2). Fig. 1 displays the degradation curves of PROP (a), ACMP (b) and SMX (c) catalyzed by the combination of 50% EDDS + 50% EDTA in both secondary effluents (MBR and CAS). In addition, the removals of three MPs using 100% EDDS and 100% EDTA were also plotted. The pH evolution was followed during each experiment. Only variations of ± 0.2 were observed since real and naturally buffered wastewater effluents were employed.

As can be observed in Fig. 1, the best removal was observed for PROP and the worst for ACMP, in all cases. With MBR effluent, similar to CAS, the trend of all three MPs was the same regardless of the employed iron chelates (see Fig. 1a, 1b and 1c). The most representative difference was observed for ACMP during the first 60 min (0.77 kJ L^{-1}). For instance, with the EDDS-EDTA mixture, the degradation of ACMP was 60.9% at 60 min, while with EDDS and EDTA the removals were 39.4 and 32.9%, respectively. This fact is related to the low kinetic rate constant of reaction between hydroxyl radicals and ACMP, so that the MPs removals

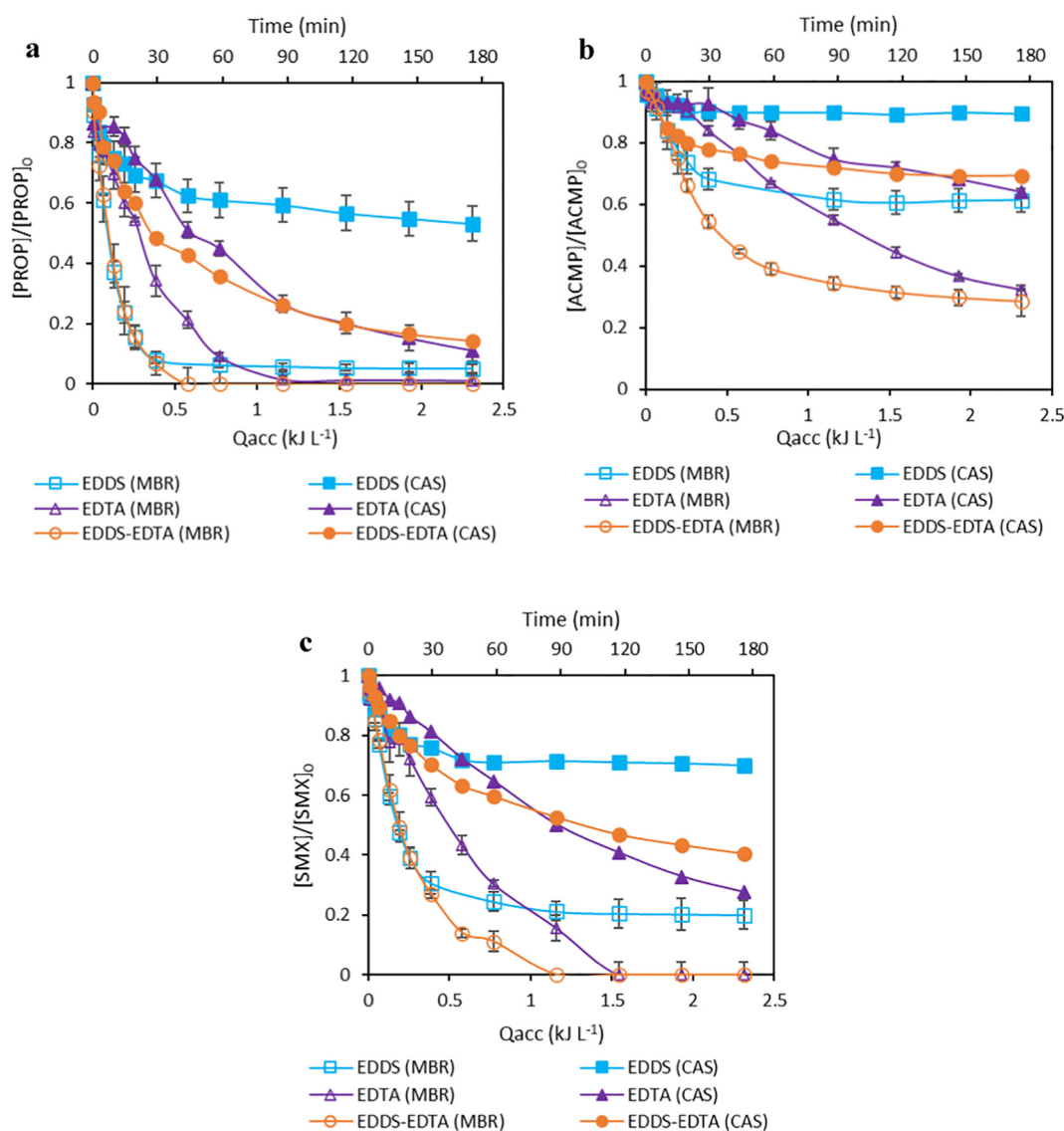


Fig. 1. Profile of a) PROP b) ACMP and c) SMX degradation as a function of the accumulated energy for photo-Fenton experiments at natural pH, with EDDS, EDTA and a mixture of both (50% EDDS + 50% EDTA), in MBR (opened symbols) and CAS (closed symbols). $[\text{PROP}]_0 = [\text{ACMP}]_0 = [\text{SMX}]_0 = 0.25 \text{ mg L}^{-1}$; $[\text{Fe}]_0 = 5 \text{ mg L}^{-1}$; $[\text{H}_2\text{O}_2]_0 = 50 \text{ mg L}^{-1}$.

were slower and an improvement in degradation with the combination is more noticeable.

The degradations at the end of the treatment with CAS were lower than those achieved in MBR, due to the higher complexity of the first matrix including a higher organic load. Thus, 100% of PROP abatement (with EDDS + EDTA) was reached in only 45 min (0.58 kJ L^{-1}) in the MBR matrix, whereas only 85.7% of PROP removal was observed at the end of the treatment (180 min, 2.31 kJ L^{-1}) in CAS matrix. This confirmed the competition for HO \cdot and probably light scattering due to high organic matter and turbidity in CAS. This fact was already observed when EDDS and EDTA were used alone. Thus, the PROP degradation was 89.9% with EDDS and 65.8% with EDTA (Fig. 1a), at 0.39 kJ L^{-1} (30 min) in MBR. However, only 32.6% and 32.2% of PROP was removed in CAS for EDDS and EDTA, respectively. The higher organic load of the CAS effluent also explains that the difference in the degradation rates of PROP with EDDS and EDTA is larger in MBR compared to CAS, as oxidation of the organic load of that matrix can prevail over the degradation of the model pollutant.

Another key aspect to consider in the behavior of iron chelates as catalysts is the rate of iron precipitation. Fig. 2 shows the iron evolution during the photo-Fenton treatment with different organic fertilizers and

their mixtures in two wastewater effluents (Fig. 2a for MBR and Fig. 2b for CAS). EDDS quickly releases iron, while EDTA releases it more slowly. This fact can explain (see Fig. 1) that EDDS contributed to a higher reaction rate at the initial 30 min while EDTA participated in less iron precipitation throughout the reaction. In addition, the precipitation of iron in CAS was higher than that in MBR, mainly in the case of EDDS which forms the iron chelate with a lower stability. For instance, when EDDS was used, at 0.39 kJ L^{-1} (30 min) the iron precipitated was 81.5% in CAS and 38.7% in MBR (see Fig. 2). This behavior could be related to the highest complexity of CAS compared to MBR. The different compounds contained in wastewaters, such as ions, can be involved in the breakdown of the iron complex since they could perform new complexes with the complexing agent if the stability constant of the new combination is higher than that with iron. This fact results in a higher precipitation of iron in CAS than MBR. It constitutes another reason why the degradation of MPs at the beginning of the reaction was slower when EDDS was used in CAS.

Coming again to the combination EDDS + EDTA, in the case of MBR, the synergistic effect appears throughout the entire experiment. It should be noted that at the beginning of the experiment the behavior of this mixture is very similar to that with EDDS alone. However,

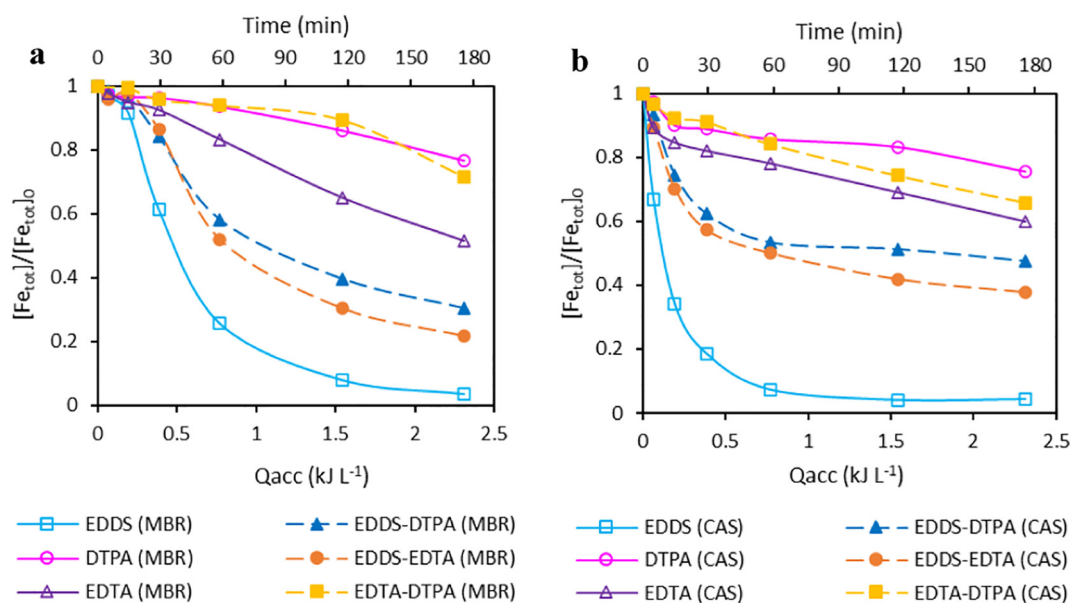


Fig. 2. Iron evolution during the experiment as a function of the accumulated energy for three chelating agents and their mixtures in photo-Fenton at natural pH in a) MBR and b) CAS. $[PROP]_0 = [ACMP]_0 = [SMX]_0 = 0.25 \text{ mg L}^{-1}$; $[Fe]_0 = 5 \text{ mg L}^{-1}$; $[H_2O_2]_0 = 50 \text{ mg L}^{-1}$.

given the presence of EDTA as well, the plateau formed when EDDS alone is used appears much later in the case of EDDS + EDTA. This shows the good synergy between the release of iron by the EDDS, at the beginning of the experiment, and the minor but continuous release of iron throughout the whole experiment by EDTA. Therefore, the decrease in PROP concentration does not reach a plateau, as it would happen using only EDDS, but it continues to go down thanks to EDTA. All of this is also corroborated by the data in Fig. 2, which shows the evolution of the concentration of iron in solution throughout the experiment, as commented before. It can be seen that at the end of the experiment and thanks to EDTA, there is still a large amount of iron in solution which causes, as mentioned before, the plateau not to appear, and therefore PROP degradation continues. The evolution of H_2O_2 decomposition of different organic fertilizers and their mixtures is decomposed in Fig. S2. In all cases, at the end of the experiment, not all the H_2O_2 was consumed. This fact evidences that the plateau observed for EDDS in MPs abatement was not caused by a lack of oxidant.

In the case of CAS, the EDDS + EDTA synergy is noticeable during the first half of the experiment and disappears towards the end, where even the use of EDTA alone offers better results than the EDDS + EDTA mixture. This could be explained because, in the case of CAS, there is a higher organic load that competes with the MPs for hydroxyl radicals. Thus, at the beginning, the effect of EDTA to avoid the EDDS plateau is noticed but, in turn, it causes a higher precipitation rate of the EDTA iron which explains that at the end of the experiment, the EDDS + EDTA mixture behaves worse than EDTA alone. As seen in Fig. 2, much less iron remains in solution at the end of the experiment for the EDDS + EDTA combination than for EDTA alone. This was also the case with MBR. However, in that assay the effect of EDDS is much more powerful and allows the PROP degradation to go a long way. With this, the supplementary effect of EDTA, even if it is less, already allowing the synergy to continue until the end of the experiment, achieving the total degradation of PROP.

In CAS matrix, the degradation of ACMP and SMX with different chelating agents followed the same trend than PROP (46.8% for EDDS, 88.8% for EDTA and 85.7% for EDDS-EDTA). ACMP achieved 10.4%, 35.8% and 30.6% and SMX presented 30%, 72.5% and 59.5% for EDDS, EDTA and the combination of both, respectively, at 180 min (2.31 kJ L^{-1}).

In CAS matrix, at the end of the treatment, EDTA and the mixture of both chelating agents presented similar results for all three MPs.

However, an enhancement in MPs degradation and dissolved iron was observed comparing EDDS with the combination of EDDS and EDTA. For instance, the degradation of PROP at the end of the treatment was 1.8 times higher and the precipitation of iron was 2 times lower with 50% EDDS + 50% EDTA than those observed for EDDS. In addition, the application of the mixture (EDDS + EDTA) to the crops is a more sustainable measure since EDDS presents a biodegradable character and EDTA was more recalcitrant, negatively affecting the soils when the plants do not absorb all the amount of applied fertilizer (López-Rayo et al., 2016). Using the mixture, less EDTA would be poured to the ecosystems and similar MPs degradation and iron precipitation could be achieved.

For a better understanding of the effect of combining different chelating agent's, two more mixtures of were tested. Fig. 3 shows the degradation curves of three MPs catalyzed by 50% EDDS + 50% DTPA, and Fig. 4 presents the results for 50% EDTA + 50% DTPA.

As can be observed in Fig. 3a for CAS effluent, both the experiment with the combination of EDDS + DTPA and 100% EDDS presented overlapped curves until 0.39 kJ L^{-1} (30 min), while DTPA showed a slow kinetic rate. Then, the PROP degradation with EDDS stopped down due to the high iron precipitation, achieving only 46.8% abatement at the end of the treatment. Nevertheless, the removal of PROP with the combination of both chelating agents reached 60.4% of degradation, equal than the experiment using only DTPA. As commented for the mix EDDS + EDTA, the higher organic load of CAS competes with the MPs for hydroxyl radicals. Being so, at the beginning of the experiment, DTPA can avoid the EDDS plateau but, in turn, the precipitation rate of iron coming from DTPA increases, explaining that at the end of the experiment, the EDDS + DTPA mixture behaved similarly to DTPA alone. In addition, for the mixture EDDS + DTPA the iron remaining in solution was higher than that observed in the test using EDDS alone, and lower than in the test with DTPA alone (see Fig. 2b). Therefore, this can explain the fact that the degradation of MPs with EDDS + DTPA followed an intermediate behavior between EDDS and DTPA separately.

In the case of experiments with the MBR matrix, iron precipitation was slower reaching good MPs abatement kinetics during the first 30 min (0.39 kJ L^{-1}). This fact implies that the difference in MPs removal between EDDS and DTPA was higher in MBR compared to CAS. Thus, the effect of iron precipitation is much more important in effluents with higher DOC and alkalinity, due to faster precipitation as

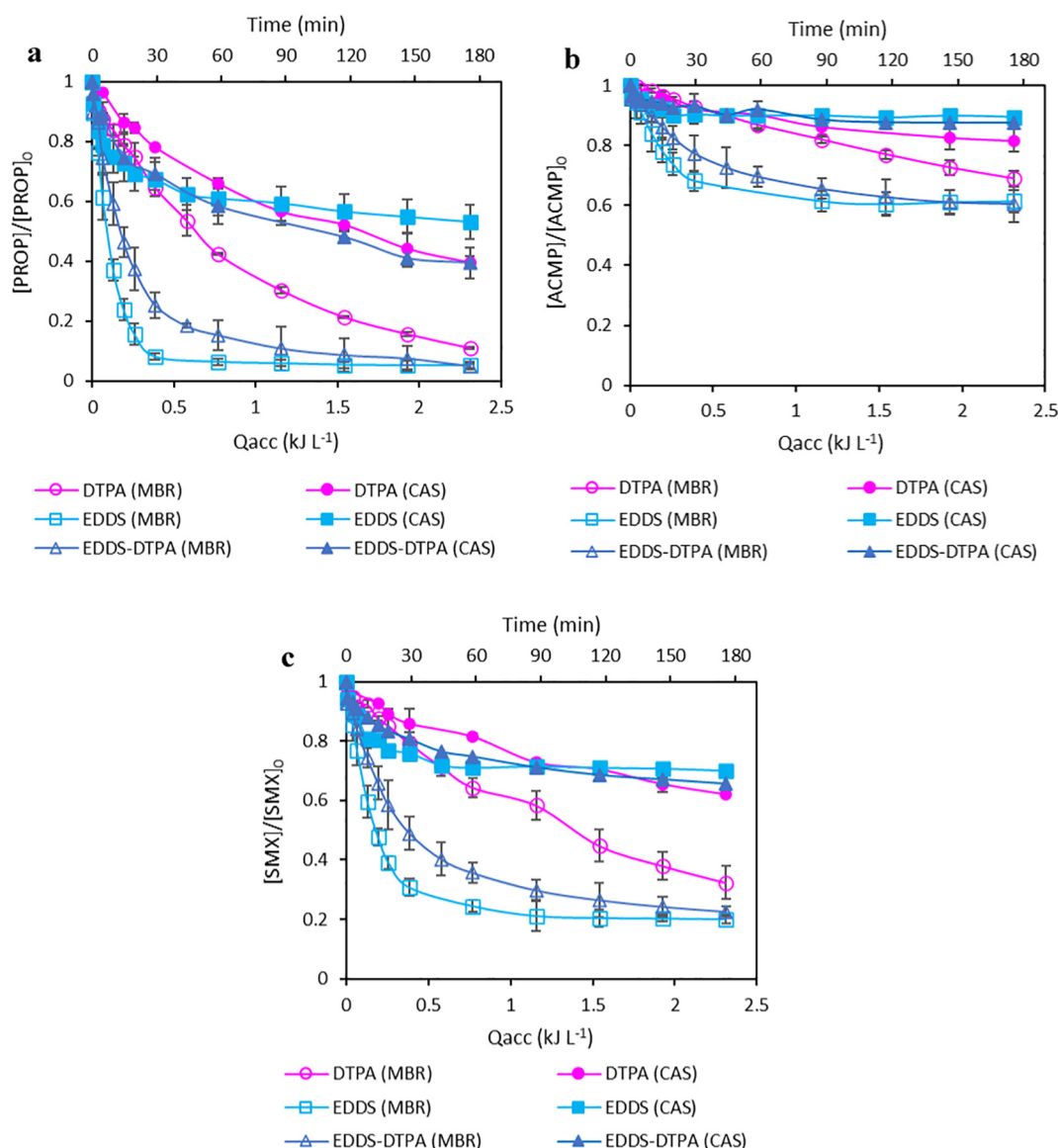


Fig. 3. Profile of a) PROP b) ACMP and c) SMX degradation as a function of the accumulated energy for experiments with EDDS, DTPA and a mixture of both (50% EDDS +50% DTPA) in photo-Fenton at natural pH in MBR (open symbols) and CAS (closed symbols). $[\text{PROP}]_0 = [\text{ACMP}]_0 = [\text{SMX}]_0 = 0.25 \text{ mg L}^{-1}$; $[\text{Fe}]_0 = 5 \text{ mg L}^{-1}$; $[\text{H}_2\text{O}_2]_0 = 50 \text{ mg L}^{-1}$.

commented before. However, DTPA did not achieve better removals than EDDS at 90 min (1.16 kJ L^{-1}), as happened in CAS effluent. The results for ACMP and SMX when the combination of two chelating agents was employed were: 12.4 and 34.4% in CAS and 39.4 and 77.4% in MBR, respectively.

Comparing the two mixtures performed with EDDS (i.e., EDDS + DTPA (Fig. 3) and EDDS + EDTA (Fig. 1)), it was noted that in the combination with EDTA better removals were achieved for all three MPs because both EDTA and EDDS presented higher degradation rates during the initial instants. This fact implies that the higher MPs degradation is produced before the iron precipitation was very pronounced. However, in the case of the EDDS + DTPA combination, the kinetic rates were slower, due to the fact that DTPA presents higher stability in its combination with iron. For this reason, the iron precipitation exerts a stronger effect when this mixture of chelates was tested because at 60 min (0.77 kJ L^{-1}) the iron in solution was about 50% in both effluents. This fact caused the reduction in the efficiency of the process, consequently failing to reach total MPs removal. The same fact was observed when 100% of EDDS was tested. At 0.39 kJ L^{-1} , the degradation of all three MPs was stopped due to the high iron precipitation. In addition, with

the EDDS-EDTA mixture this fact was also seen in ACMP, since this compound presents slower oxidation kinetics with hydroxyl radical. Thus, the removal was stopped at 0.77 kJ L^{-1} , when the iron precipitation was very high, and total degradation was not reached.

Fig. 4 displays the results obtained through the combination of 50% EDTA +50% DTPA for PROP (Fig. 4a), ACMP (Fig. 4b) and SMX (Fig. 4c) degradation in MBR and CAS effluents. The EDTA-DTPA chelates mixture allowed to reach similar degradation kinetics than EDTA alone, achieving the same PROP abatement (about 87% in CAS at 180 min and 100% at 90 min in MBR). EDTA + DTPA mixture improves the behavior of DTPA since only 60.5% of PROP removal was achieved with DTPA alone, at 180 min. The same fact happened with ACMP and SMX. In addition, in experiments using the combination EDTA-DTPA about 1.2 times less iron precipitated compared to tests with EDTA, which is better for the agricultural purposes as it avoids iron chlorosis in plants.

On the other hand, and comparing the mixtures of chelating agents tested, EDTA + DTPA (see Fig. 4) achieved better results than the combination EDDS + DTPA (see Fig. 3) in both effluents (MBR and CAS) at the end of the treatment (180 min). Until 0.6 kJ L^{-1} (45 min) the

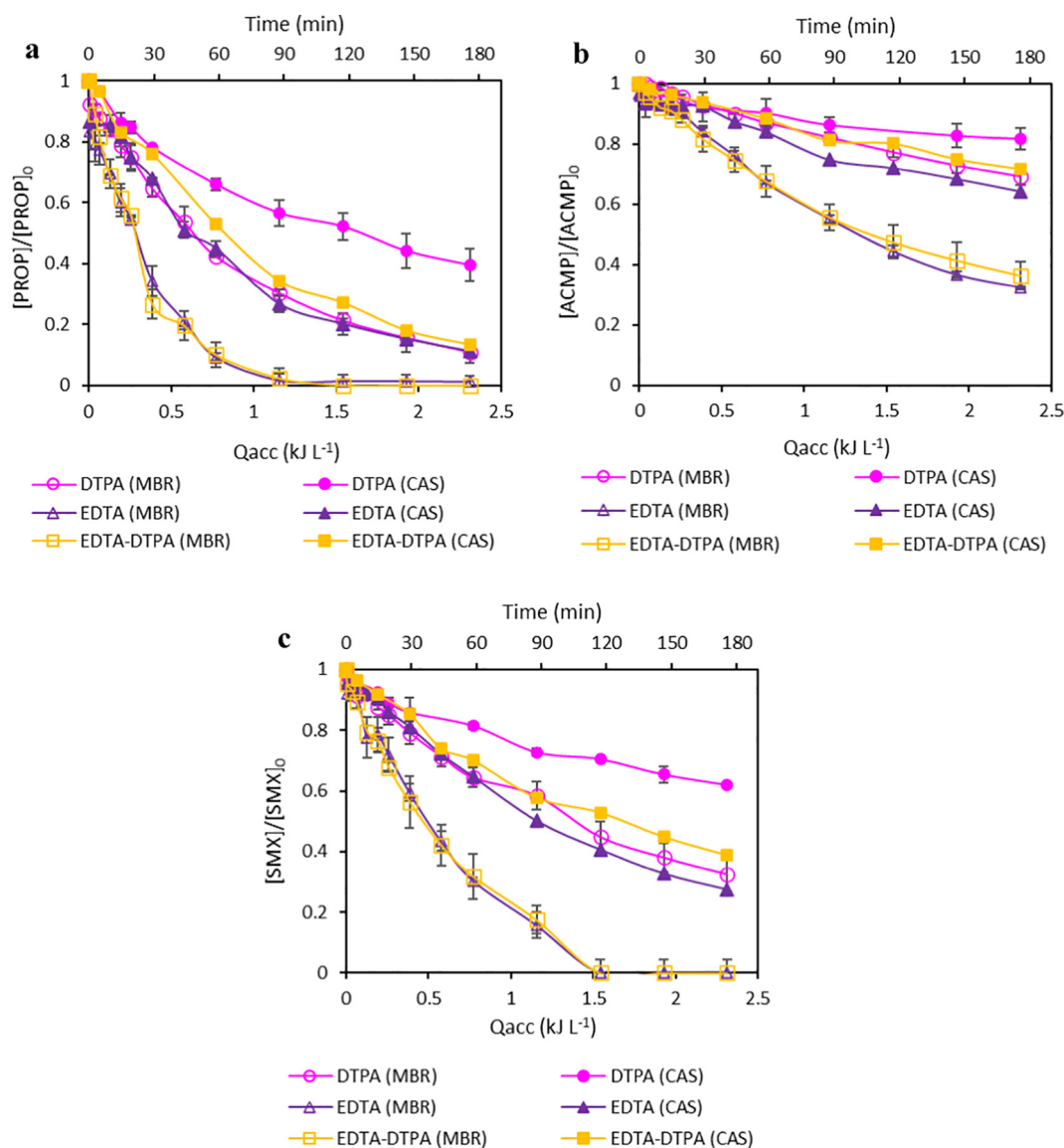


Fig. 4. Profile of a) PROP b) ACMP and c) SMX degradation as a function of the accumulated energy for experiments with EDTA, DTPA and a mixture of both (50% EDTA + 50% DTPA) in photo-Fenton at natural pH in MBR (opened symbols) and CAS (closed symbols). $[\text{PROP}]_0 = [\text{ACMP}]_0 = [\text{SMX}]_0 = 0.25 \text{ mg L}^{-1}$; $[\text{Fe}]_0 = 5 \text{ mg L}^{-1}$; $[\text{H}_2\text{O}_2]_0 = 50 \text{ mg L}^{-1}$.

degradations of all three MPs were similar in both effluents and chelating agent's combinations. Then, the mixture EDTA + DTPA presented higher removals in all the experiments. The reason is the higher iron precipitation when EDDS + DTPA was tested (approximately 2.5 times higher than EDTA + DTPA). The different behavior of the three mixtures of chelating agents can also be explained from this different rate of iron precipitation, similarly to the EDDS + EDTA mixture. Thus, EDTA and DTPA release iron in a more sustained way during the experiment, and not abruptly at the beginning and very slowly at the end as observed for EDDS. This would explain why the EDTA + DTPA mixture had better results than the EDDS + DTPA mixture, as DTPA releases iron very slowly and, at the end of the experiment, it cannot compensate the lack of iron caused by the fact that EDDS released it so quickly. In the case of the EDDS + EDTA combination, EDDS also releases iron very quickly but EDTA is capable to release it to a higher extent than DTPA. Therefore, ensuring that, at the end of the experiment, enough iron remains in solution allowing the continuity of the MPs degradation reactions. That is why the EDDS + EDTA mixture gave the best results.

3.2. Bacterial inactivation in Conventional Activated Sludge effluent

E. coli inactivation was also evaluated in CAS. Fig. 5 displays the inactivation curves corresponding to experiments employing the three chelating agents (EDDS, EDTA and DTPA) and their corresponding binary mixtures. The quantification of wild *E. coli* disclosed concentrations in the range of 10^3 – 10^4 colony-forming units per mL (CFU mL⁻¹) at initial time. Experiments with only hydrogen peroxide demonstrated that under darkness conditions disinfection does not occur. A photolysis test was also carried out, achieving only 0.2 log-inactivation at 180 min (2.31 kJ L⁻¹).

Regarding the experiments with different chelating agents, EDTA showed the worst results with inactivation levels of 1.3 log at the end of the experiment. EDDS presented a 1.8 log inactivation. The two combinations of chelating agents including EDDS (EDDS + EDTA and EDDS + DTPA) achieved the best inactivation: 2.1 log-inactivation. On its part, DTPA and the mixture EDTA + DTPA showed the same inactivation: 1.5 log. Total inactivation was not reached in any of the studied cases. However, no regrowth was observed in any case at 48 and 72 h.

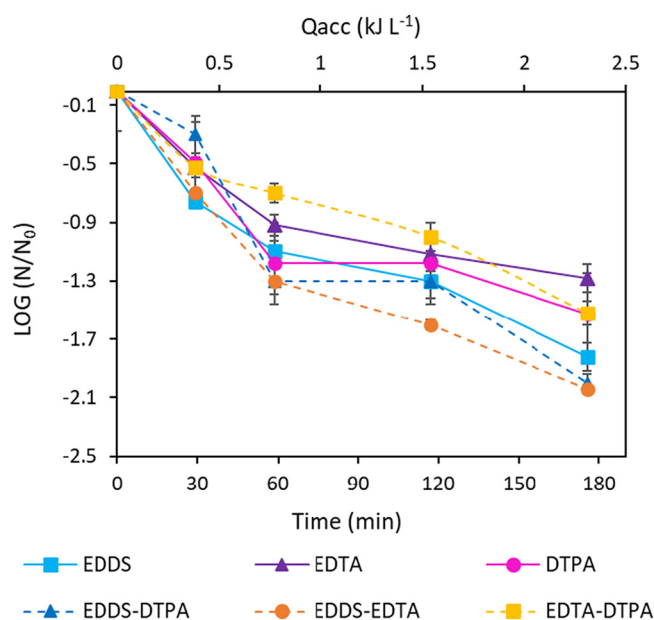


Fig. 5. *E. coli* inactivation in CAS with photo-Fenton process at natural pH catalyzed by DTPA, EDTA, EDDS and three different combinations of these chelating agents. $[\text{Fe}]_0 = 5 \text{ mg L}^{-1}$; $[\text{H}_2\text{O}_2]_0 = 50 \text{ mg L}^{-1}$.

Hydroxyl radicals formed in photo-Fenton at natural pH can affect proteins, lipids and DNA causing mortality in bacteria (Spuhler et al., 2010; García-Fernández et al., 2012). Moreover, intracellular diffusion of Fe (II) can generate internal Fenton reactions and also produce the inactivation of bacteria (Halliwell and Gutteridge, 1984; Polo-López et al., 2013). Nevertheless, in photo-Fenton at natural pH with high concentrations of iron (10 mg L^{-1}) the presence of Fe (II) is almost negligible, as observed in a previous work. In that case, the formation of oxyhydroxides was very fast and experiments with EDDS, which presented high iron precipitation, achieved worst inactivation results (López-Vinent et al., 2020b). However, in the present study combinations of EDDS with two other chelating agents allowed to reach the best log-inactivation. In this case, however, the initial iron concentration was lower and the formation of oxyhydroxides consequently slower, thus favoring the inactivation of bacteria. In addition, the MPs degradation kinetics and the inactivation rate of bacteria do not have to follow necessarily the same trend. Thus, if we compare all the chelates and mixtures of chelates tested, when working with EDDS and its mixtures the amount of iron in solution at the beginning of experiments is larger than that for the other mixtures, as has been reasoned in previous sections. Therefore, although there is competition between inactivation of bacteria and degradation of MPs, there is enough iron for contributing to both. However, in the case of EDTA and DTPA, these and their mixtures slowly release the iron and therefore there is less iron available in the reaction medium.

3.3. Phytotoxicity and BOD₅ assays

Biochemical oxygen Demand at 5 days ($\text{mgO}_2 \text{ L}^{-1}$) is an important parameter in wastewater reuse for agricultural purposes. The Regulation of the European Parliament and of the Council (European Commission, 2020) lists the minimum requirements for agricultural wastewater reuse, establishing four water classes (A-D, A fixes $\text{BOD}_5 \leq 10 \text{ mgO}_2 \text{ L}^{-1}$ and B-D $\leq 25 \text{ mgO}_2 \text{ L}^{-1}$). More information about the classes of reclaimed water quality can be found in Tables S2 and S3. In this study, BOD₅ at the end of the treatment was evaluated for all three organic fertilizers and their respective mixtures, when applied to MBR and CAS treatment (Fig. 6). In addition, phytotoxicity was evaluated

using seeds of *E. sativa*, with the aim of exploring if the final treated effluent could be used for agricultural purposes.

As can be observed in Fig. 6, using EDDS yielded the highest BOD₅ at the end of the treatment, for both matrices MBR and CAS. This behavior was expected because of EDDS was the more biodegradable chelating agent among those tested. The experiments conducted with mixtures containing EDDS also exhibited high values of BOD₅, especially in the case of MBR. However, in the case of CAS, experiments with only EDDS showed significantly high BOD₅ values, whereas the rest of chelators and respective mixtures show very similar values.

Finally, all treated MBR effluents were suitable for reuse for agricultural purposes, according to the values listed in the Regulation for agricultural water reuse (European Commission, 2020) (Tables S2 and S3). Nevertheless, taking into account the values of *E. coli* at the end of the treatment in CAS matrix, these effluents were not appropriate for this use, even though the BOD₅ values were within the range for their reuse.

Regarding phytotoxicity, Table 2 displays the germination index (GI) at different reaction times for MBR and CAS matrices. The equations for GI estimation can be found in Table S1. The control tests were carried out in deionized water.

Zucconi et al. (1981a, 1981b) proposed different categories depending on the percentage of GI to determine the phytotoxicity grade:

- Inhibition of seed germination and root elongation: <20% GI.
- Presence of phytotoxicity: 20–50% GI.
- No significant injury to the plant: >50–60% GI.
- Disappearance of phytotoxicity: >80–85% GI.
- Stimulation of the root elongation: >100% GI (better than control, which represent 100% of GI).

As can be observed, at initial time only experiments with EDTA and DTPA showed a stimulation of the root in MBR. Nevertheless, the other experiments did not present phytotoxicity at initial time. On the contrary, in CAS matrix all treatments displayed values of GI > 100%, being this indicative of root stimulation. This difference between both matrices could be related to the higher organic matter content present in CAS compared to MBR, which can stimulate the growth of seeds. Regarding the differences between employed chelators, these could be associated to their effectiveness as fertilizers, being EDTA and DTPA those more employed in agriculture. The percentage of GI varied without a clear trend (between 15 min and 120 min), in all experiments. This fact was likely due to the presence of by-products (Freitas et al., 2017) probably more toxic than the initial MPs, as well as to transformation products from the chelating agents. However, evidences for phytotoxicity, inhibition of seed germination or root elongation were not observed.

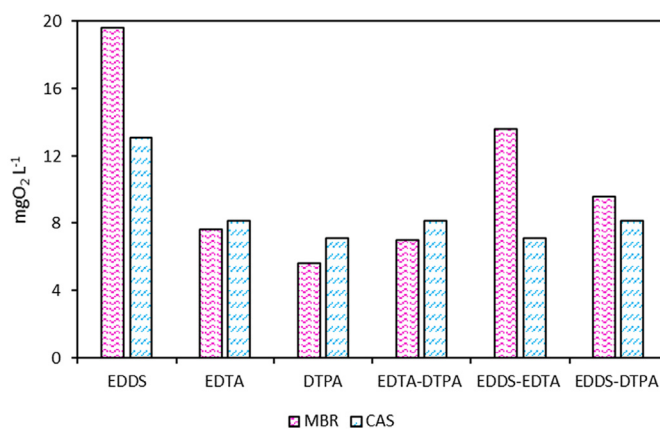


Fig. 6. Biochemical Oxygen Demand at 5 days at the end of the treatment with photo-Fenton at natural pH, using EDDS, EDTA, DTPA and three mixtures of these organic fertilizers, in MBR and CAS matrices. $[\text{Fe}]_0 = 5 \text{ mg L}^{-1}$; $[\text{H}_2\text{O}_2]_0 = 50 \text{ mg L}^{-1}$.

Table 2

Percentage of germination index of *E. sativa* in MBR and CAS matrix with photo-Fenton process at natural pH using DTPA, EDTA, EDDS and three different combinations of these chelating agents. $[Fe]_0 = 5 \text{ mg L}^{-1}$; $[H_2O_2]_0 = 50 \text{ mg L}^{-1}$.

Matrix	(%)	EDDS	EDTA	DTPA	50%EDDS 50%EDTA	50%EDDS 50%DTPA	50%EDTA 50%DTPA
MBR	0 min	76	153	117	68	96	86
	15 min	82	96	97	80	102	236
	30 min	108	71	132	63	119	202
	60 min	106	175	51	82	89	207
	120 min	79	139	73	67	132	209
	180 min	148	223	187	132	199	172
CAS	0 min	136	215	109	148	119	198
	15 min	51	93	150	104	112	93
	30 min	132	138	114	122	134	73
	60 min	126	154	101	104	193	185
	120 min	112	111	243	116	151	106
	180 min	168	186	122	237	151	139

Probably, the different changes in the experiments were caused by the distinct kinetics of MPs removal, implying different by-products formation and subsequent removal. In CAS, the tendency in all treatments to show lower values of GI throughout the experiment was minor than that in MBR. In that case, as the degradations of all three MPs were slower, the subsequent formation of more toxic by-products could also be minor causing the observed trend.

To conclude, at the end of the treatment, final treated effluents displayed values of GI higher than 100% (stimulation of the root) for both matrices MBR and CAS and for different chelating agents and their mixtures. This fact means that these effluents would be suitable for its reuse in agricultural irrigation without causing any damage to crops, as long as in CAS matrix the final values of *E. coli* are within the legal limit.

4. Conclusions

The capability of three Fe-complexes (EDDS, EDTA and DTPA) as iron sources has been demonstrated in photo-Fenton process for micropollutants abatement in Membrane Bioreactor and Conventional Activated Sludge effluents.

Propranolol and sulfamethoxazole have been successfully removed from MBR with three organic fertilizers achieving degradations higher than 70% at 180 min (2.31 kJ L^{-1}). Acetamiprid presented the lowest removals: 67.6% was the maximum degradation reached by EDTA at 180 min. This fact was related to the low kinetics of reactions between hydroxyl radical and this compound.

Regarding the differences between the two wastewaters tested, the MPs removals at the end of the treatment with CAS were always lower than those observed in MBR, due to the higher complexity of the matrix and its higher organic load. Additionally, the higher hardness of CAS promoted the higher precipitation of iron when treating this water, decreasing the efficiency of the process. For instance, when EDDS was employed, 90% of propranolol abatement was achieved at 30 min (0.39 kJ L^{-1}) with MBR while only 46.9% was reached with CAS at 180 min (2.31 kJ L^{-1}).

Concerning the Fe-complexes, the one with EDDS allowed the fastest degradation rate until the first 30 min, and then the reaction stopped failing to reach the complete degradation of the model micropollutants. For its part, the use of EDTA as chelating agent also yielded good kinetics, achieving the total degradation in propranolol and sulfamethoxazole. The lowest reaction rate was observed in experiments with DTPA. The different stability of organic fertilizers with iron affects degradation kinetics of MPs as well as iron release. To solve these inconveniences, three mixtures of organic fertilizers were also tested (50%EDDS + 50%EDTA; 50%EDDS + 50%DTPA; 50%EDTA + 50%DTPA). In all three cases, a yield improvement was observed in experiments with both

MBR and CAS, compared to the treatment using the chelates separately. The mixture of EDDS + EDTA gave the best results reducing the treatment time about four and two times in propranolol removal compared to single EDDS and EDTA, respectively. Additionally, final soluble iron availability was 30% higher with the corresponding mixture, compared to the use of single EDDS. *E. coli* inactivation was also evaluated in CAS matrix, with EDDS + EDTA and EDDS + DTPA mixtures achieving the best inactivation at the end of the treatment with 2.1 log-inactivation.

Finally, the results obtained in BOD₅ tests and phytotoxicity suggested the suitability of both treated effluents MBR and CAS for its reuse in irrigation. Additionally, in CAS effluent the inactivation values of *E. coli* were within the legal limits for its application.

CRedit authorship contribution statement

N. López-Vinent: Conceptualization, Investigation, Data curation, Writing – original draft, Writing – review & editing, Visualization, Project administration. **A. Cruz-Alcalde:** Conceptualization, Investigation, Data curation, Writing – original draft, Writing – review & editing, Visualization, Project administration. **J. Giménez:** Writing – review & editing, Supervision, Project administration. **S. Esplugas:** Writing – review & editing, Supervision, Project administration.

Declaration of competing interest

The authors declare that they have no known competing financial interests or personal relationships that could have appeared to influence the work reported in this paper.

Acknowledgments

The authors wish to thank the Ministry of Economy and Competitiveness of Spain (project CTQ2017-86466-R, MINECO/FEDER, UE), AGAUR-Generalitat de Catalunya (project 2017SGR-131) and Nuria López FPU research fellowship (FPU-16/02101) financed by Ministry of Science, Innovation and Universities of Spain.

Appendix A. Supplementary data

Supplementary data to this article can be found online at <https://doi.org/10.1016/j.scitotenv.2021.147416>.

References

- Ahile, U.J., Wuana, R.A., Itodo, A.U., Sha'Ato, R., Malvestiti, J.A., Dantas, R.F., 2021. Are iron chelates suitable to perform photo-Fenton at neutral pH for secondary effluent treatment? *J. Environ. Manag.* 278, 111566. <https://doi.org/10.1016/j.jenvman.2020.111566>.
- Ayers, R.S., Westcot, D.W., 2004. *Water Quality for Agriculture; Food and Agriculture Organization of the United Nations: Rome, Italy, 1985.*
- Benner, J., Salhi, E., Ternes, T., von Gunten, U., 2008. Ozonation of reverse osmosis concentrate: kinetics and efficiency of beta blocker oxidation. *Water Res.* 42, 3003–3012. <https://doi.org/10.1016/j.watres.2008.04.002>.
- Cruz-Alcalde, A., Sans, C., Esplugas, S., 2019. Priority pesticides abatement by advanced oxidation water technologies: the case of acetamiprid removal by ozonation, *Science of the Total Environment* 599–600 (2017) 1454–1461. <https://doi.org/10.1016/j.scitotenv.2017.05.065>.
- Cruz-Alcalde, A., Sans, C., Esplugas, S., 2020. Continuous versus single H₂O₂ addition in peroxide process: performance improvement and modelling in wastewater effluents. *J. Hazard. Mater.* 387, 121993. <https://doi.org/10.1016/j.jhazmat.2019.121993>.
- De la Cruz, N., Romero, V., Dantas, R.F., Marco, P., Bayarri, B., Giménez, J., Esplugas, S., 2013. O-Nitrobenzaldehyde actinometry in the presence of suspended TiO₂ for photocatalytic reactors. *Catal. Today* 209, 209–214. <https://doi.org/10.1016/j.cattod.2012.08.035>.
- De Luca, A., Dantas, R.F., Esplugas, S., 2014. Assessment of iron chelates efficiency for photo-Fenton at neutral pH. *Water Res.* 61, 232–242. <https://doi.org/10.1016/j.watres.2014.05.033>.
- European Commission, 2003. *Regulation (EC) No 2003/2003 of the European Parliament and of the Council of 13 October 2003 relating to fertilizers.* *Off. J. Eur. Communities.*
- European Commission, 2020. *Regulation 2020/741/EU of the European Parliament and of the Council of 25 May of 2020 on minimum requirements for water reuse.* *Off. J. Eur. Union* 177, 32–55.
- Fiorentino, A., Esteban, B., Garrido-Cardenas, J.A., Kowalska, K., Rizzo, L., Aguera, A., Sánchez Pérez, J.A., 2019. Effect of solar photo-Fenton process in raceway pond

- reactors at neutral pH on antibiotic resistance determinants in secondary treated urban wastewater. *J. Hazard. Mater.* 378, 120737. <https://doi.org/10.1016/j.jhazmat.2019.06.014>.
- Freitas, A.M., Rivas, G., Campos-Mañas, M.C., Casas López, J.L., Agüera, A., Sánchez Pérez, J.A., 2017. Ecotoxicity evaluation of a WWTP effluent treated by solar photo-Fenton at neutral pH in a raceway pond reactor. *Environmental Science Pollution & Research* 24, 1093–1104. <https://doi.org/10.1007/s11356-016-7101-7>.
- García-Fernández, I., Polo-López, M., Oller, I., Fernández-Ibáñez, P., Bacteria and fungi inactivation using Fe^{3+} /sunlight, H_2O_2 /sunlight and near neutral photo-Fenton: a comparative study, *Applied Catalysis B: Environmental* 121–122 (2012) 20–29. <https://doi.org/10.1016/j.apcatb.2012.03.012>.
- García-Fernández, I., Miralles-Cuevas, S., Oller, I., Malato, S., Fernández-Ibáñez, P., Polo-López, M.I., 2019. Inactivation of *E.coli* and *E. faecalis* by solar photo-Fenton with EDDS complex at neutral pH in municipal wastewater effluents. *J. Hazard. Mater.* 372, 85–93. <https://doi.org/10.1016/j.jhazmat.2018.07.037>.
- Halliwell, B., Gutteridge, J., 1984. Oxygen toxicity, oxygen radicals, transition metals and disease. *Biochemical Journal* 219, 1–14. <https://doi.org/10.1042/bj2190001>.
- Huang, W., Brigante, M., Wu, F., Hanna, K., Mailhot, G., 2012. Development of a new homogeneous photo-Fenton process using Fe(III) -EDDS complexes. *J. Photochem. Photobiol. A Chem.* 239, 17–23. <https://doi.org/10.1016/j.jphotochem.2012.04.018>.
- Huber, M.M., Canonica, S., Park, G.Y., Von Gunten, U., 2003. Oxidation of pharmaceuticals during ozonation and advanced oxidation processes. *Environ. Sci. Technol.* 37, 1016–1024. <https://doi.org/10.1021/es025896h>.
- Iglesias, A., Garrote, L., Flores, F., Moneo, M., 2007. Challenges to manage the risk of water scarcity and climate change in the Mediterranean. *Water Resour. Manag.* 21, 775–788. <https://doi.org/10.1007/s11269-006-9111-6>.
- ISO-16075-2, International Standard (ISO 16075-2), 2015-part 2: guidelines for treated wastewater use for irrigation projects-part 2: development of the project, 1st ed. (2015).
- Lima Perini, J.A., Tonetti, A.L., Vidal, C., Montagner, C.C., Pupo Nogueira, R.F., 2018. Simultaneous degradation of ciprofloxacin, amoxicillin, sulfathiazole and sulfamethazine, and disinfection of hospital effluent after biological treatment via photo-Fenton process under ultraviolet germicidal irradiation. *Appl. Catal. B Environ.* 224, 761–771. <https://doi.org/10.1016/j.apcatb.2017.11.021>.
- López, N., Marco, P., Giménez, J., Esplugas, S., 2018. Photocatalytic diphenhydramine degradation under different radiation sources: kinetic studies and energetic comparison. *Appl. Catal. B Environ.* 220, 497–505. <https://doi.org/10.1016/j.apcatb.2017.08.077>.
- López-Rayó, S., Nadal, P., Lucena, J.J., 2016. Novel chelating agents for iron, manganese, zinc and copper mixed fertilization in high pH soil-less cultures. *Journal of the Science Food and Agriculture* 96, 1111–1120. <https://doi.org/10.1002/jsfa.7183>.
- López-Vinent, N., Cruz-Alcalde, A., Romero, L.E., Chávez, M.E., Marco, P., Giménez, J., Esplugas, S., 2019. Synergies, radiation and kinetics in photo-Fenton process with UVA-LEDs. *J. Hazard. Mater.* 380, 120882. <https://doi.org/10.1016/j.jhazmat.2019.120882>.
- López-Vinent, N., Cruz-Alcalde, A., Gutiérrez, C., Marco, P., Giménez, J., Esplugas, S., Micropollutant removal in WW by photo-Fenton (circumneutral and acid pH) with BLB and LED lamps, *Chem. Eng. J.* 379 (2020a) 122416. <https://doi.org/10.1016/j.cej.2019.122416>.
- López-Vinent, N., Cruz-Alcalde, A., Malvestiti, J.A., Marco, P., Giménez, J., Esplugas, S., Organic fertilizer as a chelating agent in photo-Fenton at neutral pH with LEDs for agricultural wastewater reuse: micropollutant abatement and bacterial inactivation, *Chem. Eng. J.* 388 (2020b) 124246. <https://doi.org/10.1016/j.cej.2020.124246>.
- Luo, H., Zeng, Y., He, D., Pan, X., 2021. Application of iron-based materials in heterogeneous advanced oxidation processes for wastewater treatment: a review. *Chem. Eng. J.* 407, 127191. <https://doi.org/10.1016/j.cej.2020.127191>.
- Malvestiti, J.A., Cruz-Alcalde, A., López-Vinent, N., Dantas, R.F., Sans, C., Catalytic ozonation by metal ions for municipal wastewater disinfection and simultaneous micropollutants removal, *Appl. Catal. B Environ.* 259 (2019a) 118104. <https://doi.org/10.1016/j.apcatb.2019.118104>.
- Malvestiti, J.A., Fagnani, E., Simao, D., Dantas, R.F., 2019b. Optimization of UV/ H_2O_2 and ozone wastewater treatment by the experimental design methodology. *Environ. Technol.* 40 (15), 1910–1922. <https://doi.org/10.1080/09593330.2018.1432698>.
- Maniakova, G., Salmerón, I., Polo-López, M.I., Oller, I., Rizzo, L., Malato, S., 2021. Simultaneous removal of contaminants of emerging concern and pathogens from urban wastewater by homogeneous solar driven advanced oxidation processes. *Sci. Total Environ.* 766, 144320. <https://doi.org/10.1016/j.scitotenv.2020.144320>.
- Meireles, A., Gíaoiris, E., Simoes, M., 2016. Alternative disinfection methods to chlorine for use in the fresh-cut industry. *Food Res. Int.* 82, 71–85. <https://doi.org/10.1016/j.foodres.2016.01.021>.
- Miralles-Cuevas, S., Oller, I., Sánchez Pérez, J.A., Malato, S., 2014. Removal of pharmaceuticals from MWTP effluent by nanofiltration and solar photo-Fenton using two different iron complexes at neutral pH. *Water Res.* 64, 23–31. <https://doi.org/10.1016/j.watres.2014.06.032>.
- Nahim-Granados, S., Oller, I., Malato, S., Sánchez Pérez, J.A., Polo-López, M.I., 2019. Commercial fertilizer as effective iron chelate (Fe^{3+} -EDDHA) for wastewater disinfection under natural sunlight for reusing in irrigation. *Appl. Catal. B Environ.* 253, 286–292. <https://doi.org/10.1016/j.apcatb.2019.04.041>.
- Ortega-Gómez, E., Esteban García, B., Ballesteros Martín, M.M., Fernández Ibáñez, P., Sánchez Pérez, J.A., 2014. Inactivation of natural enteric bacteria in real municipal wastewater by solar photo-Fenton at neutral pH. *Water Res.* 63, 316–324. <https://doi.org/10.1016/j.watres.2014.05.034>.
- Polo-López, M.I., Oller, I., Fernández-Ibáñez, P., 2013. Benefits of photo-Fenton at low concentrations for solar disinfection of distilled water. A case study: *Phytophthora capsici*. *Catal. Today* 209, 181–187. <https://doi.org/10.1016/j.cattod.2012.10.006>.
- Pupo Nogueira, R.F., Oliveira, M.C., Paterlini, W.C., 2005. Simple and fast spectrophotometric determination of H_2O_2 in photo-Fenton reactions using metavanadate. *Talanta* 66, 86–89. <https://doi.org/10.1016/j.talanta.2004.10.001>.
- Rodríguez-Chueca, J., Laski, E., García-Cañibano, C., Martín de Vidales, M.J., Encinas, Á., Kuch, B., Marugán, J., 2018. Micropollutants removal by full-scale UV-C/sulfate radical based Advanced Oxidation Processes. *Sci. Total Environ.* 630, 1216–1225. <https://doi.org/10.1016/j.scitotenv.2018.02.279>.
- Romero Olarte, R.V., Degradation of Metoprolol by Means of Advanced Oxidation Processes (Doctoral Thesis). University of Barcelona, Spain (2015). <http://hdl.handle.net/2445/65724>.
- Soriano-Molina, P., Miralles-Cuevas, S., Esteban García, B., Plaza-Bolaños, P., Sánchez-Pérez, J.A., 2021. Two strategies of solar photo-Fenton at neutral pH for the simultaneous disinfection and removal of contaminants of emerging concern. Comparative assessment in raceway pond reactors. *Catal. Today* 361, 17–23. <https://doi.org/10.1016/j.cattod.2019.11.028>.
- Spuhler, D., Rengifo-Herrera, A.J., Pulgarin, C., 2010. The effect of Fe^{2+} , Fe^{3+} , H_2O_2 and the photo-Fenton reagent at near neutral pH on the solar disinfection (SODIS) at low temperatures of water containing *Escherichia coli* K12. *Appl. Catal. B Environ.* 96, 126–141. <https://doi.org/10.1016/j.apcatb.2010.02.010>.
- Tam, N.F.Y., Tiquia, S., 1994. Assessing toxicity of spent pig litter using a seed germination technique. *Resources, Conservation and Recycling* 11, 261–274. [https://doi.org/10.1016/0921-3449\(94\)90094-9](https://doi.org/10.1016/0921-3449(94)90094-9).
- Zucconi, F., Pera, A., Forte, M., 1981a. Evaluating toxicity of immature compost. *Biocycle* 54–57.
- Zucconi, F., Forte, M., Monaco, A., Biological evaluation of compost maturity, *Biocycle* (1981b) 27–29.

Supplementary Information for

Mixtures of chelating agents to enhance photo-Fenton process at natural pH: influence of wastewater matrix on micropollutant removal and bacterial inactivation

N. López-Vinent^{a*}, A. Cruz-Alcalde^{ab}, J. Giménez^a, S. Esplugas^a

^a *Department of Chemical Engineering and Analytical Chemistry, Faculty of Chemistry, Universitat de Barcelona, C/Martí i Franqués 1, 08028 - Barcelona, Spain. Tel: +34934021293. Fax: +34934021291*

^b *Institute of Environmental Assessment and Water Research – Spanish National Research Council (IDAEA-CSIC), C/Jordi Girona 18-26, 08034 – Barcelona, Spain. Tel: +34934006100 (ext. 5203).*

*Corresponding author:

Núria López Vinent, phone: +34 934 02 01 54, e-mail: nuria.lopez@ub.edu

Table of Contents

Figure S1. Experimental setup.....	p.2
Figure S2. Evolution of H ₂ O ₂ decomposition during the experiments with three organic fertilizers and their mixtures in a) MBR effluent and b) CAS effluent.....	p.2
Table S1. Phytotoxicity conditions and equations.....	p. 3
Table S2. Reclaimed water quality requirements for agricultural irrigation.....	p.3

Table S3. Classes of reclaimed water quality and allowed agricultural use and irrigation method.....p.4

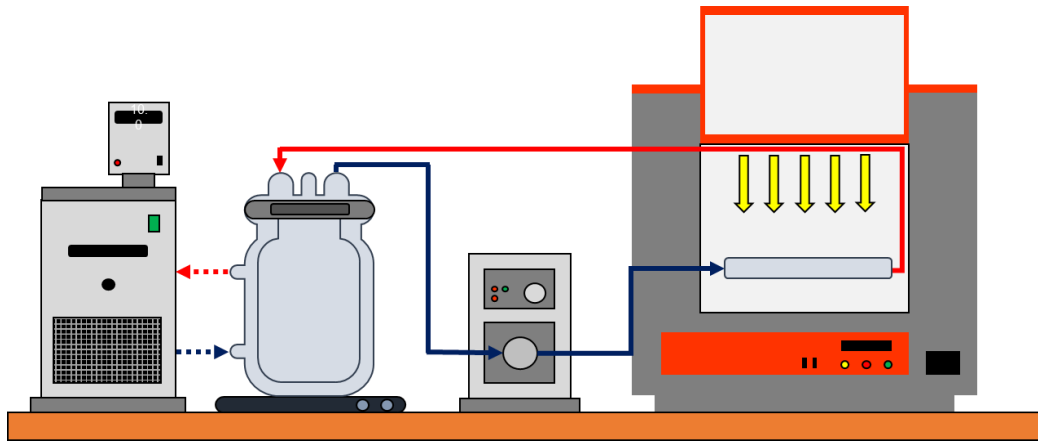


Figure S1. Experimental setup

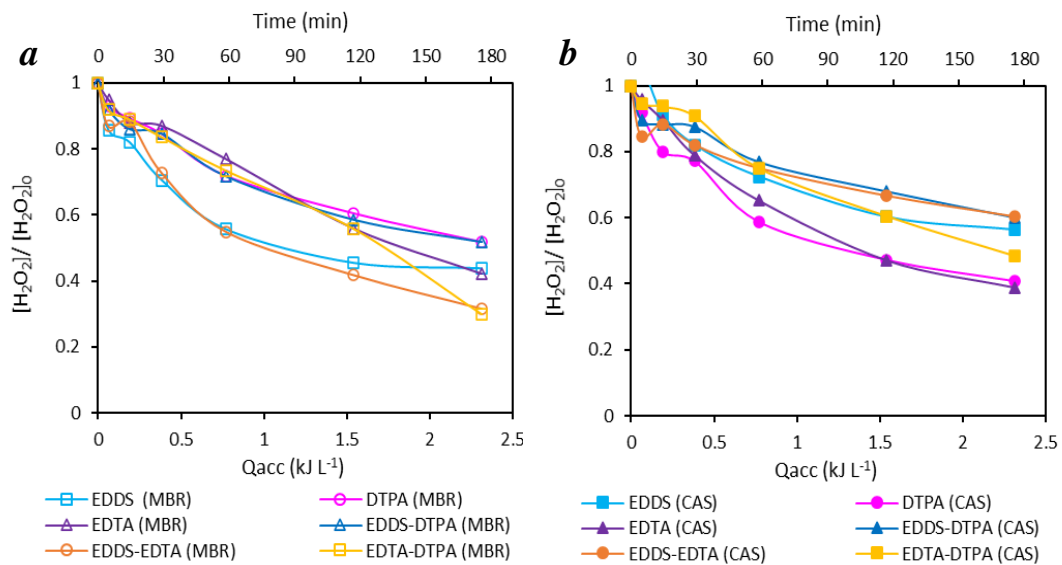


Figure S2. Evolution of H₂O₂ decomposition during the experiments with three organic fertilizers and their mixtures in a) MBR effluent and b) CAS effluent.

Table S1. Phytotoxicity conditions and equations (Tam and Tiquia, 1994)

Parameters	Conditions
Temperature	22.0 °C
Light	No
Test volume	4 mL per plate
Control	Distilled water
Number of seeds	10 seeds
Test duration	5 days
Test vessel	100 x 10 mm culture plate with 1 filter paper
Equation 1 (% seed germination)	$\% SG = \frac{n^{\circ} \text{ seeds germinated in the sample}}{n^{\circ} \text{ seeds germinated in the control}} \times 100$
Equation 2 (% root growth)	$\% RG = \frac{\text{mean root length in the sample}}{\text{mean root length in the control}} \times 100$
Equation 3 (Germination index)	$GI = \frac{\% \text{ seed germination} \times \% \text{ root growth}}{100}$

Table S2. Reclaimed water quality requirements for agricultural irrigation (European Commission, 2020).

Reclaimed water quality class	Quality requirements				
	<i>E. coli</i> (CFU/100 mL)	BOD ₅ (mg/L)	TSS (mg/L)	Turbidity (NTU)	Other
A	≤ 10 Or below detection limit	≤ 10	≤ 10	≤ 5	Legionella spp.: <1000 CFU/L where there is risk of aerosolization in greenhouses
B	≤ 100			-	Intestinal nematodes (helminth eggs): ≤1 egg/L for irrigation of pastures or forage
C	≤ 1000	≤ 25	≤ 35	-	
D	≤ 10000			-	

Table S3. Classes of reclaimed water quality and allowed agricultural use and irrigation method (European Commission, 2020).

Minimum reclaimed water quality class	Crop category	Irrigation method
A	Food crops, including root crops consumed raw and food crops where the edible part is in direct contact with reclaimed water	All
B	Food crops consumed raw where the edible part is produced above ground and is not in direct contact with reclaimed water, processed food crops and non-	All
C	food crops including crops to feed milk- or meat-producing animals	Drip *
D	Industrial, energy, and seeded crops	All

(*) Drip irrigation (also called trickle irrigation) is a micro-irrigation system capable of delivering water drops or tiny streams to the plants and involves dripping water onto the soil or directly under its surface at very low rates (2-20 liters/hour) from a system of small diameter plastic pipes fitted with outlets called emitters or drippers.

Part VI

Role of sunlight and oxygen on the performance of photo-Fenton process at near neutral pH using organic fertilizers as an iron chelates

Núria López-Vinent, Alberto Cruz-Alcalde, Claudia Lai, Jaime Giménez, Santiago
Esplugas, Carmen Sans

Department of Chemical Engineering and Analytical Chemistry, Faculty of Chemistry,
University of Barcelona, C/Martí i Franqués 1, 08028 Barcelona, Spain.

Submitted to *Journal of Hazardous Materials*

Role of sunlight and oxygen on the performance of photo-Fenton process at near neutral pH using organic fertilizers as iron chelates

N. López-Vinent ^{a*}, A. Cruz-Alcalde ^{ab}, C. Lai ^a, J. Giménez ^a, S. Esplugas ^a, C. Sans ^a

^a *Department of Chemical Engineering and Analytical Chemistry, Faculty of Chemistry, University of Barcelona, C/Martí i Franqués 1, 08028 - Barcelona, Spain. Tel: +34934021293. Fax: +34934021291*

^b *Institute of Environmental Assessment and Water Research – Spanish National Research Council (IDAEA-CSIC), C/Jordi Girona 18-26, 08034 – Barcelona, Spain. Tel: +34934006100 (ext. 5203).*

*Corresponding Author: nuria.lopez@ub.edu

ABSTRACT

Nowadays reaction mechanisms of photo-Fenton process with chelated iron are not yet clearly defined. In this study, five organic fertilizers were used as iron complexes to investigate the role of sunlight and oxygen in photo-Fenton at near neutral pH. UV absorbance and stability constant of each selected iron chelate is different, and this work demonstrates that these parameters affect the reaction mechanisms in SMX degradation. Irradiation experiments without H₂O₂ revealed that EDDS-Fe and DTPA-Fe achieved SMX degradation, but different iron release. These results, together with soluble oxygen free experiments, allowed the proposal of complementary reaction mechanisms to the classical photo-Fenton one. The proposed mechanisms start through the potential photoexcitation of the iron complex and subsequent oxygen-mediated hydroxyl radical generation reactions, which are different for EDDS-Fe and DTPA-Fe. Moreover,

irradiation experiments using EDTA-Fe and HEDTA-Fe had negligible SMX degradation, but iron release were observed, evidencing the differences for iron chelates.

KEYWORDS

Photochemistry, Iron complexes, Organic fertilizers, Reactive Oxygen Species, Photoexcitation

1. Introduction

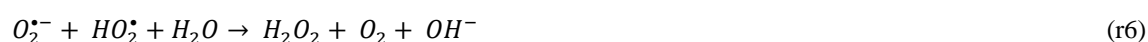
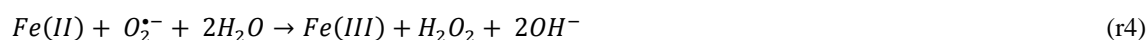
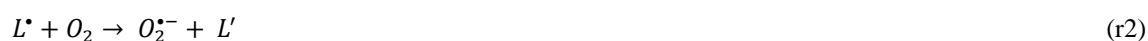
According to UNESCO, around 70% of the total consumed freshwater (up to 90% in some developing countries) is destined to agriculture [1]. In a water scarcity scenario, reusing wastewater (WW) for agricultural purposes might be a good strategy to reduce the freshwater consumption. Nevertheless, the treated wastewater must accomplish some minimum quality requirements to be reused in crop irrigation. These parameters (like biochemical oxygen demand (BOD₅), *E. coli* and turbidity) are established in a Proposal for a Regulation of the European Parliament and of the Council on minimum requirements for water reuse [2].

In the last decades, Advanced Oxidation Processes (AOPs) have demonstrated their efficiency in the removal of contaminants of emerging concern and bacterial inactivation [3-6]. Among AOPs, photo-Fenton process is a promising technology to remove persistent micropollutants (MPs) [7-11]. The possibility to use solar light as irradiation source makes the process more economic, reducing a large part of operating costs. Photo-Fenton runs better at acidic pH, implying a subsequent neutralization. However, the possibility of working at neutral pH exists, making the process more attractive for full-scale application [12]. Recent studies are focused on the performance of photo-Fenton process at neutral pH using organic fertilizers as an iron source to treat wastewater and reuse it for agricultural purposes [13-15]. Organic fertilizers are widely used in agriculture

as iron chelates, increasing the bioavailability of iron for crops, preventing iron chlorosis, and avoiding the plant disease, since iron is an essential micronutrient for plant growth [16]. Thus, wastewaters treated by photo-Fenton with organic fertilizers as iron chelates could be directly applied in soils without the need of chelates removing. However, these organic fertilizers applied to agriculture may not be completely absorbed by the plants and therefore may appear in surface or groundwater. So far, their reactivity in the aquatic environment has not been deeply studied. In the literature, there is evidence of the iron chelates reactivity with UV (ultraviolet) radiation and dissolved oxygen, and how these processes could potentially lead to the generation of reactive oxygen species (ROS) [17-20]. These reactions and the photo-redox cycle of iron (III) complexes may be important to the environment, which could contribute to the self-depuration of the aquatic compartments by oxidation of some persistent organic pollutants [21,22].

The mechanisms of photo-Fenton with chelated iron are not yet clearly defined. Both UV absorbance and complex stability vary for the different chelating agents, and therefore the reactions involving radiation and free iron could be also distinct. In particular, organic fertilizers such as DTPA-Fe, HEDTA-Fe and EDDHA-Fe have not yet been studied in this regard. Their stability constant with iron is very different compared to EDDS-Fe, which is the most investigated iron complex. Despite this, some authors use the mechanistic knowledge obtained for the EDDS-Fe chelate in a general way, making it extensive to any polycarboxylic acid ligand (L). In the case of photo-Fenton using EDDS-Fe, there is evidence of additional mechanisms to produce hydroxyl radicals (HO^\bullet) apart from classical photo-Fenton reactions. According to the literature [23-25], the photoexcitation of EDDS-Fe leads to the generation of EDDS radical (EDDS^\bullet) expressed as L^\bullet in reaction r1. According to reaction r1, the complexes chelated with Fe(III) under irradiation could generate both Fe(II) and ligand-free radical (L^\bullet) by ligand-to-metal

charge transfer (LMCT). The superoxide radical ($O_2^{\bullet-}$) could be formed by the reaction between dissolved oxygen and L^{\bullet} (see r2). Meanwhile $O_2^{\bullet-}$ and its conjugated acid form could generate hydrogen peroxide (H_2O_2) via r3-7 reactions. Finally, HO^{\bullet} is generated by the Fenton reaction with available dissolved iron (i.e., H_2O_2 with Fe(II) (r9)). However, the pH is an important factor to consider given that, at neutral pH, reactions r3, r5, r6 and r7 would take place slower than under acidic conditions, influencing the amount of H_2O_2 formed and consequently the quantity of HO^{\bullet} available to react. In addition, at pH values higher than 4 the concentration of both dissolved iron and photoactive $FeOH^{2+}$ decreases, forming precipitated iron hydroxides and thus affecting reactions r4, r5 and r8.



The aim of this work is to study the reactivity of some widely used organic fertilizers in photo-Fenton process under solar radiation and the main involved reaction mechanisms at near neutral pH. The selected commercial iron chelates were EDDS, EDTA, DTPA, HEDTA and EDDHA, which are approved by the European Commission for their agricultural use [26]. Sulfamethoxazole (SMX) was chosen as a target compound due to their occurrence in aquatic systems [27-30]. The organic fertilizers present different iron-ligand stability constant and different UV absorbance, which has helped to investigate the

contribution of these parameters on the reaction mechanisms. This includes mechanisms about ROS formation because of the interactions between these agricultural products with both sunlight and dissolved oxygen in aquatic systems.

2. Material and methods

2.1. Chemicals

Sulfamethoxazole (SMX), diethylene triamine pentaacetic acid (DTPA), hydrogen peroxide (H₂O₂) (30% w/w), *tert*-butyl alcohol (tBuOH), catalase from bovine liver and EDDS-Na were purchased from Sigma-Aldrich (USA). DTPA-Fe (7% iron), EDTA-Fe (13.3% iron) and HEDTA-Fe (13.0% iron) were bought from Phygenera (Germany). EDDHA-Fe (6.0% iron) was acquired from Fertiberia (Spain). Acetonitrile, orthophosphoric acid, sodium bicarbonate (NaHCO₃) and iron sulphate heptahydrate (FeSO₄ 7H₂O) were obtained from Panreac Quimica (Spain). Nitrogen gas (N₂ > 99.995) was supplied by Abelló Linde (Spain).

2.2. Experimental set-up and procedure

A Solar simulator (Xenonterm-1500RF.CCI) with a Xenon lamp (1.5 kW) equipped with a UV filter, removing the wavelengths under 290 nm, was employed to perform all experiments. The apparatus contains a tubular photoreactor (25 cm length x 2 cm diameter) located in the axis of a parabolic mirror made of reflective aluminum, at the bottom of simulator. An external stirred tank (1 L) was used as a reservoir. During the experiments, the solution from the reservoir tank was continuously pumped (peristaltic pump Ecoline VC-280) to the tubular photoreactor and recirculated back to the reservoir. O-nitrobenzaldehyde actinometry [31] was carried out to evaluate the photonic flowrate entering the photoreactor (wavelength range: 290-400 nm), obtaining a value of $6.6 \cdot 10^{-7}$ Einstein s⁻¹

(13.9 W m⁻²). Temperature was kept constant at 25°C by means of a Haake C-40 cooling bath. A scheme of the irradiation setup can be found elsewhere [13].

For solutions preparation, 1.64 mM of HCO₃⁻ (representing a relative contribution to HO• scavenging less than 3%) was added to ultrapure water to keep pH constant at 7.5±0.2. An appropriate amount of each organic fertilizer chelated with iron was added to achieve a value of 5 mg L⁻¹ of iron (maximum allowed concentration for irrigation water) [32, 33], considering the percentage of iron in each organic fertilizer presented in section 2.1. As EDDS was not found chelated with iron, a molar ratio of 1:1 (EDDS-Fe(II)) was selected [3]. In that especial case, iron (5 mg L⁻¹) was added to the stirred EDDS solution to guarantee the chelation. More details about the experimental procedure of chelation can be found elsewhere [15]. Then SMX, used as a model target compound, was spiked to ultrapure water to have a concentration of 1 mg L⁻¹. Finally, hydrogen peroxide (concentration of 50 mg L⁻¹) was appended just before turning on the solar simulator. The contribution of dissolved oxygen on the process was evaluated by bubbling N₂ gas during 30 minutes before starting the experiment and throughout the whole reaction time. WTW Oxi 340i Oximeter was used during the experiment to measure the O₂ concentration. A concentration of 25 mM of tBuOH (contributing to 95% of HO• scavenging) was used to study the role of hydroxyl radical in photo-Fenton experiments with and without H₂O₂. All experiments were performed in duplicate and error bars are shown in the plots.

For different analyses, samples were withdrawn from the feeding tank throughout the entire reaction time and catalase (200 mg L⁻¹) was employed to quench the residual H₂O₂. When iron in solution was determined, the samples were filtered with 0.20 µm PVDF filter to analyze only the dissolved iron. Then, excess of ascorbic acid was added to obtain total soluble iron.

The accumulated energy (Q_{acc} , kJ L^{-1}) was calculated according to Eq.1 [34].

$$Q_{acc} = \sum_{i=1}^n \frac{I \Delta t_i}{V} \quad (\text{Eq.1})$$

Where I corresponds to the irradiation entering the photoreactor (kJ s^{-1}), Δt_i is the increment of the reaction' time (s) and V is the volume (L).

2.3. Analytical methods

SMX concentrations were determined by High Performance Liquid Chromatography (HPLC) with UV detection (1260 Infinity Series from Agilent). Acetonitrile and orthophosphoric water solution acidified at pH=3 (60:40 volumetric mixture, respectively) were employed as a mobile phase. An isocratic method at 1 mL min^{-1} and $100 \mu\text{L}$ of volume injection was selected. The column used was a Tecknokroma Mediterrania C-18 (250 x 4.6 mm i.d, $5 \mu\text{m}$ particle size) and the UV detector was set at 270 nm. For the determination of hydrogen peroxide, a colorimetric method based on the use of metavanadate was employed [35]. A procedure based on o-phenatroline (ISO 6332) was employed to measure the total dissolved iron. Absorbance spectra were obtained by using a spectrophotometer DR6000 UV-Vis by Hach (USA).

3. Results and discussion

The photodegradation of three new iron chelates (DTPA-Fe, HEDTA-Fe and EDDHA-Fe) was studied over a long period of time to emphasize the importance of the iron chelates stability. EDDS-Fe and EDTA-Fe were also investigated for comparison purposes.

The absorption spectra of iron chelates were obtained in ultrapure water and it was used to evaluate the possibility of iron complexes undergoing photodegradation (Figure 1). The light absorption band, in all these organic fertilizers, overlap to solar simulator

emission spectrum (290-600 nm). Therefore, Figure 1 elucidates the capacity of these iron complexes to absorb radiation at the UVA and UVB range.

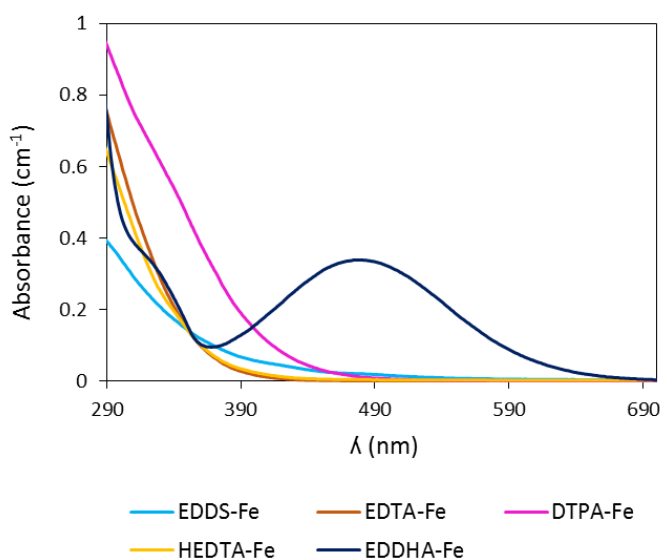


Figure 1. UV-Vis absorption spectrum of five iron chelates (EDDS-Fe, EDTA-Fe, DTPA-Fe, HEDTA-Fe and EDDHA-Fe) at 5 mg L⁻¹ of iron.

3.1. Contribution of solar simulated radiation

3.1.1. Photo-Fenton and dark Fenton experiments

To elucidate the contribution of simulated solar radiation on SMX abatement when the five iron chelates (EDDS-Fe, EDTA-Fe, DTPA-Fe, HEDTA-Fe and EDDHA-Fe) were used in photo-Fenton at pH=7.5 ± 0.2, photo-Fenton tests (chelate-Fe + H₂O₂ + sunlight) together with Fenton reaction (chelate-Fe + H₂O₂) and experiments without H₂O₂ (chelate-Fe + sunlight) were performed and the SMX depletion results are shown in Figures 2a,3a and 4a respectively. The evolution of total iron corresponding to each experiment is displayed in Figures 2b, 3b and 4b. The plots present results for 1.5 kJ L⁻¹, corresponding to 2h of experiment. Blank tests were also carried out to clarify the potential SMX degradation mechanisms. No removal was observed in the photolysis experiment. In addition, H₂O₂ combined with radiation led a value of 9.7% of SMX

abatement, corresponding to H_2O_2 decomposition by radiation giving place to two hydroxyl radical molecules (see reaction r9). However, in photo-Fenton experiments this contribution was probably lower due to the strong “inner filter effect” because of the absorption of light by Fe-complexes [36].

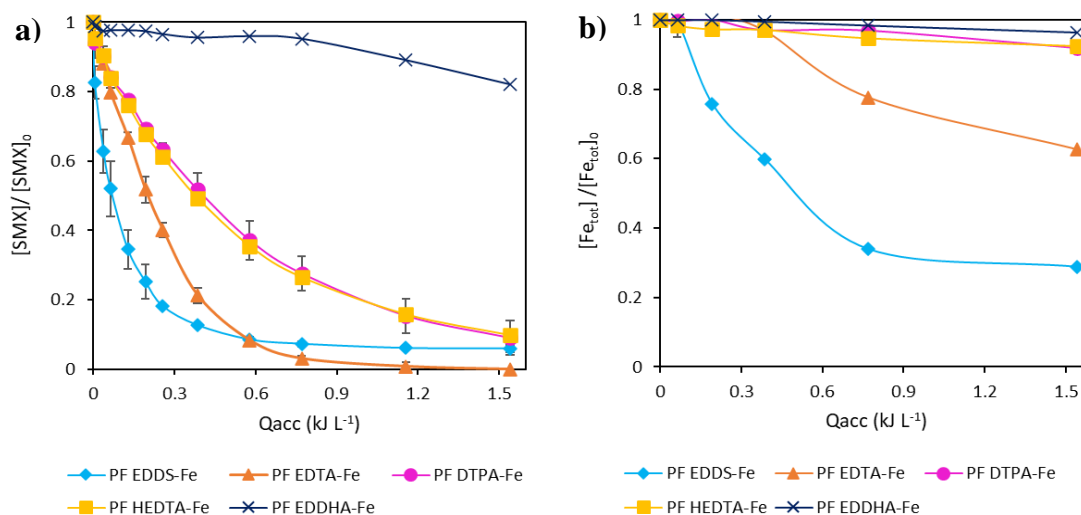
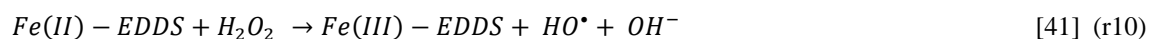


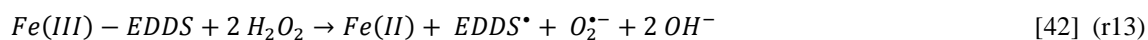
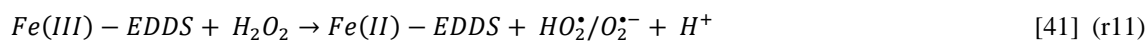
Figure 2. a) SMX abatement and b) evolution of total dissolved iron plotted as a function of the accumulated energy for photo-Fenton experiments with five different iron chelates at $\text{pH} = 7.5 \pm 0.2$. $[\text{SMX}]_0 = 1 \text{ mg L}^{-1}$; $[\text{Fe}]_0 = 5 \text{ mg L}^{-1}$; $[\text{H}_2\text{O}_2]_0 = 50 \text{ mg L}^{-1}$.

From Figure 2a, different behaviour on SMX degradation can be appreciated in photo-Fenton at near neutral pH, depending on the iron chelate. Total SMX removal was achieved at the end of the treatment when using EDTA-Fe (1.5 kJ L^{-1} ; 120 min) while in the case of EDDHA-Fe only a 17.8% of degradation was observed. Experiments with EDDS-Fe showed the highest degradation kinetics until 0.6 kJ L^{-1} (corresponding to 45 min) and then it dropped significantly until nearly complete degradation (93.3% at 1.5 kJ L^{-1}). DTPA-Fe and HEDTA-Fe mediated treatments resulted in close removal profiles throughout entire experiment, obtaining a degradation of 91.0 and 90.2% at 1.5 kJ L^{-1} , respectively. As mentioned before, the characteristics of the ligand is important in

reactions involving iron chelates. In this sense, the stability constant of each ligand with iron is a parameter to consider, but not the only one. Highest stability constant value of the studied chelates is 35.1, corresponding to EDDHA-Fe(III) [37]. This value is in accordance with the lowest total iron precipitation (3.6% at the end of the experiment) displayed in Figure 2b, and also with the lowest SMX degradation (see Fig. 2a). On the contrary, EDDS showed the highest precipitation of iron (71.2% at 1.5 kJ L⁻¹), in accordance with its stability constant with iron (III) that is 22.0 [38]. The stability constants with iron (III) for EDTA, DTPA and HEDTA are 25.1, 28.6 [39] and 19.8 [40], respectively, and the iron precipitation at the end of the experiment was 37.4%, 8.1% and 7.7%, respectively (see Figure 2b). From these results it seems that a high chelate-Fe stability constant reduces the SMX degradation. However, a clear trend in this way was not observed. For instance, even though HEDTA and DTPA have different stability constants of their complexes with iron (III), iron precipitation and SMX removal were very similar. This fact could evidence the existence of other structural factors of iron chelates that could affect to mechanisms in hydroxyl radical generation apart from the classical Fenton and photo-Fenton reactions.

In the literature related to the Fenton reactions with EDDS-Fe chelates, some authors state that reactions between oxidants and EDDS-Fe complexes could be interpreted analogously to homogeneous processes taking place with free iron at acidic pH (reaction r10 and r11) [41]. Other works propose the contribution of the breakdown of Fe-EDDS complex in Fenton reactions, forming EDDS radical (EDDS[•]) (reaction r12 and r13) [42] or EDDS^{•+} (reaction r14) [43] together with radical species like hydroxyl and superoxide radicals.





To determine the possible contribution of iron chelate breakdown on the Fenton performance when using the studied fertilizers, experiments (without light) were performed (see Figure 3a). The evolution of total iron was also evaluated and displayed in Figure 3b. EDDHA-Fe was not included due to the low degradation in Fenton tests at the end of the treatment.

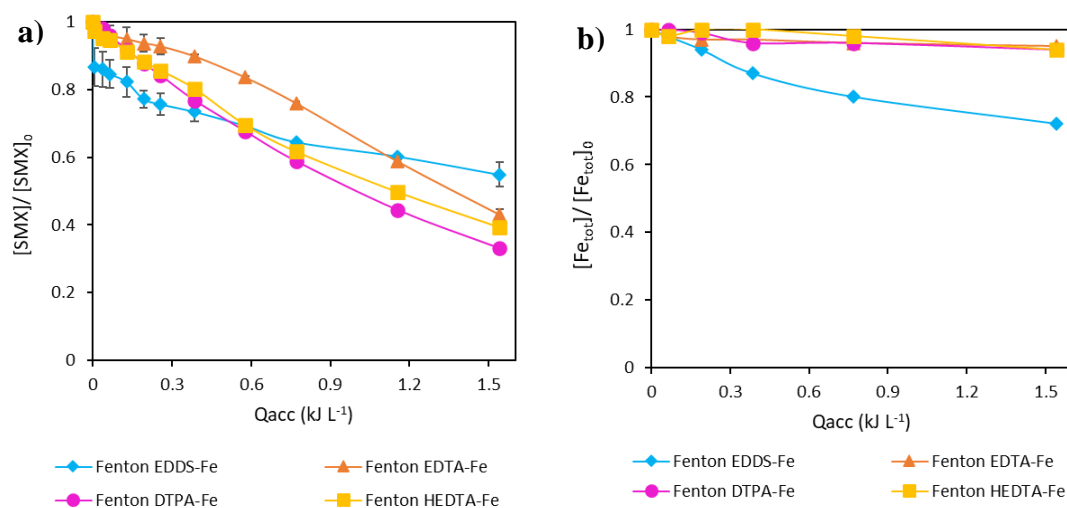


Figure 3. a) SMX abatement and b) evolution of total dissolved iron plotted as a function of the accumulated energy for Fenton experiments with four different iron chelates. $[SMX]_0 = 1 \text{ mg L}^{-1}$; $[Fe]_0 = 5 \text{ mg L}^{-1}$; $[H_2O_2]_0 = 50 \text{ mg L}^{-1}$.

From the iron precipitation gathered in Fig. 3b, it was deduced that the main reactions in Fenton process when using DTPA-Fe, HEDTA-Fe and EDTA-Fe are reaction r10 and r11, since the chelate-Fe ligand breakdown and iron release is minimum. In the case of EDDS-Fe, the iron precipitation was significantly higher, up to 28.4% after 2 hours of treatment. Therefore, these results are in accordance with previous works performed with EDDS (reactions r10-13).

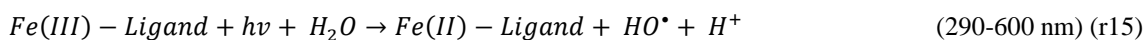
Comparing Figures 2a and 3a, the role of solar irradiation in the photo-Fenton experiments can be appreciated. Pseudo-first order kinetics was also fitted for Fenton and photo-Fenton experiments and presented in Table 1. In photo-Fenton experiments with EDDS-Fe, high iron release was observed from 30 minutes of reaction. This fact implies that the kinetics from this point cannot be considered as pseudo-first order, and EDDS-Fe kinetics were determined until 30 minutes. The kinetics of EDDS-Fe were not compared with the kinetics of other organic fertilizers since in these cases the pseudo-first order kinetics was evaluated until 120 minutes.

Table 1. Removal of SMX and total iron in solution in photo-Fenton and Fenton tests at near neutral pH, with different organic fertilizers. The presented values are at the end of the treatment (1.5 kJ L^{-1} ; 120 min). k is the calculated kinetic constant (pseudo-first order) for each ligand-Fe (from 0 to 1.5 kJ L^{-1} , 120 min). *For EDDS, kinetic constants for both treatments were calculated considering data obtained from 0 to 0.39 kJ L^{-1} (30 min), i.e., within the linear range of the pseudo first-order plot.

Treatment	Iron chelates	SMX degradation (%)	k (kJ^{-1})	R^2	Fe_{tot} in solution (%)
photo-Fenton	EDDS-Fe	93.3	5.32*	0.97*	28.8
	EDTA-Fe	100.0	3.85	0.99	62.6
	DTPA-Fe	91.0	1.56	0.99	91.9
	HEDTA-Fe	90.2	1.52	0.99	92.3
Fenton	EDDS-Fe	47.5	0.63*	0.85*	71.6
	EDTA-Fe	56.8	0.35	0.98	95.0
	DTPA-Fe	66.9	0.71	0.99	94.0
	HEDTA-Fe	60.6	0.60	0.99	94.2

DTPA-Fe, HEDTA-Fe and EDTA-Fe photo-Fenton tests achieved higher degradations than Fenton experiments at the end of the treatment (see Table 1). This can be related to the existence of a photoredox cycle for iron, which in presence of solar light, reduces iron

chelates from Fe(III) to Fe(II), leading the generation of hydroxyl radicals (r15) (*Ligand* applicable to DTPA, HEDTA and EDTA).



However, there were significant differences in the precipitation of iron in all cases (see Figures 2b, 3b and Table 1). In the presence of solar light, the breakdown of iron complexes may be due to the attack of hydroxyl radical and/or photodegradation, depending on the structure of the ligand. The iron precipitation in experiments performed with DTPA-Fe and HEDTA-Fe was only 2% higher in photo-Fenton than in Fenton process. Thus, in that cases, the contribution of irradiation on the breakage of the iron complexes was minimum. This is in accordance with their higher stability. For EDTA, iron remained chelated with the chelate during Fenton reaction (5% of iron precipitation) but the metal precipitation reached 37.4% at the end of the photo-Fenton treatment, indicating the contribution of photodegradation of EDTA-Fe ligand. In the case of EDDS-Fe, interestingly, this breakage seems to proceed through both pathways (28.4% and 71.2% of iron precipitation for Fenton and photo-Fenton tests, respectively). In that case, the influence of irradiation together with the possible HO[•] contribution on iron complex breakage is more evidenced in photo-Fenton. These results are in accordance with the lowest stability constant of EDDS with iron.

From the results of SMX degradation in Fenton and photo-Fenton experiments shown in Table 1, it is also observed that the irradiation affects differently depending on the stability of iron chelate with iron. The SMX oxidation rates in DTPA-Fe and HEDTA-Fe mediated photo-Fenton were only 2.2 and 2.5 times higher than those in Fenton, respectively, in accordance with their higher stability. On the other hand, the degradation kinetics were 11 and 8.4 times faster when employing less stable EDTA-Fe and EDDS-Fe complexes. Nevertheless, a special case is that of EDDS-Fe. At initial times (until 0.39

kJ L^{-1}) presented the highest kinetic rate but then reached the lowest degradation at the end of the treatment (only 47.5%). This fact could be related to the r10 reaction where the Fe(II)-EDDS reacts with H_2O_2 giving a great amount of hydroxyl radicals due to the low stability of that chelating agent with iron.

Summarizing and according with our results and those from the literature, there are strong evidences of photoexcitation of EDDS-Fe and subsequent potential formation of EDDS radical (EDDS $^{\bullet}$), which can be involved in further reactions to generate hydroxyl radicals. In that case, the precipitation of iron was very high. However, the precipitation of iron for the other organic fertilizers was significantly lower. These data, together with the comparison between Fenton and photo-Fenton experiments exposed, point out that the generated species and mechanisms participating in the solar photo-Fenton process could be different for each chelating agent.

3.1.2. Irradiation experiments without H_2O_2

With this in mind, irradiation experiments without H_2O_2 were carried out with the different iron chelates (see Figures 4a, 4b) to establish the relative photo-susceptibilities of the different complexes and its influence on the target MPs degradation mechanisms.

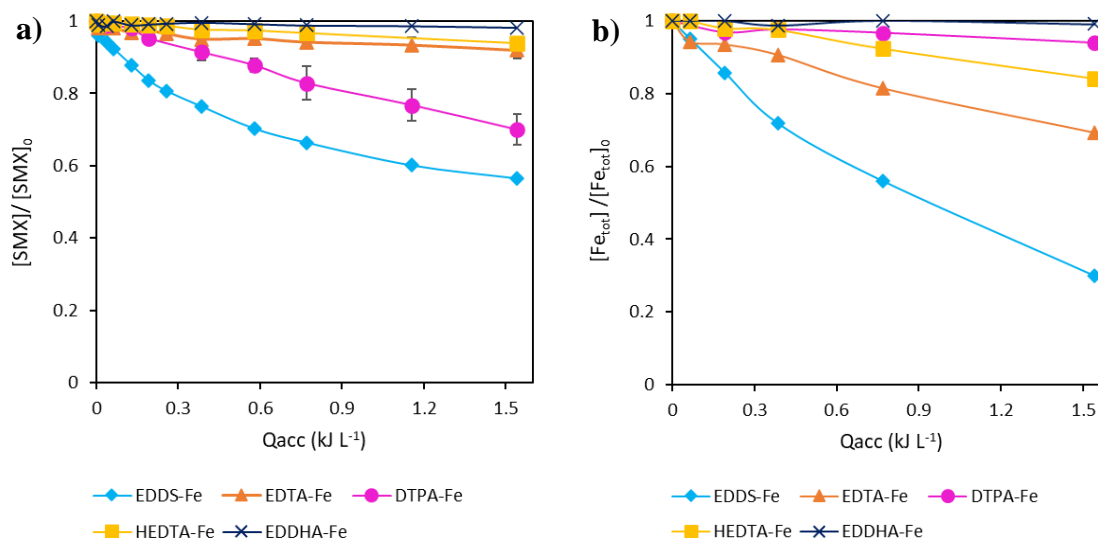


Figure 4. a) SMX abatement and b) evolution of total dissolved iron plotted as a function of the accumulated energy for irradiation experiments without H₂O₂ for five different iron chelates at pH = 7.5 ± 0.2. [SMX]₀ = 1 mg L⁻¹; [Fe]₀ = 5 mg L⁻¹.

As it can be observed in Figure 4a, the irradiation tests with EDDS-Fe and DTPA-Fe yielded significant SMX removal. At the end of the experiment (1.5 kJ L⁻¹; 120 min), the degradation results were 43.5 and 30.0% for EDDS-Fe and DTPA-Fe, respectively. The result of EDDS-Fe was not fully unexpected, as the same behavior has been observed in previous studies related to photodegradation of this iron complex [17, 22, 24, 41]. In Particular, Ciésła and coworkers [22] proposed a photodegradation mechanisms for EDDS-Fe that lies in the photoreduction of Fe(III) complex induced by light by the ligand-to-metal charge transfer (LMCT) (reaction r16; 290-600 nm). This excitation can lead to a reduction of Fe(III) to Fe(II) followed by one-electron oxidation of the ligand by the inner-sphere photoinduced electron transfer [22].



The radical formed via reaction r16 (EDDS^{*3-}) tends to reach its stable oxidation state requiring a second electron transfer through reaction with dissolved oxygen (reaction r17) [22].

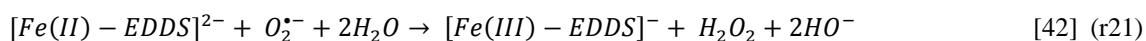
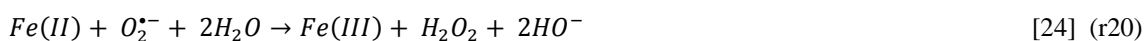


The superoxide radical generated in r17 can take part in additional reactions as a precursor of hydroxyl radical.

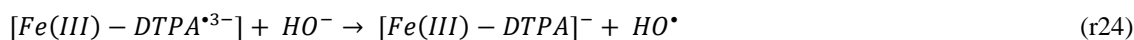
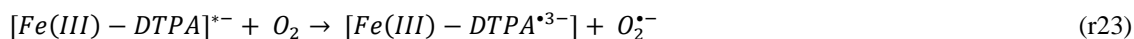
Additionally, $EDDS^{*3-}$ can react with the Fe(III) complex, enhancing the Fe(III)/Fe(II) cycle (reaction r18), as well as with hydroxyl ion (OH^-) to generate HO^\bullet (reaction r19).



According to our data gathered in Figures 4a and b, the results with EDDS-Fe appear to indicate the possibility of generating $EDDS^{*3-}$ due to the photodegradation of Fe-complex causing great amount of Fe (II) release during the experiment. This is supported by the fact that a large part of the iron precipitates when the complex breaks up. However, a small part of this could react with superoxide radical to generate H_2O_2 (reaction r20) [24]. On its part, $[Fe(II)-EDDS]^{2-}$ formed in reaction (r18) can also react with superoxide radical to produce H_2O_2 (reaction r21).



As observed in Figures 4a and b, not all Fe-complexes had the same behavior as that observed for EDDS-Fe. DTPA-Fe irradiation experiments resulted in 30.0% of SMX abatement but only 8.0% iron precipitation and, consequently, the reduction of Fe(III) to Fe(II) from the photoexcitation of the complex and subsequent iron complex breakage (reaction r22), did not significantly occur. Thus, the main photo-induced reactions mechanism for oxidants generation with DTPA-Fe would be different from those of EDDS-Fe. The main involved reactions are proposed for first time in this study, and presented in r23 and r24.



For DTPA, the electron transfer to molecular oxygen would proceed through the excited Fe(III)-complex ($[Fe(III)-DTPA]^{*-}$) to generate superoxide radical (reaction r23), which would be involved in further reactions to generate hydroxyl radical. However, the reduction of $[Fe(III)-DTPA]^-$ to $[Fe(II)-DTPA]^{2-}$ is possible by reaction (r15), and subsequent formation of H_2O_2 according to reaction (r21). In addition, H_2O_2 could also be generated by reaction (r20) even though it is unlikely as only 8.0% of iron release was observed with this organic fertilizer.

Further experiments without H_2O_2 were performed to investigate the possible formation of H_2O_2 by means of irradiation (290-600 nm) of DTPA-Fe solutions (without peroxide addition). The results suggested the generation of small amounts of H_2O_2 , with maximum observed concentrations of 0.7 mg L^{-1} after two hours of experiment. Increasing iron concentration (chelated with DTPA) to 20 mg L^{-1} , which also implies an increase of the ligand concentration, the maximum detected concentration of H_2O_2 was 5.2 mg L^{-1} . Thus, in the experiments without initial H_2O_2 (Figure 4a), its generation could produce HO^{\bullet} by photo-Fenton reactions, a fact which agreed with the little hydrogen peroxide consumed during the photo-Fenton experiments (data not shown). Additionally, to ensure that the photoactive species were the Fe-complexes, experiments without iron were performed. No SMX degradation was observed, confirming the suggested reactions.

EDTA-Fe and HEDTA-Fe presented a completely different behaviour. In these cases, especially for EDTA-Fe, a photoexcitation of iron complex was observed on the basis of iron precipitation throughout the experiment (30.7% of iron release for EDTA-Fe at 2

hours). This amount is higher than that for DTPA-Fe (only 6.0% at the end of the experiment), but the degradation of SMX was almost null in EDTA-Fe (only 6.3%). In the case of HEDTA-Fe, these percentages at the end of the experiment were 15.8% and 6.2% for iron precipitation and SMX removal, respectively. These results suggest that the species formed by the photodegradation of EDTA-Fe and HEDTA-Fe would not be involved in the same way as the EDDS-Fe and DTPA-Fe, concerning the generation of ROS. For this reason, when degradation mechanisms are evaluated, it is important to study diverse iron complexes, as their different characteristics can lead to different behaviours.

To understand the role of superoxide radical probably formed in the above reaction mechanisms, experiments with *tert*-butyl alcohol in the photo-Fenton tests were also carried out and depicted in Figure 5. EDDHA-Fe was not studied in this regard due to its low SMX degradation in photo-Fenton experiments. *t*BuOH has an elevated reaction rate with HO[•] ($6 \times 10^8 \text{ M}^{-1} \text{ s}^{-1}$) [44]. Scavengers of superoxide radical, like benzoquinone, were not employed in this study because they are not completely selective for O₂^{•-} (in general they also react with HO[•]) [45].

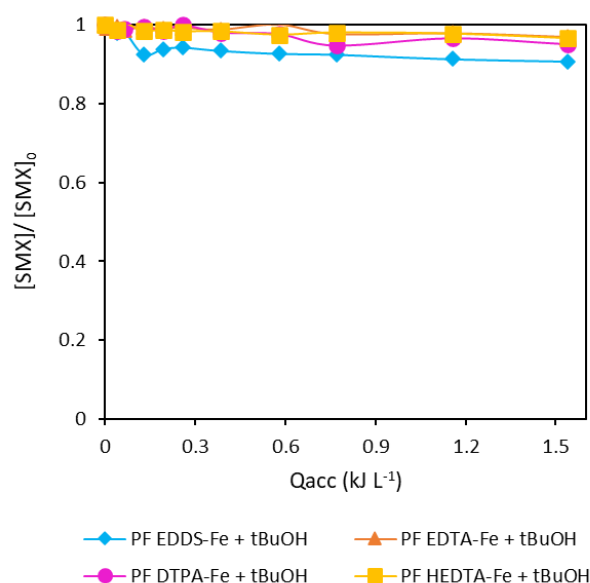


Figure 5. SMX degradation as a function of the accumulated energy for photo-Fenton experiments with tBuOH for four different iron chelates at $\text{pH}=7.5 \pm 0.2$. $[\text{SMX}]_0 = 1 \text{ mg L}^{-1}$; $[\text{Fe}]_0 = 5 \text{ mg L}^{-1}$; $[\text{H}_2\text{O}_2] = 50 \text{ mg L}^{-1}$; $[\text{tBuOH}] = 25 \text{ mM}$.

As it can be observed in Figure 5, the same level of SMX degradation was reached for all EDTA-Fe, DTPA-Fe and HEDTA-Fe when tBuOH was present in the reaction medium (about 5.0% of SMX removal at the end of the treatment). Only EDDS-Fe achieved the slightly higher value of 9.2% in 2 hours. As tBuOH was calculated for 95% of scavenging effect, the results indicated that HO^\bullet generated directly by photo-Fenton reactions and mediated by the photoexcitation of Fe-complexes (EDDS-Fe and DTPA-Fe) was the specie involved in the degradation of SMX. In the case of EDDS-Fe, although it is the main specie in the removal of SMX, the abatement of 9.2% (when tBuOH was added) confirmed that other ROS would be implicated in the degradation mechanisms of SMX in the presence of dissolved oxygen.

To complete this section, experiments with non-chelated iron were investigated in an attempt of elucidating the possible involvement of free iron in solution in the degradation

mechanisms of SMX. This iron is formed from the breakdown of the iron complex and before generating $\text{Fe}(\text{OH})_2^+$, which is the predominant specie at $\text{pH}=7.5$ [36]. As observed, when organic fertilizers complexed with iron were used, the greater iron release was followed by higher reaction rate in SMX. This fact can lead to confusion in the degradation mechanisms. For this reason, the precipitation curves in photo-Fenton experiments catalyzed by EDDS-Fe and DTPA-Fe (Figure 2b) were used to determine the potential free iron in solution for both experiments. From Figure 2b, the difference in concentration of chelated iron in solution at two different times DTPA-Fe and EDDS-Fe (for instance concentration of iron precipitated between 0 and 5 min (0 and 0.1 kJ L^{-1}), 5 and 15 min (0.1 kJ L^{-1} and 0.2 kJ L^{-1}) ...) was used to elaborate a Fe(II) dosing plan during the experiments without chelating agent. The selection of these two organic fertilizers was thought with the objective to study the iron dose at different concentrations, being the highest iron dose with EDDS-Fe and the lowest with DTPA-Fe since EDDS-Fe presents the highest iron release and DTPA-Fe the lowest one. The dosage plan is depicted in Figures 6a and 6b. Figure 6a corresponds to the iron concentration added at each time (min) or energy (kJ L^{-1}). Thus, the iron concentration added at 0 kJ L^{-1} (0 min) corresponds to the concentration of iron which was precipitated in the photo-Fenton experiments between 0 and 5 minutes (0 and 0.1 kJ L^{-1}). In the same way, the iron concentration added at 0.8 kJ L^{-1} (60 min) corresponds the iron release between 60 and 120 minutes (0.8 and 1.5 kJ L^{-1}). The same can be commented for the other intervals considered (0.1 , 0.2 and 0.4 kJ L^{-1}). Figure 6b was referred to accumulated iron added during the Fe (II) dosage experiment, not corresponding to the total dissolved iron. As the pH was 7.5 , part of this added Fe (II) precipitated due to the formation of $\text{Fe}(\text{OH})_2^+$. In Figure 6b it is observed that a total of 2.2 mg L^{-1} of Fe (II) was added in one case, following the precipitation curve of iron in EDDS-Fe (see Figure 2b where 2.2 mg L^{-1} of

iron were precipitated at 120 minutes). Following the iron precipitation curve of DTPA-Fe, only 0.4 mg L^{-1} of Fe (II) were precipitated at the end of the experiment, which corresponds with the total iron added in the experiments without chelating agent (Figure 6b). To perform these experiments a stock solution of Fe (II) at $\text{pH}=2.8$ was prepared. From these stock solution different aliquots, at established times, were taken and added to the solution to be treated. To compare with photo-Fenton experiments with organic fertilizers, the pH of the solution was followed during the entire reaction, remaining constant until the end of the experiment ($\text{pH} = 7.5 \pm 0.2$).

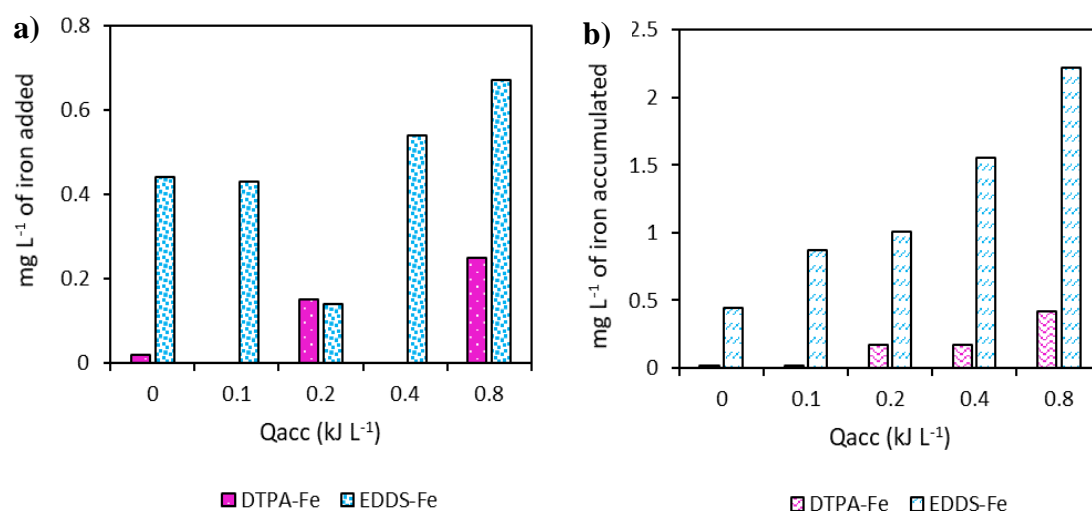


Figure 6. a) Iron dosification b) accumulated iron as a function of the accumulated energy in photo-Fenton experiments without chelating agents following the iron precipitation curves of photo-Fenton catalyzed by EDDS-Fe and DTPA-Fe. $\text{pH}=7.5 \pm 0.2$. $[\text{SMX}]_0 = 1 \text{ mg L}^{-1}$; $[\text{H}_2\text{O}_2] = 50 \text{ mg L}^{-1}$.

The results of the SMX removal at the end of the experiment (2 hours, 1.5 kJ L^{-1}) were 16.6 and 13.7% for the total dosage of 2.2 and 0.4 mg L^{-1} , corresponding to the iron precipitation curve of EDDS-Fe and DTPA-Fe, respectively. These results represented a great reduction of SMX removal compared to photo-Fenton using organic fertilizers where 94.7 and 91.0% were reached at 2 hours. This fact evidenced that at studied conditions, iron chelates were involved in the photo-Fenton reactions. A small part of the

SMX degradation could be caused by dissolved iron before precipitating as Fe(III) oxyhydroxides. However, it was not the main generation pathway of HO[•].

3.2. Contribution of dissolved oxygen

To corroborate the role of dissolved oxygen on photo-Fenton reactions catalyzed by Fe-complexes, photo-Fenton tests were subjected to continuous N₂ bubbling. The results are depicted in Figures 7a, b, c and d, corresponding to experiments with EDDS-Fe, EDTA-Fe, DTPA-Fe and HEDTA-Fe, respectively. In the case of EDDS-Fe and DTPA-Fe, experiments without H₂O₂ were also tested under N₂ bubbling. The results are also shown in Figures 7a and 7c. Table 2 reports the corresponding pseudo-first order reaction rates.

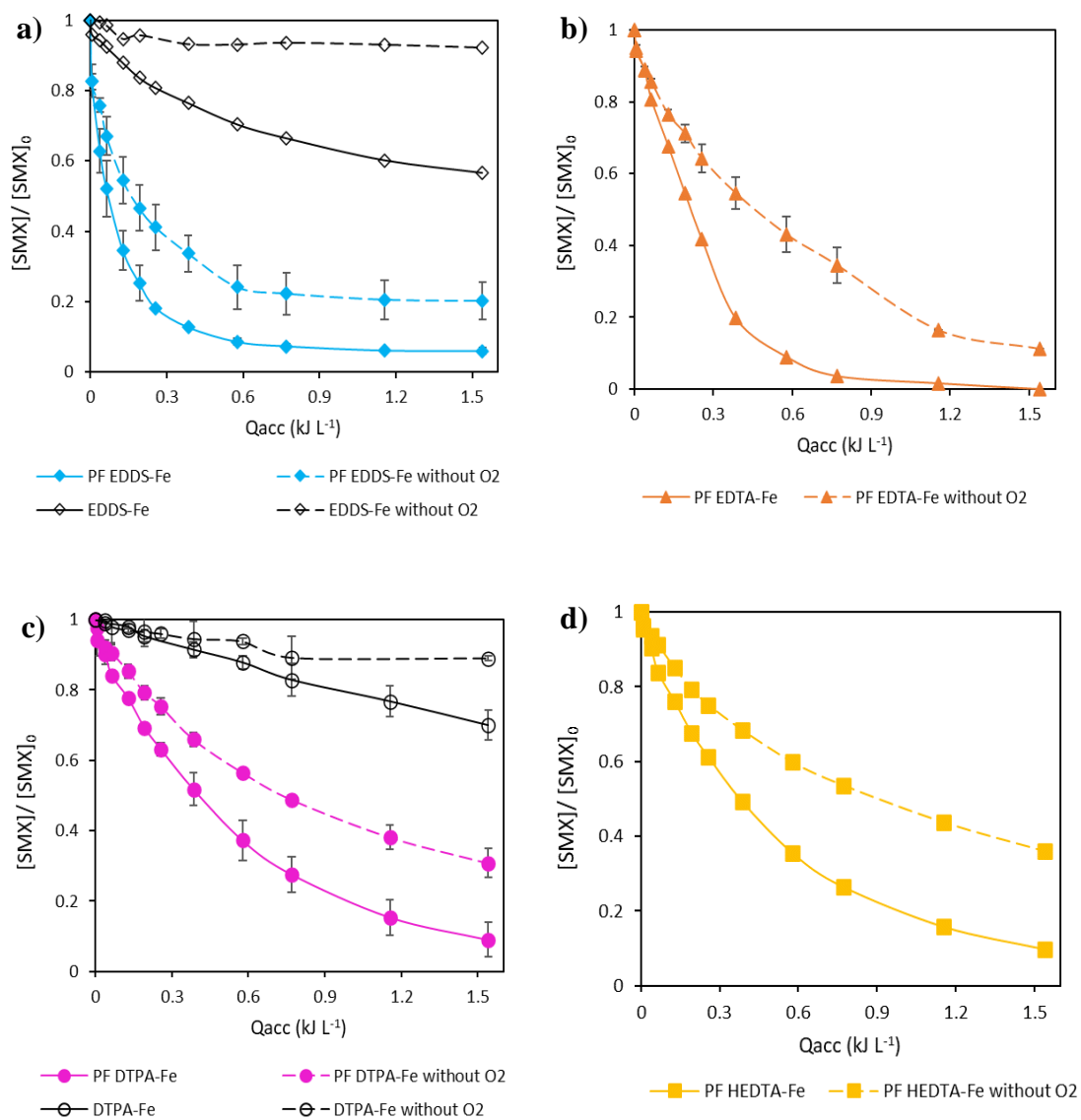


Figure 7. Photo-Fenton experiments without dissolved O_2 (continuously bubbling N_2) for a) EDDS-Fe, b) EDTA-Fe, c) DTPA-Fe and d) HEDTA-Fe as a function of the accumulated energy. Opened symbols corresponds to irradiation experiments without H_2O_2 and closed symbols refers to photo-Fenton experiments. $pH = 7.5 \pm 0.2$. $[SMX]_0 = 1 \text{ mg L}^{-1}$; $[H_2O_2] = 50 \text{ mg L}^{-1}$.

Table 2. Pseudo-first order kinetics and SMX removal for each organic fertilizer in photo-Fenton with and without dissolved O₂ (from 0 to 1.5 kJ L⁻¹, 120 min). *For EDDS, kinetic constants for two treatments were calculated considering data obtained from 0 to 0.39 kJ L⁻¹ (30 min), i.e., until a linear trend is observed in the pseudo first-order plot.

Treatment	Iron chelates	SMX degradation (%)	k (kJ ⁻¹)	R ²
photo-Fenton with O ₂	EDDS-Fe	93.3	5.32*	0.97*
	EDTA-Fe	100.0	3.85	0.99
	DTPA-Fe	91.0	1.56	0.99
	HEDTA-Fe	90.2	1.52	0.99
photo-Fenton without O ₂	EDDS-Fe	79.8	1.41*	0.86*
	EDTA-Fe	88.8	1.42	0.99
	DTPA-Fe	69.2	0.77	0.99
	HEDTA-Fe	64.0	0.66	0.98

As can be seen from the results, dissolved oxygen plays an important role in the SMX degradation mechanisms in all cases. The reductions in kinetic constants in anoxic conditions, compared to photo-Fenton experiments with dissolved oxygen, were: 3.8, 2.7, 2.0 and 2.3 times for EDDS-Fe, EDTA-Fe, DTPA-Fe and HEDTA-Fe, respectively. As the iron release was the same in the two types of experiments, the results suggested that the role of the oxygen was more important at greater iron precipitation (and possible subsequent ligand radical formation). This fact evidenced the reactions explained in section 3.1.2 where the Fe-complexes together with irradiation (290-600 nm) could lead the formation of superoxide radical as a precursor of hydroxyl radicals. This fact can also be observed in Figures 7a and 7c, where results of experiments using EDDS-Fe and DTPA-Fe without H₂O₂ nor O₂ were represented. Irradiation experiments without H₂O₂ achieved 43.5% and 30.0% of SMX removal EDDS-Fe and DTPA-Fe, respectively. In

the same experiments under anoxic conditions the SMX degradations were reduced to 7.8 and 11.0% for EDDS-Fe and DTPA-Fe, respectively, evidencing the role of oxygen in the removal mechanisms. The low SMX abatement seen in these last experiments could be related to the no generation of H_2O_2 through reactions explained in section 3.1.2.

Finally, in the case of EDTA-Fe and HEDTA-Fe it was seen that the mechanisms could be a little different due to low SMX degradation was observed in the experiments without H_2O_2 . Probably in these cases, due to the characteristics of the organic fertilizers, the superoxide radical generated can affect more the Fe(III)/Fe(II) cycle which in photo-Fenton process is an additional way to produce hydroxyl radicals [17, 36].

4. Conclusions

This work has demonstrated that radical's production mechanisms of the photo-Fenton process using the five organic fertilizers studied (EDDS-Fe, EDTA-Fe, DTPA-Fe, HEDTA-Fe and EDDHA-Fe) present differences, due to different UV absorbance and stability constant of chelate with iron. All iron complexes obtained more than 90% of SMX removal at 2 hours, except EDDHA-Fe which achieved only 17.8%. The organic fertilizers with lower stability with iron achieved the best kinetic rates (EDDS-Fe and EDTA-Fe) together with higher iron release at the end of the experiment (about 70% and 40% for EDDS-Fe and EDTA-Fe, respectively). This fact was evidenced comparing Fenton and photo-Fenton experiments, which revealed that radiation plays an important role in the photoredox cycle of iron and subsequent hydroxyl radical generation, especially for iron complexes less stable.

The results obtained from irradiation tests without H_2O_2 evidenced differences in the five organic fertilizers tested and, although all of them absorb in the range of 290-400 nm, only EDDS-Fe and DTPA-Fe showed significant SMX degradation (43.5% and 30.0%, respectively). Since the iron release was very different (70.0 and 8.0% for EDDS-Fe and

DTPA-Fe, respectively), the mechanisms in hydroxyl radical formation are potentially different. According to the literature, photoexcitation of EDDS-Fe(III) complex gives EDDS radical ($\text{EDDS}^{\cdot 3-}$), which react with dissolved O_2 to form superoxide radical. This specie is involved in further reactions to produce hydroxyl radicals. However, since in tests using DTPA-Fe the iron precipitation was minimum, the proposed mechanisms established that the electron transfer to molecular oxygen would proceed through the excited Fe(III)-complex ($[\text{Fe(III)-DTPA}]^*$) to generate the superoxide radical and subsequent hydroxyl radicals generation. The scavenging experiments with tBuOH determined that hydroxyl radicals were the final specie responsible to SMX removal. Additionally, the production of H_2O_2 was observed during this test and, although its concentration was very low, can promote the photo-Fenton reactions and subsequent formation of hydroxyl radicals. The experiments performed with EDTA-Fe and HEDTA-Fe evidenced again that photoexcitation mechanisms are different for iron complexes. In that cases, only 6% of SMX degradation was achieved and 30.7 and 15.8% of iron release were observed for EDTA-Fe and HEDTA-Fe, respectively.

The photo-Fenton experiments bubbling N_2 revealed the importance of oxygen-mediated reactions in the in the generation of radicals at neutral pH with iron complexes, being reinforced by the increase in SMX abatement in presence of dissolved oxygen. Finally, photo-Fenton tests with non-chelated iron were done to elucidate the possible involvement of free iron in solution (formed in the breakdown of the iron complex and before it precipitates) in the SMX degradation mechanisms. Experiments showed a low SMX removal (16.6% at 2 hours, with higher iron concentration added), demonstrating that the photo-Fenton reactions with iron chelates are the main pathway in the process.

Acknowledgments

The authors are grateful with the Ministry of Economy and Competitiveness (project CTQ2017-86466-R, MINECO/FEDER, UE), AGAUR-Generalitat de Catalunya (project 2017SGR-131) and Nuria López FPU research fellowship (FPU-16/02101) financed by Ministry of Science, Innovation and Universities.

References

- [1] Food and Agriculture Organization of the United Nations. (2021). Land & Water: Water scarcity. Consulted at: <http://www.fao.org/land-water/world-water-day-2021/water-scarcity/en/>.
- [2] European Commission, Proposal for a Regulation of the European Parliament and of the Council of 28 May 2018 establishing the minimum requirements for water reuse, Off. J. Eur. Communities. 337 (2018) 1-27.
- [3] A. Cruz-Alcalde, C. Sans, S. Esplugas, Priority pesticides abatement by advanced oxidation water technologies: The case of acetamiprid removal by ozonation, Science of the Total Environment 599-600 (2017) 1454-1461.
- [4] M.M. Huber, S. Canonica, G.Y. Park, U. Von Gunten, Oxidation of pharmaceuticals during ozonation and advanced oxidation processes, Environmental Science and Technology 37 (2003) 1016–1024
- [5] Y. Aguas, M. Hincapie, P. Fernández-Ibáñez, M.I. Polo-López, Solar photocatalytic disinfection of agricultural pathogenic fungi (*Curvularia sp.*) in real urban wastewater, Science of the Total Environment 607-608 (2017) 1213-1224.

- [6] N. López, S. Plaza, A. Afkhami, P. Marco, J. Giménez, Treatment of diphenhydramine with different AOPs including photo-Fenton at neutral pH, *Chemical Engineering Journal* 318 (2017) 112-120.
- [7] S. Miralles-Cuevas, D. Darowna, A. Wanag, S. Mozia, S. Malato, I. Oller, Comparison of UV/H₂O₂, UV/S₂O₈²⁻, solar/Fe(II)/H₂O₂ and solar/Fe(II)/S₂O₈²⁻ at pilot plant scale for the elimination of micro-contaminants in natural water, *Chemical Engineering Journal* 310 (2017) 514–524.
- [8] J. Rodríguez-Chueca, M.P. Ormad, R. Mosteo, J.L. Ovelleiro, Kinetic modelling of *Escherichia coli* and *Enterococcus spp.* Inactivation in wastewater treatment by photo-Fenton and H₂O₂ UV-vis processes, *Chemical Engineering Science* 138 (2015) 730-740.
- [9] N. López-Vinent, A. Cruz-Alcalde, C. Gutiérrez, P. Marco, J. Giménez, S. Esplugas, Micropollutant removal in WW by photo-Fenton (circumneutral and acid pH) with BLB and LED lamps, *Chemical Engineering Journal* 379 (2020) 122416.
- [10] A. Serra-Clusellas, L. De Angelis, C.H. Lin, P. Vo, M. Bayati, L. Sumner, Z. Lei, N.B. Amaral, L.M. Bertini, J. Mazza, L.R. Pizzio, J.D. Stripeikis, J.A. Rengifo-Herrera, M.M. Fidalgo de Cortalezzi, Abatement of 2,4-D by H₂O₂ solar photolysis and solar photo-Fenton-like process with minute Fe(III) concentrations, *Water Research* 144 (2018) 572-580.
- [11] I. Carra, J.A. Pérez Sánchez, S. Malato, O. Autin, B. Jefferson, P. Jarvis, Application of high intensity UVC-LED for the removal of acetamiprid with the photo-Fenton process, *Chemical Engineering Journal* 264 (2015) 690-696.

- [12] I. De la Odra, L. Ponce-Robles, S. Miralles-Cuevas, I. Oller, S. Malato, J.A. Sánchez Pérez, Microcontaminant removal in secondary effluents by solar photo-Fenton at circumneutral pH in raceway pond reactors, *Catalysis Today* 287 (2017) 10–14.
- [13] N. López-Vinent, A. Cruz-Alcalde, J.A. Malvestiti, P. Marco, J. Giménez, S. Esplugas, Organic fertilizer as a chelating agent in photo-Fenton at neutral pH with LEDs for agricultural wastewater reuse: Micropollutant abatement and bacterial inactivation, *Chemical Engineering Journal* 388 (2020) 124246.
- [14] S. Nahim-Granados, I. Oller, S. Malato, J.A. Sánchez Pérez, M.I. Polo-López, Commercial fertilizer as effective iron chelate (Fe^{3+} -EDDHA) for wastewater disinfection under natural sunlight for reusing in irrigation, *Applied Catalysis B: Environmental* 253 (2019) 286-292.
- [15] N. López-Vinent, A. Cruz-Alcalde, J. Giménez, S. Esplugas, C. Sans, Improvement of the photo-Fenton process at natural condition of pH using organic fertilizers mixtures: potential application to agricultural reuse of wastewater, *Applied Catalysis B: Environmental*, 290 (2021) 120066.
- [16] W. Schenkeveld, E. Temminghoff, The effectiveness of FeEDDHA chelates in mending and preventing iron chlorosis in soil-grown soybean plants, in: H.A. El-Shemy (Ed.), *Soybean Physiology and Biochemistry*, InTech, Rijeka, Croatia, 2011, pp 83-108.
- [17] W. Huang, M. Brigante, F. Wu, K. Hanna, G. Mailhot, Development of a new homogeneous photo-Fenton process using Fe(III)-EDDS complexes, *Journal of Photochemistry and Photobiology A: Chemistry* 239 (2012) 17-23.

- [18] L. Clarizia, D. Russo, I. Di Somma, R. Marotta, R. Andreozzi, Homogeneous photo-Fenton processes at near neutral pH: A review, *Applied Catalysis B: Environmental* 209 (2017) 358-371.
- [19] S. Miralles-Cuevas, I. Oller, J.A. Sánchez Pérez, S. Malato, Removal of pharmaceuticals from MWTP effluent by nanofiltration and solar photo-Fenton using two different iron complexes at neutral pH, *Water Research* 64 (2014) 23-31.
- [20] U.J. Ahile, R.A. Wuana, A.U. Itodo, R. Sha'Ato, R.F. Dantas, A review on the use of chelating agents as an alternative to promote photo-Fenton at neutral pH: Current trends, knowledge gap and future studies, *Science of the Total Environment* 710 (2020) 134872.
- [21] C.A.L. Graça, A. Correia de Velosa, A.C. S.C. Teixeira, Role of Fe(III)-carboxylates in AMZ photodegradation: A response surface study based on Doehlert experimental design, *Chemosphere* 184 (2017) 981-991.
- [22] P. Ciésła, P. Kocot, P. Mytych, Z. Stasicka, Homogeneous photocatalysis by transition metal complexes in the environment, *Journal of Molecular Catalysis A: Chemical* 224 (2004) 17-33.
- [23] Z. Stasicka, Chapter 7-Transition metal complexes as solar photocatalysts in the environment: a short review of recent development, in: van Eldik, Rudi, Stochel, Grazyna (Ed.), *Advances in Inorganic Chemistry*, 63, 2011, Academic Press, pp. 291e343.
- [24] J. Li, G. Mailhot, F. Wu, N. Deng, Photochemical efficiency of Fe(III)-EDDS complex: •OH radical production and 17-estradiol degradation, *Journal of Photochemistry and Photobiology A: Chemistry* 212 (2010) 1-7.

- [25] U. J. Ahile, R. A. Wuana, A. U. Itodo, R. Sha'Ato, R. F. Dantas, A review on the use of chelating agents as an alternative to promote photo-Fenton at neutral pH: Current trends, knowledge gap and future studies, *Science of the Total Environment* 710 (2020) 134872.
- [26] European Commission, Regulation (EC) No 2003/2003 of the European Parliament and of the Council of 13 October 2003 relating to fertilizers, *Official Journal of the European Communities*.
- [27] O. Golovko, S. Örn, M. Söregard, K. Friedberg, W. Nassazi, F.Y. Lai, L. Ahrens, Occurrence and removal of chemicals of emerging concern in wastewater treatment plants and their impact on receiving water systems, *Science of the Total Environment* 754 (2021) 142122.
- [28] L. Chen, W. Fu, Y. Tan, X. Zhang, Emerging organic contaminants and odorous compounds in secondary effluent wastewater: Identification and advanced treatment, *Journal of Hazardous Materials* 408 (2021) 124817.
- [29] S.Y. Bunting, D.J. Lapworth, E.J. Crane, J. Grima-Olmedo, A. Korosa, A. Kuczynska, N. Mali, L. Rosenqvist, M.E. van Vliet, A. Togola, B. López, Emerging organic compounds in European groundwater, *Environmental Pollution* 269 (2021) 115945.
- [30] Y. Luo, W. Guo, H.H. Ngo, L.D. Nghiem, F.I. Hai, J. Zhang, S. Liang, A review on the occurrence of micropollutants in the aquatic environment and their fate and removal during wastewater treatment, *Science of the Total Environment* 473–474 (2014) 619–641.

- [31] N. De la Cruz, V. Romero, R.F. Dantas, P. Marco, B. Bayarri, J. Giménez, S. Esplugas, O-Nitrobenzaldehyde actinometry in the presence of suspended TiO₂ for photocatalytic reactors, *Catalysis Today* 209 (2013) 209–214.
- [32] Guidelines for Water Reuse 600/R-12/618; Environmental Protection Agency: Washington, DC, USA, 2012.
- [33] R.S. Ayers, D.W. Westcot, *Water Quality for Agriculture*; Food and Agriculture Organization of the United Nations: Rome, Italy, 1985.
- [34] Rossmary Violette Romero Olarte (2015) Degradation of metoprolol by means of advanced oxidation processes (Doctoral Thesis). University of Barcelona, Spain.
- [35] R.F. Pupo Nogueira, M.C. Oliveira, W.C. Paterlini, Simple and fast spectrophotometric determination of H₂O₂ in photo-Fenton reactions using metavanadate, *Talanta* 66 (2005) 86-89.
- [36] J.J. Pignatello, E. Oliveros, A. Mackay, Advanced Oxidation Processes for organic contaminant destruction based on the Fenton reaction and related chemistry, *Critical Reviews in Environmental Science and Technology* 36 (1) (2006) 1-84.
- [37] M.A. Sierra, M. Gómez-Gallego, R. Alcázar, J.J. Lucena, F. Yunta, S. García-Marco, Effect of the tether on the Mg(II), Ca(II), Cu(II) and Fe(II) stability constants and pM values of chelating agents related to EDDHA, *Dalton Transactions* 21 (2004) 3741-3747.
- [38] M. Orama, H. Hyvönen, H. Saarinen, R. Aksela, Complexation of [S,S] and mixed stereoisomers of N,N'-ethylendiaminedisuccinic acid (EDDS) with Fe(III), Cu(II), Zn(II) and Mn(II) ions in aqueous solution, *Journal of the Chemical Society, Dalton Transactions* 24 (2002) 4644-4648.

- [39] Dojindo Molecular Technologies, Inc, Table of Stability Constants, (2020). https://www.dojindo.eu.com/images/Product%20Photo/Chelate_Table_of_Stability_Constants.pdf (accessed April 20, 2021).
- [40] A.E. Martell, R.J. Motekaitis, D. Chen, R.D. Hancock, D. McManus, Selection of new Fe(III)/Fe(II) chelating agents as catalysts for the oxidation of hydrogen sulphide to sulfur by air, *Canadian Journal of Chemistry* 74 (1996) 1872-1879.
- [41] W. Huang, M. Brigante, F. Wu, C. Mousty, K. Hanna, G. Mailhot, Assessment of the Fe(III)–EDDS Complex in Fenton-Like Processes: From the Radical Formation to the Degradation of Bisphenol A, *Environmental Science & Technology* 47 (4) (2013) 1952-1959.
- [42] S. Miralles-Cuevas, I. Oller, A. Ruíz-Delgado, A. Cabrera-Reina, L. Cornejo-Ponce, S. Malato, EDDS as complexing agent for enhancing solar advanced oxidation processes in natural water: Effect of iron species and different oxidants, *Journal of Hazardous Materials* 372 (2019) 129-136.
- [43] Y. Wu, M. Passananti, M. Brigante, W. Dong, G. Mailhot, Fe(III)–EDDS complex in Fenton and photo-Fenton processes: from the radical formation to the degradation of a target compound, *Environmental Science & Pollution Research* 21 (1) (2014) 12154-12162.
- [44] M. Piechowski, M.A. Thelen, J. Hoigné, R.E. Bühler, tert-Butanol as an OH scavenger in the pulse radiolysis of oxygenated aqueous systems. *Berichte der Bunsengesellschaft für Physikalische Chemie* 96 (1992) 1448–1454.

[45] N. Bustos, A. Cruz-Alcalde, A. Iriel, A. Fernández Cirelli, C. Sans, Sunlight and UVC-254 irradiation induced photodegradation of organophosphorus pesticide dichlorvos in aqueous matrices, *Science of the Total Environment* 649 (2019) 592-600.

5 Conclusions and recommendations

5.1 Conclusions

Conclusions are divided in three parts, according to the objectives of the research.,

Concerning the **efficiency of photo-Fenton using ultraviolet light emitting diodes (LEDs) as irradiation source**, it could be concluded that:

- Photo-Fenton with two UV-A LEDs wavelengths (380-390 nm and 390-400 nm) is effective for MPs removal in water.
- The combination of two wavelengths ranges reaches better performances on MPs, TOC, and COD removal than the use of a single range.
- The concentrations of Fenton reagents as well as an appropriate ratio $\text{Fe}^{2+} : \text{H}_2\text{O}_2$ are key parameters to achieve high kinetic rates and removals.
- Kinetic studies highlight the importance of Fe^{2+} concentration during the removal in first 30 seconds of reaction.

Regarding **the study and comparison of different irradiation sources (BLB lamps and LEDs) to perform photo-Fenton at acidic pH in four secondary effluents matrices**, it could be concluded that:

- The replacement of conventional lamps by LEDs in photo-Fenton tests is feasible, since similar yields were achieved in ultrapure water. However, the tests performed in secondary wastewater effluents using LEDs required higher irradiance to obtain reaction rates similar to BLB lamps.
- LED are punctual sources and the dark zones generated in the photoreactor, greatly affect the experiments carry out in secondary wastewater matrices. This is attributed to the turbidity and organic matter present in effluents influencing on the radiation field throughout the photoreactor.
- High DOC, turbidity and alkalinity of water matrices affect negatively to the efficiency of photo-Fenton process on MPs degradation.
- Photo-Fenton at circumneutral pH, catalyzed by EDDS-Fe(II), demonstrates its effectivity on MPs removal with more than 90% of abatement in ultrapure water.

- In wastewater effluents similar performances are obtained in photo-Fenton at acid and circumneutral pH, even best degradations are reached at circumneutral pH at the end of the treatment, except in IFAS.
- Comparing the process efficiency at acid and circumneutral pH in ultrapure water, the tests at acidic conditions give best yield. This is attributed to the fact that, in the first 30 seconds, about 50% of PROP is degraded in acid pH while only 10% in the experiments catalyzed by EDDS-Fe(II).

From the study of **new iron complexes to carry out the photo-Fenton process more efficiently in terms of iron release, MPs abatement and bacterial inactivation**, it could be concluded that:

- The use of the new organic fertilizers DTPA and HEDTA, as iron chelating agents, are effective in simultaneous MP removal and bacterial inactivation by photo-Fenton at natural pH.
- The stability constant with iron is a key factor in photo-Fenton tests at natural pH. Low stability corresponds to high reaction rates at initial times but also high iron release. The opposite happens with chelating agents with high stability constant with iron.
- Organic fertilizer EDDHA is not appropriate for photo-Fenton at natural pH, because the high stability constant with iron.
- High iron release diminishes the catalytic activity decreasing the efficiency of the process.
- The combination of organic fertilizers with different stability constant with iron enhances the process efficiency. Using 50%EDDS+50%EDTA, total PROP removal is achieved 1 hour before comparing to tests with only EDTA. Additionally, iron in solution at the end of the treatment is 5.5 times higher than experiments with only EDDS.
- MBR effluent, which presents low DOC, turbidity, and alkalinity, reaches higher performances than CAS. It is also attributed to higher iron release in CAS due to the larger amount of ions and organic matter, which can break the iron complex, decreasing the process efficiency.
- Phytotoxicity and BOD₅ results suggest that all treated MBR effluents accomplish with the minimum requirements for their reuse in irrigation. However, in the case of

- CAS, high reaction time is needed to reach greater yields in *E. coli* reduction, since the final CFU mL⁻¹ exceeded the maximum value proposed in the Regulation.
- Concerning the reactivity of iron complexes in aquatic ecosystem, radiation plays an important role in the photoredox cycle of iron, especially for iron complexes less stable with iron.
 - Irradiation experiments without H₂O₂ evidenced important differences in the five organic fertilizers. Although all of them absorb in the range of 290-400 nm, only EDDS-Fe and DTPA-Fe reach significant SMX degradation.
 - Photo-Fenton tests without O₂ revealed that this specie contributes on the generation of hydroxyl radicals, which are responsible of the final MPs degradation.
 - Photo-Fenton experiments with dosing of non-chelated iron achieve low MP removal, showing that iron chelates are the main via to generate hydroxyl radicals.

5.2 Recommendations

After the results obtained from this investigation and in the current water scarcity scenario, some recommendations are provided related to the potential reuse of wastewater treated by photo-Fenton process.

Firstly, it would be recommended further investigation on the use of LEDs as irradiation source. The effect of combined UV-LEDs at various wavelengths could be deeply studied to investigate more synergies. In addition, the optimization of the photoreactor design is essential to replace the conventional lamps by UV-LEDs.

Concerning the photo-Fenton process at circumneutral pH, the expansion of the study to priority compounds, regulated in Directive 2013/39/EU and watch list of Decision 2018/840/EU, would be highly recommendable due to their concern on environment. Additionally, the inactivation studies of various microorganisms could be interesting (*i.e.* *Enterococcus spp.*, *Salmonella spp.*, *Pseudomonas spp.*). The evaluation of the toxicity of the treated effluents using organisms with different sensibilities and different trophic levels (*Vibrio fishery*, *Daphnia magna*, fishes, phytotoxicity...) could be also required. Further studies on stability of iron with chelates in different matrices are essential to determine which iron complex could be applied in a specific wastewater to obtain good efficiencies.

Experiments of photo-Fenton process at circumneutral pH would be done at pilot plant scale to study the effectiveness. Besides, to perform an economic study and life cycle analysis is important to know the feasibility of the process.

Finally, a more accurate determination of all reactive oxygen species, formed when iron chelates are used in photo-Fenton, would allow a better understanding of the mechanisms. The investigation of more iron chelates is also needed.

6 Other contributions by the author

Besides the journal articles included in this thesis, the author has participated in other studies carried out during her predoctoral period. Thus, additional papers were derived from other works carried out in our laboratories and from short research stays fulfilled by the author. Additionally, she has participated in several contributions in international and national congresses derived from her PhD thesis or collaborations.

6.1 Journal articles from research stays

Three short research stays were carried out during her PhD. An article was published from the investigation performed during the stay in the University of Alberta (Canada), under the supervision of Dr. Mohamed Gamal El-Din. The investigation was focused on the treatment of Combined Sewer Overflows by coagulation-flocculation and subsequent catalytic ozonation. The second research stay was carried out in the University of Porto, under the supervision of Dr. Adrián Tavares Da Silva. In this period, it was investigated the activation of commercial graphene oxide by persulfate to remove MPs from water. The publication derived from this study is under the first revision in Chemical Engineering Journal. Finally, from the stay performed in University Polytechnic of Madrid, under the supervision of Dr. Stefanos Giannakis, interesting results were obtained, and a journal publication is currently in preparation. The study deals on disinfection of different microorganisms (*K12* and wild *E.coli*, *B. subtilis*, *R. planticola*, *S. cerevisiae* and *Enterococcus*) by means of ferrate activation by diverse oxidants (persulfate, hydrogen peroxide, peroxymonosulfate) and sunlight.

N. López-Vinent, A. Cruz-Alcalde, S.O. Ganiyu, S. Sable, S.A. Messele, D. Lillico, J. Stafford, C. Sans, J. Giménez, S. Esplugas, M. Gamal El-Din, Coagulation-flocculation followed by catalytic ozonation processes for enhanced primary treatment during wet weather conditions, *Journal of Environmental Management*, 283 (2021) 111975.

A. Cruz-Alcalde, N. López-Vinent, R.S. Ribeiro, C. Sans, J. Giménez, A.M.T. Silva, Persulfate activation by reduced graphene oxide membranes: practical and mechanistic insights concerning organic pollutants abatement, submitted to *Chemical Engineering Journal* (2021) and currently under 1st review.

6.2 Other journal articles

J.A. Malvestiti, A. Cruz-Alcalde, N. López-Vinent, R.F. Dantas, C. Sans, Catalytic ozonation by metal ions for municipal wastewater disinfection and simultaneous micropollutants removal, *Applied Catalysis B: Environmental* 259 (2019) 118104.

O. Porcar-Santos, A. Cruz-Alcalde, N. López-Vinent, D. Zanganas, C. Sans, Photocatalytic degradation of sulfamethoxazole using TiO₂ in simulated seawater: Evidence for direct formation of reactive halogen species and halogenated by-products, *Science of the Total Environment* 736 (2020) 139605.

B. Bayarri, A. Cruz-Alcalde, N. López-Vinent, M.M. Micó, C. Sans, Can ozone inactivate SARS-CoV-2? A review of mechanisms and performance on viruses, *Journal of Hazardous Materials* 415 (2021) 125658.

6.3 Congress communications

A. Cruz-Alcalde, N. López-Vinent, Removal of contaminants of emerging concern by means of Advanced Oxidation Processes, in: 2nd IdRA Young Researchers Seminar, Barcelona (Spain), May 2017.

N. López, A. Cruz-Alcalde, L. Romero, M. Chávez, P. Marco, J. Giménez, S. Esplugas, Application of UV-A LED Photo-Fenton in a Batch Reactor Evaluating Different Wavelengths, in: 10th European Meeting on Solar Chemistry and Photocatalysis: Environmental Applications (SPEA10), Almeria (Spain), June 2018. ISBN: 978-84-17261-27-6.

N. López, A. Cruz-Alcalde, L. Romero, M. Chávez, P. Marco, J. Giménez, S. Esplugas, Photo-Fenton treatment of Histamine 1 with UV-A LED and BLB radiation: energetic efficiency comparison, in: 10th European Meeting on Solar Chemistry and Photocatalysis: Environmental Applications (SPEA10), Almeria (Spain), June 2018. ISBN: 978-84-17261-27-6.

N. López, A. Cruz-Alcalde, L. Romero, M. Chávez, P. Marco, J. Giménez, S. Esplugas, Assessment of different reactor configurations for a Diphenhydramine Removal by UV-A LED Photo-Fenton Process, in: 10th European Meeting on Solar Chemistry and

Photocatalysis: Environmental Applications (SPEA10), Almeria (Spain), June 2018. ISBN: 978-84-17261-27-6.

N. López-Vinent, Emerging pollutants abatement by UV-A LED photo-Fenton in a batch reactor, in: 3rd IdRA Young Researchers Seminar, Barcelona (Spain), May 2018.

N. López, C. Gutiérrez, P. Marco, J. Giménez, S. Esplugas, Reducción del propanolol en efluentes secundarios usando el proceso foto-Fenton: comparación de UV-A LED y lámpara convencional BLB, in: XIII Congreso Español de Tratamiento de Aguas (META 2018), León (Spain), June 2018.

N. López-Vinent, Photo-Fenton at neutral pH using organic fertilizer as a chelating agent for wastewater reuse, in: 4th *IdRA Young Researchers Seminar*, Barcelona (Spain), June 2019.

S. Esplugas, J. Giménez, C. Sans, P. Marco, A. Cruz-Alcalde, N. López, Eliminación de contaminantes emergentes en aguas residuales mediante POAs, in: 1^o Simposio Novedar, Santiago de Compostela (Spain), June 2019.

N. López-Vinent, A. Cruz-Alcalde, J.A. Malvestiti, P. Marco, J. Giménez, S. Esplugas, C. Sans, Chelating agents comparison for photo-Fenton at neutral pH using UV-A LEDs in urban wastewaters: disinfection and micropollutant abatement, in: ANQUE-ICCE-CIBIQ, Santander (Spain), June 2019.

J.A. Malvestiti, A. Cruz-Alcalde, N. López-Vinent, R.F. Dantas, C. Sans, Advanced Oxidation Processes based on peracetic acid (PAA) for urban wastewater disinfection and micropollutants abatement, in: 6th European Conference on Environmental Applications of Advanced Oxidation Processes (EEAOP-6), Portoroz (Slovenia), June 2019. ISBN: 978-961-93849-5-4.

N. López-Vinent, A. Cruz-Alcalde, C. Gutiérrez, P. Marco, J. Giménez, S. Esplugas, Application of UV-A LED photo-Fenton process at neutral pH in real wastewaters: matrix influence and economical consideration, in: 6th European Conference on Environmental Applications of Advanced Oxidation Processes (EEAOP-6), Portoroz (Slovenia), June 2019. ISBN: 978-961-93849-5-4.

N. López-Vinent, A. Cruz-Alcalde, P. Marco, J. Giménez, S. Esplugas, Comparative study of photo-Fenton at neutral pH, in: 6th European Conference on Environmental Applications

of Advanced Oxidation Processes (EEAOP-6), Portoroz (Slovenia), June 2019. ISBN: 978-961-93849-5-4.

N. López-Vinent, A. Cruz-Alcalde, J.A. Malvestiti, P. Marco, J. Giménez, S. Esplugas, Strategies in photo-Fenton at neutral pH for wastewater reuse, in: IWA Young Water Professionals Spain Conference, Madrid (Spain), November 2019. ISBN: 978-84-09-19073-7.

A. Cruz-Alcalde, N. López-Vinent, L. Sánchez-Fontanet, S. Esplugas, C. Sans, Degradation of organic compounds during ozonation in the presence of zero-valent iron, in: IOA World Congress, Nice (France), October 2019. ISBN: 979-10-92607-05-5.

N. López-Vinent, A. Cruz-Alcalde, J. Giménez, P. Marco, B. Bayarri, S. Esplugas, C. Sans, New insights in photo-Fenton process at neutral pH: organic fertilizer as an iron complex for agricultural irrigation reuse, in: 14th Mediterranean Congress of Chemical Engineering (MeCCE), virtual event, November 2020.

N. López-Vinent, A. Cruz-Alcalde, J. Giménez, P. Marco, B. Bayarri, S. Esplugas, C. Sans, Photo-Fenton treatment for the removal of contaminants of emerging concern in wastewaters, in: 14th Mediterranean Congress of Chemical Engineering (MeCCE), virtual event, November 2020.

O. Porcar-Santos, A. Cruz-Alcalde, N. López-Vinent, B. Bayarri, P. Marco, J. Giménez, S. Esplugas, C. Sans, TiO₂ photocatalyst reactivity in highly saline water under simulated sunlight irradiation, in: 14th Mediterranean Congress of Chemical Engineering (MeCCE), virtual event, November 2020.

References

- [1] I. Shiklomanov, World fresh water resources, in: Water Cris. A Guid. to World's Fresh Water Resour., Oxford University Press, New York, NY (USA), 1993.
- [2] AQUASTAT. n.d. AQUASTAT website. Food and Agriculture Organization of the United Nations (FAO). www.fao.org/nr/water/aquastat/water_use/index.stm (accessed february 5, 2021).
- [3] WWAP (United Nations World Water Assessment Programme)/UN-Water, The United Nations World Water Development Report 2016: Water and jobs, UNESCO (United Nations Educational Scientific and Cultural Organization), Paris (France), 2016.
- [4] UN (United Nations) website. International Decade for Action 'WATER FOR LIFE' 2005-2015. Water scarcity. <https://www.un.org/waterforlifedecade/scarcity.shtml> (accessed february 8, 2021).
- [5] WWAP (United Nations World Water Assessment Programme)/UN-Water, The United Nations World Water Development Report 2019: Leaving no One Behind. UNESCO (United Nations Educational Scientific and Cultural Organization), Paris (France), 2019.
- [6] WWAP (United Nations World Water Assessment Programme)/UN-Water, The United Nations World Water Development Report 2018: Nature-Based Solutions for Water, UNESCO (United Nations Educational Scientific and Cultural Organization), Paris (France), 2018.
- [7] OECD (Organization for Economic Co-operation and Development), OECD Environmental Outlook to 2050: The Consequences of Inaction, OECD Publishing, Paris (France), 2012.
- [8] IWMI (International Water Management Institute), World Water Supply and Demand in 2025, World Water Scenario Analyses, World Water Council, Marseille (France), 2000.
- [9] FAO (Food and Agriculture Organization of the United Nations), The State of the World. Overcoming water challenges in agriculture, Rome (Italy), 2020.
- [10] European Commission, EU-level instruments on water reuse: final report to support the Commission's impact assessment, Publications Office of the European Union, Luxembourg (Luxembourg), 2016.

[11] WWAP (United Nations World Water Assessment Programme)/UN-Water, The United Nations World Water Development Report 2017: Wastewater – The Untapped Resource. UNESCO (United Nations Educational Scientific and Cultural Organization), Paris (France), 2017.

[12] O. Golovko, S. Örn, M. Söregard, K. Friedberg, W. Nassazi, F.Y. Lai, L. Ahrens, Occurrence and removal of chemicals of emerging concern in wastewater treatment plants and their impact on receiving water systems, *Sci. Total Environ.* 754 (2021) 142122. doi:10.1016/j.scitotenv.2020.142122.

[13] P. Gago-Ferrero, M. Gros, L. Ahrens, K. Wiberg, Impact of on-site, small and large scale wastewater treatment facilities on levels and fate of pharmaceuticals, personal care products, artificial sweeteners, pesticides, and perfluoroalkyl substances in recipient waters, *Sci. Total Environ.* 601-602 (2017) 1289–1297. doi: 10.1016/j.scitotenv.2017.05.258.

[14] B. Petrie, R. Barden, B. Kasprzyk-Hordern, A review on emerging contaminants in wastewaters and the environment: current knowledge, understudied areas and recommendations for future monitoring, *Water Res.* 72 (2015) 3–27. doi:10.1016/j.watres.2014.08.053

[15] J.L. Liu, M.H. Wong, Pharmaceuticals and personal care products (PPCPs): a review on environmental contamination in China. *Environ. Int.* 59 (2013) 208–224. doi:10.1016/j.envint.2013.06.012.

[16] X. Jin, Y. Wang, W. Jin, K. Rao, J.P. Giesy, H. Hollert, K.L. Richardson, Z. Wang, Ecological risk of nonylphenol in China surface waters based on reproductive fitness. *Environ. Sci. Technol.* 48 (2) (2014) 1256–1262. doi:10.1021/es403781z.

[17] K. Styszko, K. Proctor, E. Castrignanò, B. Kasprzyk-Hordern, Occurrence on pharmaceutical residues, personal care products, lifestyle chemicals, illicit drugs and metabolites in wastewater and receiving surface waters of Krakow agglomeration in South Poland, *Sci. Total Environ.* 768 (2021) 144360. doi:10.1016/j.scitotenv.2020.144360.

[18] L. Chen, W. Fu, Y. Tan, X. Zhang, Emerging organic contaminants and odorous compounds in secondary effluent wastewater: Identification and advanced treatment, *J. Hazard. Mater.* 408 (2021) 124817. doi:10.1016/j.jhazmat.2020.124817.

[19] J.C.G. Sousa, A.R. Ribeiro, M.O. Barbosa, M.F.R. Pereira, A.M.T. Silva, A review on environmental monitoring of water organic pollutants identified by EU guidelines, *J. Hazard.*

Mater. 344 (2018) 146–162. doi:10.1016/j.jhazmat.2017.09.058.

[20] S.Y. Bunting, D.J. Lapworth, E.J. Crane, J. Grima-Olmedo, A. Korosa, A. Kuczynska, N. Mali, L. Rosenqvist, M.E. van Vliet, A. Togola, B. López, Emerging organic compounds in European groundwater, *Environ. Pollut.* 269 (2021) 115945. doi:10.1016/j.envpol.2020.115945.

[21] Y. Luo, W. Guo, H.H. Ngo, L.D. Nghiem, F.I. Hai, J. Zhang, S. Liang, A review on the occurrence of micropollutants in the aquatic environment and their fate and removal during wastewater treatment, *Sci. Total Environ.* 473–474 (2014) 619–641. doi:10.1016/j.scitotenv.2013.12.065.

[22] F.G. Calvo-Flores, J. Isac-García, J.A. Dobado, *Emerging pollutants: Origin, Structure and Properties*, 1st ed., Wiley-VCH, Weinheim (Germany), 2018.

[23] J. Rogowska, M. Cieszynska-Semenowicz, W. Ratajczyk, L. Wolska, Micropollutants in treated wastewater, *Ambio* 49 (2020) 487–503. doi:10.1007/s13280-019-01219-5

[24] NCIthesaurus (National Cancer Institute). Diphenhydramine Hydrochloride (Code C300).https://ncit.nci.nih.gov/ncitbrowser/ConceptReport.jsp?dictionary=NCI_Thesaurus&ns=NCI_Thesaurus&code=C300 (accessed february 12, 2021).

[25] L. Joseph, B-M. Jun, M. Jang, C.M. Park, J.C. Muñoz-Senmache, A.J. Hernández-Maldonado, A. Heyden, M. Yu, Y. Yoon, Removal of contaminants of emerging concern by metal-organic framework nanoadsorbents: A review, *Chem. Eng. J.* 369 (2019) 928–946. doi:10.1016/j.cej.2019.03.173.

[26] Y. Choi, J-H. Lee, K. Kim, H. Mun, N. Park, J. Jeon, Identification, quantification, and prioritization of new emerging pollutants in domestic and industrial effluents, Korea: Application of LC-HRMS based suspect and non-target screening, *J. Hazard. Mater.* 402 (2021) 123706.

[27] S.L. Bartelt-Hunt, D.D. Snow, T. Damon, J. Shockley, K. Hoagland, The occurrence of illicit and therapeutic pharmaceuticals in wastewater effluent and surface waters in Nebraska, *Environ. Pollut.* 157 (2009) 786–791. doi:10.1016/j.envpol.2008.11.025.

[28] R.P. Deo, Pharmaceuticals in the surface water of the USA: A review, *Curr. Environ. Health Rep.* 1 (2014) 113–122. doi:10.1007/s40572-014-0015-y.

[29] J.P. Berninger, B. Du, K.A. Connors, S.A. Eytcheson, M.A. Kolkmeier, K.N. Prosser,

T.W. Valenti, C.K. Chambliss, B.W. Brooks, Effects of the antihistamine diphenhydramine to select aquatic organisms. *Environ Toxicol Chem.* 30 (2011) 2065–2072. doi.org/10.1002/etc.590.

[30] NCIthesaurus (National Cancer Institute). Propranolol hydrochloride (Code C29382).https://ncit.nci.nih.gov/ncitbrowser/ConceptReport.jsp?dictionary=NCI_Thesaurus&ns=NCI_Thesaurus&code=C29382 (accessed february 12, 2021).

[31] I. Ferrer, E.M. Thurman, Analysis of 100 pharmaceuticals and their degradates in water samples by liquid chromatography/quadrupole time-of-flight mass spectrometry, *J. Chromatogr. A*, 1259 (2012) 148-157. doi:10.1016/j.chroma.2012.03.059.

[32] M. Cleuvers, Aquatic ecotoxicity of pharmaceuticals including the assessment of combination effects, *Toxicol. Lett.* 142 (2003) 185-194. doi:10.1016/S0378-4274(03)00068-7.

[33] D.B. Huggett, B.W. Brooks, B. Peterson, C.M. Foran, D. Schlenk, Toxicity of select beta adrenergic receptor-blocking pharmaceuticals (B-blockers) on aquatic organisms, *Arch. Environ. Contam. Toxicol.* 43 (2002) 229–235. doi: 10.1007/s00244-002-1182-7.

[34] P.A. Segura, M. François, C. Gagnon, S. Sauvé, Review of the occurrence of anti-infectives in contaminated wastewaters and natural and drinking waters. *Environ Health Perspect.* 117 (2009) 675–684. doi:10.1289/ehp.11776.

[35] D.C.G. Bedor, T.M. Gonçalves, M.L.L. Ferreira, C.E.M. de Sousa, A.L. Menezes, E.J. Oliveira, D.P. de Santana, Simultaneous determination of sulfamethoxazole and trimethoprim in biological fluids for high-throughput analysis: Comparison of HPLC with ultraviolet and tandem mass spectrometric detection, *J. Chromatogr. B Anal. Technol. Biomed. Life Sci.* 863 (2008) 46-54. doi:10.1016/j.jchromb.2007.12.027.

[36] J.C. Underwood, R.W. Harvey, D.W. Metge, D.A. Repert, L.K. Baumgartner, R.L. Smith, T.M. Roane, L.B. Barber, Effects of antimicrobial sulfamethoxazole on groundwater bacterial enrichment, *Environ. Sci. Technol.* 45 (2011) 3096-3101. doi:10/1021/es103605e.

[37] Y-M. Kang, M-K. Kim, T. Kim, T-K. Kim, K-D. Zoh, Occurrence and fate of micropollutants in private wastewater treatment facility (WTF) and their impact on receiving water, *Environ. Manage.* 64 (2019) 650-660. doi:10.1007/s00267-019-01211-5.

[38] Y. Zhou, J. Meng, M. Zhang, S. Chen, B. He, H. Zhao, Q. Li, S. Zhang, T. Wang, Which

type of pollutants need to be controlled with priority in wastewater treatment plants: traditional or emerging pollutants?, *Environ. Int.* 131 (2019) 104982. doi.org/10.1016/j.envint.2019.104982.

[39] D.W. Kolpin, E.T. Furlong, M.T. Meyer, E.M. Thurman, S.D. Zaugg, L.B. Barber, H.T. Buxton, Pharmaceuticals, hormones, and other organic wastewater contaminants in US streams, 1999-2000: a national reconnaissance, *Environ Sci Technol.* 36 (2002) 1202–11. doi:10.1021/es011055j.

[40] M. Isidori, M. Lavorgna, A. Nardelli, L. Pascarelli, A. Parrella, Toxic and genotoxic evaluation of six antibiotics on non-target organisms, *Sci. Total Environ.* 346 (2005) 87–98. doi:10.1016/j.scitotenv.2004.11.017.

[41] Y. Kim, K. Choi, J. Jung, S. Park, P-G. Kim, J. Park, Aquatic toxicity of acetaminophen, carbamazepine, cimetidine, diltiazem and six major sulfonamides, and their potential ecological risks in Korea, *Environ. Int.* 33 (2007) 370–375. doi:10.1016/j.envint.2006.11.017.

[42] N. Simon-Delso, V. Amaral-Rogers, L.P. Belzunces, J.M. Bonmatin, M. Chagnon, C. Downs, L. Furlan, D.W. Gibbons, C. Giorio, V. Girolami, D. Goulson, D.P. Kreutzweiser, C.H. Krupke, M. Liess, E. Long, M. McField, P. Mineau, E.A.D. Mitchell, C.A. Morrissey, D.A. Noome, L. Pisa, J. Settele, J.D. Stark, A. Tapparo, H. Van Dyck, J. Van Praagh, J.P. Van der Sluijs, P.R. Whitehorn, M. Wiemers, Systemic insecticides (neonicotinoids and fipronil): trends, uses, mode of action and metabolites., *Environ. Sci. Pollut. Res. Int.* 22 (2015) 5–34. doi:10.1007/s11356-014-3470-y.

[43] D. Gibbons, C. Morrissey, P. Mineau, A review of the direct and indirect effects of neonicotinoids and fipronil on vertebrate wildlife, *Environ. Sci. Pollut. Res. Int.* 22 (2015) 103–118. doi:10.1007/s11356-014-3180-5.

[44] J. Kimura-Kuroda, Y. Komuta, Y. Kuroda, M. Hayashi, H. Kawano, Nicotine-Like Effects of the Neonicotinoid Insecticides Acetamiprid and Imidacloprid on Cerebellar Neurons from Neonatal Rats, *PLoS One.* 7 (2012) e32432. doi:10.1371/journal.pone.0032432.

[45] EFSA (European Food Safety Authority), Scientific Opinion on the developmental neurotoxicity potential of acetamiprid and imidacloprid, *EFSA J.* 11 (2014) 1–47. doi:10.2903/j.efsa.2013.3471.

-
- [46] J.T. Marfo, K. Fujioka, Y. Ikenaka, S.M.M. Nakayama, H. Mizukawa, Y. Aoyama, M. Ishizuka, K. Taira, Relationship between Urinary N-Desmethyl-Acetamiprid and Typical Symptoms including Neurological Findings: A Prevalence Case-Control Study, *PLoS One*. 10 (2015) e0142172. doi:10.1371/journal.pone.0142172.
- [47] L. Li, X. Chen, D. Zhang, X. Pan, Effects of insecticide acetamiprid on photosystem II (PSII) activity of *Synechocystis* sp. (FACHB-898), *Pestic. Biochem. Physiol.* 98 (2010) 300–304. doi:10.1016/j.pestbp.2010.06.022.
- [48] X. Yao, H. Min, Z. Lü, H. Yuan, Influence of acetamiprid on soil enzymatic activities and respiration, *Eur. J. Soil Biol.* 42 (2006) 120–126. doi: 10.1016/j.ejsobi.2005.12.001.
- [49] T. Iwasa, N. Motoyama, J.T. Ambrose, R.M. Roe, Mechanism for the differential toxicity of neonicotinoid insecticides in the honey bee, *Apis mellifera*, *Crop Prot.* 23 (2004) 371–378. doi:10.1016/j.cropro.2003.08.018.
- [50] A.K. El Hassani, M. Dacher, V. Gary, M. Lambin, M. Gauthier, C. Armengaud, effects of sublethal doses of acetamiprid and thiamethoxam on the behavior of the honeybee (*Apis mellifera*), *Arch. Environ. Contam. Toxicol.* 54 (2008) 653–661. doi:10.1007/s00244-007-9071-8.
- [51] European Commission, Decision 2018/840/EU of 5 June 2018 establishing a watch list of substances for Union-wide monitoring in the field of water policy pursuant to Directive 2008/105/EC of the European Parliament and of the Council and repealing Decision 2015/495/EU, *Off. J. Eur. Union*, 141 (2018) 9–12.
- [52] F. Sánchez-Bayo, R. V. Hyne, Detection and analysis of neonicotinoids in river waters - Development of a passive sampler for three commonly used insecticides, *Chemosphere* 99 (2014) 143–151. doi:10.1016/j.chemosphere.2013.10.051.
- [53] A. Tsaoulou, E.N. Papadakis, Z. Vryzas, A. Kotopoulou, K. Kintzikoglou, E. Papadopoulou-Mourkidou, Environmental and human risk hierarchy of pesticides: A prioritization method, based on monitoring, hazard assessment and environmental fate, *Environ. Int.* 91 (2016) 78–93. doi:10.1016/j.envint.2016.02.008.
- [54] E.N. Papadakis, A. Tsaoulou, A. Kotopoulou, K. Kintzikoglou, Z. Vryzas, E. Papadopoulou-Mourkidou, Pesticides in the surface waters of Lake Vistonis Basin, Greece: Occurrence and environmental risk assessment, *Sci. Total Environ.* 536 (2015) 793–802. doi:10.1016/j.scitotenv.2015.07.099.

- [55] T. Radović, S. Grujić, A. Petković, M. Dimkić, M. Laušević, Determination of pharmaceuticals and pesticides in river sediments and corresponding surface and ground water in the Danube River and tributaries in Serbia, *Environ. Monit. Assess.* 187 (2015). doi:10.1007/s10661-014-4092-z.
- [56] N. Antić, M. Radišić, T. Radović, T. Vasiljević, S. Grujić, A. Petković, M. Dimkić, M. Laušević, Pesticide Residues in the Danube River Basin in Serbia - a Survey during 2009-2011, *Clean - Soil, Air, Water.* 43 (2015) 197–204. doi:10.1002/clen.201200360.
- [57] E.C. Kalogridi, C. Christophoridis, E. Bizani, G. Drimaropoulou, K. Fytianos, Part I: Temporal and spatial distribution of multiclass pesticide residues in lake sediments of northern Greece: Application of an optimized SPE-UPLC-MS/MS pretreatment and analytical method, *Environ. Sci. Pollut. Res.* 21 (2014) 7239–7251. doi:10.1007/s11356-014-2794-y.
- [58] S. Zheng, B. Chen, X. Qiu, M. Chen, Z. Ma, X. Yu, Distribution and risk assessment of 82 pesticides in Jiulong River and estuary in South China, *Chemosphere.* 144 (2016) 1177–1192. doi:10.1016/j.chemosphere.2015.09.050.
- [59] European Commission, Directive 2000/60/EC of the European Parliament and of the Council of 23 October 2000 establishing a framework for Community action in the field of water policy, *Off. J. Eur. Communities*, 327 (2000) 1–72.
- [60] European Commission, Decision 2001/2455/EC of the European Parliament and of the Council of November 2001 establishing the list of priority substances in the field of water policy and amending Directive 2000/60/EC, *Off. J. Eur. Communities*, 331 (2001) 1–5.
- [61] Secretariat of the Stockholm Convention, Stockholm Convention, (2008). <http://chm.pops.int/> (accessed February 15, 2021).
- [62] European Commission, Regulation 2004/850/EC of the European Parliament and of the Council of 29 April 2004 on persistent organic pollutants and amending Directive 79/117/EEC, *Off. J. Eur. Union*, 158 (2004) 7–49.
- [63] European Commission, Directive 2008/105/EC of the European Parliament and of the Council of 16 December 2008 on environmental quality standards in the field of water policy, *Off. J. Eur. Union*, 348 (2008) 84–97.
- [64] European Commission, Directive 2013/39/EU of the European Parliament and of the

Council of 12 August 2013 amending Directives 2000/60/EC and 2008/105/EC as regards priority substances in the field of water policy, *Off. J. Eur. Union*, 226 (2013) 1–17.

[65] European Commission, Decision 2015/495/EU of 20 March 2015 establishing a watch list of substances for Union-wide monitoring in the field of water policy pursuant to Directive 2008/105/EC of the European Parliament and of the Council, *Off. J. Eur. Union*, 78 (2015) 40–42.

[66] EEA (European Environmental Agency), *Guidelines on Integrating Water Reuse into Water Planning and Management in the context of the WFD*, Policy Document, Common Implementation Strategy for the Water Framework Directive, Amsterdam (Netherlands), 2016.

[67] L. Alcalde-Sanz, B.M. Gawlik, *Minimum Quality Requirements for Water Reuse in Agricultural Irrigation and Aquifer Recharge Towards a Legal Instrument on Water Reuse at EU Level*, Publications Off. Eur. Union, Luxembourg, 2017. doi:10.2760/804116.

[68] European Commission, Proposal for a Regulation of the European Parliament and of the Council of 28 May 2018 establishing the minimum requirements for water reuse, *Off. J. Eur. Union*. 337 (2018) 1-27.

[69] European Commission, Regulation 2020/741/EU of the European Parliament and of the Council of 25 May of 2020 on minimum requirements for water reuse, *Off. J. Eur. Union*, 177 (2020) 32-55.

[70] Real Decreto 1620/2007, por el que se establece el régimen jurídico de la reutilización de las aguas depuradas. «BOE» núm. 294, de 8 de diciembre de 2007, BOE-A-2007-21092, 50639-50661.

[71] G. Centi and S. Perathoner, *Handbook of Advanced Methods and Processes in Oxidation Catalysis. From Laboratory to Industry*, Chapter 10: Advanced Oxidation Processes in Water Treatment, Imperial Collage Press, 2014, 251-290. doi:10.1142/9781848167513_0010.

[72] J. Poyatos, M. Muñio, M. Almecija, J.C. Torres, E. Hontoria, F. Osorio, *Advanced Oxidation Processes for Wastewater Treatment: State of the Art*, *Water Air Soil Pollut.* 205 (2010) 187-204. doi: doi.org/10.1007/s11270-009-0065-1.

[73] P. Robertson, *Advanced Oxidation Technologies for Waste and Potable Water*

Treatment, John Wiley & Sons Inc., New York (USA), 2011.

[74] C. von Sonntag, Advanced oxidation processes: mechanistic aspect, *Water Sci. Technol.* 58 (2008) 1015-1021. doi:10.2166/wst.2008.467.

[75] O. Legrini, E. Oliveros, A.M. Braun, Photochemical processes for water treatment, *Chem. Rev.* 93 (1993) 671-698. doi:10.1021/cr00018a003.

[76] J.J. Pignatello, E. Oliveros, A. Mackay, Advanced oxidation processes for organic contaminant destruction based on the Fenton reaction and related chemistry, *Crit. Rev. Environ. Sci. Technol.* 36 (2006) 1-84. doi:10.1080/10643380500326564.

[77] Y. Mokhbi, M. Korichi, Z. Akchiche, Combined photocatalytic and Fenton oxidation for oily wastewater treatment, *App. Water Sci.* 9 (2019) 35. doi:10.1007/s13201-019-0916-x.

[78] S.C. Ameta, Advanced oxidation processes for waste water treatment, Chapter 1: Introduction, *Emerging Green Chem. Technol.* 2018, 1-12. doi: 10.1016/B978-0-12-810499-6.00001-2.

[79] C. Comninellis, A. Kapalka, S. Malato, S.A. Parsons, I. Poulios, D. Mantzavinos, Advanced oxidation processes for water treatment: advances and trends for R&D, *J. Chem. Technol. Biotechnol.* 83 (2008) 769–776. doi: 10.1002/jctb.1873.

[80] M. Petrovic, J. Radjenovic, D. Barcelo, Advanced oxidation processes (AOPs) applied for wastewater and drinking water treatment. Elimination of pharmaceuticals. *Holist Approach to Environ.* 1 (2011) 63–74.

[81] U. von Gunten, Oxidation processes in water treatment: are we on track?, *Environ. Sci. Technol.* 52 (2018) 5062–5075. doi:10.1021/acs.est.8b00586.

[82] U. von Gunten, Ozonation for enhanced wastewater treatment: kinetics and mechanisms for micropollutant abatement, oxidation by-product formation and toxicological assessment, in: *5th Eur. Conf. Environ. Appl. Adv. Oxid. Process.*, Prague (Czech Republic), 2017: p. 37.

[83] Swissinfo, A look inside the Zurich's water treatment system, [https://www.swissinfo.ch/eng/clean-water-for-all_a-look-inside-zurich-s-water-treatment - system/43833918](https://www.swissinfo.ch/eng/clean-water-for-all_a-look-inside-zurich-s-water-treatment-system/43833918) (accessed february 18, 2021).

-
- [84] WaterWorld, Switzerland's first CeraMac water treatment plant operational, <https://www.waterworld.com/international/potable-water/article/16203319/switzerlands-first-ceramac-water-treatment-plant-operational> (accessed february 18, 2021).
- [85] PWNT Water Technology, Andijk III- PWN, The Netherlands, <https://pwntechnologies.com/portfolio-item/andijk-iii/> (accessed february 18, 2021).
- [86] K. Agrawal and P. Verma, Advanced oxidation processes for effluent treatment plants, Chapter 5: advanced oxidative processes: an overview of their role in treating various wastewaters, Elsevier, 2020, 87-102. doi:10.1016/B978-0-12-821011-6.00005-0.
- [87] G. V. Buxton, C. L. Greenstock, W. P. Helman, A. B. Ross, Critical review of rate constants for reactions of hydrated electrons, hydrogen atoms and hydroxyl radicals ($\cdot\text{OH}/\cdot\text{O}$) in aqueous solution, *J. Phys. Chem. Ref. Data* 17 (2) (1988) 513-883. doi.org/10.1063/1.555805.
- [88] F.M.M. Morel, J.G.Hering, Principles and Applications of Aquatic Chemistry, Wiley, New York (USA), 1993.
- [89] D. Schowanek, T.C.J. Feijtel, C.M. Perkins, F.A. Hartman, T.W. Federle, R.J. Larson, Biodegradation of [S,S], [R,R] and mixed stereoisomers of ethylene diamine disuccinic acid (EDDS), a transition metal chelator, *Chemosphere* 34 (11) (1997) 2375–2391. doi:10.1016/S0045-6535(97)00082-9.
- [90] J.D. Englehardt, D.E. Meeroff, L. Echegoyen, Y. Deng, F.M. Raymo, T. Shibata, Oxidation of aqueous EDTA and associated organics and coprecipitation of inorganics by ambient iron-mediated aeration, *Environ. Sci. Technol.* 41 (2006) 270–276. doi:10.1021/es061605j.
- [91] S. Metsarinne, T. Tuhkanen, R. Aksela, Photodegradation of ethylenediaminetetraacetic acid (EDTA) and ethylenediamine disuccinic acid (EDDS) within natural UV radiation range, *Chemosphere* 45 (2001) 949–955. doi:10.1016/s0045-6535(01)00022-4.
- [92] J. Li, 17 β -Estradiol degradation photoinduced by iron complex, clay and iron oxide minerals: effect of the iron complexing agent ethylenediamine-ethylenediamine-N, N-disuccinic acid, University Blaise Pascal, Aubière, 2010, PhD Thesis.
- [93] W. Huang, M. Brigante, F. Wu, C. Mousty, K. Hanna, G. Mailhot, Assesment of the Fe(III)-EDDS complex in Fenton-Like process: from the radical formation to the

degradation of bisphenol A, *Environ. Sci. Technol.* 47 (2013) 1952–1959. doi:10.1021/es304502y.

[94] B.H.J. Bielski, D.E. Cabelli, R.L. Arudi, A.B. Ross, Reactivity of HO_2/O_2^- radicals in aqueous solution, *J. Phys. Chem. Ref. Data* 14 (1985) 1041–1100. doi:10.1063/1.555739.

[95] H.J.H. Fenton, Oxidation of tartaric acid in presence of iron, *J. Chem. Soc.* 65 (1894) 899–910. doi:10.1039/CT8946500899.

[96] F. Haber and J. Weiss, The catalytic decomposition of hydrogen peroxide by iron salts, *Proc. Roy. Soc. A.* 134 (1934) 332–351. doi: 10.1098/rspa.1934.0221.

[97] F. Millero, Speciation of metals in natural waters, *Geochim. Trans.* 57 (2) (2001). doi: 10.1186/1467-4866-2-57.

[98] T. Rigg, W. Taylor, J. Weiss, The rate constant of the reaction between hydrogen peroxide and ferrous ions, *J. Chem. Phys.* 22 (1954) 575. doi:10.1063/1.1740127.

[99] C. Walling and A. Goosen, Mechanism of the ferric ion catalyzed decomposition of hydrogen peroxide. Effect of organic substrates. *J. Am. Chem. Soc.* 95 (1973) 2987–2991. doi:10.1021/ja00790a042.

[100] B.H.J. Bielski and D.E. Cabelli, Highlights of current research involving superoxide and perhydroxyl radicals in aqueous solutions, *Int. J. Radiat. Biol.* 59 (1991) 291–319. doi:10.1080/09553009114550301.

[101] S. Malato, P. Fernández-Ibáñez, M.I. Maldonado, J. Blanco, W. Gernjak, Decontamination and disinfection of water by solar photocatalysis: recent overview and trends, *Catal. Today* 147 (2009) 1–59. doi:10.1016/j.cattod.2009.06.018.

[102] Guidelines for Water Reuse 600/R-12/618; Environmental Protection Agency: Washington, DC, USA, 2012.

[103] R.S. Ayers, D.W. Westcot, Water Quality for Agriculture; Food and Agriculture Organization of the United Nations: Rome, Italy, 1985.

[104] A. Gallego-Schmid, R.R.Z. Tarpani, S. Miralles-Cuevas, A. Cabrera-Reina, S. Malato, A. Azapagic, Environmental assessment of solar photo-Fenton processes in combination with nanofiltration for the removal of micro-Contaminants from real wastewaters, *Sci. Total Environ.* 650 (2019) 2210–2220. doi:10.1016/j.scitotenv.2018.09.361.

-
- [105] S. Arzate, S. Pfister, C. Oberschelp, J.A. Sánchez-Pérez, Environmental impacts of an advanced oxidation process as tertiary treatment in a wastewater treatment plant. *Sci. Total Environ.* 694 (2019) 133572. doi:10.1016/j.scitotenv.2019.07.378.
- [106] R.J. Tayade, T.S. Natarajan, H.C. Bajaj, Photocatalytic degradation of methylene blue dye using ultraviolet light emitting diodes, *Ind. Eng. Chem. Res.* 48 (2009) 10262–10267. doi:10.1021/ie9012437.
- [107] M.A. Würtele, T. Kolbe, M. Lipsz, A. Kulberg, M. Weyers, M. Kneissl, M. Jekel, Application of GaN-based ultraviolet-C light emitting diodes-UV-LEDs-for water disinfection, *Water Res.* 45 (2011) 1481–1489. doi:10.1016/j.watres.2010.11.015.
- [108] S. Miralles-Cuevas, D. Darowna, A. Wanag, S. Mozia, S. Malato, I. Oller, Comparison of UV/H₂O₂, UV/S₂O₈²⁻, solar/Fe(II)/H₂O₂ and solar/Fe(II)/S₂O₈²⁻ at pilot plant scale for the elimination of micro-contaminants in natural water, *Chem. Eng. J.* 310 (2017) 514–524. doi:10.1016/j.cej.2016.06.121.
- [109] M.H. Rasoulifard, M. Fazli, M.R. Eskandarian, Performance of the light emitting diodes in a continuous photoreactor for degradation of Direct Red using UV-LED/S₂O₈⁻ process, *J. Ind. Eng. Chem.* 24 (2015) 121–126. doi:10.1016/j.jiec.2014.09.018.
- [110] N.F.F. Moreira, J.M. Sousa, G. Macebo, A.T. Ribeiro, L. Barrientos, M. Pedrosa, J.L. Faria, F.R. Pereira, S. Castro-Silva, M.A. Segundo, C.M. Manaia, O.C. Nunes, A.M.T. Silva, Photocatalytic ozonation of urban wastewater and surface water using immobilized TiO₂ with LEDs: micropollutants, antibiotic resistance genes and estrogenic activity. *Water Res.* 94 (2016) 10–22. doi: 10.1016/j.watres.2016.02.003.
- [111] J. Kosman, J.F.H. Leandro Monteiro, V. Mariani Lenart, P. Los Weinert, E.R. Lopes Tiburtius, UV-Vis LED-assisted photo-Fenton process for mineralization of losartan and hydrochlorothiazide: optimization using desirability function, *Environ. Sci. Poll. Res.* (2021). doi:10.1007/s11356-020-12011-4.
- [112] J. Rodríguez-Chueca, C. Amor, J.R. Fernandes, P.B. Tavares, M.S. Lucas, J.A. Peres, Treatment of crystallized-fruit wastewater by UV-A LED photo-Fenton and coagulation-flocculation, *Chemosphere* 145 (2016) 351-359. doi:10.1016/j.chemosphere.2015.11.092.
- [113] I. de la Obra, B. Esteban García, J.L. García Sánchez, J.L. Casas López, J.A. Sánchez Pérez, Low cost UVA-LED as a radiation source for the photo-Fenton process: a new

approach for micropollutant removal from urban wastewater, *Photochem. Photobiol. Sci.* 16 (2017) 72-78. doi:10.1039/c6pp00245e.

[114] I. Carra, J.A. Pérez Sánchez, S. Malato, O. Autin, B. Jefferson, P. Jarvis, Application of high intensity UVC-LED for the removal of acetamiprid with the photo-Fenton process, *Chem. Eng. J.* 264 (2015) 690-696. doi:10.1016/j.cej.2014.11.142.

[115] K. Davididou, J.M. Monteagudo, E. Chatzisyneon, A. Durán, A.J. Expósito, Degradation and mineralization of antipyrine by UV-A LED photo-Fenton reaction intensified by ferrioxalate with addition of persulfate, *Sep. Purif. Technol.* 172 (2017) 227-235. doi:10.1016/j.seppur.2016.08.021.

[116] M. Douglas Marchetti, E. Bessa Azevedo, Degradation of NSAIDs by optimized photo-Fenton process using UV-LEDs at near-neutral pH, *J. Water Process Eng.* 35 (2020) 101171. doi: 10.1016/j.jwpe.2020.101171.

[117] Z. Stasicka, Chapter 7-Transition metal complexes as solar photocatalysts in the environment: a short review of recent development, *Adv. Inorg. Chem.* 63 (2011) 291-343. doi:10.1016/B978-0-12-385904-4.00004-4.

[118] X. Xue, K. Hanna, C. Despas, F. Wu, N. Deng, Effect of chelating agent on the oxidation rate of PCP in the magnetite/H₂O₂ system at neutral pH, *J. Mol. Catal. A: Chem.* 311 (2009) 29–35. doi: 10.1016/j.molcata.2009.06.016.

[119] Y. Sun and J.J. Pignatello, Chemical treatment of pesticide wastes. Evaluation of iron(III) chelates for catalytic hydrogen peroxide oxidation of 2,4- D at circumneutral pH. *J. Agric. Food Chem.* 40 (1992) 322–327. doi:10.1021/jf00014a03.

[120] European Commission, Regulation (EC) No 2003/2003 of the European Parliament and of the Council of 13 October 2003 relating to fertilizers, *Official Journal of the European Communities*.

[121] M. Cho, Y. Lee, H. Chung, J. Yoon, Inactivation of *Escherichia Coli* by photochemical reaction of ferrioxalate at slightly acidic and near-neutral PHs. *Appl. Environ. Microbiol.* 70 (2) (2004) 1129–1134. doi:10.1128/AEM.70.2.1129-1134.2004.

[122] M. Cho, J. Yoon, Measurement of OH radical CT for inactivating *Cryptosporidium Parvum* using photo/ferrioxalate and photo/TiO₂ systems. *J. Appl. Microbiol.* 104 (3) (2008) 759–766. doi:10.1111/j.1365-2672.2007.03682.x.

-
- [123] N. Klammerth, S. Malato, A. Agüera, A. Fernández-Alba, G. Mailhot, Treatment of municipal wastewater treatment plant effluents with modified photo-Fenton as a tertiary treatment for the degradation of micro pollutants and disinfection. *Environ. Sci. Technol.* 46 (5) (2012) 2885–2892. doi:10.1021/es204112d.
- [124] W. Huang, M. Brigante, F. Wu, K. Hanna, G. Mailhot, Development of a new homogeneous photo-Fenton process using Fe(III)-EDDS complexes, *J. Photochem. Photobiol. A: Chem.* 239 (2012) 17-23. doi:10.1016/j.jphotochem.2012.04.018.
- [125] J.A. Perini, M. Perez-Moya, R.F.P. Nogueira, Photo-Fenton degradation kinetics of low ciprofloxacin concentration using different iron sources and pH. *J. Photochem. Photobiol. A Chem.* 259 (2013) 53–58. doi:10.1016/j.jphotochem.2013.03.002.
- [126] A. De Luca, R.F. Dantas, S. Esplugas, Assessment of iron chelates efficiency for photo-Fenton at neutral pH, *Water Res.* 61 (2014) 232–242. doi:10.1016/j.watres.2014.05.033.
- [127] S. Papoutsakis, S. Miralles-Cuevas, I. Oller, J.L. Garcia Sanchez, C. Pulgarin, S. Malato, Microcontaminant degradation in municipal wastewater treatment plant secondary effluent by EDDS assisted photo-Fenton at near-neutral pH: an experimental design approach. *Catal. Today* 252 (2015) 61–69. doi:10.1016/j.cattod.2015.02.005.
- [128] C. Ruales-Lonfat, J.F. Barona, A. Sienkiewicz, J. Vélez, L.N. Benítez, C. Pulgarín, Bacterial inactivation with iron citrate complex: a new source of dissolved iron in solar photo-Fenton process at near-neutral and alkaline pH. *Appl. Catal. B: Environ.* 180 (2016) 379–390. doi:10.1016/j.apcatb.2015.06.030.
- [129] P. Villegas-Guzman, S. Giannakis, R.A. Torres-Palma, C. Pulgarin, Remarkable enhancement of bacterial inactivation in wastewater through promotion of solar photo-Fenton at near-neutral pH by natural organic acids. *Appl. Catal. B: Environ.* 205 (2017) 219–227. doi:10.1016/j.apcatb.2016.12.021.
- [130] P. Soriano-Molina, J.L. García Sánchez, S. Malato, L.A. Pérez-Estrada, J.A. Sánchez Pérez, Effect of volumetric rate on photon absorption on the kinetics of micropollutant removal by solar photo-Fenton with Fe³⁺-EDDS at neutral pH, *Chem. Eng. J.* 331 (2018) 84–92. doi: 10.1016/j.cej.2017.08.096.
- [131] I. García-Fernández, S. Miralles-Cuevas, I. Oller, S. Malato, P. Fernández-Ibáñez, M.I. Polo-López, Inactivation of *E. coli* and *E. faecalis* by solar photo-Fenton with EDDS

complex at neutral pH in municipal wastewater effluents. *J. Hazard. Mater.* 372 (2019) 85–93. doi:10.1016/j.jhazmat.2018.07.037.

[132] W. Dong, Y. Jin, K. Zhou, S-P. Sun, Y. Li, X. Dong Chen, Efficient degradation of pharmaceutical micropollutants in water and wastewater by Fe^{III}-NTA-catalyzed neutral photo-Fenton process, *Sci. Total Environ.* 688 (2019) 513-520. doi: 10.1016/j.scitotenv.2019.06.315.

[133] P. Soriano-Molina, P. Plaza-Bolaños, A. Lorenzo, A. Agüera, J.L. García Sánchez, S. Malato, J.A. Sánchez Pérez, Assessment of solar raceway pond reactors for removal of contaminants of emerging concern by photo-Fenton at circumneutral pH from very different municipal wastewater effluents. *Chem. Eng. J.* 366 (2019) 141-149. doi:10.1016/j.cej.2019.02.074.

[134] S. Nahim-Granados, I. Oller, S. Malato, J.A. Sánchez Pérez, M.I. Polo-López, Commercial fertilizer as effective iron chelate (Fe³⁺-EDDHA) for wastewater disinfection under natural sunlight for reusing in irrigation, *App. Cat. B: Environ.* 253 (2019) 286-292. doi:10.1016/j.apcatb.2019.04.041.

[135] E.P. Costa, M. Roccamante, C.C. Amorim, I. Oller, J.A. Sánchez Pérez, S. Malato, New trend on the open solar photoreactors to treat micropollutants by photo-Fenton at circumneutral pH: Increasing optical pathway, *Chem. Eng. J.* 385 (2020) 123982. doi: 10.1016/j.cej.2019.123982.

[136] U.J. Ahile, R.A. Wuana, A.U. Itodo, R. Sha'Ato, J.A. Malvestiti, R.F. Dantas, Are iron chelates suitable to perform photo-Fenton at neutral pH for secondary effluent treatment? *J. Environ. Manage.* 278 (2021) 111566. doi: 10.1016/j.jenvman.2020.111566.

[137] H.J. Kuhn, S.E. Braslavsky, R. Schmidt, Chemical actinometry (IUPAC technical report). *Pure Appl. Chem.* 76 (2004) 2105–2146. doi:10.1351/pac200476122105.

[138] E.S. Galbavy, K. Ram, C. Anastasio, 2-Nitrobenzaldehyde as a chemical actinometer for solution and ice photochemistry, *J. Photochem. Photobiol. A: Chem.* 209 (2010) 186–192. doi:10.1016/j.jphotochem.2009.11.013.

[139] N. De la Cruz, V. Romero, R.F. Dantas, P. Marco, B. Bayarri, J. Giménez, S. Esplugas, O-Nitrobenzaldehyde actinometry in the presence of suspended TiO₂ for photocatalytic reactors, *Cat. Today* 209 (2013) 209–214. doi:10.1016/j.cattod.2012.08.035.

-
- [140] K.L. Willet, R.A. Hites, Chemical Actinometry: using o-Nitrobenzaldehyde to measure lamp intensity in photochemical experiments, *J. Chem. Educ.* 77 (2000) 900. doi:10.1021/ed077p900.
- [141] Rossmary Violette Romero Olarte, Degradation of metoprolol by means of advanced oxidation processes (Doctoral Thesis). University of Barcelona, Spain, 2015.
- [142] S.A. Huber, A. Balz, M. Abert, W. Pronk, Characterisation of aquatic humic and non-humic matter with size-exclusion chromatography - organic carbon detection - organic nitrogen detection (LC-OCD-OND), *Water Res.* 45 (2011) 879–885. doi:10.1016/j.watres.2010.09.023.
- [143] Organic Carbon Detector – DOC-Labor Dr. Huber, (2017). <http://doc-labor.de> (accessed february 4, 2021).
- [144] American Public Health Association/American Water Works Association/Water Pollution Control Federation, *Standard Methods for the Examination of Water and Wastewater*, 21st ed., Washington, D.C. (USA), 2005.
- [145] R.F.P. Nogueira, M.C. Oliveira, W.C. Paterlini, Simple and fast spectrophotometric determination of H₂O₂ in photo-Fenton reactions using metavanadate, *Talanta* 66 (2005) 86–91. doi:10.1016/j.talanta.2004.10.001.
- [146] US EPA, *Protocols for short term toxicity screening of hazardous waste sites. A. 8.7, Lettuce root elongation (Lactuca sativa)*. EUA, Chicago (1989).
- [147] N.F.Y. Tam, S. Tiquia, Assessing toxicity of spent pig litter using a seed germination technique, *Resources, Conservation and Recycling* 11 (1-4) (1994) 261-274. doi:10.1016/0921-3449(94)90094-9.
- [148] F. Zucconi, M. Forte, A. Monaco, Biological evaluation of compost maturity, *Biocycle* (1981) 27–29.
- [149] F. Zucconi, A. Pera, M. Forte, Evaluating toxicity of immature compost, *Biocycle* (1981) 54–57.